MAPPING PENNSYLVANIAN STRATIGRAPHY AND ELEVATION OF THE FRESH-SALINE GROUNDWATER INTERFACE USING GEOPHYSICAL WELL LOGS IN CARROLL COUNTY, OHIO

By

LAURA ERICHSEN

Bachelor of Science in Geology

Northland College

Ashland, WI

2010

Submitted to the Faculty of the
Graduate College of the
Oklahoma State University
in partial fulfillment of
the requirements for
the Degree of
MASTER OF SCIENCE
December, 2022

MAPPING PENNSYLVANIAN STRATIGRAPHY

AND ELEVATION OF THE FRESH-SALINE

GROUNDWATER INTERFACE

USING GEOPHYSICAL WELL LOGS

IN CARROLL COUNTY, OHIO

Thesis Approved:

Dr. Todd Halihan

Thesis Adviser

Dr. Mary Hileman

Dr. Jack Pashin

ACKNOWLEDGEMENTS

I would like to thank my advisor, Dr. Halihan, as well as committee members Dr. Pashin and Dr. Hileman. Their guidance and patience was imperative to the completion of this study and to the success of this chapter in my academic career. I would also like to thank Chesapeake Energy for supplying the vast majority of data for this study and allowing me to use it and share the results for the benefit of those who live and work in Carroll County. I am also grateful for the mentorship and encouragement of former colleagues, Brent Wilson and Mark Becker, who played a vital role in developing this project and encouraging me to pursue my Master's degree. Lastly, I would like to thank my husband, Andrew, for his emotional and technical support throughout this project.

Name: LAURA ERICHSEN

Date of Degree: DECEMBER, 2022

Title of Study: MAPPING PENNSYLVANIAN STRATIGRAPHY AND ELEVATION OF THE FRESH-SALINE GROUNDWATER INTERFACE USING GEOPHYSICAL WELL LOGS IN CARROLL COUNTY, OHIO

Major Field: GEOLOGY

Abstract: Carroll County in eastern Ohio overlies the western portion of the Appalachian Basin and is dominated by surface sediments consisting of Pennsylvanian fluvial deposits. These deposits are approximately 30.48 meters (1,000 feet) thick and contain complex patterns of sandstone, siltstone, shale, and coal beds and are the main source of underground drinking water for the county. The distribution, geometry, and connectivity of porous sandstone beds plays a large role in the flow and recharge of meteoric water in this aquifer, and thus the elevation of the interface of fresh and deeper saline waters. Previously, the elevation this interface was not mapped in the study area due to stratigraphic complexity. This study's purpose is to map this interface, which involves first delineating the Pennsylvanian fluvial stratigraphy in order to map the structure and thickness of connected porous sandstone beds using well logs. Specific conductance data collected from fluid samples gathered while drilling through the aquifer are then used in conjunction with well logs to allow two methods from which to calculate total dissolved solids (TDS) of formation water at each well log location. Total dissolved solids (TDS) interface elevations are determined at each well location for transitions of 1,000, 5,000, and 10,000 mg/L. These elevations are combined with the results of the stratigraphic analysis, which drive the interpretation of TDS interface contour geometries based on thickness and distribution of connected sandstone units. The integration of fluid and stratigraphic data results in a set of contour maps for each TDS transition elevation that allow for accurate prediction of each interface elevation at any location within the study area, which can help with protection and planning regarding freshwater resources.

TABLE OF CONTENTS

Chapter Page

LIST OF FIGURES

Figure Page

Figure Page

Figure Page

CHAPTER I

INTRODUCTION

The importance of groundwater resources to communities throughout the world cannot be overstated. Significant research has been undertaken on how to best maintain and protect groundwater from potential sources of contamination (Turcan, 1962; Roberts, 2001; Hamlin and de la Rocha, 2015). One source of potential contamination is mixing of deep, saline groundwater with shallower freshwater zones during and after oil and gas drilling, which by nature has the potential to create a conduit between shallow and deep subsurface environments. If shallow zones are improperly isolated by well casing and cement, saline fluids can potentially travel up the wellbore and into a freshwater aquifer. Proper identification of the fresh-saline groundwater interface depth is important information to prevent this mixing and contamination from occurring.

Identification of the fresh-saline interface elevation necessitates having a strong understanding of the aquifer's physical properties since that is what often controls the way fluids move through the subsurface. High geologic complexity can make predicting groundwater flow and recharge difficult, which in turn leads to difficulty in mapping and predicting elevation of the fresh-saline groundwater interface depth.

In addition to understanding the geologic properties of the aquifer, the chemical properties of the groundwater must also be analyzed. Specific conductance (SC) measurements of fluids captured during oil and gas drilling, known as "returned drilling fluids", can be used as a proxy for groundwater SC at the associated wellbore depths when air-drilling methods are used since this method does not involve addition of drilling fluids and chemicals to the borehole (Brassington and Taylor, 2012). The SC measurements of these fluid samples, collected while drilling through the freshwater aquifer, can then be used to calibrate well log data in order to accurately calculate the total dissolved solids (TDS) of groundwater for a given study area (Brassington and Taylor, 2012).

Carroll County, Ohio, the location for this study, is underlain by an aquifer consisting of Pennsylvanian fluvial deposits, which have high stratigraphic complexity dominated by discrete lenses of porous sandstone beds separated by low-porosity shales and siltstones, as well as coal beds (Adams et al., 1984; Stout, 1944). This results in complex groundwater movement, which has caused difficulty in previous analyses of the fresh-saline groundwater interface in this area (Riley, et al., 2012).

The study area also has both historical and current oil and gas drilling operations (Whieldon and Pierce, 1965). These more recent operations, specifically those conducted by Chesapeake Energy beginning in 2012, included the collection of well logs and borehole fluid SC data while drilling through the Pennsylvanian aquifer within the study area. These data can be used to delineate the stratigraphy as well as determine TDS of formation water within the aquifer throughout the study area.

HYPOTHESIS

Through integration of stratigraphic and groundwater TDS analyses, the elevation of the fresh-saline groundwater interface can be mapped and modeled in a predictive manner by using well

logs and SC measurements of returned drilling fluids within the study area. This hypothesis will be testable through the consistent and repeatable determination of 5,000 mg/L and 10,000 mg/L TDS groundwater salinity interfaces on well logs and the hydrogeological reasonableness of the resultant interface maps.

Connectivity of porous sandstone beds can be delineated in the subsurface using well logs and correlation between data points (Jordan and Pryor, 1992; Bridge and Tye, 2000; Gibling, 2006). SC measurements of returned fluids captured during drilling operations can be used as direct representations of groundwater measurements when captured during air-rotary drilling operations (Brassington and Taylor, 2012). These measurements can then be used to calibrate well log values to the study area using known physical and chemical relationships, allowing groundwater TDS to be determined solely from well log data after final calibration (Turcan, 1962; Gaither, 1994; Roberts, 2001). Elevation of the fresh-saline groundwater interface, or any groundwater TDS value of interest, can then be evaluated on individual well logs throughout the study area.

After completion of final stratigraphic correlation and mapping the thickness and structure of porous sandstone units, as well as selection of the fresh-saline groundwater interface on well logs, these two datasets can be integrated to create a predictive map of the interface elevation. Analyzing the structure and thickness of individual porous units allows confinement of the shape and slope of the contours of the fresh-saline groundwater interface elevation, which leads to accurate prediction of elevation of the fresh-saline interface based on the vertical and lateral geometries of the mapped sandstone units.

OBJECTIVES

The objectives of this study include the following: 1) use Carroll County, Ohio well logs to define stratigraphically connected sandstones using defined physical parameters, 2) map the thickness and structure of each sandstone bed, 3) outline an improved methodology for calculating

groundwater TDS from well logs and SC measurements of returned drilling fluid samples, 4) determine elevations of 1,000 mg/L, 5,000 mg/L, and 10,000 mg/L groundwater TDS transitions on each well log, and 5) integrate sandstone thickness and structure maps with TDS transition elevations to create hand-contoured maps of the elevations of each of the three groundwater TDS interfaces listed above. The ultimate goal of this study is to create an accurate, predictive model of the fresh-saline groundwater interface using the steps listed.

RESEARCH SIGNIFICANCE

This study provides a framework for characterizing stratigraphic controls on groundwater quality in the study area. Additionally, it outlines an improved methodology for integration of well log data with groundwater SC measurements to create a mathematical relationship for accurate calculation of groundwater TDS from well logs. Finally, integration of stratigraphic and groundwater TDS analyses result in a predictive hydrogeological model for determining the elevation of the fresh-saline water interface in the study area.

The broader significance of this study is that the methods outlined will be useful for evaluating the elevation of the fresh-saline groundwater interface in other geologically complex settings where available data sets include well logs and measurements of SC of groundwater (whether by direct measurement or by using returned drilling fluids as a proxy for direct groundwater samples). This could be particularly useful in areas with previous or current oil and gas drilling where this data has already been collected or could be collected in the future. Ultimately, these evaluations can lead to better protection of fresh groundwater resources when elevation of fresh-saline groundwater interfaces can be mapped in an accurate and predictive manner.

CHAPTER II

REVIEW OF LITERATURE

A significant amount of literature was evaluated for this work. In this review, the stratigraphic concepts required for the evaluation of the lithology of the fluvial depositional environment of the study site will be evaluated. Second, the literature for converting well log data to information on the properties of the formation fluids will be reviewed. This will be utilized to determine the structure of the saline water interface.

STRATIGRAPHY

Stratigraphic correlation of logs in fluvial depositional environments is notoriously difficult due to the constant lateral and vertical movement of stream beds throughout time, which result in complex facies patterns in the subsurface (Jordan and Pryor, 1992; Shepherd, 2009). These can be difficult to interpret on well logs since each one only shows a singular vertical data set, and greater well spacing makes it difficult to trace correlative units between them.

Geometries of Fluvial Deposits

There is abundant literature that discusses fluvial depositional geometries, which gives a starting point of what to expect when interpreting the subsurface from well logs (Jordan and Pryor, 1992; Bridge and Tye, 2000; Gibling, 2006). Understanding lateral facies changes and geographic extents, as well as vertical stacking patterns, is imperative to interpretation – and thus correlation – of fluvial stratigraphy. Shepherd (2009) outlined geometries of meandering vs. braided streams, including the scale of the various depositional features. Features of meandering stream deposits include point bars, crevasse splays, and fine-grained flood plain deposits (Figures 2.1 and 2.2). Generally, meandering streams do not create deposits as thick as those of braided streams (Shepherd, 2009). Gibling (2006) noted from outcrop data that meandering stream deposits range in thickness from 3.96-19.81m (13-65 ft). In contrast, the braided stream deposits from that study were commonly up to 60.05 m (197 ft) thick.

Fluvial features that contain coarser sediment are of particular interest to this research as this leads to deposits with higher porosity and permeability. These features include point bars, channel sands, and crevasse splays (Jordan and Pryor, 1992). Several studies have been conducted on these types of features since they can make effective oil and gas plays due to potentially high porosity, including one by Jordan and Pryor (1992) who studied point bars in a section of the Mississippi River with the intention of applying the findings to oil and gas reservoir studies. The data for Jordan and Pryor (1992) included cores, trenches, and vibracores. The study focused on heterogeneity in this meander belt system at multiple scales, from large scale at the size of an entire oil field, down to individual sand laminae found within a point bar.

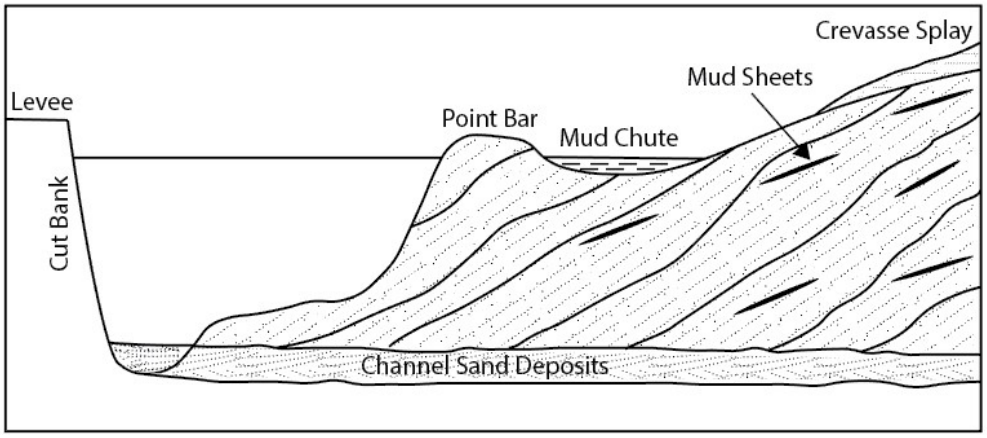

Figure 2.1: Vertically exaggerated cross section of meandering stream showing commonly associated depositional features, including stream channel, point bar, mud chute, and crevasse splay (modified from Jordan and Pryor, 1992).

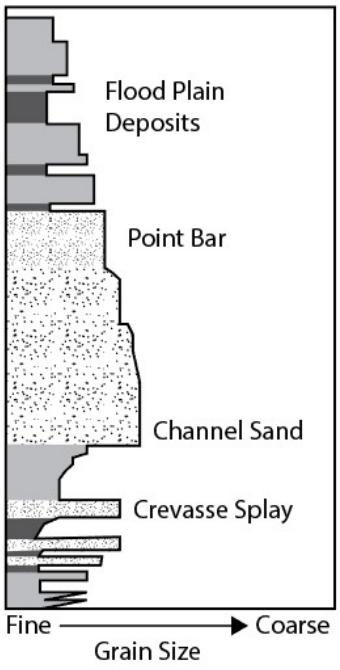

Figure 2.2: Stratigraphic profile of meandering channel deposits showing typical fining-upward sequence as well as sharp contact between base of channel sand and underlying fine-grained deposits; note heterogeneity of sediment grain sizes also typical of fluvial depositional systems (modified from Shepherd, 2009).

The most applicable scale they described is the "pool within an oil field" scale, defined as "individual meander scroll of highly permeable, laterally accreted channel point-bar and splay sands, partly or wholly isolated from other laterally contiguous bodies by low-permeability, abandoned-channel clay plugs." The sand bodies in this scale were 15.24-45.72 m (50-150 ft) thick and 3.22-8.05 km (2-5 miles) wide (Jordan and Pryor, 1992). The grain size content of clay plugs and chutes depends on how quickly they are cut off from the main river; they may be made up of entirely fine-grained mud, or they may also contain some sand within the mud. Sand deposits from abandoned channels can be either U-shaped or asymmetric. They are generally coarser-grained with more consistent grain sizes at the base of the sand body, with the tops of most sands showing increasing interfingering of silt and mud (Figure 2.2). Ultimately, these bodies are capped by fine-grained floodplain or levee deposits, though oftentimes these are reworked and possibly eroded away as the river meanders through the floodplain over time (Jordan and Pryor, 1992). Overall, this study shows there is a high level of heterogeneity one can expect within a fluvial reservoir. Understanding possible geometries of coarse-grained and fine-grained deposits is useful, as well as noting that these systems change frequently and textbook depositional patterns may be disrupted and changed by future erosion and reworking (Jordan and Pryor, 1992).

Another important aspect of fluvial systems related to this research is the connectivity of high porosity sand deposits such as point bars and channel sands. Donselaar and Overeem (2008) used outcrop data to determine the connectivity of amalgamated and stacked porous, sandy point bar deposits. The authors concluded that coarse channel sand deposits were preserved during channel meander and abandonment in their study area, connecting successive point bar deposits with high-porosity sand units (Figure 2.3). The implications from Donselaar and Overeem (2008) are important to this research, as it was similarly focused on the study of connectivity and fluid flow within high porosity fluvial sand deposits, and they show a higher degree of connectivity of point

bar deposits than expected prior to their study. By using outcrop data, the authors were able to get a finer level of detail than is available on well logs, but their conclusions are useful to keep in mind during correlation and interpretation using less-detailed data sets.

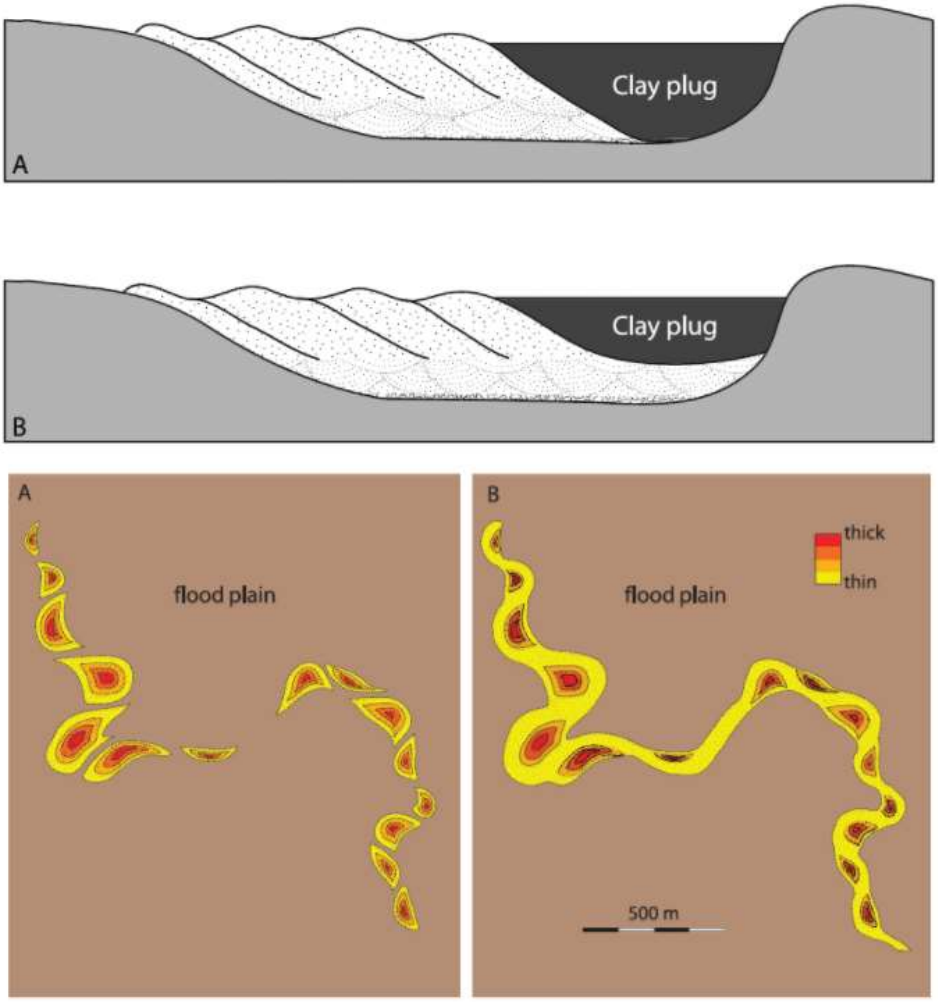

Figure 2.3: Cross section and related isopach maps showing two scenarios for fluvial sandstone connectivity; A) point bar and channel sand deposits are cut off from each other laterally with mud/clay plugs, and B) basal channel sands are contiguous beneath clay plugs, allowing for connectivity between porous channel/point bar deposits (from Donselaar and Overeem, 2008).

In addition to porous sandstone deposits, coal beds are a very important aspect of fluvial deposition with respect to this research, as they are a helpful guide by adding vertical and lateral reference datums to stratigraphic interpretation. Coals form in low-energy areas of fluvial systems

from the buildup of peat (Shepherd, 2009). To form, they require a lack of oxygen, drainage, and sediment input. They also require time to accumulate and thus can indicate periods of stability in the areas they form within fluvial systems, such as areas away from stream channels including poorly-drained, swampy floodplains and abandoned meander belts (Flores, 1984; Tibert and Gibling, 1999). This makes them useful in correlation of fluvial systems as they tend to be more laterally extensive and consistent than other types of fluvial deposits, and they are easily recognized on well logs (Figure 2.5) (Flores, 1984; Tibert and Gibling, 1999; Fanti and Catuneanu, 2010).

Correlation of Fluvial Deposits

Several studies are available regarding subsurface fluvial correlation and are discussed below. Many of these studies rely on well logs while others use different data types, including outcrop data, cores, 3D seismic data, or Ground-Penetrating Radar (GPR) (Bridge and Tye, 2000; Carter, 2003). These additional data sources provide more detail and accuracy, but where well log data is sufficient in quantity and quality, reasonably accurate correlation is possible as noted in the studies discussed below.

Crawley and Atkinson (1982) evaluated the Mesaverde Group in the Piceance Basin in Colorado. They used well logs to correlate lenticular sandstones between various wells, calculating changes in formation thickness, shale volume, and porosity. They used gamma-ray curve data to calculate shale volumes and the density curve data to calculate porosity, methods for which are outlined in Asquith and Krygowski (2004). The authors then used the calculated porosity and shale volumes, as well as formation thickness, to implement cutoffs to constrain the vertical and lateral boundaries of the mapped sandstones. The purpose of implementing cutoffs was to confine their stratigraphic correlations to sandstone units capable of effective fluid transport. As is expected, the authors noted that well spacing had a large effect on the confidence of their correlations. They

noted the physical properties, and thus log signatures, of each sandstone unit changed throughout the study area, as would be expected when considering the geometries and heterogeneity of fluvial deposits.

One method of increasing confidence in fluvial sandstone correlations is using coal seams as marker beds, as discussed above. Alqahtani (2013) used a regionally expansive coal seam within one of two fluvial formations as a structural datum from which to correlate connected sandstones on well logs. The author also noted that many thinner coal beds were eroded away by sandstones intermittently from well to well as shown on the well logs, which is similar to observations in the study area for this work. Coal marker beds are useful when trying to correlate sandstones in areas with sparse data points and in situations where stream beds have cut deeply into the underlying sediment, as it can show a relatively steady depositional horizon in the subsurface from which to base stratigraphic interpretations (Figures 2.4 and 2.5). Other researchers have discussed the use of coals in fluvial stratigraphic correlations, even to the point of discussing their use in non-marine sequence stratigraphic studies by using them as marker beds in a similar manner to how shales are used in marine sequence stratigraphic studies (Tibert and Gibling, 1999; Fanti and Catuneanu, 2010). All of these studies show using coals as traceable marker beds in fluvial systems is vital to increasing the confidence and accuracy of stratigraphic correlation of surrounding sediments.

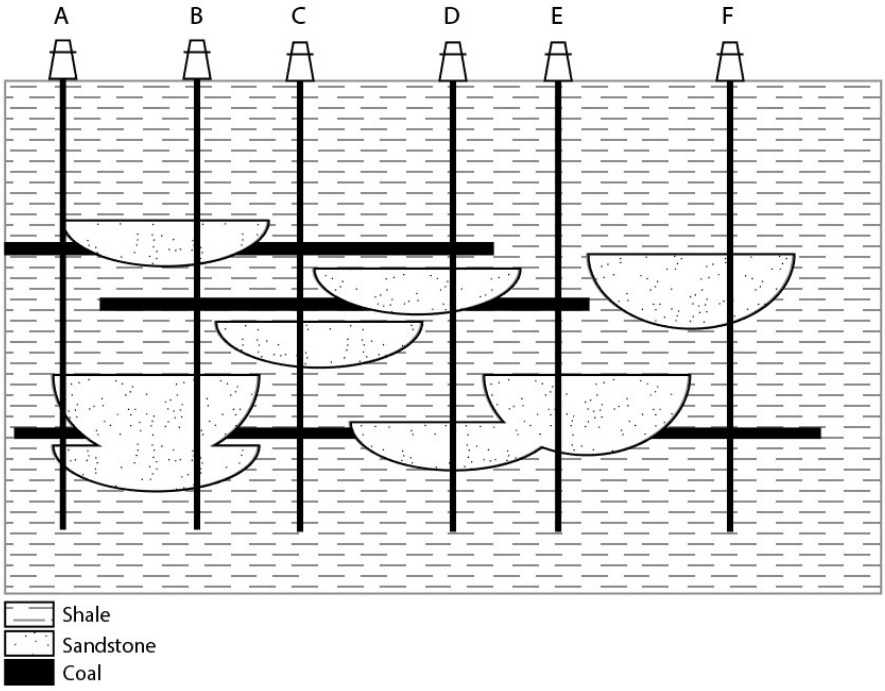

Figure 2.4: Cross-sectional view of wellbores intersecting sandstone lenses and coal seams; laterally continuous coal seams can help determine whether sandstone lenses are connected when interpreting stratigraphy using well logs (Tibert and Gibling, 1999; Fanti and Catuneanu, 2010).

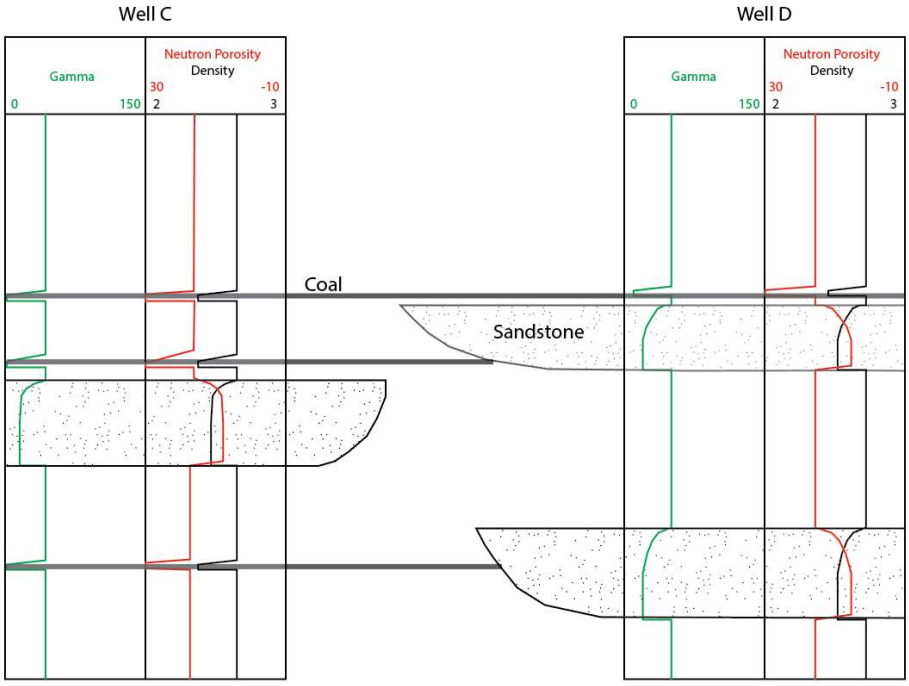

Figure 2.5: Example well log cross section of wells C and D in Figure 2.4; coal beds help constrain interpretation when determining connectivity of sandstone beds on adjacent well logs and tend to be easily recognizable from other lithologies on logs (Tibert and Gibling, 1999; Fanti and Catuneanu, 2010).

Calculating Fluid Properties from Well Logs

Evaluating the salinity of pore water is the next step in mapping a fresh-saline water interface. Oilfield well logs have been evaluated in several studies for their usefulness and accuracy in aquifer studies in areas where they are available (Turcan, 1962; Gaither, 1994). They often extend much deeper than the saline water interface depth and can show the physical properties of an entire aquifer. The drawback of using oilfield well logs in aquifer studies is that the logging tools are often designed for petroleum reservoirs, where the goal is to differentiate between different types of fluids (oil, gas, and water), and not necessarily changing salinities in groundwater. In addition, borehole conditions are often quite different in oil/gas wells and water wells (borehole size, drilling processes, drilling fluids, etc.), which can affect the performance of logging tools, so consideration of that must be taken into account when using oilfield well logs to evaluate freshwater aquifers (Gaither, 1994).

Resistivity is a major indicator of water salinity, though in well log data, values are a combination of formation resistivity and fluid resistivity and are commonly relied upon for calculating TDS from logs. Most of the principles used in these calculations are based off "Archie's equation" (1942). Archie (1942) developed a well-known equation used in petroleum reservoir investigations to calculate percent water saturation, the difference of which gives oil saturation (Equation 2.1).

$$S_w^n = \frac{(R_w \times a)}{(\phi^m \times R_o)} \tag{2.1}$$

where S_w is water saturation, n is the saturation exponent, R_w is the resistivity of the formation water, R_o is the resistivity of a 100% water-saturated formation, a is the tortuosity factor, ϕ is porosity, and m is the cementation exponent (Archie, 1942).

To obtain Equation 2.1, Archie (1942) initially defined a relationship between R_w and R_o, a ratio which he called the Formation Factor (F) (Equation 2.2). An alternative definition of F relates porosity, tortuosity factor, and cementation factor (Equation 2.3) (Waxman and Smits, 1968). These relationships are the foundation for Equation 2.1 and have been commonly used to evaluate formation water salinity.

$$F = \frac{R_O}{R_W} \tag{2.2}$$

$$F = \frac{a}{\phi^m} \tag{2.3}$$

In hydrocarbon exploration, where a 100% water-saturated formation is not expected during evaluation, R_o is substituted with the true formation resistivity (R_t) in Equation 2.2 to give Equation 2.4 (Asquith and Krygowski, 2004). R_t values are determined from deep resistivity readings from well logs and are corrected for invasion (Asquith and Krygowski, 2004).

$$S_w^n = \frac{(R_w \times a)}{(\phi^m \times R_t)} \tag{2.4}$$

where S_w is water saturation, n is the saturation exponent, R_w is the resistivity of the formation water, R_t is the true formation resistivity, a is the tortuosity factor, ϕ is porosity, and m is the cementation exponent (Asquith and Krygowski, 2004).

Turcan (1962) used Archie's relationships to evaluate an aquifer in Louisiana, specifically using the resistivity relationship (Equation 2.2). The author used measured Specific Conductance (SC) values of the formation water from each of the wells in his dataset, converting SC to resistivity and using this value for R_w. The conversion from SC to resistivity is a simple unit conversion:

$$SC\left(\frac{\mu mohs}{cm}\right) = \frac{10{,}000}{R_w\left(\frac{ohmm^2}{m}\right)} \tag{2.5}$$

After correcting each resistivity value to 25º C (77º F) using Arp's (1953) equation, the author used R_o values from the well logs and then converted R_w from the SC of the associated measured water samples to determine F for each sample interval using Equation 2.2. Turcan (1962) then calculated an average value of F for the study area. Next, water samples were collected from water wells that penetrated the subject formation within the study area and measured for SC and TDS. These values were plotted against each other on a scatter plot, and a linear best-fit line was used to define the mathematical relationship between TDS and SC for the study area, allowing for conversion of any particular value of TDS to SC. Using Equation 2.5, this value was then converted to R_w. Equation 2.2 was then solved for R_o, and the previously determined R_w value was multiplied by the average F for the study area to calculate R_o. That R_o value represents a log resistivity reading that directly correlates with the TDS value that was input into Equation 2.5. In this way, this method allows for calculation of a specific value of R_o that correlates to any given TDS value (Turcan, 1962).

Roberts (2001) used these principles in evaluating an aquifer in Oklahoma, but took the additional step of considering formation water type, specifically the dominant ions, when calculating the formation factor. Different anions and cations have different electrical properties, and can thus influence conductance and resistivity readings differently. This can lead to errors when using multiple different water types to calculate a regional formation factor, as SC readings

for a water sample dominated by one anion/cation may be different than a water sample dominated by a different anion/cation for the same TDS level (Roberts, 2001; Robinson and Lupton, 2018). By comparing the dominant ions from water samples at various depths and TDS levels, Roberts (2001) found a noticeable shift in the dominant anions at approximately 1,000 mg/L TDS, while cations remained consistent. Due to this, the author limited his dataset to water samples with greater than 1,000 mg/L TDS for determining the regional formation factor in that particular study area. In this way, the ionic makeup of the water used for comparison was consistent, and the effects of different ions on conductivity, and thus fluid resistivity, were mitigated.

An important piece of data for Roberts (2001) was the chemical analyses of water samples with which to determine the resistivity of the formation water. The data for Roberts's (2001) study were obtained from USGS test wells that were drilled with the specific goal of evaluating water in the aquifer as well as several municipal water test wells. Oil and gas wells are not often used for direct freshwater evaluation. They are frequently drilled using fluids (mud filtrate) with constituents that are meant to stick to the sides of the wellbore and seal the formation off from the borehole. These often contain clay, which can interfere with accurate SC and resistivity readings, and the nature of this drilling method means there is an abundance of added drilling fluids in the wellbore, with which the formation water mixes before it reaches the surface. These issues can be avoided if the well is drilled using air rotary drilling, which does not use significant external drilling fluids and little to no chemical additives to the water sampled from the resulting well. This method allows formation water to come to the surface relatively unaltered, which can then be measured to provide an accurate formation fluid resistivity value. Brassington and Taylor (2012) discuss obtaining water samples from oil and gas wells that are drilled with air. They evaluated the accuracy of the SC measurements of water samples taken from the returned fluids while using air rotary drilling methods by using piezometers to obtain water samples from the

same wellbores at varying depths, and comparing them to the measurements of the returned drilling fluids. Their results showed that the fluid conductivities measured by the two different methods were similar in correlative sample intervals, meaning measuring SC of returned fluids while drilling can result in an accurate representation of in-situ formation water SC when using air rotary drilling methods.

Alger (1966) discusses a caveat to Equation 2.2 in shallower formations with varying porosity and grain size. Using laboratory measurements, he concluded that the formation factor is influenced by surface conductance of the grains in the formations, with smaller grain size causing a decrease in formation factor. This needs to be kept in mind when evaluating aquifers with varying porosities and highly variable grain size.

Hamlin and de la Rocha (2015) used an even simpler method to evaluate the upper portion of the Carrizo-Wilcox aquifer, directly comparing TDS to R_o. The TDS values came from direct water sample measurements of water wells, and R_o values were determined from oil and gas well logs. The TDS and R_o values were from the same zones, and well pairs were a median distance of 2,693 m (8,835 ft) apart according to the authors. TDS and R_o were plotted on a scatter plot using a log-log scale and these data showed strong correlation (R^2=0.87). The authors then further separated their data into three regions to assure similar lithologies, porosities, and general aquifer properties. This method worked in the upper portion of this aquifer because it is lithologically relatively uniform and free of low permeability layers, so groundwater salinity gradually increases with depth and flows uniformly throughout the aquifer.

The deeper portion of the Carizzo-Wilcox aquifer is separated hydraulically from the upper portion, has higher lithologic variability, and the authors had no water well samples from which to directly measure TDS (Hamlin and de la Rocha, 2015). The methods the authors used on the upper portion of the aquifer were thus unsuitable for the lower portion, and they instead used the

combination of Equations 2.2 and 2.3 (assuming a=1 after Archie, 1942) which resulted in Equation 2.6.

$$R_w = \phi^m \times R_o \tag{2.6}$$

They used constant values for $ø$ and m from previous research to determine R_o at various TDS values using Equation 2.5, first converting TDS to R_w as discussed above using Equation 2.5. This is similar to Roberts's (2001) method but considers porosity as well, though it assumes constant porosity through the entire aquifer. The ionic makeup of the water is not considered in either of the methods the authors used. For the lower portion of the aquifer, they did have historical R_w measurements from previous research from which they were able to quality-control the values used for $ø$ and m.

Alger and Harrison (1989), building on Archie's (1942) work, noted another proportional relationship of common well log resistivity measurements: the resistivity of the mud filtrate (R_{mf}) and resistivity of the formation filled 100% with mud filtrate (R_{xo}), shown in Equation 2.7:

$$\frac{R_{mf}}{R_w} = \frac{R_{xo}}{R_o} \tag{2.7}$$

This essentially assumes the ratio between the resistivity of the mud filtrate and the formation water must be similar to that of the 100% mud-filled formation and 100% water-filled formation. In this way, they are able to determine R_w from log readings alone instead of using water samples like Roberts (2001), provided the drilling method allows for sufficient invasion of the mud filtrate into the formation. Drilling on air does not allow for this method, and direct measurements of formation water resistivity must be obtained. As discussed by Robinson and Lupton (2018), this method also assumes formation water is highly saline and is generally dominated by sodium and chloride ions; therefore, correction for specific ions is required for using this method in fresh formation water. Robinson and Lupton (2018) were also studying multiple aquifer units within

the larger Trinity Aquifer, each with different dominant ions, rather than one aquifer like Roberts (2001), and thus required specific TDS conversions for each aquifer unit. This study ultimately shows how to calculate TDS from log resistivity readings for each of the aquifer units in the study area, rather than a resistivity cutoff for a specific TDS value. It also shows another way to determine R_w from logs instead of water samples.

Structure of Fresh-Saline Water Interface

Due to the importance of freshwater resources, numerous studies have been conducted across the world to identify and map fresh-saline water interfaces (Hamlin and de la Rocha, 2015; Robinson and Lupton, 2018). The structure of the boundary of saltwater and freshwater varies between different geologic settings, and differing stratigraphy can have a strong influence as grain size affects porosity and permeability, and thus water movement underground (Hamlin and de la Rocha, 2015; Gillespie, et al., 2017). Other factors such as structure, climate, and proximity to fresh or saline water bodies also affect this structure (Barker and Ardis, 1996; Brassington and Taylor, 2012).

As discussed above, many aquifers show increasing TDS with increasing depth, which is generally a result of residence time of the water in the aquifer (Hamlin and de la Rocha, 2015; Robinson and Lupton, 2018). This is the case for many aquifers, though the complexity can vary significantly depending on the stratigraphy within the aquifer (Gillespie, et al., 2017). As discussed by Hamlin and de la Rocha (2015), the presence of aquitards can have a strong effect on the groundwater variability within an aquifer, as is the case between the upper and lower portions of the Carizzo-Wilcox aquifer (Figure 2.6). In some cases, fine-grained beds are not thick enough or consistent enough to fully separate porous units hydraulically, as is the case in a study of aquifers near El-Sadat City, Egypt (Atwia, et al., 1997). In this case, the authors showed that water is able to travel vertically through nearly 25 m (82 ft) of clay due to the presence of

sandy layers within the clay bed, which was shown through chemical analysis of water samples collected from zones above and below the clay layer.

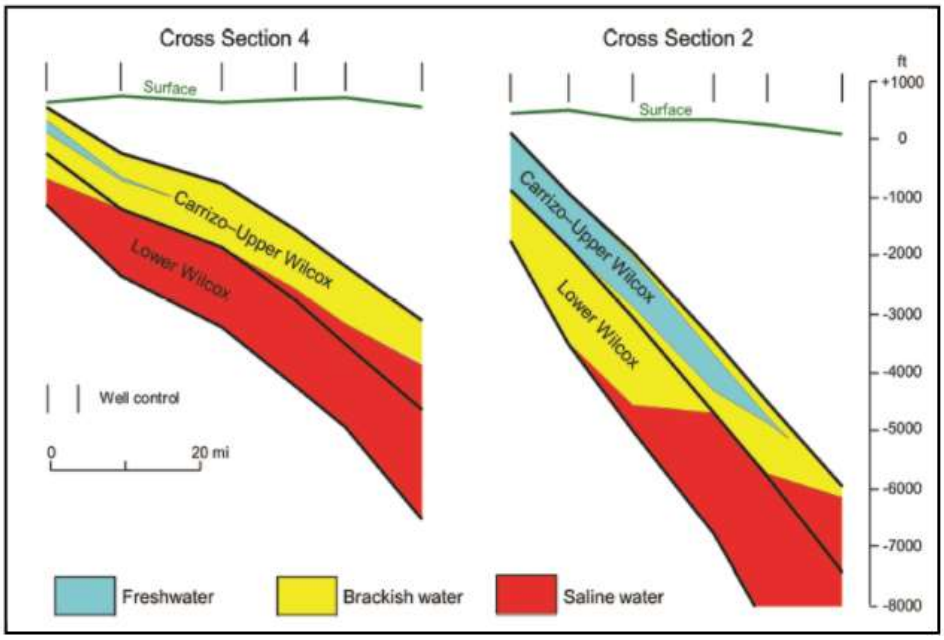

Figure 2.6: Example of increasing TDS with depth in Carrizo-Wilcox aquifer as well as influence of aquitards (black lines) on the aquifer's salinity profile (from Hamlin and de la Rocha, 2015).

Lithology may also have an effect on the groundwater salinity depending on the type and abundance of various minerals. In addition, the depositional environment of the formation, indicated by the lithology (e.g. marine vs. inland), affects the type of connate water originally in the formation (Gillespie, et al., 2017). Authors in some areas have noted that the interface may not be clear due to the lithology of the underlying unit. Atwia et al. (1997) and Gillespie, et al. (2017) both studied aquifers that are underlain by crystalline basement rock, which was then used as a proxy for the saline interface depth.

Recharge can also have a large effect on the structure of the fresh/saline water interface, which can be affected by climate and geologic structure. The region studied by Atwia et al. (1997) is an arid environment, so recharge from rain and surface water is minimal, and the water table is up to

80 m (262.5 ft) below land surface. On the contrary, Roberts's (2001) study area contains several major streams and receives an average of 83.82 cm (33 inches) of rainfall per year, meaning surface recharge to the aquifer is expected to be much higher. In areas with faulting, faults can act as a conduit for fresh surface water to enter and recharge much deeper areas of the aquifer, as discussed by Brassington and Taylor (2012) (Figure 2.7). This deep recharge is visible on saline interface maps as a structural low in the saline interface depth contours, and it is highly dependent on the size of the fault.

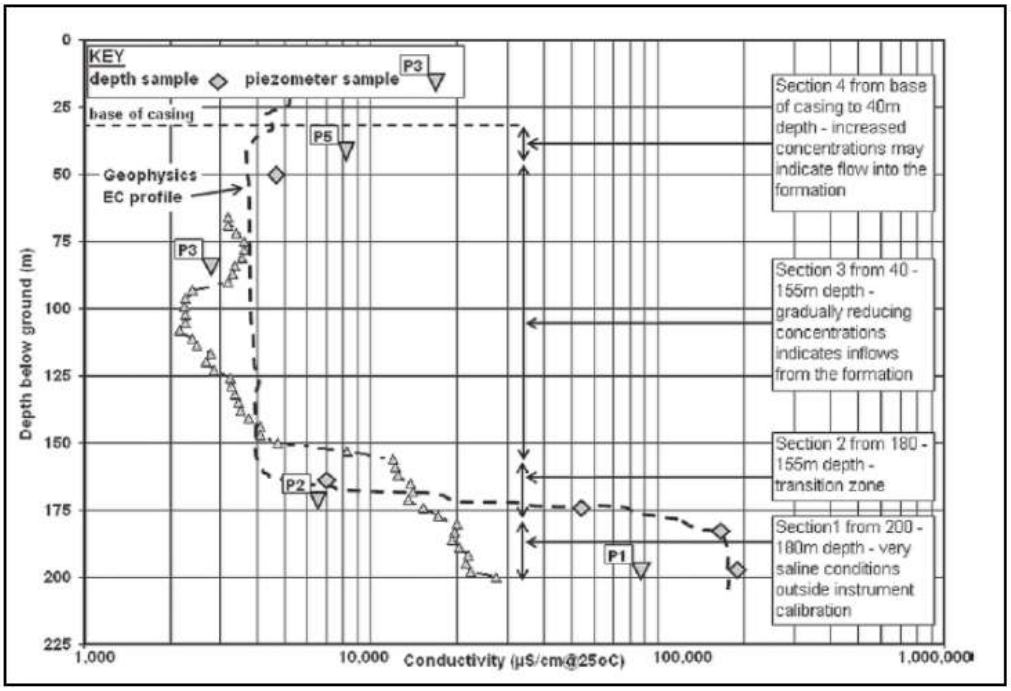

Figure 2.7: Groundwater salinity profile of aquifer showing reduction in salinity at approximately 30 m (90 ft) below ground surface, indicating source of fresh water recharge at this depth: authors indicate this is likely due to a fault that creates a conduit from surface to this depth (from Brassington and Taylor, 2012).

All the factors discussed above not only control the depth/elevation of the saline interface, but the character of the interface as well. The local stratigraphy plays a large part of this, as discussed by Hamlin and de la Rocha (2015) regarding the Carrizo-Wilcox aquifer. The upper portion of that aquifer showed a gradual increase in TDS with depth, largely due to the higher sand percentage and general lack of low porosity beds throughout that portion of the aquifer. In contrast, areas

where the upper portion of the aquifer contained fresh water throughout the entire interval showed a sharper fresh/saline interface contact due to the presence of shales that hydraulically separate the upper and lower portions of the aquifer.

The type of data available in evaluating the saltwater interface can also affect the interpretation. Brassington and Taylor (2012), while studying an aquifer in England, discuss the assumption that the fresh/saline interface in that aquifer was thought to be a sharp transition based on the evaluation of water samples during previous research. These water samples had not been compared to well logs due to lack of available data. The authors were able to take water samples during drilling of several new wells in their study area, after which well logs were run. The well logs revealed a much more gradual transition than would be expected from only the well fluid conductivity data. While well logs alone have their limits, the smaller sampling scale allows for finer detail in aquifer changes to be visible. The water samples, which were collected from larger intervals, did not show as much detail, but were necessary to effectively calibrate the well log measurements to the study area aquifer.

Mapping the Interface

The main goal in calculating TDS and determining the structure of the fresh/saline water interface is to develop a map delineating the elevation of that interface in the case of this study. There are some useful techniques provided in the literature for spatially mapping the well data, which are described below.

Roberts (2001) described one method used for picking the interface based on both the R_o cutoff and stratigraphy derived from well log data. In porous intervals (assumed to be water-bearing) that showed the transition of resistivity from above the R_o cutoff to below it, he selected the interface at the base of the next shallower porous sand interval. This method errs on the side of a

shallower interface, essentially showing the deepest water well depth that would produce water less than 10,000 mg/L TDS (Figure 2.8).

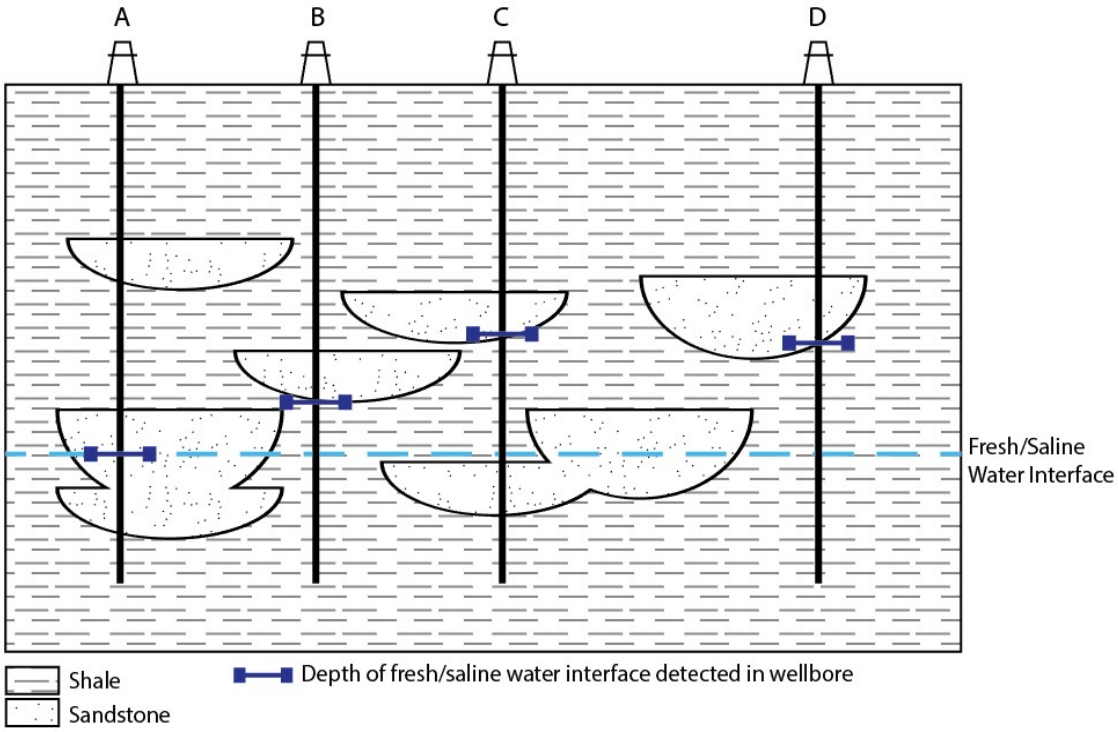

Figure 2.8: Cross-sectional view showing example of isolated sandstone lenses influencing detection of fresh-saline water interface depth in four wellbores; wellbore A shows most accurate interface depth as it drills through a sandstone lens containing the fresh-saline transition; Wellbores B, C, and D show how interface depth may be determined when the transition occurs at a depth in between discrete sandstone beds.

Robinson and Lupton (2018) separated the larger Trinity Aquifer into five separate aquifer units based on the stratigraphy and hydraulic connectivity of porous water-bearing sandstones. They assumed that the five units were not in communication with each other and mapped each separately. Instead of contouring on the elevation or depth of the saline interface, the authors plotted the TDS values at the top of each aquifer unit on a map, then hand contoured the location depicting where the water at the top of each unit crosses the saline interface. They also chose three TDS thresholds to map: 1000 mg/L, 3,000 mg/L, and 10,000 mg/L and mapped the location of each interface for each aquifer unit. This results in maps that illustrate which aquifer unit will

have the freshest water based on geographic location, which could then be compared to structure maps of each aquifer unit to determine the depth/elevation to the saline water interface (or any of the mapped TDS interfaces). Two of these maps are shown as examples in Figure 2.9.

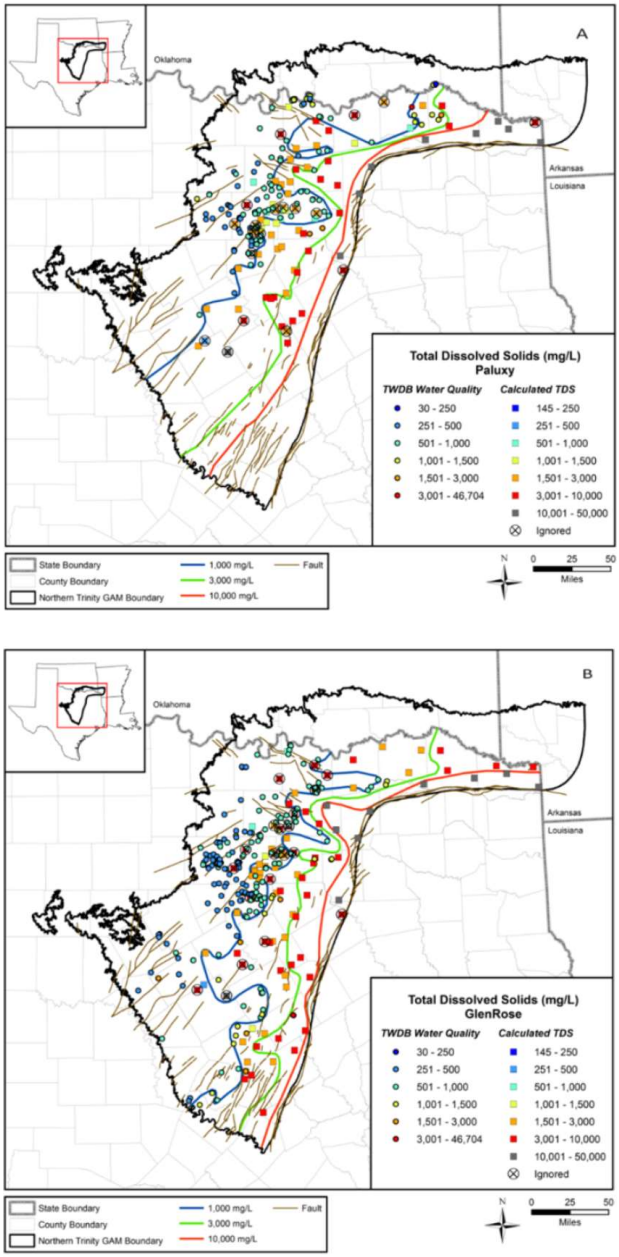

Figure 2.9: Example of two individual aquifer unit maps (Paluxy and Glen Rose) showing salinity changes over the study area, including lines depicting locations for each unit where TDS transitions over 1,000 mg/L (blue), 3,000 mg/L (green), and 10,000 mg/L (red) (from Robinson and Lupton, 2018).

CHAPTER III

STUDY AREA

The location of this study includes the entirety of Carroll County, Ohio. This county is in the east-central part of the state near the Ohio River and the West Virginia panhandle. In this section, the geologic setting, stratigraphy, and hydrogeology of the study area will be discussed. This information is necessary for accurately interpreting lithology and fluid data in order to map the fresh-saline water interface.

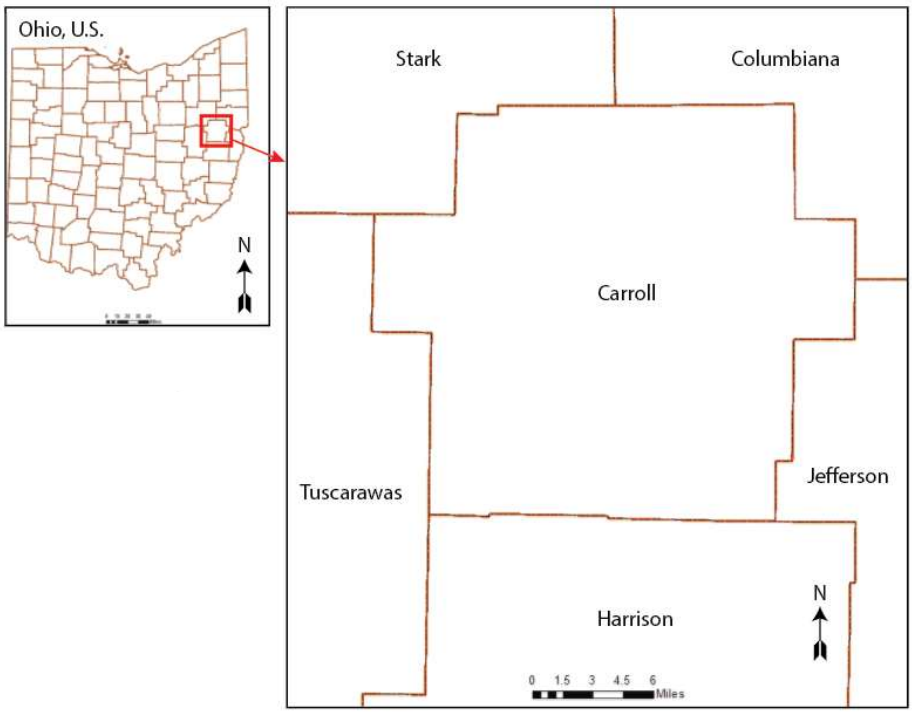

Figure 3.1: Study area location.

GEOLOGIC SETTING

Carroll County lies in the western Appalachian Basin (Branson, 1962; Adams et al., 1984). The top of Mississippian interval, which consists of the Sunbury shale in this area, was deposited in a marine environment and was highly eroded prior to Pennsylvanian deposition, creating a disconformable contact between the formations (Beuthin, 1994). The Pennsylvanian was marked by increased fluvial deposition with intermittent marine deposition in the study area (Mrakovich and Coogan, 1974; Nadon and Kelly, 2004). Due to the erosion of the top of the Mississippian, Pennsylvanian deposition was highly influenced by valleys and ridges, which allowed for preferential deposition of sandstone units within valleys (Beuthin, 1994). As is typical of fluvial settings, the Pennsylvanian consists primarily of sandstone, siltstone, shale, and coal.

The Ohio Department of Natural Resources has compiled research on the Pennsylvanian system and defined the nomenclature and descriptions of several broad groups within the Pennsylvanian Period (Ohio Division of Geological Survey, 1990). The groups of interest for this research include the Pottsville Group, the Allegheny Group, and the Conemaugh Group (Figure 3.2). Several pieces of literature discussed in detail below describe these groups and define the framework for the stratigraphic analysis for this study.

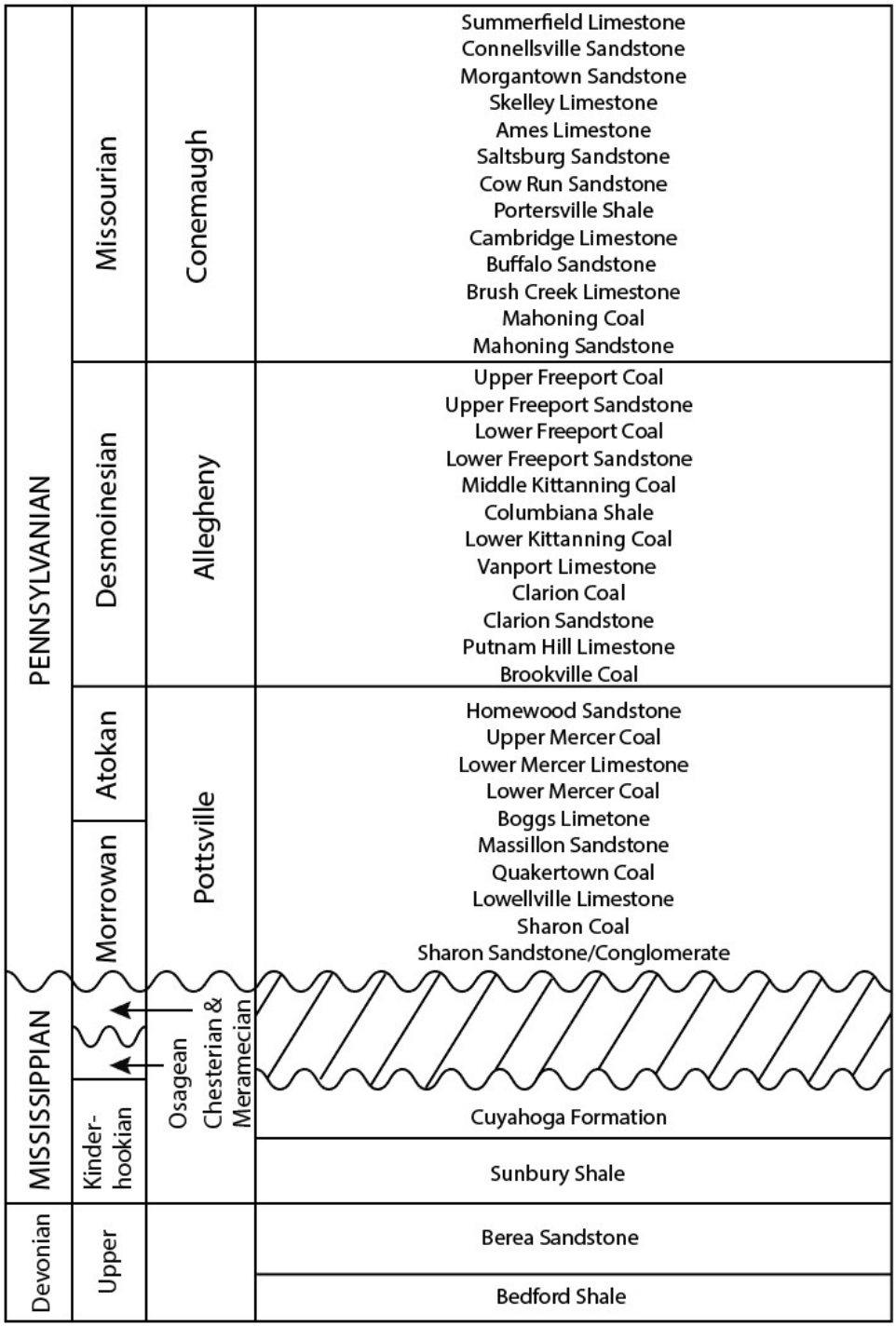

Figure 3.2: Stratigraphic column of southeastern Ohio (modified from Ohio Division of Geological Survey, 1990; Stout, 1944).

Devonian

The Upper Devonian Berea Sandstone lies below the Mississippian-aged Sunbury Shale and above the Bedford Shale (Potter et al., 1983). Thought to be composed of delta and shoreline facies, it is contiguous across this study area and is distinguishable on well logs as it is a sandstone that sits between two massive shale beds (Potter et al., 1983). The Berea has been studied extensively throughout Kentucky and southeastern Ohio as it is capable of producing oil and gas (Stout et al., 1935; Channas, 1969). There is historic Berea oil and gas production in Carroll County, beginning with the first discovery in 1896 (Whieldon and Pierce, 1965). The Berea was drilled and produced in several small fields throughout the county (Figure 3.3). According to Ohio Geological Survey's state Underground Sources of Drinking Water (USDW) map, the Berea is the deepest freshwater-bearing zone throughout a large portion of central Ohio, west of the study area.

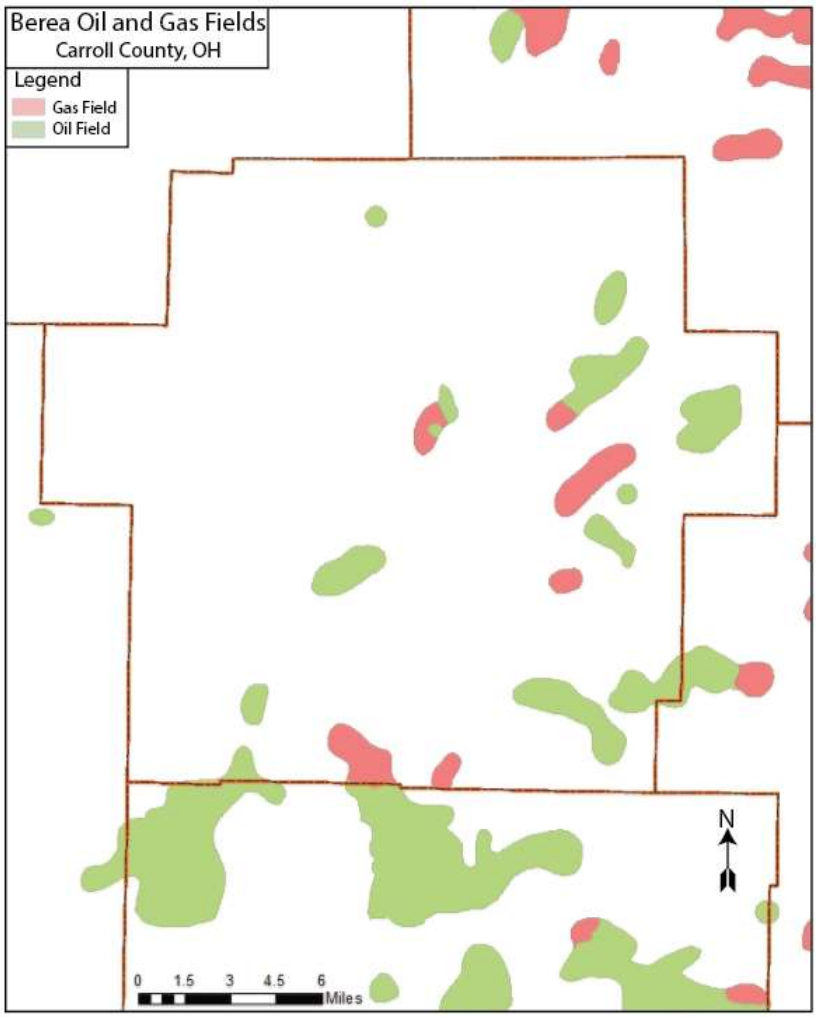

Figure 3.3: Berea Sandstone oil and gas fields (from Ohio DNR GIS Mapping Services, accessed March 2022).

Mississippian

The oldest formation in the Mississippian in the study area is the Sunbury Shale (Stout, 1944). The base of the Pennsylvanian sits disconformably on top of the Mississippian (Stout, 1944; Mrakovich and Coogan, 1973). Where the Sharon Sandstone is present, well logs show a sharp transition from fine-grained Mississippian shale to coarse-grained Pennsylvanian sandstone. In many of the well logs used for this research in the study area, the base of the Pennsylvanian consists of fine-grained material that grades into the top of the Mississippian, making the exact transition indiscernible on geophysical well logs. Defining the base of the Pennsylvanian/top of

Mississippian boundary on well logs presents a challenge in the study area due to this, which leads to problems mapping fresh-saline groundwater interface with ODNR's model of defining the fresh-saline water interface as the base of the Pennsylvanian.

Pennsylvanian

a. Pottsville Group

The Pottsville Group ranges from 60.96-91.44 m (200-300 ft) thick and, according to Stout (1944), includes the interval from the top of the Mississippian to the base of the Brookville coal. The Sharon Sandstone/Conglomerate is currently the accepted marker for the base of the Pottsville Group and records the disconformable surface between the base of the Pennsylvanian and the top of the Mississippian (Adams et al., 1984; Stout, 1944).

Branson (1962) outlines ten cyclothems in the Pottsville, each containing a coal bed. In Ohio, the main coal beds in this group include, in ascending order, the Sharon, Quakertown, Lower Mercer, and Upper Mercer coals. The Sharon Coal outcrops in northeastern and southeastern Ohio and is generally sporadic throughout the eastern part of the state, ranging from a few centimeters up to 1.2 m (4 ft) thick. It is cut by channel sands in many areas. The Quakertown, Lower Mercer, and Upper Mercer coals are similarly discontinuous and often very thin, enough so that they are only mined locally and infrequently (Adams et al., 1984).

The Sharon Coal overlies the Sharon Conglomerate, which ranges from medium-grained sandstone to course, pebbly conglomerate and is known for its fluid and gas storage capability (Stout, 1944). This formation is an important marker bed for this research because the current map of the fresh-saline groundwater interface provided by the Ohio DNR is contoured on the estimated base of the Sharon Sandstone around the northern and western edges of Carroll County (Riley et al., 2012). Within Carroll County, the well logs used for this study show that a consistent, connected conglomerate topped with coal is not always present at depths where the

Sharon would be expected, causing the base of the Pennsylvanian to be difficult to distinguish from the fine-grained Mississippian below. Stout (1944) notes that the Sharon tends to occur in "broad, deep depressions, resembling erosion valleys, cut in the older Mississippian floor" but the deposits are erratically distributed, which may explain why a large, massive conglomerate is not always present to mark the base of the Pennsylvanian. The Sharon Sandstone can range from 3.05-76.2 m (10-250 ft) in thickness and has been drilled for brine and natural gas in southeastern Ohio (Stout, 1944). The depositional environment was originally thought to be deltaic, but later studies indicate evidence of alluvial plain deposition dominated by braided streams (Mrakovich and Coogan, 1973).

b. Allegheny Group

The Allegheny Group is the interval from the base of the Brookville Coal to the top of the Upper Freeport Coal (Ohio Division of Geological Survey, 1990). Branson's (1962) maps show the Allegheny ranging in thickness from approximately 60.96 m (200 ft) in the southeast of Carroll County to 45.72 m (150 ft) in the northwest of the county where it crops out. He also notes that there are 13 defined cyclothems, with mostly incomplete sequences of (from base to top) 1) sandstone and shale, 2) freshwater limestone, 3) underclay, 4) coal, and 5) marine shale or limestone at the top. He also notes that sandstones in this group are "erratic in distribution and thickness, and at places rest in channels cut into older beds" (Branson, 1962).

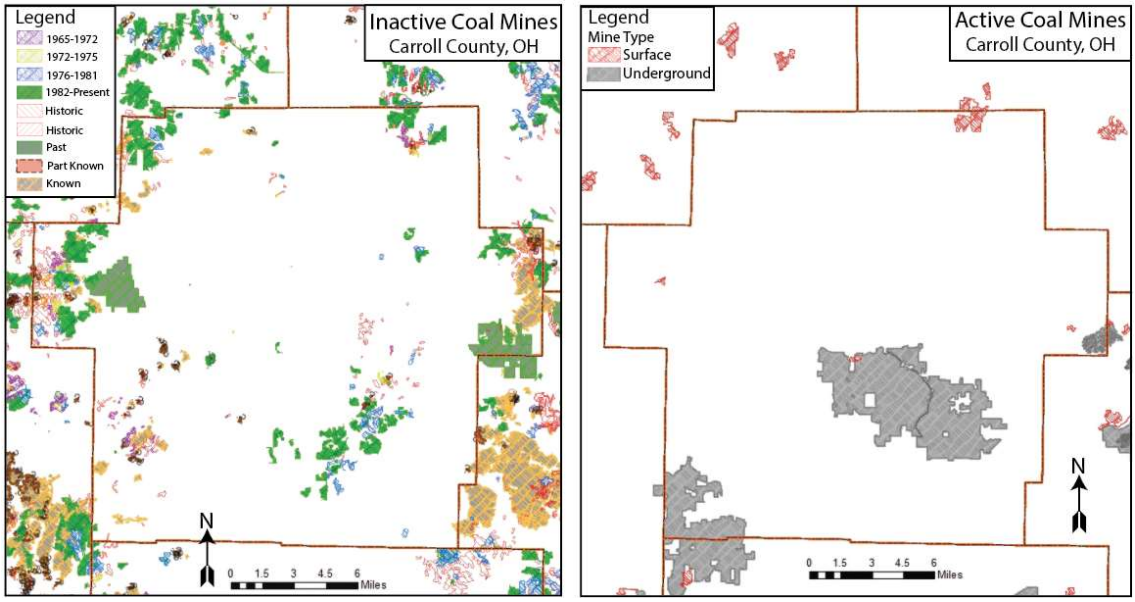

Figure 3.4: Past and current surface and underground coal mines within the study area (from Ohio DNR GIS Mapping Services, accessed March 2022).

Several coal beds from the Allegheny Group are mined within the study area using both surface and underground mining methods (Adams et al., 1984). The ODNR Mines of Ohio GIS shapefiles show geographical extents of historical and current surface and underground coal mining operations throughout the study area, highlighting the prevalence of coal mining in Carroll County (Figure 3.4). Important named coal beds in this group include the Clarion, Brookville, Lower and Middle Kittanning, and Upper Freeport Coals (Branson, 1962; Adams et al., 1984; Ohio DNR GIS Mapping Services, accessed March 2022). The Brookville is 0.3-0.76 m (1-2.5 ft) thick on average, and better developed in the study area than the Clarion, which ranges from 0-1.22 m (0-4 ft) thick. The Lower Kittanning contains multiple stacked coal beds throughout the basin, and ranges from 0.61-1.22 m (2-4 ft) thick in Ohio. The Middle Kittanning is similarly extensive throughout eastern Ohio, averaging 1.22 m (4 ft) thick and is the target of the Carrollton Mine, which is visible in Figure 3.4 as a large active underground mine in the middle of Carroll County (Figure 3.4) (Ohio DNR GIS Mapping Services, accessed March 2022). The elevation of the Middle Kittanning Coal within the Carrollton Mine is not published

publically. The Upper Freeport is one of the most prolific coal seams in Ohio and is mined heavily in the southeastern part of the state, ranging in thickness from 0.76-2.13 m (2.5-7 ft) (Adams et al., 1984). Several abandoned mines on the Ohio DNR Mines of Ohio map are identified as targeting the Upper Freeport Coal throughout Carroll County, including areas near the Carrolton Mine as well as mines in the southeast and west-central parts of the county ((Ohio DNR GIS Mapping Services, accessed March 2022). These shapefiles identify the elevation of the Upper Freeport Coal in some of the abandoned mines, though not the exact location where the elevation was determined, and it appears as though this coal is within 30.5 m (100 ft) of the ground surface (Ohio DNR GIS Mapping Services, accessed March 2022).

The major named sandstone units in this group include, from oldest to youngest, the Clarion Sandstone, Lower Freeport Sandstone, and Upper Freeport Sandstone. Where the Clarion Sandstone is present, it can be useful in aiding the identification of the Clarion Coal since it often occupies the entire interval from the Putnam Hill Limestone to the Clarion Coal and is generally massive and ranges from 6.1-16.76 m (20-55 ft) in thickness (Stout, 1944). The Lower Freeport Sandstone outcrops in Carroll County as well as adjacent Columbiana and Tuscarawas counties and is fairly continuous in this area, ranging from 1.5-22.86 m (5-75 ft) or more in thickness. The Upper Freeport Sandstone is less continuous in this area and is not present in many areas throughout eastern Ohio. In areas where it is present, it may be very thin, or it may be eroded and replaced underlying beds, adding complexity to stratigraphic identification (Stout, 1944). It is reported to contain iron and clay, which may affect well log readings. It ranges from 0.31-18.29 m (1-60 ft) thick (Stout, 1944).

c. Conemaugh Group

The Conemaugh Group is the youngest Pennsylvanian Group present in the study area (Adams et al., 1984; Branson, 1962) (Figure 3.2). This group includes the interval from the top of the Upper

Freeport Coal to top of the Summerfield Limestone (Branson, 1962). This interval includes the Ames Limestone, which Branson (1962) notes is an important marine limestone marker bed used for coal exploration in eastern Ohio. Branson (1962) indicates the Conemaugh outcrops in southeastern Carroll County and is non-existent in the northwestern part of the county. Throughout southeastern Ohio, in a belt running northeast to southwest parallel to the Ohio River, approximately 4828.03 square km (3000 square miles) of Conemaugh are exposed at the surface (Stout, 1944). The Mahoning Sandstone is one of the major sandstones in the Conemaugh Group. It lies between the Upper Freeport Coal and the Mahoning Coal, and is generally 4.57-10.67 m (15-35 ft) thick. It ranges from a fine-grained sandstone to a conglomerate in some areas and often contains cross-bedding indicative of fluvial depositional environment (Stout, 1944). Stout's assessment of the Mahoning Sandstone is regional in scale.

Adams et al., (1984) describes the regional coal resources in a very broad sense and outlines general characteristics of each group, as well as general depositional settings. They also address coal thicknesses and patterns in general terms for each of the Pennsylvanian groups, giving framework for what to expect of the different coal intervals described. They describe the Conemaugh coals as "multiple-bedded," "patchy," "thin and discontinuous," and generally less than three meters (ten feet) thick throughout eastern Ohio (Adams et al., 1984).

GEOLOGIC STRUCTURE

Ohio is home to several large geologic structural features, including the Cincinnati Arch and the Cambridge arch, as well as some minor folding and faulting features throughout the state (Ver Steeg, 1944). Carroll County is part of the Appalachian Plateau, which is the area west of the Appalachian Valley and Ridge Province (Elizalde et al., 2016). Due to this, the area was subject to much less structural deformation than much of the areas to the east in West Virginia and Pennsylvania (Elizalde et al., 2016). Carroll County contains no major geologic structures, but a

few minor anticlines and synclines were noted by Ver Steeg (1944) from mapping the "No. 7 Coal" which is a Pennsylvanian-aged coal, but it is unclear which modern formation Ver Steeg was mapping. He also notes that there is no major faulting in this area, but there are very small faults with little lateral continuity and vertical throw.

This coincides with findings by Elizalde et al. (2016), who researched faults in subsurface Pennsylvanian rock exposed in a Carroll County coal mine. The authors noted thrust faults in shales of the floor and ceiling of the mine, determining that they largely consist of low-angle thrust faults striking northwest-southeast. The offset of these faults ranged from several centimeters to less than a meter (several inches to less than 3 ft). Becker (2013) studied the same mine and noted a normal fault with 38 cm (15 in) of throw, which was relatively large for that study. Overall, research indicates some deformity occurred during the Pennsylvanian Period which led to small magnitude faults with low vertical offset in Pennsylvanian-aged formations in the study area.

The structure of the Berea Sandstone has been studied in eastern Ohio for oil and gas exploration purposes. Root and Martin (1995) studied the structure of the Berea Sandstone in Portage County, including history and timing of fault movement. They determined that some deformation likely occurred during Permo-Pennsylvanian time, shortly after the Alleghanian orogeny. They also concluded that deformation likely did not occur much after this time and that the region has since been relatively structurally stable. The Berea Sandstone dips to the east-southeast at 5.9 m/km (31 ft/mile) on average throughout the region (Gray et al., 1982).

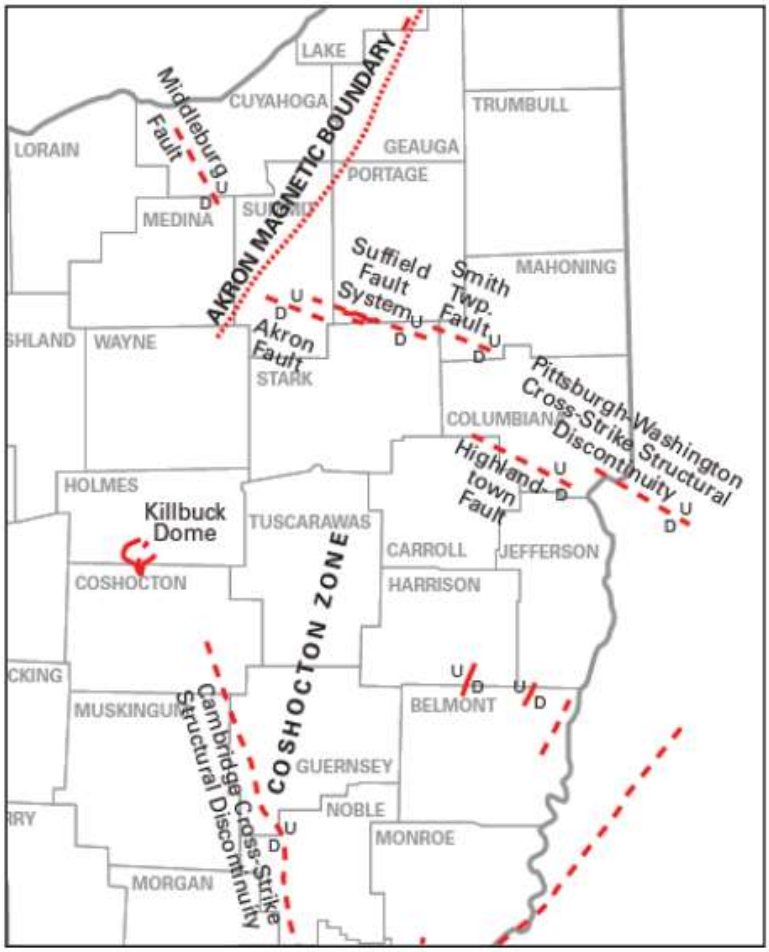

Figure 3.5: Map of eastern Ohio showing major structural features, including the Highlandtown Fault in the northeast corner of the study area (from Hansen and Fox, 2020).

One large Precambrian basement fault is noted in the study area. The Highlandtown Fault trends northwest-southeast across the northeastern corner of Carroll County, continuing across southern Columbiana County. It has a maximum vertical offset of 73.15 m (240 ft) in the Precambrian structure with the northeastern block being upthrown (Root et al., 1986). This fault is evident on maps of the Berea Sandstone in the northeast area of the study area (Figure 3.6). This fault is thought to be the result of Paleozoic deformation with multiple periods of reactivation throughout the Cambrian to the Pennsylvanian (Root et al., 1986; Root and Martin, 1995). The Highlandtown fault is in the northeastern quarter of study area and is the only structure of notable magnitude within the study area.

Overall, the geologic structure of the Pennsylvanian and top of the Mississippian within the study area consists of a few faults with very minor vertical offset of often less than one meter (3 ft) and little lateral continuity, except for the Highlandtown Fault. The Alleghanian Orogeny was occurring during the deposition of the stratigraphic interval of interest in this study, but the study area lies west of much of the deformation that occurred during that period (Gray et al., 1982; Root et al., 1986; Root and Martin, 1995).

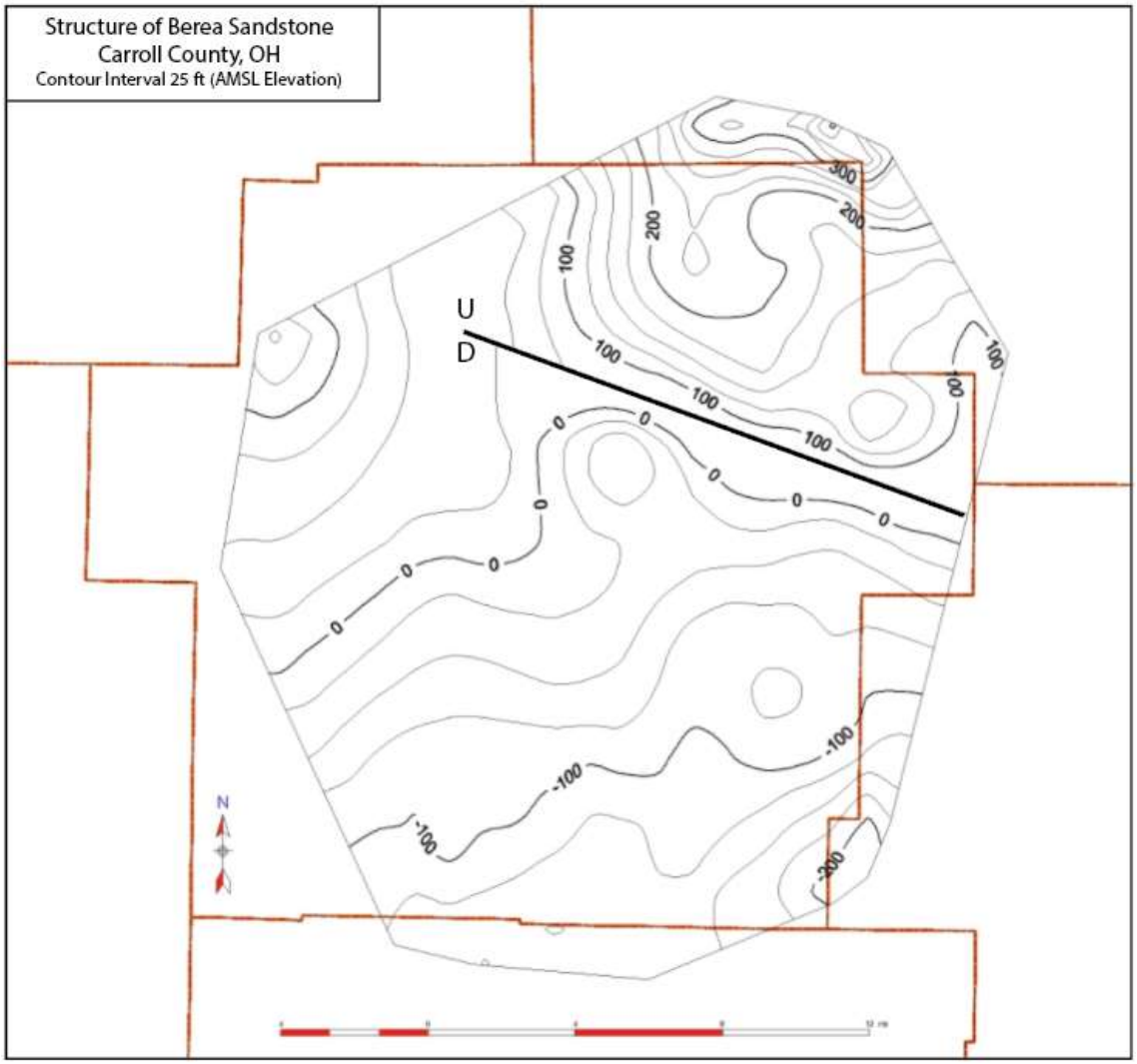

Figure 3.6: Structural map of Berea Sandstone as depicted on well logs used for this study. The Highlandtown Fault can be seen trending southwest to northeast. The northeastern block is upthrown with approximately 30.48 m (100 ft) of vertical offset.

HYDROGEOLOGY

Shallow Aquifers

Due to the geologic nature of the Pennsylvanian Formation in the study area, groundwater movement is largely controlled by stratigraphy (Riley et al., 2012). The structural and stratigraphic characteristics discussed previously, including the absence of both large faults and thick, brittle formations which might create conduits for deep groundwater recharge, are important considerations for interpretation of the fresh-saline groundwater interface in this area. Without major structural deformities, the stratigraphic connectivity of porous and permeable sandstone units is the primary controller of aquifer recharge in the study area, and is thus what drives the fresh-saline groundwater interface structure.

The Ohio DNR published a statewide map showing the deepest underground source of drinking water (USDW), which is defined as 10,000 mg/L TDS, by mapping specific stratigraphic units over large areas of the state (Riley, et al., 2012). This map shows that the deepest USDW occurs in the basal Pennsylvanian Sharon Sandstone formation in the northern half of Carroll County. The map contours do not cover the southern half of the county because, "The lenticular, braided, and intertwining nature of these deposits prohibits reliably naming and mapping a lowest USDW across any appreciable portions of [the southeastern part of Ohio]" (Riley et al., 2012). The Ohio EPA identifies the general aquifer type in this area as sandstone.

Water well production rates vary from 11 to more than 380 liters per minute (LPM) (3-100 gallons per minute (GPM)) according to the map of water resources in Carroll County published by ODNR (Walker, 1991). The highest groundwater yields are found in the northwestern part of the county in large valley fill deposits. Outside of these valley fills, yields in that area are typically 38-95 LPM (10-25 GPM). The average yield decreases to the southeast of the county to less than 11 LPM (<3 GPM) (Walker, 1991). ODNR provides a water well database that shows

private water well depths, locations, test yields, and lithology. These data show water wells in Carroll County range from 2.13-205.44 m (7 to 674 ft) in depth below ground surface (BGS), with median depth of 41.45 m (135 ft) BGS. These data do not include water quality data.

Siegel et al. (2015) evaluated water well sampling data collected on behalf of Chesapeake Energy Corporation in the study area. These data were collected within 762-1,219 m (2,500-4,000 ft) of planned oil and gas wells prior to Chesapeake commencing the associated drilling operations and include many data points in Carroll County, as well as surrounding areas within eastern Ohio, southwestern Pennsylvania, and northwestern West Virginia. The results of this study show water wells in these areas have a mean TDS of 425 mg/L and consist of dominantly calcium and bicarbonate ions. Of 7,962 analyzed samples, 3% exceeded the EPA secondary maximum contaminant levels (SMCLs) for chlorides, 5% exceeded the SMCLs for sulfate, and 23% exceeded SMCLs for TDS. The researchers noted increased sulfate concentrations in some samples, which they attributed to the oxidation of pyrite within coal deposits. They also noted that these samples frequently contained increased iron, manganese, sodium, and TDS. The effects of coal mining on groundwater chemistry have been studied by other researchers in nearby areas in Ohio, West Virginia, and Pennsylvania, and those studies similarly found elevated sulfate and TDS concentrations associated with the oxidation of pyrite in coals in these areas (Van Horn et al., 2007; McAuley and Kozar, 2006; Razem and Sedam, 1985).

An Ohio EPA report (2008) on Ohio's groundwater quality compares TDS and chemistry of different aquifer types throughout the state. The study shows several samples were obtained from the study area and classifies different samples as both sandstone and sand-gravel type aquifers. These data show average TDS for sandstone aquifers is 515 mg/L and the TDS of sand-gravel aquifers is 543 mg/L. The study contains piper plots showing the average ionic makeup for each aquifer type as well (Figure 3.7). The sandstone aquifers show even distribution of calcium and sodium as the dominant cations, while the dominant anion is bicarbonate. Sand-gravel aquifers

show calcium to be the dominant cation and both sulfate and bicarbonate as evenly dominant anions (Ohio EPA, 2008).

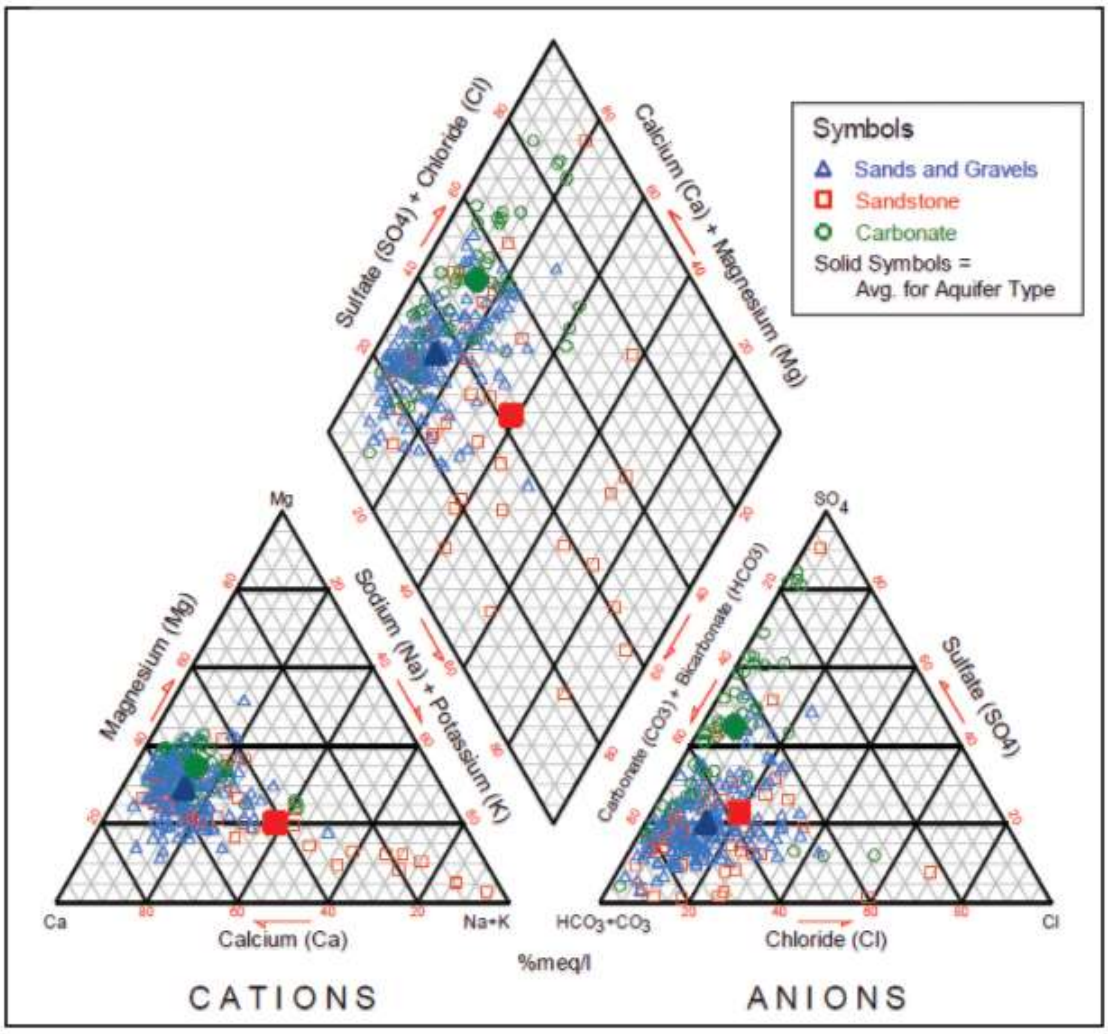

Figure 3.7: Piper plot showing dominant ions in different aquifer types in Ohio (from Ohio EPA, 2008).

Ohio EPA maintains an ambient groundwater-monitoring network throughout the state, which shows information on the chemical constituents of water in each of the monitoring wells (Ohio EPA, 2016). Carroll County contains one of these wells in the Carrollton Wellfield near the center of the county. There are six other monitoring wells within 80.47 km (50 miles) of the border of Carroll County that are completed in sandstone aquifers (Figure 3.8). The depth of the

Carroll County well is 38.1 m (125 ft) BGS and the other surrounding wells are 27.43 m (90 ft), 37.19 m (122 ft), 42.67 m (140 ft), 47.24 m (155 ft), 82.3 m (270 ft), and 121 m (397 ft) BGS. According to the most recent published reports for each monitoring well, the TDS range from 269 mg/L to 1,897 mg/L, with four of the samples being below 500 mg/L TDS and the remaining samples measuring at 775 mg/L, 1,016 mg/L, and 1,897 mg/L. Though data is sparse from 500-200 mg/L TDS, the data show that there is some pattern of dominant anions and cations in relation to TDS concentrations. In general, wells with less than 500 mg/L TDS show both sodium and calcium to be dominant cations and bicarbonate as the dominant anion. From 500-1,000 mg/L TDS, calcium and sodium continue to both be dominant cations and the dominant anion shifts to chloride. The monitoring well in Muskingum County ("The Wilds", shown in Figure 3.8) shows a dramatically higher sulfate concentration at 1,897 mg/L TDS relative to all other monitoring wells, which all show a general increase in chloride with increasing TDS. Literature shows water from this particular area to be affected by local surface coal mining and reclamation, causing increased calcium and sulfate concentrations (Eberle and Razem, 1985; Van Horn et al., 2007). Due to this, the inorganic constituent data from that particular monitoring well were not used in this evaluation.

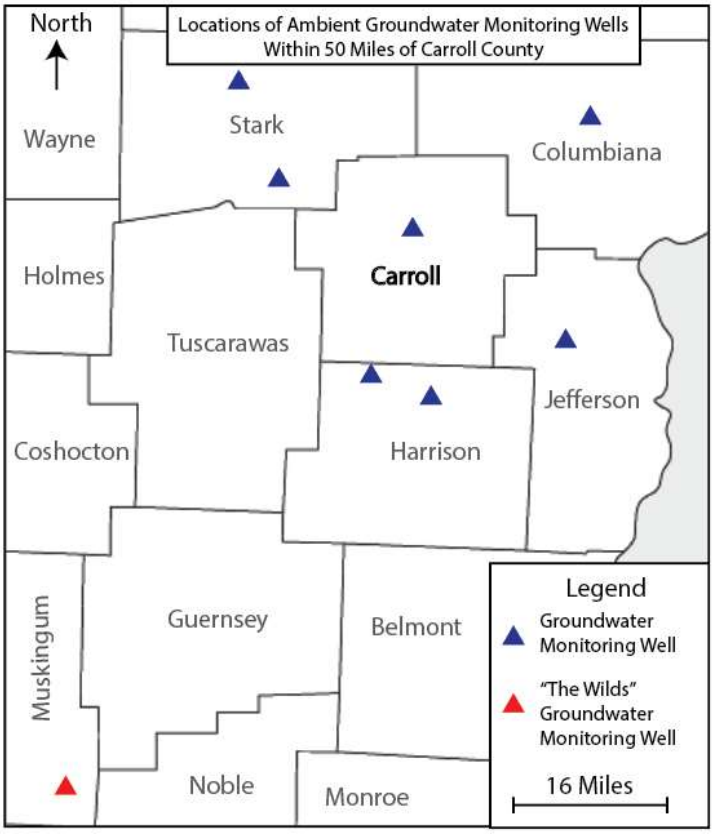

Figure 3.8: Locations of Ohio EPA Ambient Groundwater Wells in sandstone aquifers within 80.47 km (50 miles) of the border of Carroll County, as well as the location of monitoring well "The Wilds" in Muskingum County.

Though this sample set is small, other literature shows a similar shift in dominant ions in relation to increasing TDS in the study area. Thomas (2018) obtained water samples from several water wells throughout Ohio in order to study methane in groundwater. The study included three samples from Stark County and one from Columbiana County, both of which are adjacent to Carroll County, and water type and TDS were determined for these samples. The TDS values of the samples are 352 mg/L, 1,120 mg/L, 1,240 mg/L, and 2,940 mg/L. The water types all show sodium as a main cation, with calcium also being dominant in the 352 mg/L TDS sample. The anions vary, similarly to the monitoring well data. Two of the samples (352 mg/L and 1,240 mg/L) show the dominant anion to be bicarbonate. The 1,120 mg/L sample shows sulfate as the dominant anion, and the 2,940 mg/L sample shows chloride as the dominant anion. Exact

concentrations of these ions aren't shown. The data from this literature correlates well with the data from the ambient groundwater monitoring network discussed above in the lower TDS ranges, and it gives further evaluation of water chemistry changes in the 2,000-3,000 mg/L TDS range. These two datasets indicate that groundwater greater than 3,000 mg/L TDS is likely to consistently be dominated by sodium and chloride ions in the study area.

Data from the Ohio EPA ambient groundwater monitoring network also tracks SC values, allowing direct comparison of TDS and SC. The linear relationship between TDS and SC is well-established (Hem, 1985), and by plotting the TDS and SC values on a scatter plot (Figure 3.9), the mathematical relationship for the study area was found to be:

$$SC = 1.42(TDS) - 18.82 \quad (3.1)$$

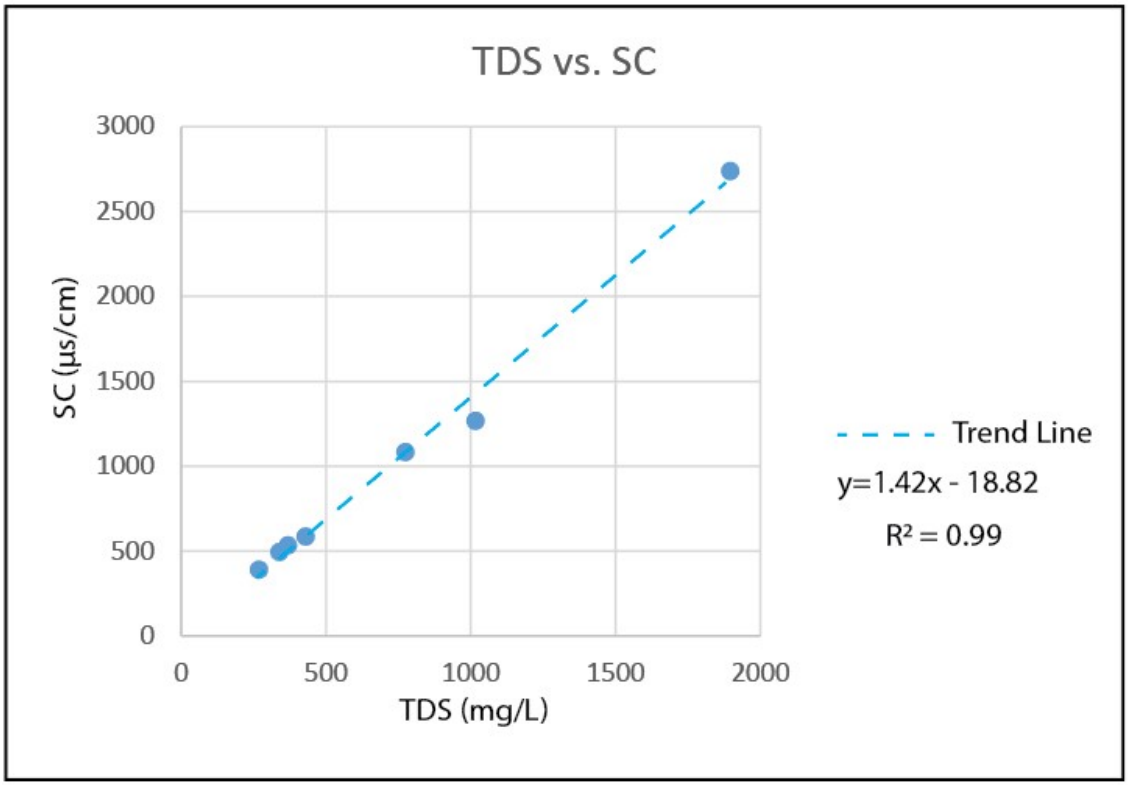

Figure 3.9: Plot showing relationship of TDS to SC in Carroll County. Water quality data sourced from Ohio EPA Ambient Ground Water Monitoring Network (Ohio EPA, 2016).

Petroleum Reservoirs

Ohio has a history of hydrocarbon exploration beginning in 1859 (Ohio DNR GIS Mapping Services, accessed March 2022). In the study area, the main formations exploited for petroleum have been Berea Sandstone (Devonian), Clinton Sandstone (Silurian) and Utica/Point Pleasant Shale (Ordovician) (Sanders, 1991; Tasker, 2020; Ohio DNR GIS Mapping Services, accessed March 2022). Produced water from these formations have been evaluated through various studies, showing how the hydrogeology of the study area changes with depth.

The Ohio DNR identifies several Berea Sandstone oil and gas fields within Carroll County (Figure 3.4). Coogan (1994) evaluated a Berea Sandstone gas field in Portage County, OH, which is approximately 32.19 km (20 miles) north of Carroll County. He noted connate water with 10,000-20,000 mg/L chloride. Additionally, he noted a transition of fresh to brackish water at approximately the Portage and Geauga County line, with fresher water to the north in Geauga County and brackish water south of that line. Another Berea Sandstone oil field in Medina County, OH, which is approximately 48.28 km (30 miles) northwest of Carroll County, contains formation waters with 80,301 mg/L TDS on average (Tomastik, 1995). Sunwall and Pushkar (1979) evaluated water from the Berea Sandstone in the Macksburg oil field in Washington County, approximately 96.56 km (60 miles) southwest of Carroll County. These data show the Berea salinity to be approximately 57,600 mg/L TDS. Data on the connate water in the Berea from within Carroll County is scarce, however the data from literature in surrounding areas allows a reasonable expectation of highly saline water likely ranging from 20,000 to 80,000 mg/L TDS.

The Silurian Clinton Sandstone has also been historically targeted for oil and gas drilling in Carroll County, namely in the East Canton Consolidated oil field (Figure 3.10) (Ohio DNR GIS Mapping Services, accessed March 2022). Sanders (1991) evaluated the geochemistry of the

water in this formation in eastern Ohio. These analyses show the water is dominated by Na, Ca, and Cl brine throughout that larger study area, which includes Carroll County. Additionally, the water in this study was found to be brine with an average TDS of 250,000 mg/L TDS. Ryder and Zagorski (2003) arrive at a similar conclusion regarding the composition of water from the Clinton Sandstone, with dominant ions of Na and Cl and a TDS range of 200,000-300,000 mg/L on average.

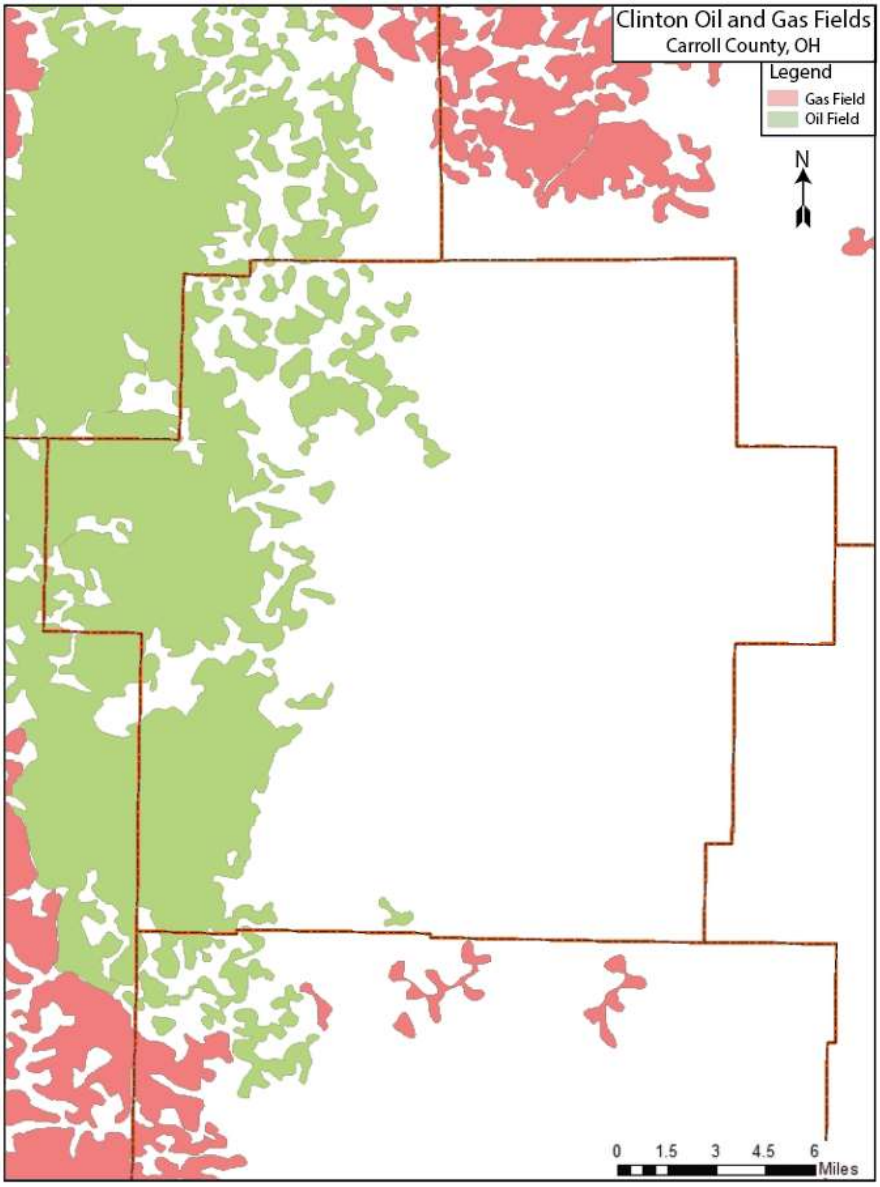

Figure 3.10: Clinton oil and gas fields (from Ohio DNR GIS Mapping Services, accessed March 2022).

The Utica/Point Pleasant Formation is an Ordovician shale that is currently developed for hydrocarbon production as an unconventional reservoir within the study area. The wells that produce from this formation are largely horizontal wells that utilize hydraulic fracturing to increase oil and gas production volumes (Ohio DNR GIS Mapping Services, accessed March, 2022). Water produced from these wells has been evaluated by Tasker (2020). The researcher limited his evaluation to samples from wells that had been producing for greater than 120 days in order to give the wells time to purge "flowback water," or water that is mainly composed of hydraulic fracturing fluids. After this time period, the researcher assumed the water being produced through these wells was primarily formation water. The water samples analyzed in this study were all greater 76,800 mg/L chloride and showed dominant ions of Na, Ca, Mg, and Cl. TDS concentrations varied widely in the samples for the study, which the author attributed to effects of hydraulic fracturing fluid even after the 120-day purging period.

These data show that groundwater salinity in the study area generally increases with depth. This coincides with the trend expected in the shallow aquifer that is being evaluated in this research, though on a larger scale. The difference in salinity between the Berea and the Clinton also shows that deep formation fluids are unlikely to be mixing with shallower formation fluids, as the Berea is much lower in TDS than the Clinton. This agrees with research discussed previously on the structure of the study area which concludes there is an absence of large faults capable of connecting shallow Pennsylvanian strata with deeper formations such as the Berea, Clinton, and Utica/Point Pleasant.

CHAPTER IV

METHODOLOGY

The methodology for this project combines an analysis of the stratigraphy, specifically porous sand units as defined below, as well as fluid properties from well logs and returned fluids during drilling. Well log data and SC data were collected on drilling rigs during drilling operations. Since the data were collected in the field under relatively uncontrolled circumstances, quality control (QC) was performed for each data set, the parameters of which are discussed below for each set of data. The individual analyses of stratigraphy and fluid properties are combined to create a final model for the study area.

DATA SOURCES

Well Log Data

Well logs for this study were obtained by Chesapeake Energy throughout the study area. The vast majority of wells were logged by a single logging company (Baker Hughes), with 14 wells logged by two other companies (12 by Schlumberger; 2 by Weatherford). A total of 180 well logs, which include gamma-ray, caliper, resistivity, bulk density, density porosity, density correction, neutron porosity, and photoelectric effect curves were available. Spontaneous potential was available on 33 of the logs. Details of each of these well log curves are discussed below.

The locations of the data points are shown in Figure 4.1. The largest groupings of data occur in the south and the northeast portions of the county, with slightly less dense data coverage in the center of the county. The northwestern part of the county has the lowest data density.

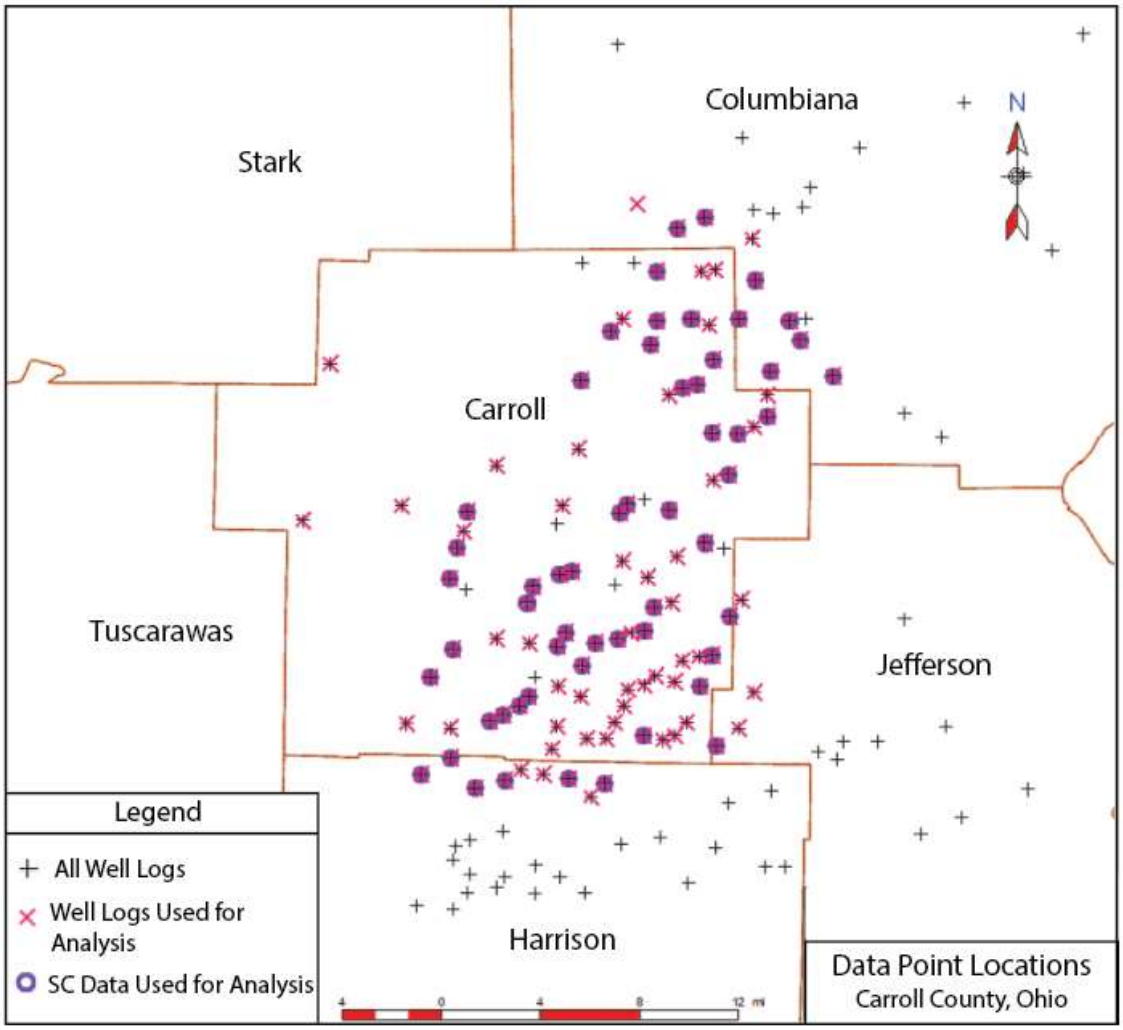

Figure 4.1: Locations of data showing all well logs in study area, well with logs used for analysis, and wells with adequate specific conductance data.

a. Curve Descriptions

The gamma-ray curve provides data on the total gamma-ray count in American Petroleum Institute (API) units with depth (Belknap et al., 1959). Throughout the interval for this study, the values generally range from less than 20 to around 200 API units. Spectral gamma-ray was not

available for this study. This curve is mainly used to aid in lithology identification in this research.

Resistivity measurements for Baker Hughes were taken using a High-Definition Induction Logging (HDIL) tool (Asquith and Krygowski, 2004). Depths of investigation (DOI) included 25.4 cm (10 inches), 50.8cm (20 inches), 76.2 cm (30 inches), 152.4 cm (60 inches), 228.6 cm (90 inches), and 304.8 cm (120 inches), though some logs did not include all of the DOI listed. Schlumberger logs used an Array Induction tool and with DOIs of 76.2 cm (30 inches), 152.4 cm (60 inches), and 228.6 cm (90 inches). Weatherford also used an Array Induction tool and included DOIs of 152.4 cm (60 inches) and 228.6 cm (90 inches). Resistivity measurements were corrected for borehole irregularities and temperature by the logging companies. These curves are shown on a logarithmic scale ranging from 0.2-2,000 ohm-meters. The resistivity curves are used for pore fluid evaluation in this research.

All logging companies used neutron and density porosity calibrated to a limestone matrix, which is typical of well logs used for oilfield applications throughout the study area. To eliminate effects of non-limestone lithologies, specifically sandstone, porosity was determined using Equation 4.1 after Asquith and Krygowski (2004).

$$\phi = \frac{\sqrt{\phi_n^2 + \phi_d^2}}{2} \tag{4.1}$$

Where ϕ_n is neutron porosity and ϕ_d is density porosity.

The neutron porosity curve was corrected by the logging companies for borehole size since the logging interval was drilled with a 445.45 cm (17.5 inch) bit through the surface casing interval and 31.12 cm (12.25 inch) through the intermediate casing interval in most wells, which is considered large for many oilfield geophysical logging applications. Bulk density was corrected

for tool separation from the borehole wall during logging by the logging companies, and a density correction curve is included on the well logs as part of data quality analysis.

b. Quality Control

The well logs were first visually checked for obvious errors, including missing curves, apparent calibration or measurement errors, and missing intervals. The well logs were checked against adjacent and/or nearby well logs for noticeable differences in the ranges/amplitudes of the various curve values. Well logs with curve data that were suspiciously different in range or amplitude from multiple adjacent well logs were not used in the dataset. Missing curves were another common quality error, and logs that were missing gamma-ray, resistivity, bulk density, density porosity, and/or neutron porosity were not considered as these curves are necessary for one or more parts of the project methodology. In some cases, all curves were missing in certain intervals, such as above or below surface casing, and these logs were also discarded from the data set. After the quality control evaluation, 109 of 180 well logs were used for stratigraphic correlation and TDS calculation in the study area.

Specific Conductance Data

a. Data Collection Methods

Mudloggers collected samples of returned fluid during drilling from well spud to approximately 152.4 m (500 ft) past surface casing and measured the specific conductance (SC) of the samples. These data were collected at the end of the flow-line where a mixture of fresh-water based drilling fluid and formation fluid exits the borehole, along with rock cuttings. All wells were drilled using air rotary drilling methods from surface spud through the surface casing interval, and all but two wells were drilled with air rotary methods through intermediate casing interval. The other two wells were drilled using fluid rotary methods with water-based drilling mud. After review of SC data collected by mudloggers for these two wells, these data were not included in

the final project as the drilling fluids contained unknown additives, which potentially included polymers, chlorides, and/or bentonite. Without knowing the composition and volume of the drilling fluids used in these two wells, there is no reliable way to differentiate drilling fluids from groundwater and the impact of each to SC measurements of the returned fluids. With air-rotary methods, very small quantities of added drilling fluids are used to bring formation cuttings up the borehole and through the flow-line. These drilling fluids are referred to as "make-up water" (MUW). Therefore, fluid returns during drilling consist largely of formation fluid when using the air-rotary drilling method (Brassington and Taylor, 2012).

The specific conductance was measured by the mudloggers while drilling using a YSI EC-300 specific conductance meter. The meter was set to automatic temperature correction (ATC) according to procedures outlined by Chesapeake Energy for the mudloggers. The mudloggers used the default temperature coefficient, which is 1.91% on these devices (YSI, 2017). No further temperature correction was performed on the measurements. MUW was also measured using the same meters and procedures prior to drilling, after completing each casing interval, and before resuming drilling after casing operations.

Spatial distribution of specific conductance data is similar to that of the log data, though in this dataset the northwest portion of the county lacks specific conductance data entirely. The south half and northeast quadrant have the greatest data density, and the data in these areas are distributed fairly evenly, offering good coverage in most of the study area (Figure 4.1).

b. Quality Control

SC data from ten wells were not included in the final dataset. These reports did not pass quality control for the following reasons: data missing from intervals greater than 60.96 m (200 ft), missing MUW records, inadequate associated log data for the well (as discussed above), and

drilling with mud instead of air-rotary methods. Ultimately, 57 wells had adequate SC and log data across the study area.

MUW SC measurements with greater than 1,000 µS/cm were noted in 13 wells. This occurred in either the surface casing interval, intermediate casing interval, or both. In eight of these wells, the highest MUW recorded was below 1,300 µS/cm, which is significantly less than 10,000 mg/L TDS and therefore would not interfere with formation water measurements in any significant way. The highest MUW recorded was in the Bauer 14-14-6 6H well at 5,360 µS/cm, and it occurred only after surface casing was complete. The calculated TDS in this well did not exceed 10,000 mg/L and so this well was included in the data set. The Ruby 15-12-5 3H also had elevated MUW measuring at 4,108 µS/cm in the intermediate casing interval. The elevated MUW measurements coincided with a large increase in the SC measurements of the returned fluids, showing calculated TDS values greater than 10,000 mg/L starting at 45.72 m (150 ft) below surface casing. This data point was still included in the data set due to the fact that the TDS cutoff was not exceeded immediately upon switching to higher TDS MUW. All MUW values greater than 1,000 µS/cm were highlighted on well logs in Geographix during analysis to add awareness and higher scrutiny of potential anomalies.

STRATIGRAPHIC CORRELATION

Techniques for correlating fluvial stratigraphy included identifying low-energy marker beds to aid in correlation of coarser sandstone beds similarly to the approach of Alqahtani (2014). The cyclothems described by Branson (1962) in the study area had significant coal beds visible in the well log data, marked by a sudden decrease in density and an increase in porosity, often times resulting in curves that were off the scale. Correlative coals are common throughout the study area and are often associated with thin limestone beds described by Branson (1962). Both were frequently discernable on well logs and often less than 3 m (10 ft) thick. These marker beds were

more laterally continuous than the sandstones and provided a local datum from which to correlate adjacent logs and confine connected sandstones. The Lower Freeport Coal and Kittanning Coal were correlated on well logs where they were visible to act as regional stratigraphic datums to aid in sandstone correlation and constrain interpretation of connectivity of sandstones. The Berea Sandstone was used as a regional stratigraphic datum to help negate some of the pre-Mississippian structural highs and lows and to help identify and correlate large erosional valleys at the top of the Mississippian, on which the Pennsylvanian was deposited (Lockett, 1927; Beuthin, 1996).

An average porosity of 5% was initially chosen as a cutoff for correlating reservoir-quality sand beds using Equation 4.1, similarly to the Western Gas Sands Project (Crawley, 1982). The porosity cutoff was an important factor in this study because it determines which sandstones can effectively transmit water downdip to recharge the aquifer with fresh groundwater. To evaluate appropriateness of using a 5% porosity cutoff in the study area for this research, well logs were reviewed for changes in resistivity between homogeneous shales and sand-containing beds, as determined from gamma-ray and porosity curve readings. The resistivity values in shale intervals were fairly constant throughout the study area (approximately 30 ohm-m), with increasing porosity showing diversion from the shale “baseline” resistivity values (Figure 4.2). By noting this pattern and associated porosity percentages, the 5% porosity cutoff was deemed appropriate for stratigraphic correlation of sands.

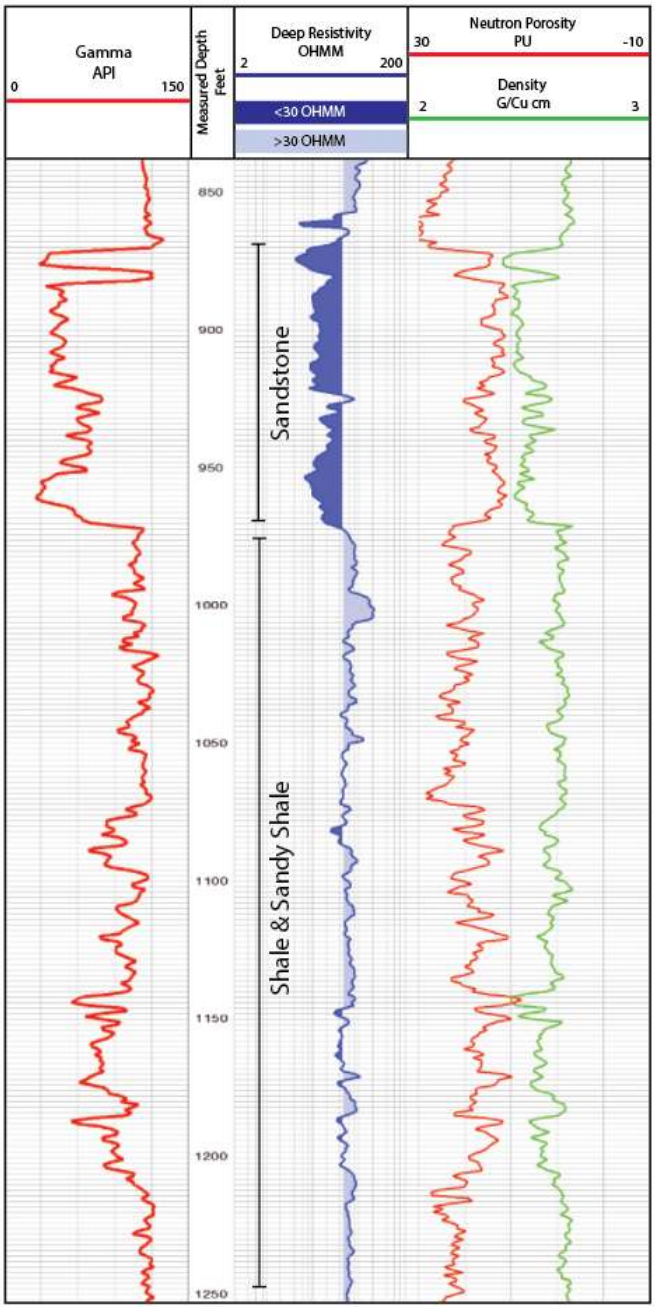

Figure 4.2: Example section of well log showing consistent shale resistivity at around 30 ohm-m; note resistivity shift from 30 ohm-m shale baseline from overlying sandstone bed at 271.27-295.66 m (890-970 ft) Measured Depth (MD).

Generally, sandstone beds less than 6 m (20 ft) thick were not mapped unless they were correlative to thicker sandstone deposits in offset wells. A definitive sandstone thickness cutoff could not be used since thin shaley and limey lenses intermittently interrupt many of the porous

sandstone units. Additionally, since most of the sandstone formations pinch out laterally into siltstone or shale, a thickness cutoff would result in inaccurate thickness maps and lateral boundaries of the mapped formations. Formation top depths were estimated for mapping purposes on the lateral extents where the porous units pinched out completely by following limestone or coal beds where possible in order to show the edges of the sandstone deposits. Shale volume was also considered from gamma-ray calculations, but the presence of coal and limestone caused the gamma-ray curve to be suppressed in many of the logs, causing erroneously high shale volume calculations. Ultimately, thickness maps and structure maps of the top and base of each sandstone unit were created based on these stratigraphic correlation methods.

TDS CALCULATIONS FROM FLUID AND LOG DATA

Two different methods to calculate TDS were used for this study. The first method used manipulates Archie's equation, using values from SC of the returned drilling fluid as a proxy for conductance of the connate formation water. The second directly correlates specific conductance to log resistivity values by evaluating the relationship between the two measurements, then uses a trend line equation for the upper envelope of the data to obtain an equation to calculate TDS directly from log resistivity values. Each method has merits and pitfalls which are outlined in the Discussion section of this study.

Method 1: Manipulating Archie's Equation

As described previously, the purpose of Archie's equation (Equations 2.1 and 2.4) is to determine water saturation to aid in hydrocarbon exploration. Since the focus of this study is a freshwater aquifer with no hydrocarbons, several assumptions are able to be made, similarly to Atwia et al. (1997).

$$S_w^n = \frac{(R_w \times a)}{(\phi^m \times R_o)} \tag{2.1}$$

$$S_w^n = \frac{(R_w \times a)}{(\phi^m \times R_t)} \quad (2.4)$$

Where S_w is water saturation, n is the saturation exponent, R_w is resistivity of the connate water, a is the tortuosity factor, ϕ is porosity, m is cementation factor, and R_o is the resistivity of the 100% water-filled formation, and R_t is the true formation resistivity.

The first assumption is that there are no hydrocarbons, and therefore water saturation is 100% (S_w=1). This also means that R_o is equal to R_t in this case, and R_t will be the variable referenced in this study. Since no hydrocarbons are present and only sand beds greater than 6.1 m (20 ft) thick were used for this portion of the study, deep resistivity measurements from well logs can be used without correction for R_t in Equation 2.4. The inverse relationship of resistivity and conductivity is then used to convert resistivity (ohm-m) to conductivity (µS/cm). Based on this unit conversion, and by assuming the returned drilling fluids consist of pure groundwater, then R_w=10,000/SC. Additionally, a = 0.81 in consolidated Pennsylvanian sandstones and n = 2 per Asquith and Krygowski (2004), but since S_w is 1, and $1^2 = 1$, n can be removed from the equation. With these assumptions, Archie's equation can be solved for R_t to get (Equation 4.2).

$$R_t = \frac{10{,}000 \times 0.81}{SC \times \phi^2} \quad (4.2)$$

This analysis was restricted to porous sand intervals at least 6.01 m (20 ft) thick and with porosity greater than 17% and gamma less than 30 API on average throughout the interval, as these values correlated with consistent, noticeable shifts (both positive and negative) in resistivity from the average of 30 ohm-m seen in shale beds within the study area, indicating sufficient porosity for possible fluid movement. Additionally, the analysis was limited to exact depths that returned drilling fluid samples were captured within these intervals since the returned fluid sample intervals were 15.24 m (50 ft), whereas log data intervals were .3 m (1 ft) or less. Measured SC and the associated porosity values from the logs at these depths were input into Equation 4.2 to

obtain values for calculated R_t, notated as R_{tCalc}. Each R_{tCalc} value was then plotted against the actual deep resistivity reading at the correlative depth from the well log (R_{tLog}). Based on data discussed in Chapter III – Study Area and similar to Roberts (2001), the intervals were reduced to those with SC greater than 4,227 µS/cm (equivalent to TDS greater than 3,000 mg/L) and plotted R_{tCalc} an R_{tLog} in a linear relationship (Figure 4.3).

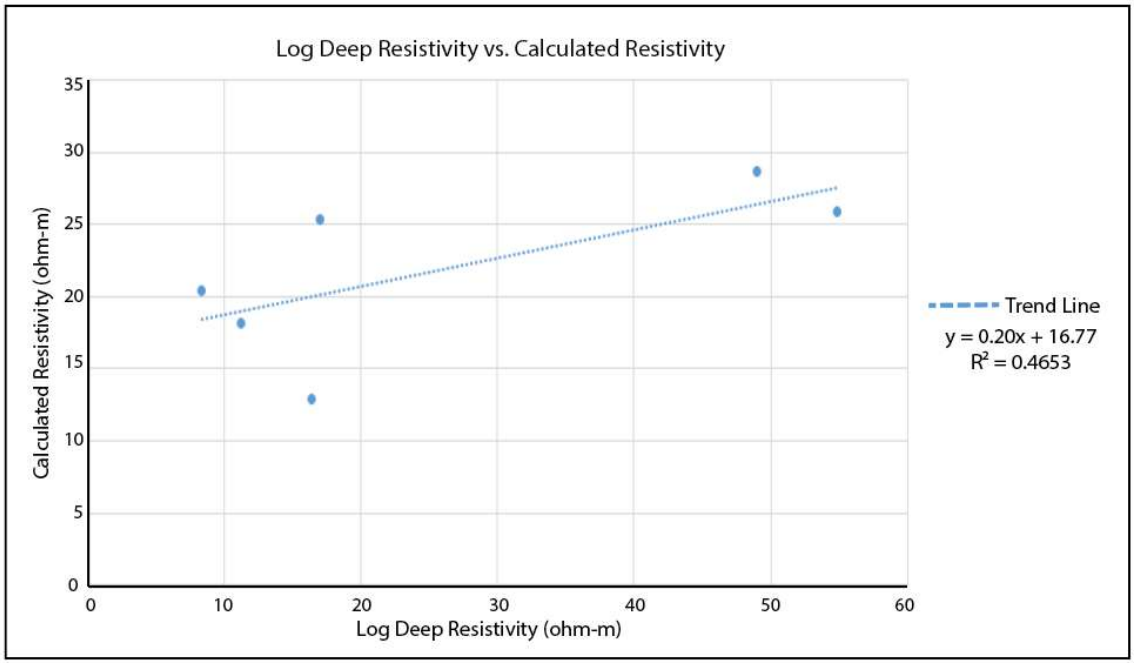

Figure 4.3: Scatter plot of deep resistivity readings from well logs vs. calculated resistivity using SC values and Archie's equation.

From this, a best-fit line was used to obtain an equation for the relationship between R_{tCalc} and R_{tLog} (Equation 4.3), shown in Figure 4.3, which gives a means to calibrate well log porosity and deep resistivity readings to measured specific conductance of groundwater.

$$R_{tCalc} = 0.20 \times R_{tLog} + 16.77 \quad (4.3)$$

Next, Equation 4.3 was substituted into Archie's equation for variable R_t with the assumptions previously discussed that resulted in Equation 4.2. This equation can then be solved for SC, which gives a calculated value for SC (SC_{calc}) that can be used to calculate groundwater SC foot-by-foot through the entire length of all porous sandstone intervals in any well log in the study area that has adequate resistivity and porosity curves, regardless of whether that well had SC samples of returned drilling fluids captured during drilling (Equation 4.4).

$$SC_{calc} = \frac{8{,}100}{\phi^2 \times (0.20R_{tLog} + 16.77)} \tag{4.4}$$

Finally, Equation 3.1, which was determined from historical water well data, is rearranged and used to calculate TDS from SC_{calc} (Equation 4.5).

$$TDS = \frac{SC_{calc} + 18.82}{1.42} \tag{4.5}$$

In this way, Archie's equation is calibrated to the study area from SC fluid sample data by determining the relationship between measured SC and well log readings of deep resistivity and porosity. This method accounts for porosity, which has a large control on water movement as higher hydraulic conductivity zones, and thus recharge and water quality distribution, in the study area.

A calculated TDS curve was created in Geographix using Equations 4.4 and 4.5. From this, the groundwater interfaces at 10,000 mg/L, 5,000 mg/L, and 1,000 mg/L TDS were able to be picked on each log. The interfaces were picked only within the mapped sandstone formations for the reasons discussed in the stratigraphic mapping section above. If the TDS curve showed a cutoff outside of a mapped porous interval rather than transitioning within the porous unit, the cutoff was picked at the base of the next shallowest mapped porous interval (Figure 4.4).

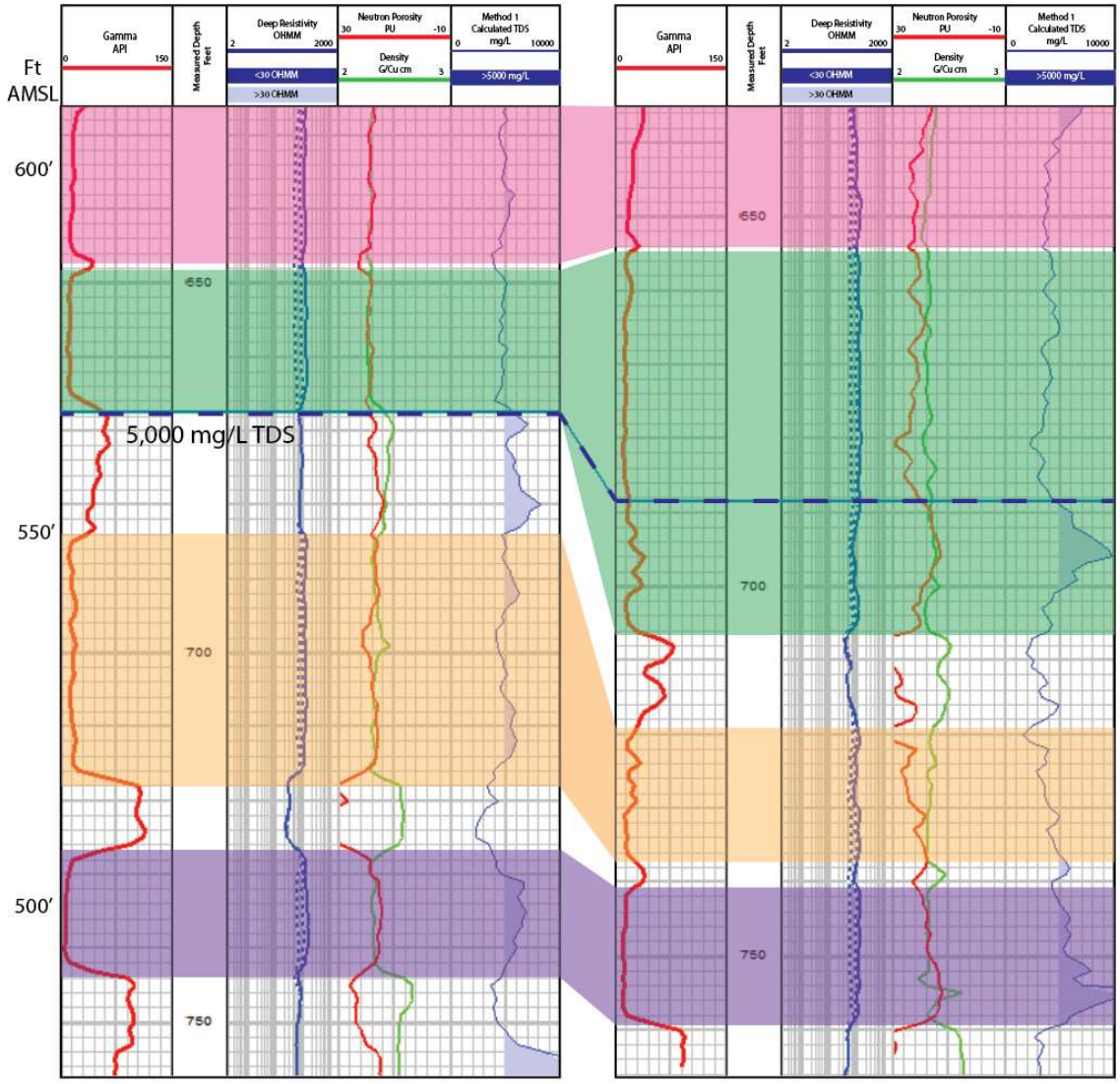

Figure 4.4: The 5,000 mg/L TDS transition interface is shown on two adjacent well logs (dashed line), as well as calculated TDS curve in far right track of each log. The light blue color-fill in the TDS curve highlights TDS values greater than 5,000 mg/L. The 5,000 mg/L TDS interface is picked at the base of the shallowest sand with <5,000 mg/L TDS if the formations below only contain water with > 5,000 mg/L TDS, otherwise it is picked at the transition within a mapped sandstone unit. Sea level is structural datum.

Method 2: Using SC and Log Deep Resistivity

As an alternative to Method 1, a direct comparison of SC samples and deep log resistivity was used to calculate TDS as well. The reasons for designing an alternative method are outlined in the Discussion section below, but one of the primary reasons is that Method 1 resulted in generally low TDS values calculated in the study area on initial review. This has environmental

conservation implications as discussed below, so Method 2 was designed to evaluate the low TDS bias and err on the side of higher calculated TDS values. Method 2 ultimately resulted in deep log resistivity values that directly correspond to TDS values of 1,000 ppm, 5,000 ppm, and 10,000 ppm in the study area, which were used to pick these interfaces on well logs.

The first step of Method 2 was plotting measured SC and deep log resistivity against each other on a simple scatter plot. The data points were limited to depths at which SC samples were taken (as recorded by the mudloggers) and the corresponding deep log resistivity value at that exact depth, which is done to correct for differing sample intervals as discussed in Method 1.

Next, the data was viewed in the scatter plot using a logarithmic scale for both axes as it resulted in the closest grouping of data points for this study area. A power law function was utlilized for the trend line which gives $y=13{,}315x^{-0.567}$ (Equation 4.6, blue line on Figure 4.5) and an R^2 value of 0.46. The power law function was chosen because it resulted in the highest R^2 value for the trend line, meaning strongest correlation to the data set, compared to alternative functions. Since the purpose of Method 2 is to err on the side of estimating higher TDS from log resistivity (see Discussion section), the "envelope method" was used to create a trend line over the upper envelope of the data (Figure 4.5). This involved using two data points from the full data set (the two points at either end of the gray trend line in Figure 4.5) to create a trend line that encompasses all of the data points beneath it, and by viewing the original trend line for all of the data, it is clear that it is a suitable trend line and follows a slope similar to that of the main trend line. The upper envelope trend line gives the equation $y=439{,}938x^{-0.978}$ (Equation 4.7).

$$y = 13{,}315x^{-0.567} \tag{4.6}$$

$$y = 439{,}938x^{-0.978} \tag{4.7}$$

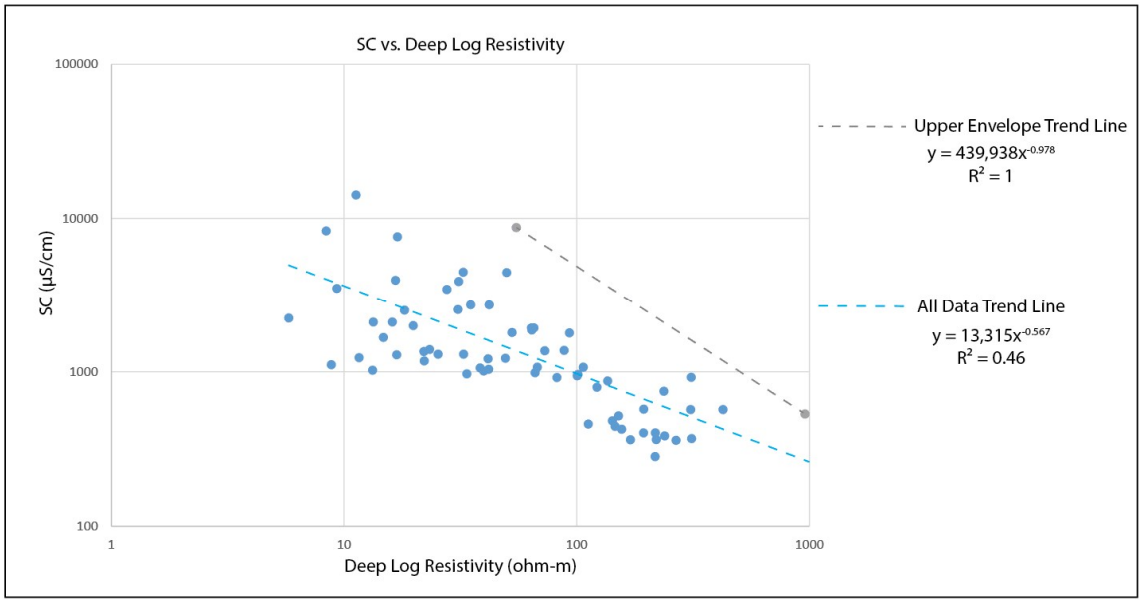

Figure 4.5: Plot showing SC and associated deep resistivity from well logs. Blue data points and trend line show relationship of total dataset. Gray trend line shows the upper envelope of the dataset, which is the result of two data points from the original data set (shown at either end of the trend line) that force a trend line that encompasses all other data points below.

Equation 3.1 was then used to calculate SC values that directly correspond to TDS values of 1,000 mg/L, 5,000 mg/L, and 10,000 mg/L, which results in SC values of 1,639 µS/cm, 8,197 µS/cm, and 16,393 µS/cm, respectively. These values were inserted for SC into Equation 4.7 as the *y*-variable in order to solve for a corresponding deep log resistivity value (x) at each of the three SC values as shown below:

$$1{,}000\,mg/L\ TDS: \quad 1{,}639\,\mu S/cm = 439{,}938x^{-0.978}$$
$$x = 304\ ohmm$$

$$5{,}000\,mg/L\ TDS: \quad 8{,}197\,\mu S/cm = 439{,}938x^{-0.978}$$
$$x = 59\ ohmm$$

$$10{,}000\,mg/L\ TDS: \quad 16{,}393\,\mu S/cm = 439{,}938x^{-0.978}$$
$$x = 29\ ohmm$$

Finally, Geographix is used to delineate the depth at which the deep resistivity curve exceeds each of these values on each well log. Individual TDS/deep log resistivity cutoffs must be analyzed visually for each well. This is simplified by using Geographix to create solid color-filled areas within the resistivity track of each well log that is bound on the right by the resistivity value of interest and on the left by the deep resistivity curve. This visually highlights the point at which the deep resistivity curve falls below the resistivity value being analyzed, and thus when TDS is above the cutoff in question (Figure 4.4). Just like Method 1, TDS interface depths are restricted to mapped porous intervals using the procedure shown in Figure 4.4.

MAPPING AND INTERPRETATION

After completion of stratigraphic mapping, TDS calculations, and picking TDS interfaces on logs, these data sets and interpretations were combined to create the final TDS interface maps. To begin, each TDS interface elevation above mean sea level (AMSL) was plotted as a point on a map. In addition to this, the formation where the interface occurred was also noted on the map.

This was then compared to the thickness and structure maps for both the top and base of associated formations that were created in the first part of the project. The lateral extents of the porous sandstones shown on thickness maps were used to initially constrain the interpretation of the TDS interface contours. Any nearby conflicting data points, such as those that showed an interface at a much different elevation or in a different formation, were considered during this step and the logs were reviewed to look for any amalgamating sandstones or other anomalies. The top and base structure maps were then used to confine contours further as they show the upper and lower limits of the interface elevation within a given sandstone as well as the slope and direction of dip, which drives the shape of the interface contours within each discrete porous unit (Figure 4.6). By overlaying structure maps of the top and base of an interface-containing sandstone, the potential area where a particular interface elevation contour can be placed on a

map is restricted geographically by the structure contours. Since the interface can't occur above the top of said sandstone, nor below the base, interface contours must be placed between the formation top and base structure contours of the same elevation. This was especially important in areas with greater spacing between well logs, allowing a more predictive set of interface contours since the formation structure and thickness maps acted to guide and constrain interface interpretation both laterally and vertically. It allowed a more three-dimensional view of the interaction of TDS interface depths with each sandstone, especially in areas with amalgamating or diverging sandstone units which add a great deal of complexity when creating predictive TDS interface contours.

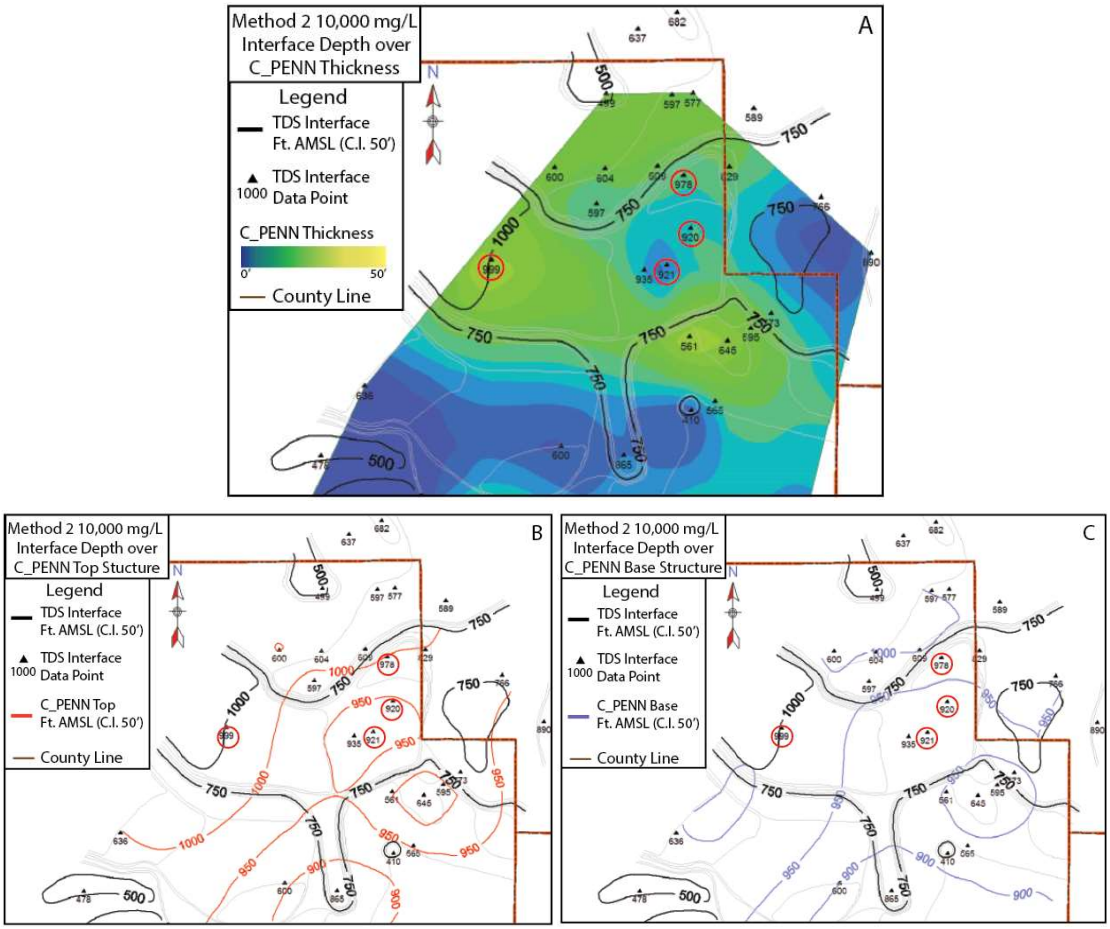

Figure 4.6: This sequence of maps shows how the fresh-saline interface contours were determined using the C_PENN formation as an example. First, data points with elevations and formation name(s) that the interface occurs in are placed on the map, listing all formations included in any amalgamated sandstones. Where the interface occurs within a particular formation within a grouping of well logs, the thickness map is first used to determine the potential general outline of the contours in the area by determining the lateral extents that the interface is likely to occur within that formation (map A). In the maps above, the points circled in red all have Method 2 10,000 mg/L interface transitions occurring in the C_PENN formation. All conflicting data points in different formations and at different elevations are considered during this step and the geographical range of influence that each formation (including the interplay of multiple amalgamated sandstones) has on the interface is determined. Next, the structure map of the top of the formation is reviewed to constrain the topmost limit of the interface elevation where it occurs as defined in the first step, in this case within the C_PENN formation (map B, red contours). The same is then done with the structure map of the base of the formation to constrain the lower limit of the interface elevation (map C, blue contours). This way, the interface elevation contours are constrained three-dimensionally: laterally by the thickness map, as well as vertically by the top and base of the sandstone formation.

CHAPTER V

RESULTS

Results of this study, including both stratigraphic and hydrogeological analyses, are outlined below. This section summarily outlines findings of the depositional nature of the study area, including depositional patterns and geometries specifically related to porous sandstones. The characteristics of the fresh-saline groundwater interface are also discussed, including detailed analyses on elevation of the interface throughout the study area, grade of TDS change as shown through mapping of multiple TDS threshold depths, and relation of this interface to stratigraphic analysis.

STRATIGRAPHY

In total, 18 separate porous sandstone formations and two named coal formations were mapped in the Pennsylvanian interval within the study area using nomenclature shown in Figure 5.1. Thickness maps, structure maps of the top of each sand, and structure maps of the base of each sand are located in Appendix A. Lateral extent varied significantly between the formations as shown on thickness maps. The lateral boundaries for some of the formations were at least partially defined within Carroll County, though most clearly extend outside of the boundaries of the dataset on one or more edges.

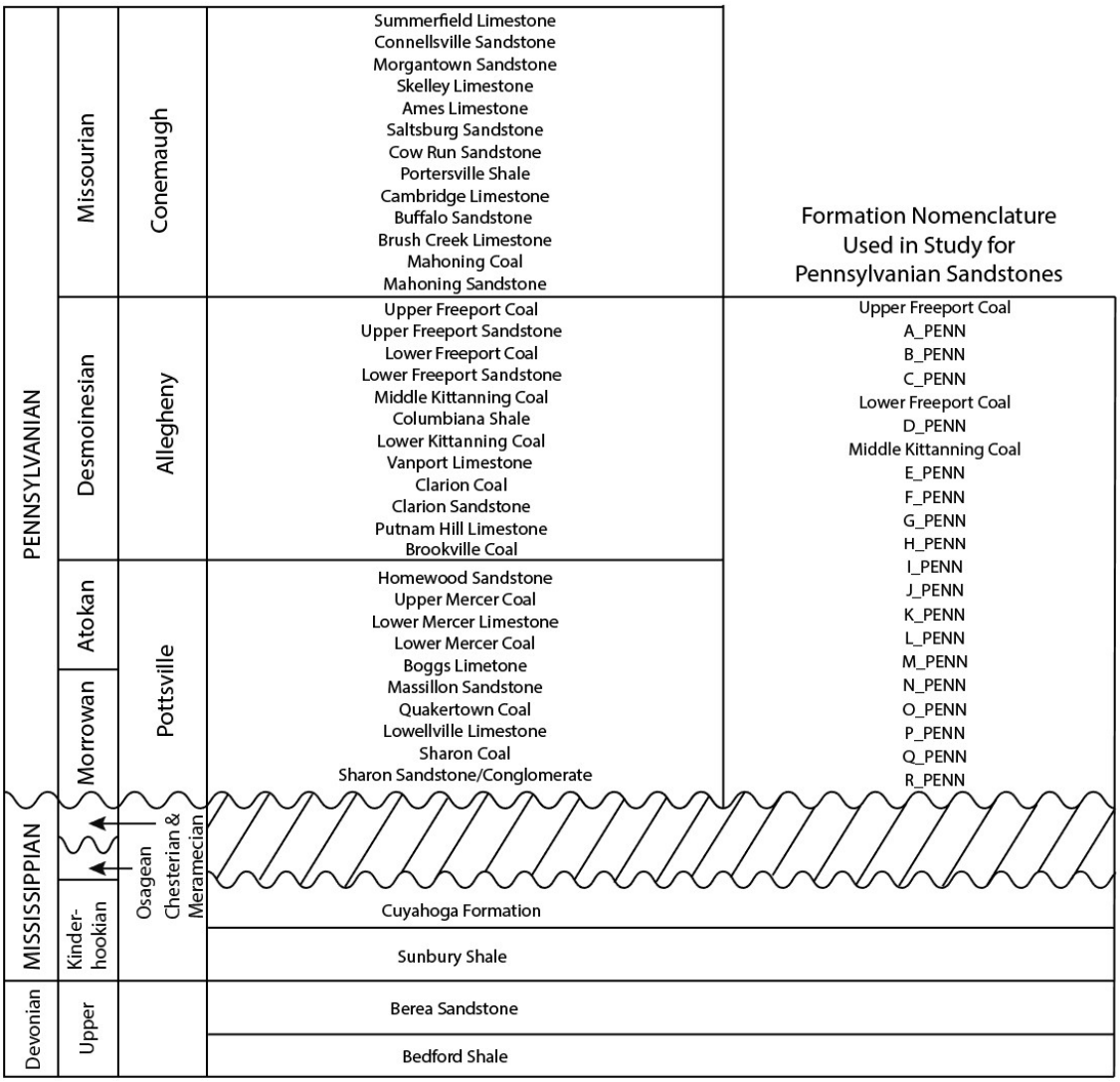

Figure 5.1: Formation nomenclature used in this study compared to published nomenclature. Study nomenclature only indicates names used for mapped sandstone formations. Positions of named coals are included for reference as correlated from historical coal mine information (modified from Larsen, 2000).

Based on the Ohio DNR's historical coal mine data discussed previously, it was determined that all mapped sandstone formations are below the Upper Freeport Coal. This is based on the published elevations of the Upper Freeport Coal from historical mines within the study area. Since this formation is fairly shallow, its elevation generally correlates with the only very top couple of meters on nearby well logs and it is most often shallower than the topmost extent of the curves, so it is not visible on well logs. The elevations of the Lower Freeport Coal and Middle

Kittanning Coal were also listed in some areas within the same Ohio DNR dataset and correlated to nearby well logs where possible. Their relative positions within the nomenclature used for the Pennsylvanian Sandstone formations for this study are shown in Figure 5.1. Structure maps of these coals are shown in Figures 5.2 and 5.3. The historical mining information does appear to have some inaccuracies based on observations of highly variable elevations reported for the same named coal seams from different closely-spaced mines. There were several of these occurrences, and those data that could not be corroborated with other nearby data were not used.

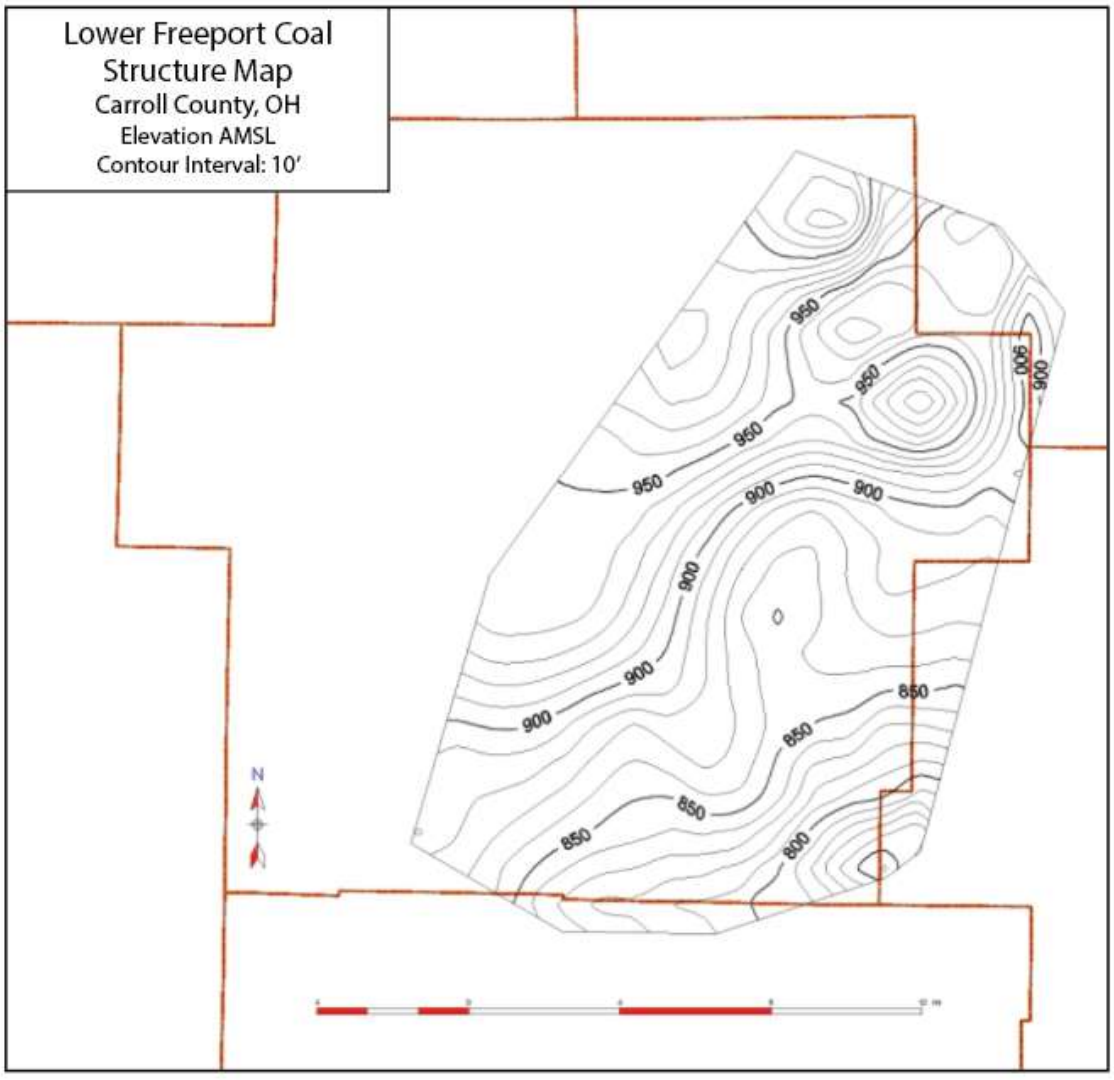

Figure 5.2: Lower Freeport Coal structure map. Contours are in mean sea level elevation.

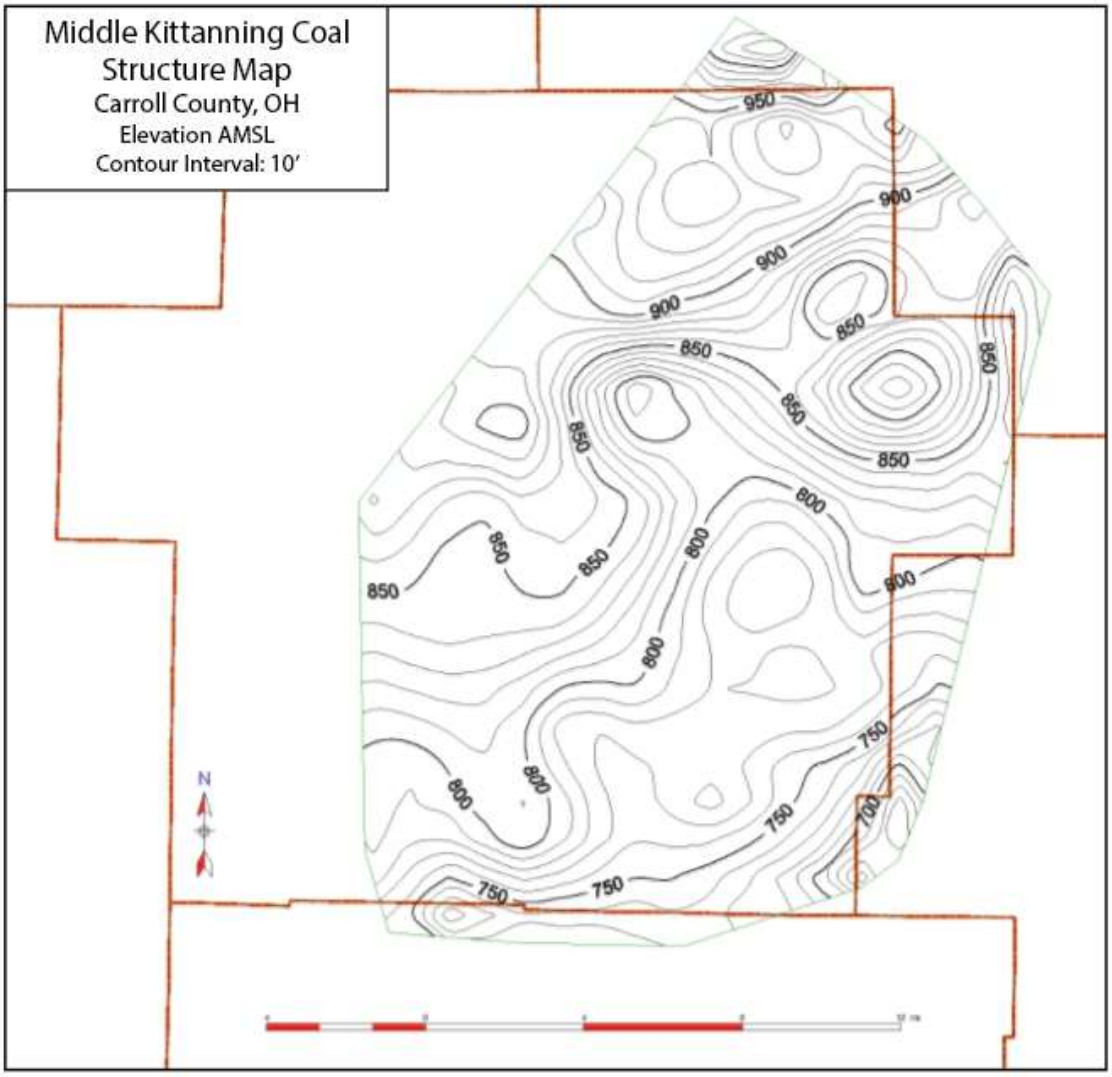

Figure 5.3: Middle Kittanning Coal structure map. Contours are in mean sea level elevation.

The A_PENN, as the shallowest mapped formation, showed smaller lateral extents than all of the other formations by a significant degree. This is partially due to the method of log data acquisition, which causes lack or distortion of data in the shallowest 30.48-60.96 m (100-200 ft) on the logs, which is coincident with the depth interval of this formation. Due to this, the A_PENN formation is not visible on many logs, though it may be physically present above the available data interval in more wells throughout the study area.

Below the A_PENN interval, the average maximum thickness was variable between the mapped formations. The smallest maximum thickness was 9.48 m (31.13 ft) and the largest maximum thickness was 31.92 m (104.72 ft) with a mean of 18.35 m (60.19 ft). Due to the mapping methodology used in this study, average thickness was not determined since all formations were mapped to either zero-foot thickness or to the boundaries of the dataset.

Sandstone depositional geometries seen during the stratigraphic mapping portion of this study include those commonly associated with fluvial depositional settings. Lateral boundaries of many of the formations are marked by increased interfingering of fine-grained sediment within the sandstones before they pinch out completely (Figure 5.4). There are both fining-up and coarsening-up sequences visible on well logs throughout the study area, especially along the lateral boundaries of deposits, with fining up sequences significantly more common (Figure 5.5). There are also many examples of blocky, coarse deposits throughout the study area, many of which occur in thicker depositional centers away from the lateral boundaries of the deposits (Figure 5.4).

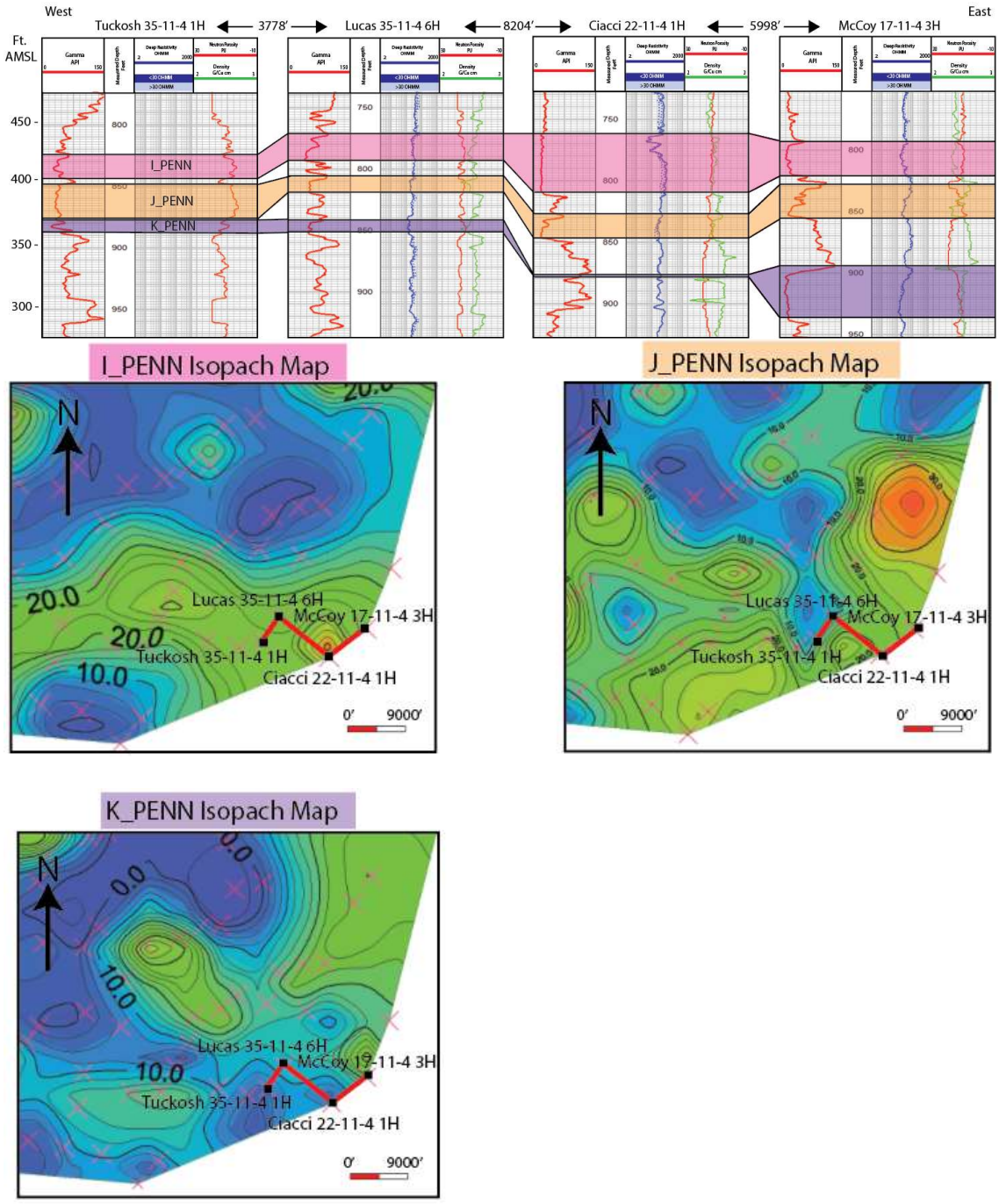

Figure 5.4: Three sandstones are identified and correlated on the well logs in this figure: I_PENN (pink), J_PENN (orange), and K_PENN (purple). Each sandstone shows varying degrees of pinching out as well as increasing interfingering of fine-grained sediments at the lateral boundaries and in thinner depositional areas, as shown on associated thickness maps. Horizontal distance between each adjacent well is noted at top of figure. Mean sea level is structural datum.

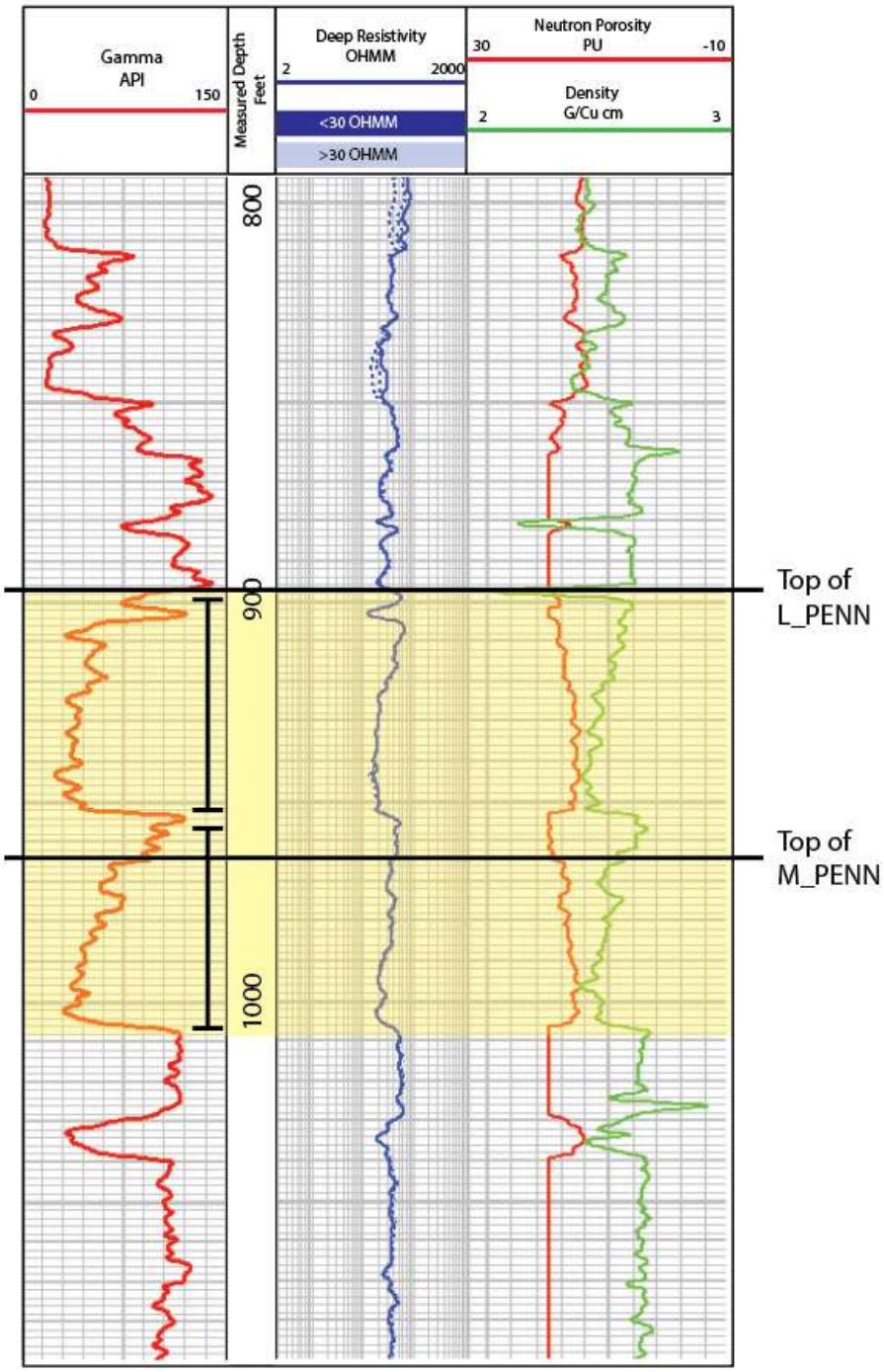

Figure 5.5: The highlighted section in this well log shows two separate fining upward sequences, indicative of point bar deposits in fluvial environments, from 304.8 m to 290.8 m (1,000 ft to 954 ft) measured depth and from 290.2 m to 274.3 m (952 ft to 900 ft) measured depth.

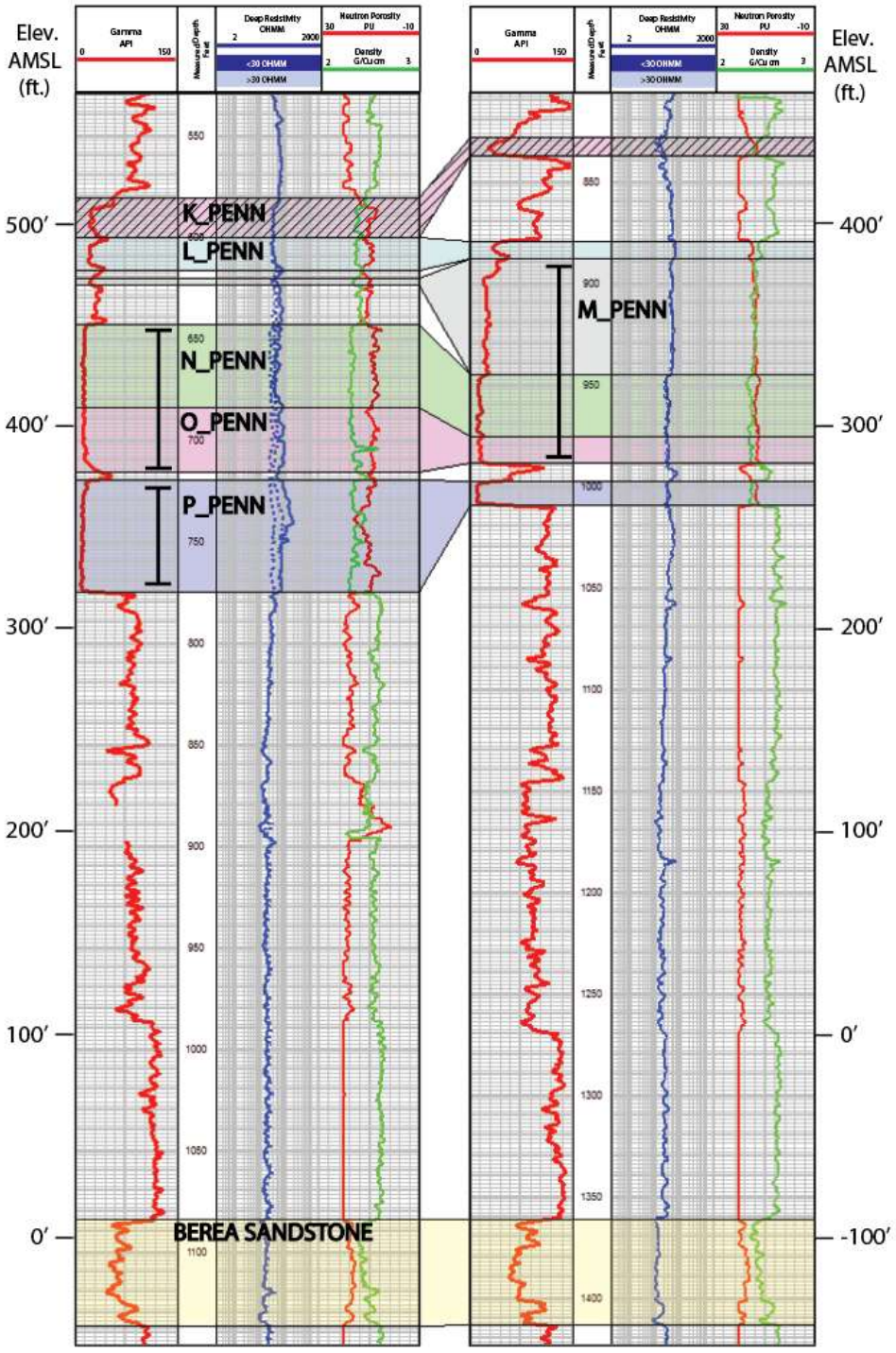

Figure 5.6: Examples of blocky sandstone deposits in two logs used in this study and indicated by the black vertical lines on each log. These wells are 9 km (29,523 ft) apart. Changes in correlative sandstones how patterns of sandstone deposition can vary greatly over several km (several miles) within a single correlative unit. Logs are hung on the Berea Sandstone. Mean sea level elevations at each location are shown as the top of the Berea has approximately 30.5 m (100 ft) of vertical elevation disparity between these two well logs.

Downcutting of sandstone deposits is very common throughout the study area in all of the mapped formations, as is expected in a fluvial depositional environment. In some instances, this results in amalgamation of separate sandstone deposits as a younger sandstone erodes down into an older one. One such amalgamation is evidenced on the Ciacci 22-11-4 1H well log, where three separate sandstones combine to create a stacked, connected sandstone deposit that is 42.7 m (140 ft) thick (Figure 5.7). These amalgamations are common throughout the study area, often being visible on adjacent well logs within a 1.6-3.2 km (1-2 mile) radius.

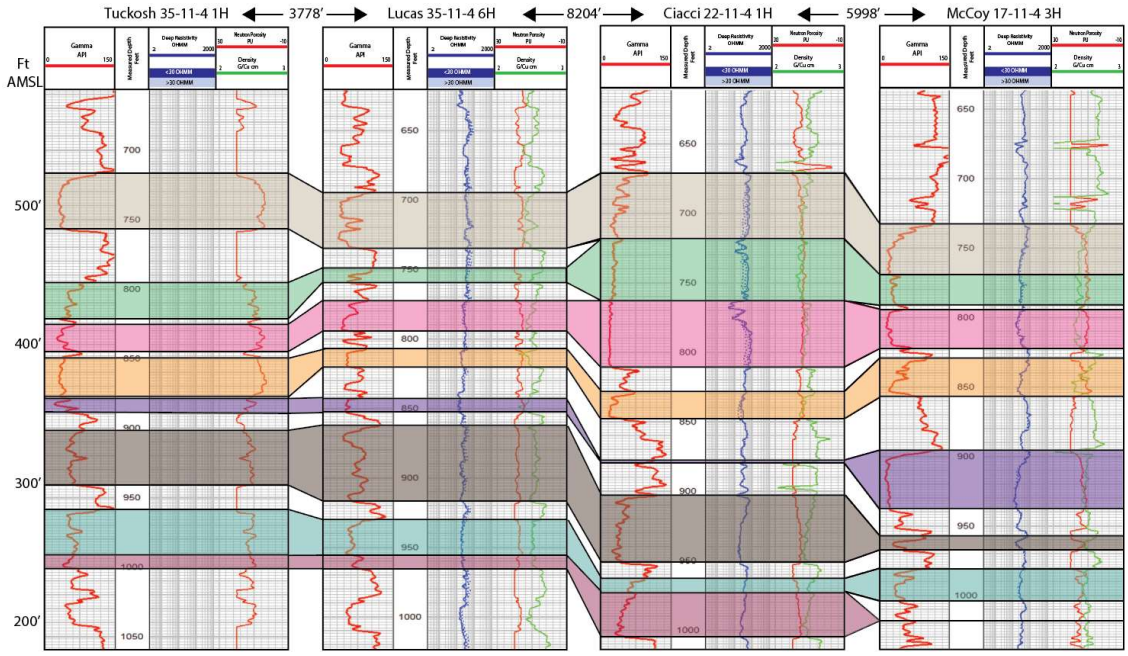

Figure 5.7: Ciacci 22-11-4 1H well log showing correlative sandstone beds amalgamating into larger, connected beds. Horizontal distance between each adjacent well is noted at top of figure. Mean sea level is structural datum.

Downcutting, especially when it does not result in amalgamation of multiple sandstones, is evident through correlation of laterally continuous coal seams, specifically in regard to their absence in certain data points. Through this, it is clear that sandstones in the study area are capable of downcutting up to 68.6 m (225 ft) at their base within 3.2 km (2 miles) laterally. Several mapped sandstones show 30.5-61 m (100-200 ft) of downcutting in wells that are approximately 3.2 km (2 miles) apart in the northeastern region of the study area, just southwest

of the border of Columbiana and Carroll counties (Figure 5.8). This correlates with the structure of the Berea as shown previously (Figure 3.6), indicating that the Highlandtown fault was likely active during the deposition of the Pennsylvanian, which allowed for sands to stack on the downthrown side of the fault.

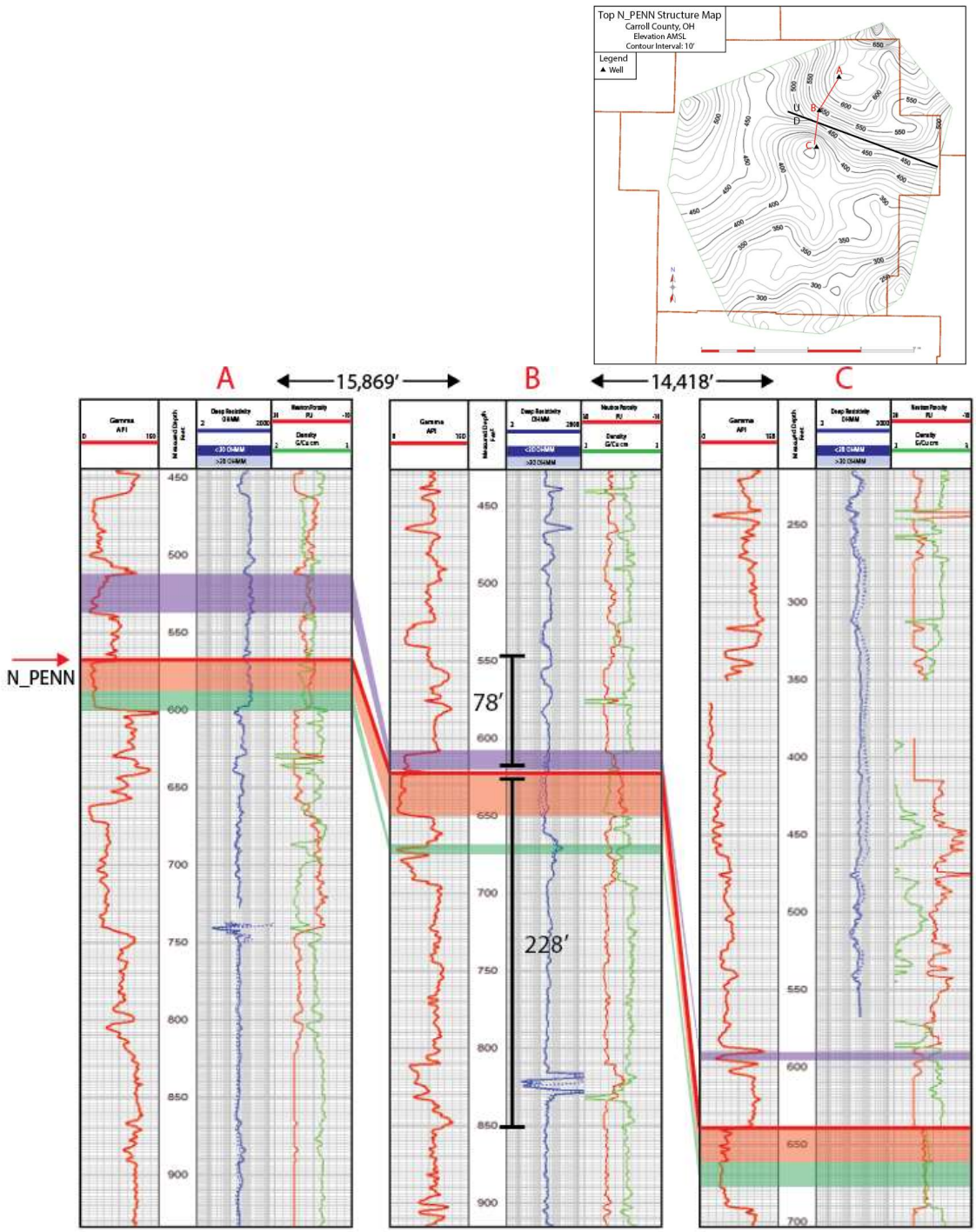

Figure 5.8: Structure map and cross section of N_PENN formation (shown in red in cross section) in northeastern Carroll County near the Highlandtown fault region. The top of the N_PENN descends 92.35 m (303 ft) from well A to well C over approximately 9.22 km (5.73 miles). From well A to well B, it descends 23.77 m (78 ft) over approximately 4.83 km (3 miles), and from well B to well C it descends 69.49 m (228 ft) over approximately 4.39 km (2.73 miles). Sea level is structural datum.

TDS interface elevations were determined for 1,000 mg/L, 5,000 mg/L, and 10,000 mg/L TDS using both Methods 1 and 2. Results of each TDS interface calculated from each method are discussed below. The results are compared after the results for each individual method.

Method 1: Using Archie's Equation to Calculate TDS from Well Logs

In total, three well logs showed a TDS value of 1,000 mg/L or less using Method 1. Two of these three wells, the Bowerston and Barnhart, are located in the southern quarter of the study area, and the third, the Pidgeon A, is in the northeast quarter of Carroll County (Figure 5.9). In all of these wells, the transition above 1,000 mg/L TDS occurs in the shallowest mapped sandstone formation on each log and is within 15.2-30.5 m (50-100 ft) of the shallowest limit of log data.

The 5,000 mg/L TDS transition was determined on 64 well logs using Method 1. The data points are well-distributed geographically across the available well logs in the study area (Figure 5.10). Only one well in this dataset also shows the 1,000 mg/L interface (Bowerston 21-13-6 106H), which is approximately 1.5 m (5 ft) shallower than the 5,000 mg/L interface. The mean elevation of the 5,000 mg/L interface calculated using Method 1 is 257.24 m (843.97 ft) above mean sea level (AMSL), the median is 261.53 m (858.04 ft) AMSL, the shallowest is 313.96 m (1,030.06 ft) AMSL, and the deepest is 155.44 m (509.97 ft) AMSL. The mean depth of this interface is 113.24 m (371.52 ft) depth below ground surface (BGS), the median is 109.20 m (358.28 ft) BGS, the minimum is 51.22 m (168.05 ft) BGS, and the maximum is 225.26 m (739.03 ft) BGS.

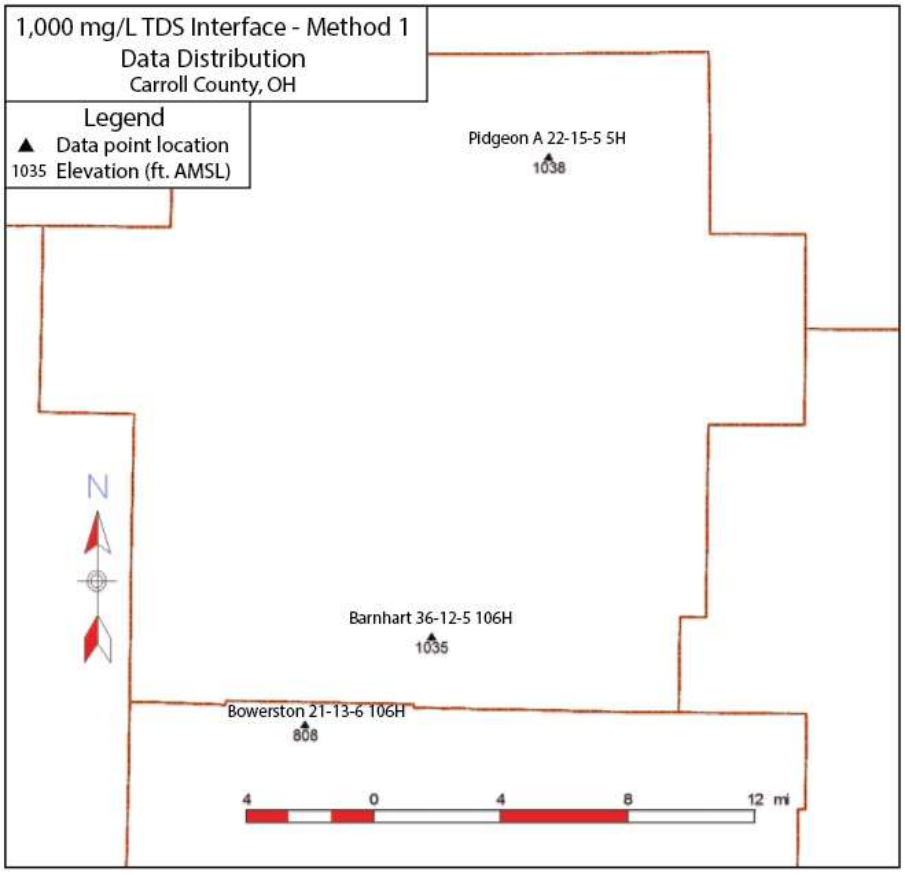

Figure 5.9 Location of well logs that show 1,000 mg/L TDS transition as calculated from Method 1.

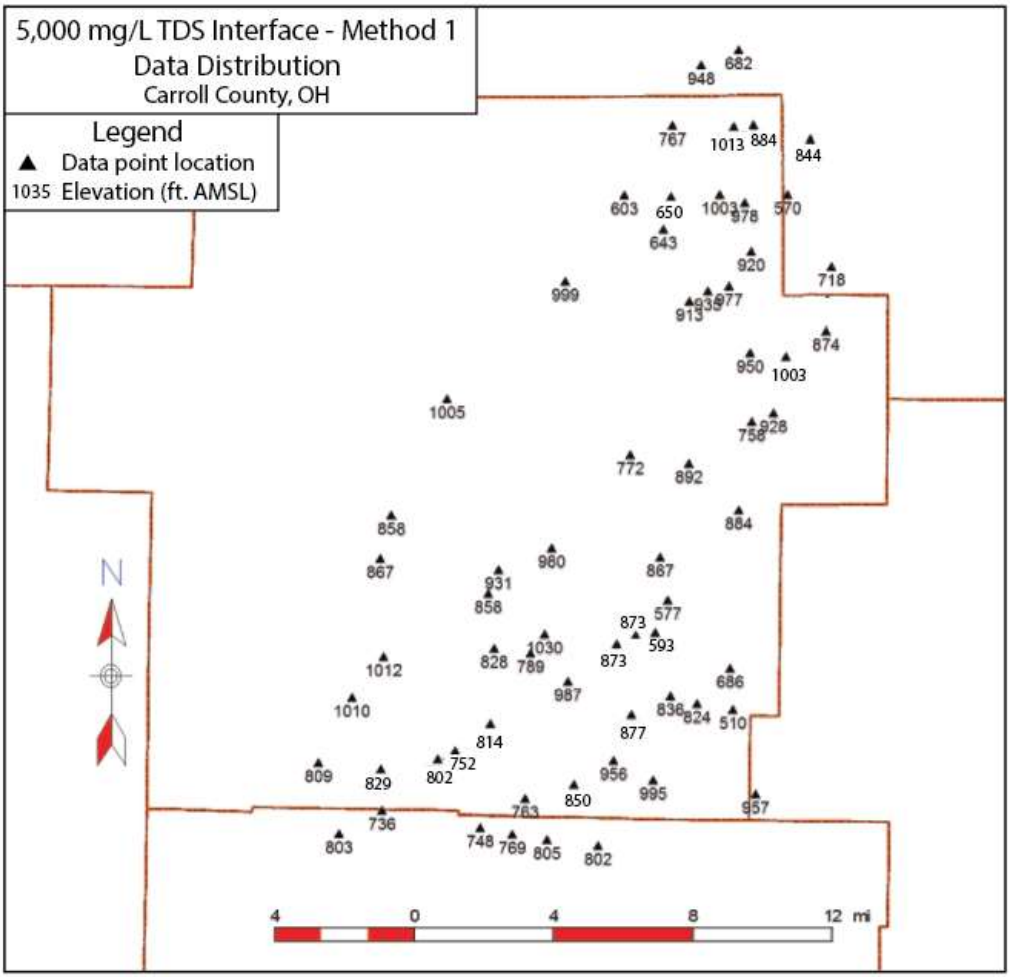

Figure 5.10: Location of well logs that show 5,000 mg/L TDS transition as calculated from Method 1.

In total, 71 wells showed the 10,000 mg/L salinity interface using Method 1. The geographical distribution is similar to that of the 5,000 mg/L interface (Figure 5.11). The mean elevation of this interface is 176.93 m (580.47 ft) AMSL, the median is 166.84 m (547.37 ft) AMSL, the shallowest is 304.50 m (999.0 ft) AMSL, and the deepest is 59.84 m (196.34 ft) AMSL. The mean depth of this interface is 194.98 m (639.69 ft) BGS, the median is 202.12 m (663.13 ft) BGS, the minimum is 51.22 m (168.05 ft) BGS, and the maximum is 313.33 m (1,028.0 ft) depth BGS. The mean distance between the 5,000 mg/L TDS interface and the 10,000 mg/L TDS interface is 80.18 m (263.06 ft), with a median of 85.55 m (280.69 ft), a minimum of 0 m (0 ft), and a maximum depth difference of 238.94 m (783.92 ft).

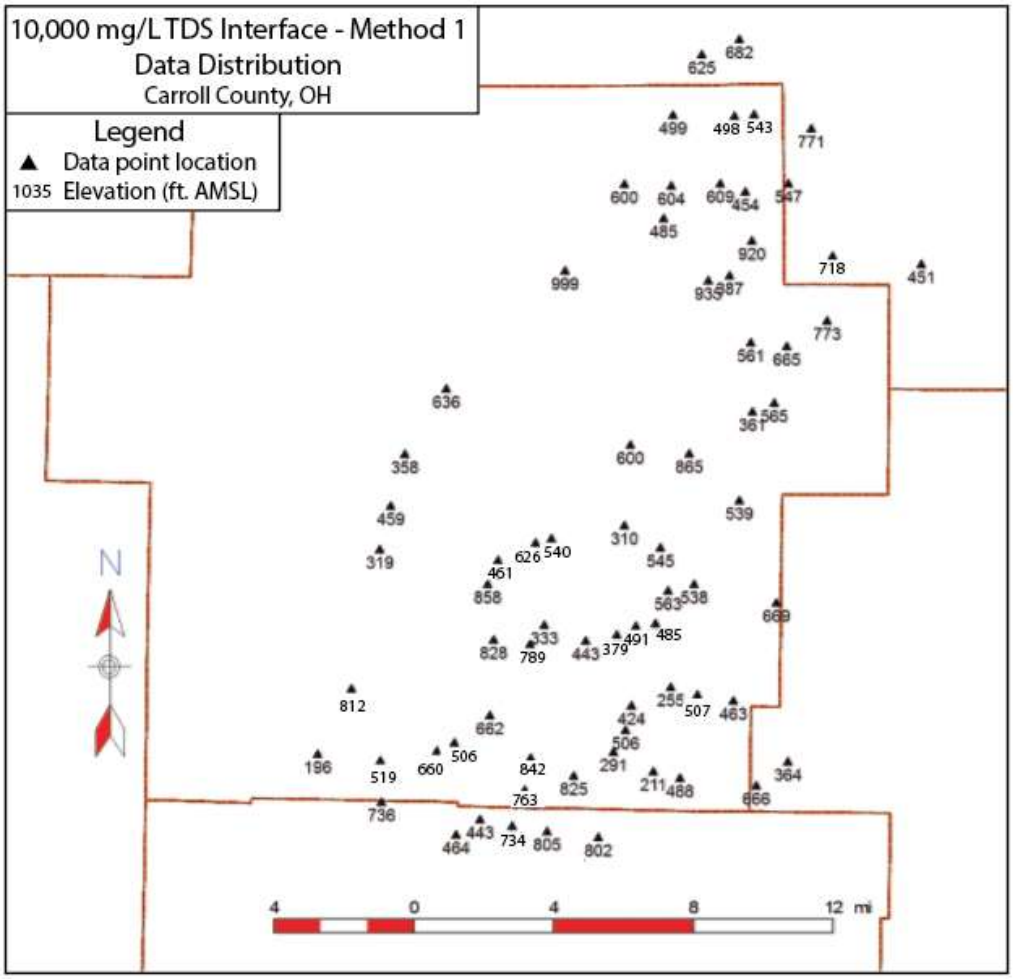

Figure 5.11: Location of well logs that show 10,000 mg/L TDS transition as calculated from Method 1.

None of the interfaces are restricted to any one formation throughout the study area. Interface formation occurrence is variable throughout the study area for each interface mapped using Method 1; however, clusters of wells within 4.83-6.44 km (3-4 miles) of each other often share the same interface formations, though many of these small clusters contain one or two wells with a different interface formation from the majority.

There is some level of uncertainty of interface elevation in some of the well logs in this dataset. The biggest cause of this uncertainty was from porosity curves being either suppressed or anomalously high when compared to nearby offset well logs. Similar issues with resistivity

curves also caused some uncertainty, but to a lesser degree since they appear to be more consistent in this dataset than the porosity data.

Method 2: Using the Envelope Method to Determine a Relationship Between SC and Resistivity on Well Logs to Calculate TDS

Like Method 1, calculating the 1,000 mg/L interface using Method 2 resulted in only 5 wells containing water fresher than 1,000 mg/L (Figure 5.12). The mean elevation of this interface is 284.53 m (933.49 ft) AMSL, the median is 287.91 m (944.60 ft) AMSL, the minimum is 317.53 m (1,041.75 ft) AMSL, and the maximum is 244.75 m (803.0 ft) AMSL. The mean depth of this interface is 71.18 m (233.52 ft) BGS, the median is 64.20 m (210.63 ft) BGS, the minimum is 53.11 m (174.25 ft) BGS, and the maximum is 103.19 m (338.56 ft) BGS.

Calculated from Method 2, the 5,000 mg/L TDS transition was present on 75 well logs. These data points are consistently distributed across the total well log dataset (Figure 5.13). The mean elevation of this interface is 252.68 m (829.18 ft) AMSL, the median is 256.10 m (840.22 ft) AMSL, the minimum is 314.25 m (1,031.0 ft) AMSL, and the maximum is 147.90 m (485.25 ft) AMSL. The mean depth of this interface is 117.40 m (385.17 ft) BGS, the median is 112.15 m (367.96 ft) BGS, the minimum is 51.22 m (168.05 ft) BGS, and the maximum is 231.27 m (758.75 ft) BGS. This set of well logs includes all four of the well logs that contain the 1,000 mg/L interface calculated using Method 2. The depth difference between the two interfaces ranges from zero to 52.86 m (173.41 ft), with a mean of 23.67 m (77.65 ft) and a median of 20.91 m (68.59 ft).

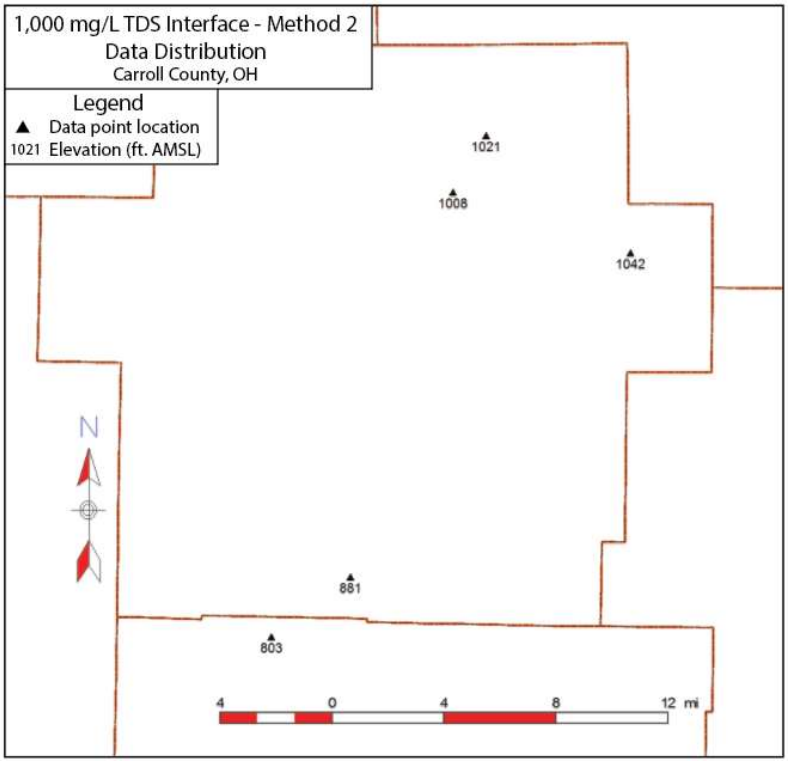

Figure 5.12: Location of well logs that show 1,000 mg/L TDS transition as calculated from Method 2.

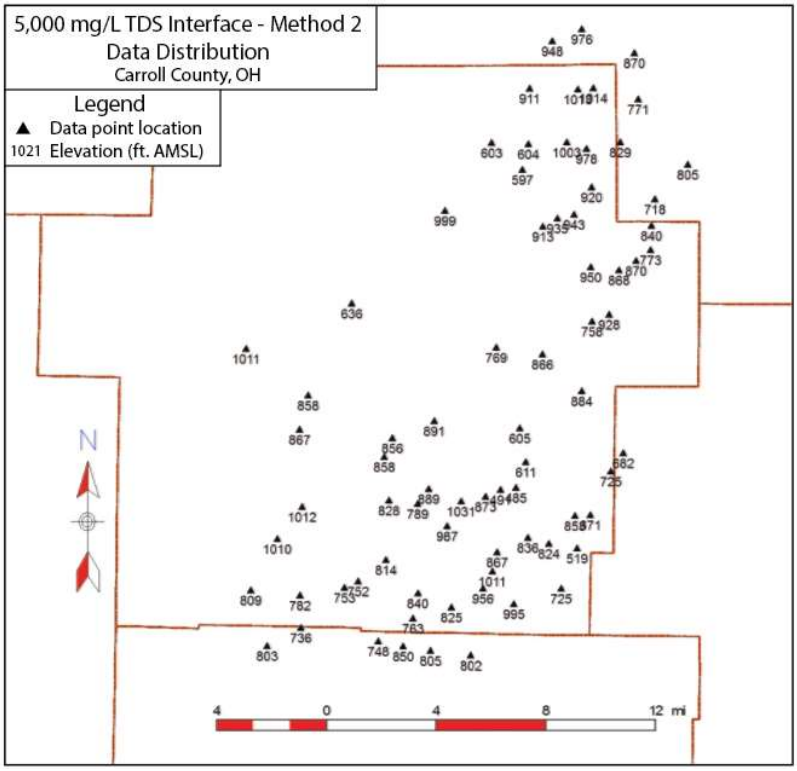

Figure 5.13: Location of well logs that show 5,000 mg/L TDS transition as calculated from Method 2.

In total, 77 well logs contained the transition to over 10,000 mg/L TDS using Method 2. This dataset is also evenly distributed among the full well log dataset in the study area (Figure 5.14). The mean elevation of this interface is 190.33 m (624.43 ft) AMSL, the median is 181.97 m (597 ft) AMSL, the minimum is 304.50 m (999 ft) AMSL, and the maximum is 97.23 m (319 ft) AMSL. The mean depth of this interface is 180.49 m (592.16 ft) BGS, the median is 192.39 m (631.20 ft) BGS, the minimum is 51.22 m (168.05 ft) BGS, and the maximum is 288.08 m (945.16 ft) BGS. This interface is separated from the depth of the 5,000 mg/L interface by a mean of 59.62 m (195.6 ft), median of 53.59 m (175.82 ft), minimum of 0 m (0 ft), and a maximum of 208.78 m (684.99 ft).

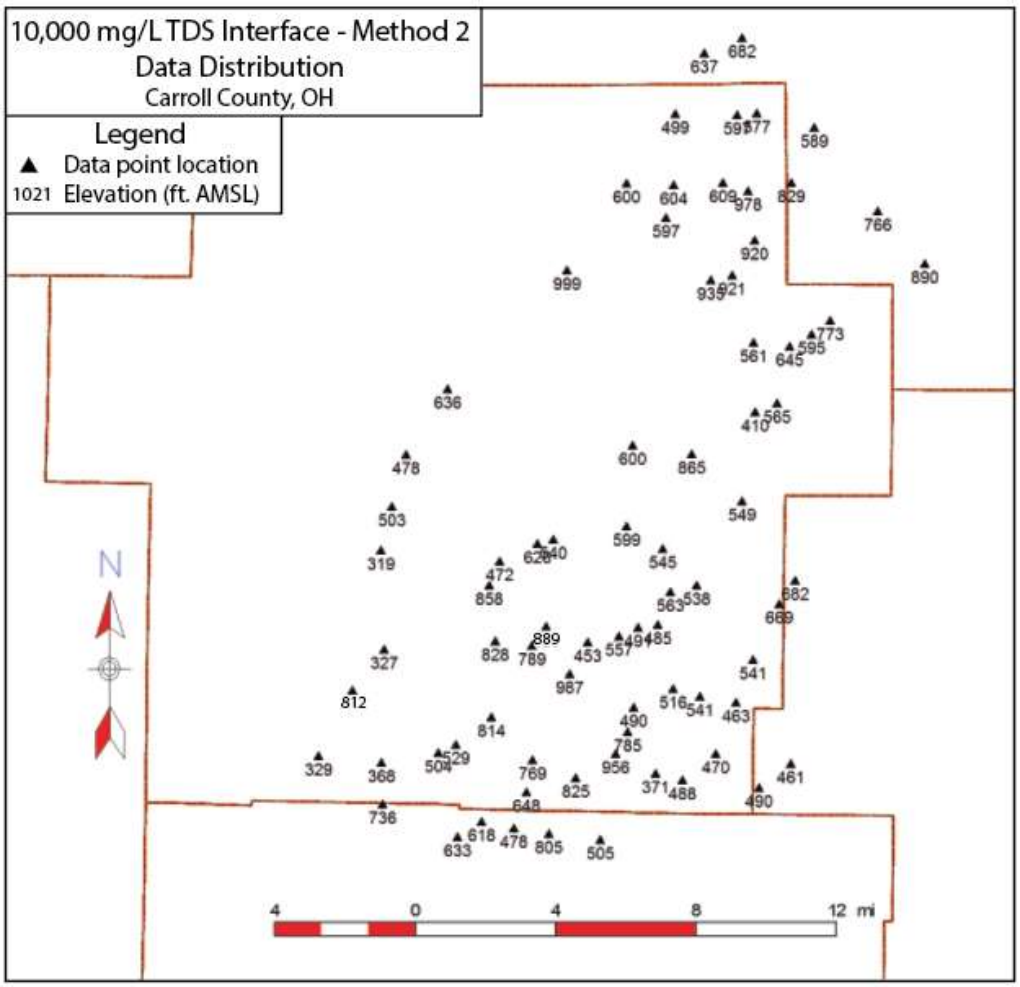

Figure 5.14: Location of well logs that show 10,000 mg/L TDS transition as calculated from Method 2.

Like Method 1, the formations in which the interfaces occur are variable for Method 2. Similarly, there are some clusters of data points where an interface occurs in the same formation, but there are also outliers within the clusters, so there is not full uniformity within any given 4.83-6.44 km (3-4 mile) radius.

The level of uncertainty of interface elevation was slightly lower with Method 2 than with Method 1. This is due to relying on fewer log curves, especially the porosity curve, which had more instances of anomalously high or low readings than the resistivity curve, which is the only curve Method 2 relies on for calculating TDS.

Comparison of Results of Methods 1 and 2

The mean elevation of the Method 1 5,000 mg/L TDS interface was 4.56 m (14.79 ft) shallower than the Method 2 mean and the Method 1 median elevation was 5.43 m (17.82 ft) shallower than the Method 2 median. There were a total of 64 well logs that showed the 5,000 mg/L TDS transition calculated from both Method 1 and Method 2, with 36 of these wells (56%) showing the transition at the same elevation for both methods. Method 1 resulted in shallower transition elevations than Method 2 on 20 wells (31%), with differences ranging from 1.22-112.47 m (4-369 ft) and a median difference of 18.29 m (60 ft). Eight wells (13%) showed Method 1 had a deeper 5,000 mg/L transition depth than Method 2, and the differences ranged from 2.44-89.61 m (8-294 ft) with a median of 40.54 m (133 ft). Of the 11 well logs on which only one method could be used to determine the 5,000 mg/L transition elevation, all were calculated only using Method 2.

The Method 1 10,000 mg/L TDS mean elevation was 10.4 m (61.96 ft) deeper than the mean Method 2 elevation, and the Method 1 median elevation was 15.13 m (49.63 ft) deeper than the Method 2 median. In total, 68 well logs showed the 10,000 mg/L TDS transition for both Methods 1 and 2. Of these, 33 well logs (49%) had this transition at the same elevation for both methods. There were 8 well logs (12%) that showed this transition to be shallower when

calculated from Method 1 versus Method 2, with differences ranging from 6.10-90.53 m (20-297 ft) and a median difference of 34.24 m (112.35 ft). 27 wells (40%) showed the Method 1 transition to be deeper than those calculated from Method 2. These differences ranged from 2.74-202.69 m (9-665 ft), with a median of 50.55 m (165.85 ft). In total, 9 well logs showed a 10,000 mg/L TDS transition from only one method or the other, with three determined from Method 1 and nine determined from Method 2.

MAPPING THE FRESH-SALINE INTERFACE

Due to the low number of data points containing the 1,000 mg/L TDS interface for both Method 1 and Method 2, this interface was not mapped for this study. Overall, four maps were created in total: one each for the 5,000 mg/L and 10,000 mg/L TDS interface elevations calculated using Method 1, and one each for the 5,000 mg/L and 10,000 mg/L TDS interface elevations calculated using Method 2.

In total, 64 data points are included in the Method 1 5,000 mg/L TDS interface map. The data points are distributed across the study area, with slightly increased well density in the southern one-third of the study area and in the far northeast quadrant as well. The average distance between wells in these two clusters is 2.41 km (1.5 miles), and in the less dense area in the center of Carroll County, the average distance between data points is 4.83 km (3 miles). This data point distribution is consistent for the other three maps as well, though there are slight changes in number of data points for each map. In the 10,000 mg/L interface map using Method 1, 71 data points are included. For the 5,000 mg/L and 10,000 mg/L interface maps calculated using Method 2, there are 75 and 77 data points, respectively.

Each map was hand-contoured using methods discussed previously, accounting for stratigraphic influence by referencing the thickness and structure of the top and base of each sand in which the interface was picked. The resultant maps are included shown in Figures 5.13 through 5.16. The

contours follow the boundaries of the associated formation thickness and structure maps that the interface occurs in. There are large vertical changes in interface depths over short lateral distances in several areas on all of the maps, which are interpreted to be largely driven by stratigraphic changes between well log data points. These results are discussed further in the following section.

Additionally, the northern and westernmost parts of the county lack sufficient data to create confident contour maps. Shown as dashed contour lines in Figures 5.13-5.16, these contours fall beyond the geographical limits of the main dataset and were mapped by projecting interface elevations from the more data-dense center of the county and by referencing the existing USDW map from Riley, et al. (2012).

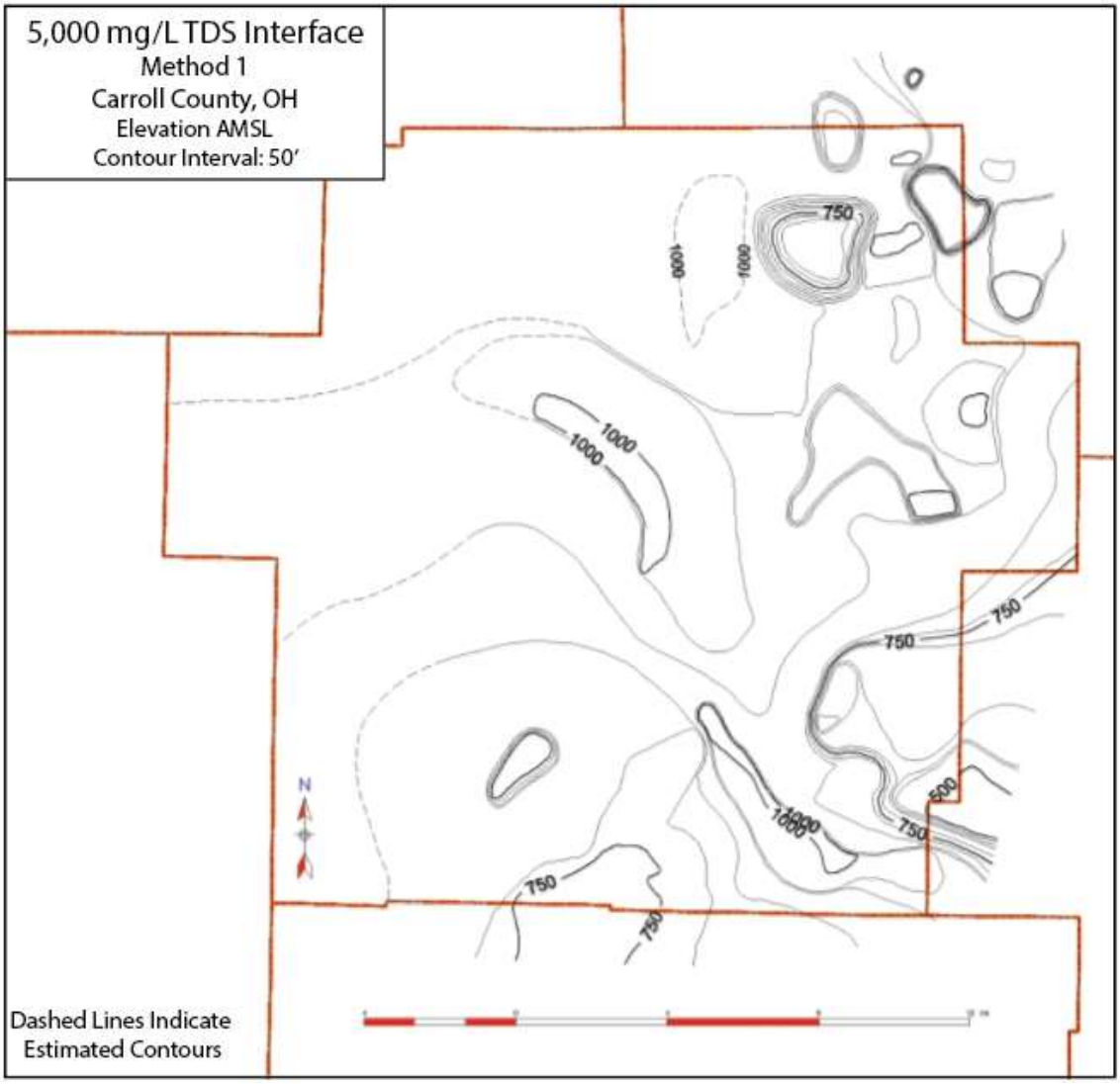

Figure 5.15: 5,000 mg/L TDS interface contours as calculated using Method 1.

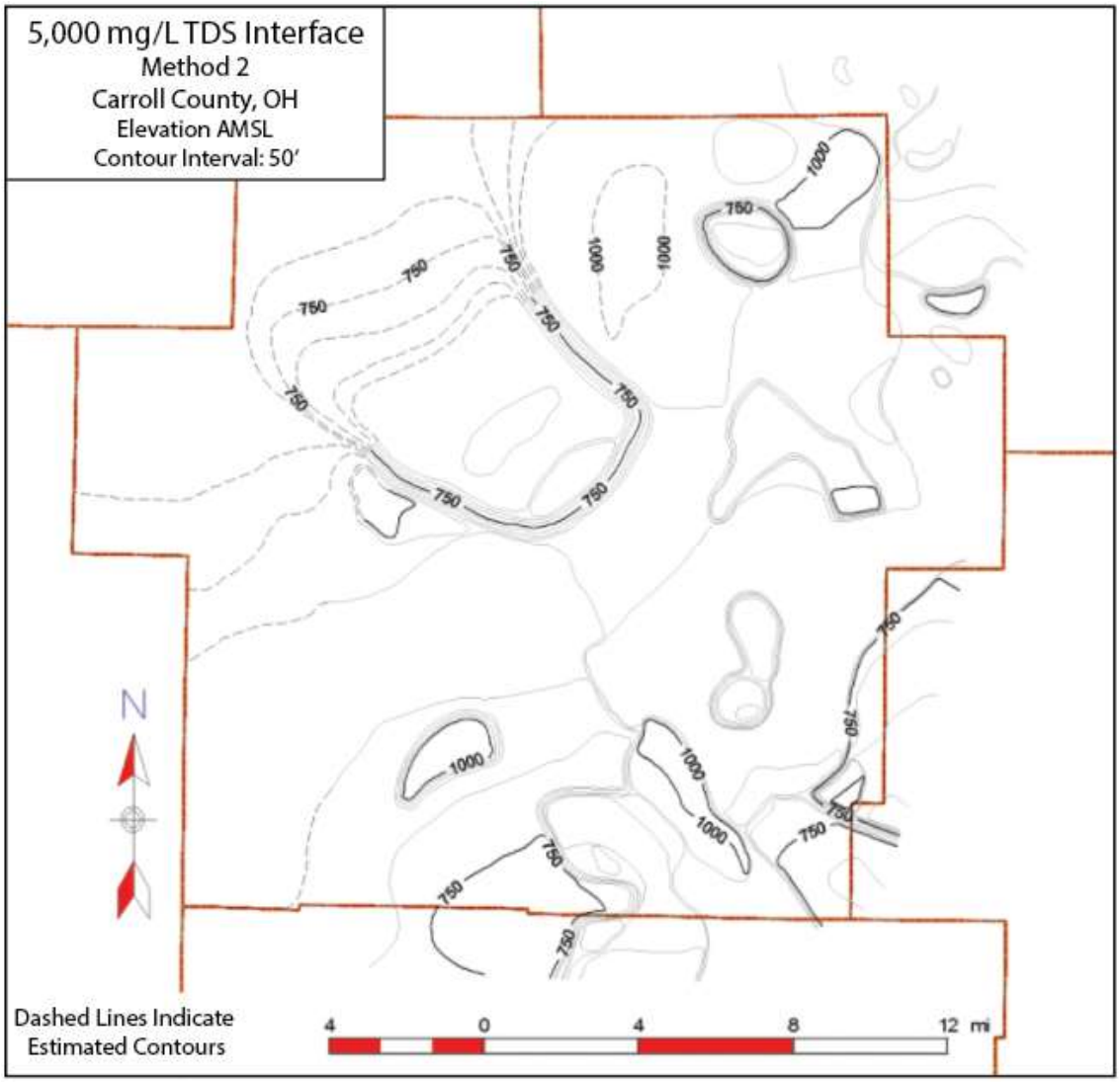

Figure 5.16: 5,000 mg/L TDS interface contours as calculated using Method 2.

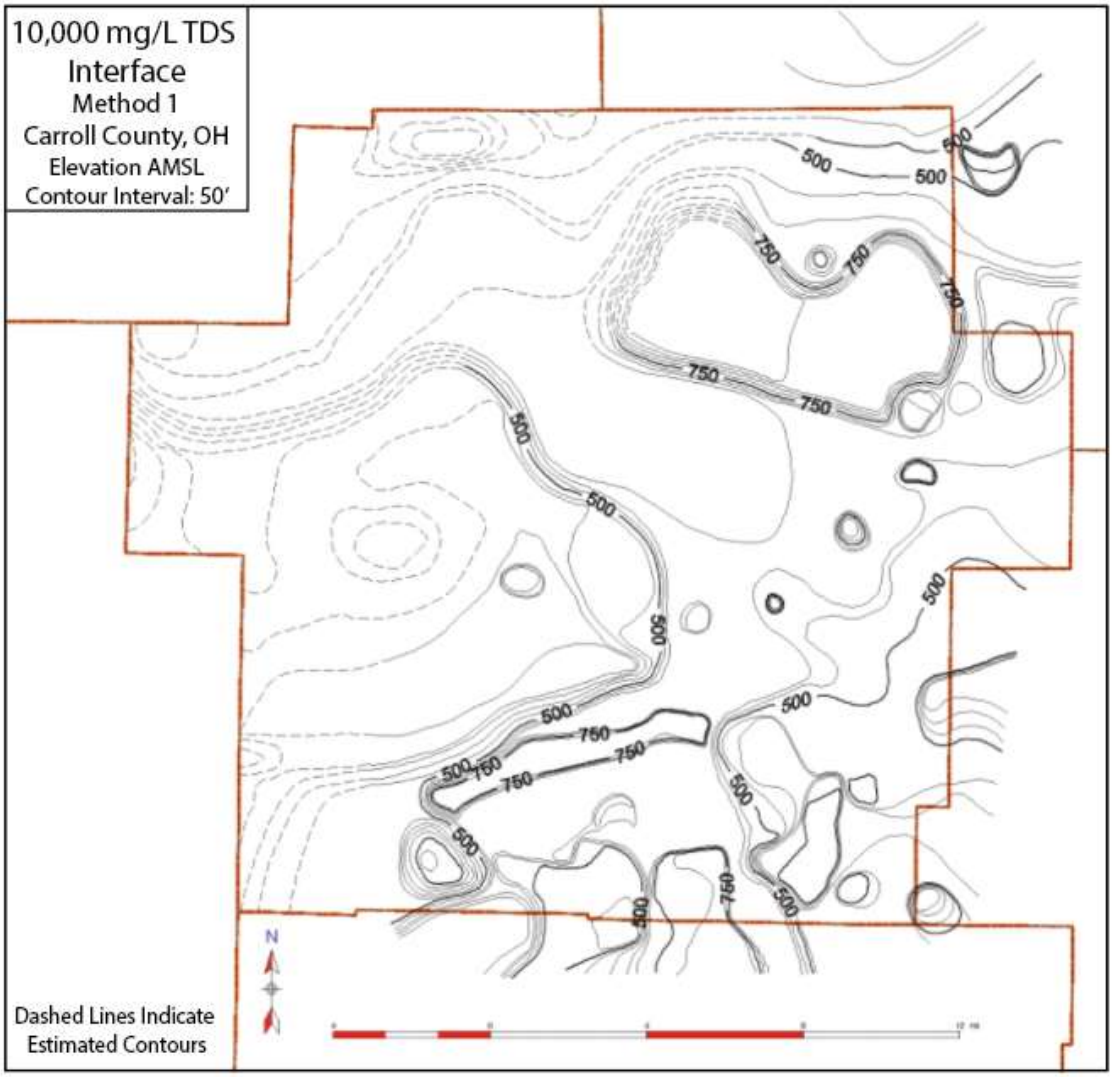

Figure 5.17: 10,000 mg/L TDS interface contours as calculated using Method 1.

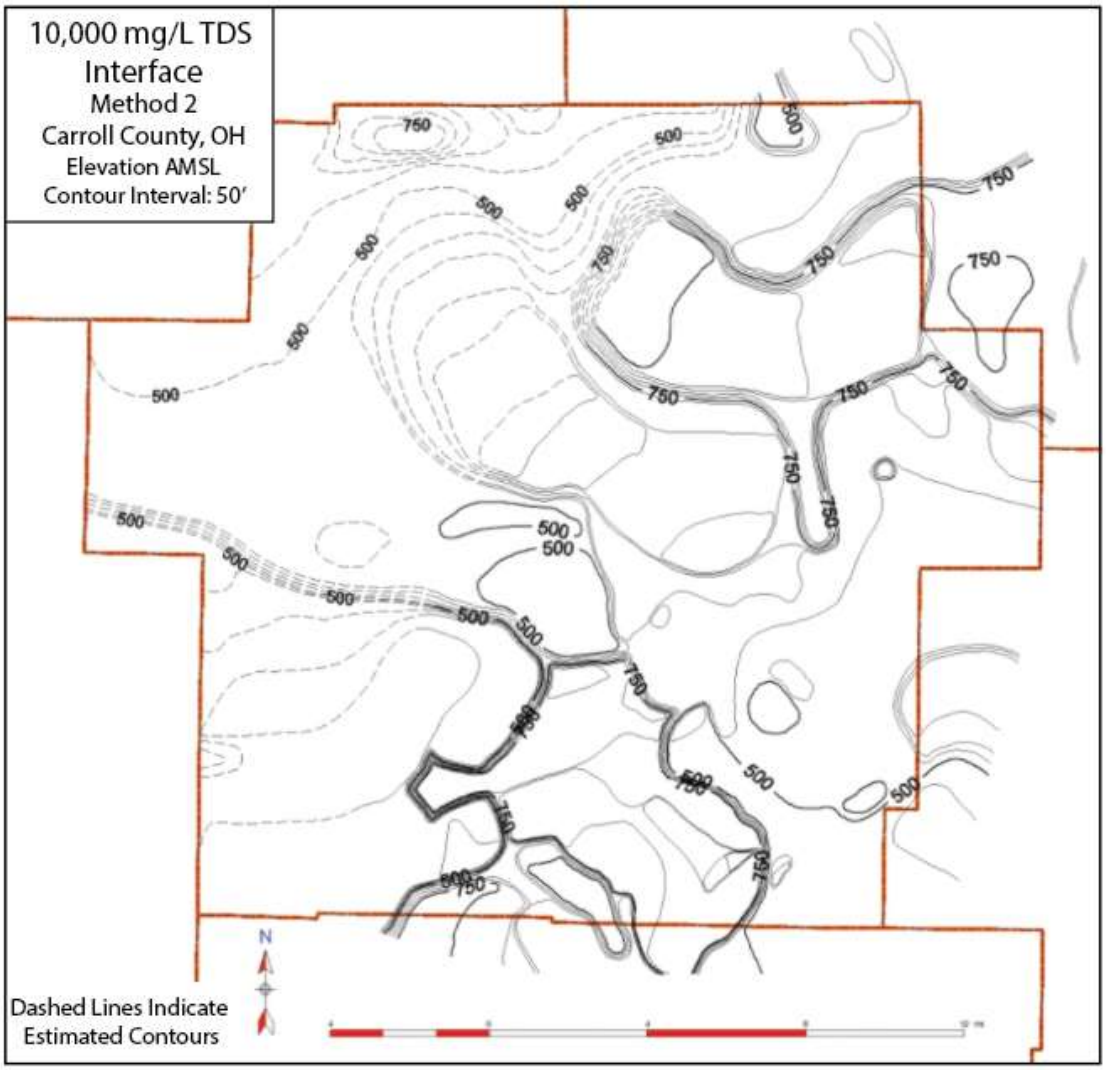

Figure 5.18: 10,000 mg/L TDS interface contours as calculated using Method 2.

CHAPTER VI

DISCUSSION

The purpose of this study is to determine the elevation of the fresh-saline groundwater interface within the study area, where the stratigraphy is highly variable, especially in terms of porosity, and is assumed to have a strong influence on groundwater recharge. The complex nature of fluvial depositional patterns and geometries, coupled with the limitations of geophysical well log data, results in some level of uncertainty in stratigraphic analysis in this study. Additionally, as discussed in other literature, oilfield geophysical well logs have limitations in evaluating freshwater, which leads to uncertainty in these analyses as well. These uncertainties are discussed in this section, as well as limits of confidence in the resultant fresh-saline water interface maps.

STRATIGRAPHIC CORRELATION

Due to the mechanisms involved in fluvial erosion and deposition, which can include relatively deep, laterally consolidated downcutting as well as shallow incision with large lateral movement of fluvial distributary channels, these deposits are notoriously difficult to map in the subsurface, as discussed previously (Jordan and Pryor, 1992; Donselaar and Overeem, 2008; Fanti and Cantuneanu, 2010; Tibert and Gibling, 1990; Crawley and Atkinson, 1982; Alqahtani, 2013).

The geophysical well logs used in this study represent a single vertical data point, which leads to ambiguity in determining correlation and connectivity of sandstone channels from well-to-well. Using coal deposits as stable marker beds helps to create boundaries when interpreting connectivity of porous sandstone deposits between well logs since they are deposited in low-energy environments during periods of little to no erosion (Alqahtani, 2013). This method was very useful in this study, as there are many coal beds visible on the well logs and they are often laterally correlative between well logs. In many instances throughout this study, the presence or absence of these coals permitted determination of whether a porous sandstone shown on one log was correlative to a porous sandstone on a nearby well log (Figure 6.1). This method proved highly effective and increased confidence in the stratigraphic correlation of porous sandstone units in this study since many wells were spaced less than 3.22 km (2 miles) apart, which led to high confidence in correlation of coal beds from well-to-well.

An additional difficulty in stratigraphic mapping of porous fluvial deposits is determining the lateral boundaries of deposits. Due to stream bed architecture and frequent lateral shifting of stream beds during deposition, the edges of sandstone deposits often become increasingly interbedded with fine-grained material. This leads to a fairly gradational edge to many sandstone deposits, which can make thickness mapping difficult. A solution to this was to incorporate a porosity cutoff of 5% when picking formations on well logs, as discussed in the Methods chapter.

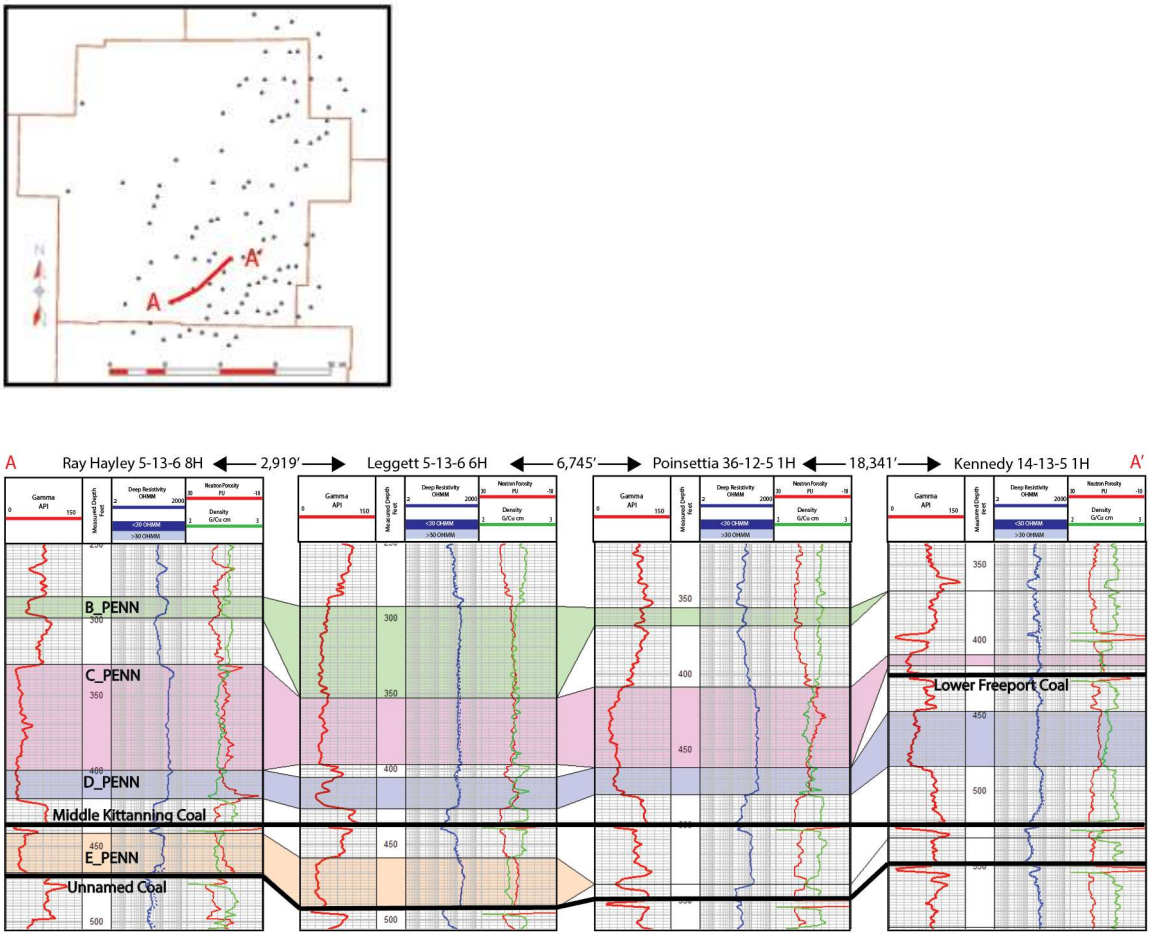

Figure 6.1: Example of using coal beds to aid in correlation of sandstones. By noting the positions of sandstone beds relative to coals that are correlative between logs, confidence increases when establishing correlation of sandstone well to well. The disappearance of a coal seam within a cross-section of logs can indicate downcutting of an overlying sandstone bed, as shown in the far right well log above. The Lower Freeport Coal at ~160 m (525 ft) MD in the Kennedy 14-13-5 1H is not present in the Poinsettia 36-12-5 1H, indicating downcutting of the sandstone above. Well logs are hung on the Middle Kittanning Coal. Horizontal distance between each adjacent log is noted at the top of the figure.

The use of a porosity cutoff reduced uncertainty in terms of mapping lateral edges of formations that pinch out, but it was not as useful in areas where sandstone deposits are interrupted with thin (<3.05 m (10 ft)) layers of low-porosity siltstones and shales within a 9.14-15.24 m (30-50 ft) thick sandstone deposit. These instances occur most frequently as the sandstone deposit is thinning near its lateral boundary, but instead of simply pinching out, these boundaries are

marked by stacked, distinct shale and sandstone beds. In these situations, a hard porosity cutoff was not used to determine vertical extents of sandstone deposits as it was clear that that the porous intervals in between the low-porosity intervals were likely connected, as shown on nearby well logs. Instead, educated interpretations of the tops and bases of formations were made for correlation purposes based on geologic understanding of fluvial systems.

This vertical thickness ambiguity was not only present on the lateral edges of sandstone deposits, but also intermittently in several formations in thicker depositional areas away from the lateral extents. Thin, low-porosity beds, including siltstone, shale, and limestone, were present at either the tops or bases of many formations, and even occasionally within the center of a vertical sandstone interval (Figure 6.2). This generally was restricted laterally to data points within a 3.22-4.83 km (2-3 mile) radius of one another, or even only present in one sandstone interval on a single well log. Again, geological interpretation was used to determine the vertical extents of connected, porous sandstone intervals in these cases, taking into consideration the porosity of the sandstone beds, overall average porosity of the unit, and thickness of the fine-grained beds in relation to that of the porous beds. This resulted in some uncertainty in determining the vertical extents of porous sandstone beds, but the interpretations are based on geologic knowledge and understanding of the study area and data.

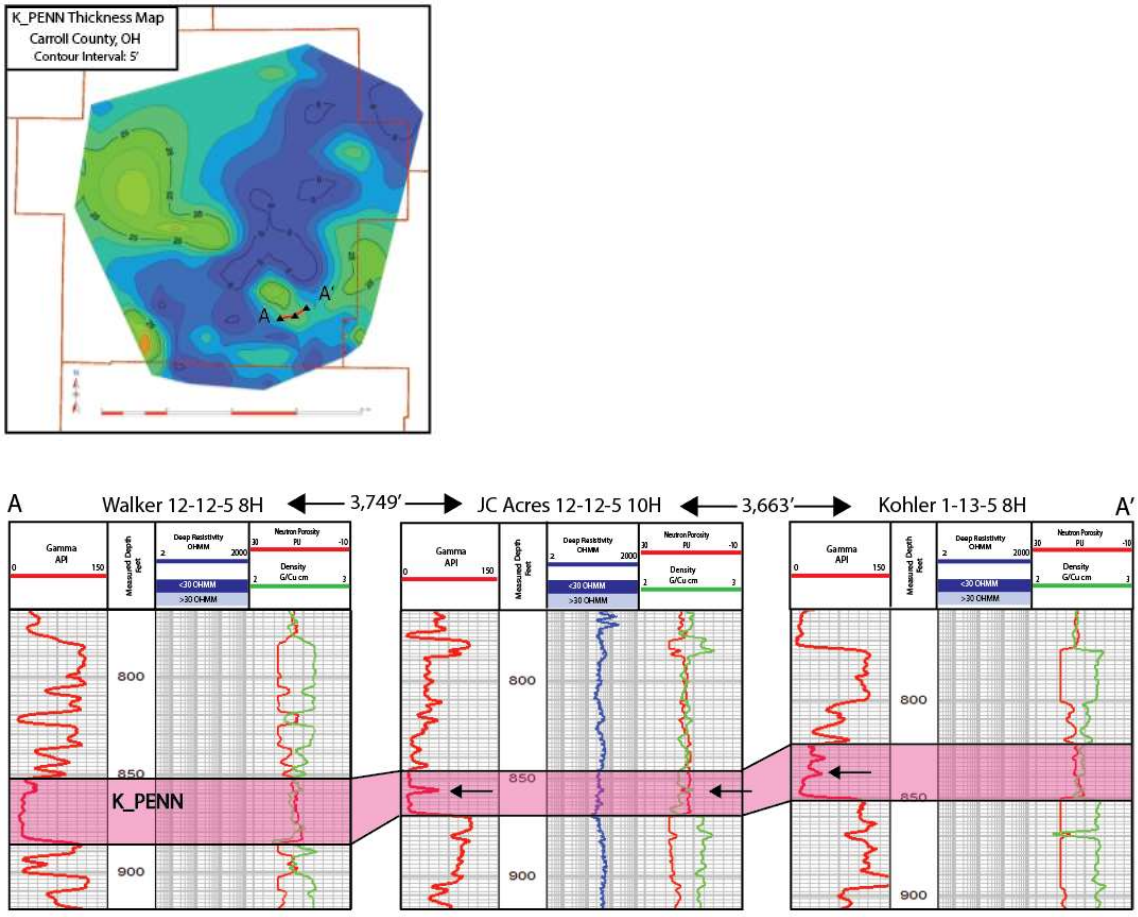

Figure 6.2: Example of sandstone being interrupted by lenses of fine-grained deposits within main depositional channel. The Walker 12-12-5 8H contains clean sandstone within the K_PENN (highlighted in cross section) while the other two wells show interfingering shaley beds. These are indicated by the black arrows and visible as spikes in the otherwise low gamma-ray curve in both wells and a minor increase in density/decrease in porosity in the JC Acres 12-12-5 10H. The cross section location relative to K_PENN thickness is shown in the map above. Well logs are hung on the top of the Berea Sandstone. Horizontal distance between each adjacent well log is noted at top of figure.

As discussed previously, extensive downcutting caused by erosion of fluvial sandstones is common in the study area and can cause amalgamation of one porous unit with an older one, or more often the amalgamation of multiple beds. In these instances, the exact bed boundaries were difficult to determine using well logs and are highly interpretive, but ultimately this uncertainty has little bearing on the results of the study since the units are assumed to be in hydrologic communication if there are no confining beds separating them. To account for this during

interpretation of the final interface maps, wherever an interface occurred in an amalgamated sand, each individual formation making up the larger deposit was noted with the associated data point. This allowed consultation of all relevant maps so that the total thickness and structure of the amalgamated sandstone package in which the interface occurred was considered as a whole, in addition to viewing nearby well logs to determine where the sandstones were separated and where they became amalgamated. This way, the interface contours within amalgamated sandstones were not dependent on the exact boundaries of the sandstones or solely on the individual thickness and structure maps for each named formation making up the bed, and instead looked at the total thickness and elevation of the top and base of the amalgamated interval and the geographical extent that the amalgamation occurred. On an observational note, since amalgamated sandstones often resulted in thicker sandstone deposits, the exact interface transition could frequently be seen within these sandstone intervals on well logs, which helped by providing a more precise interface elevation data point to anchor the contour interpretations.

One other point of uncertainty in stratigraphic correlation for this study was determining the lateral boundaries of the sandstone deposits, which required estimation of equivalent sandstone formation top elevations outside of sandstone depositional boundaries in order to fully map the edges of the deposits. This was also important for determining sandstone correlation and connectivity at the edges of the study area as sandstone deposits came in and out of view of the dataset. The majority of shale beds in the study area showed low organic content, meaning low gamma-ray curve values on well logs, and so were not easily definable from one another and were generally not helpful in confining the stratigraphic analysis. Where possible, coal deposits were used as marker beds to determine equivalent sandstone formation top depths (Figure 6.3), which also aided in correlation across the study area as sandstone deposits meandered, pinched out, and amalgamated. In some instances, sandstone bed horizons were able to be traced through very thin limestone beds within shale or siltstone on well logs outside of the primary fluvial

channel sandstone's lateral boundaries, which resulted in high confidence in those zero-thickness formation top picks.

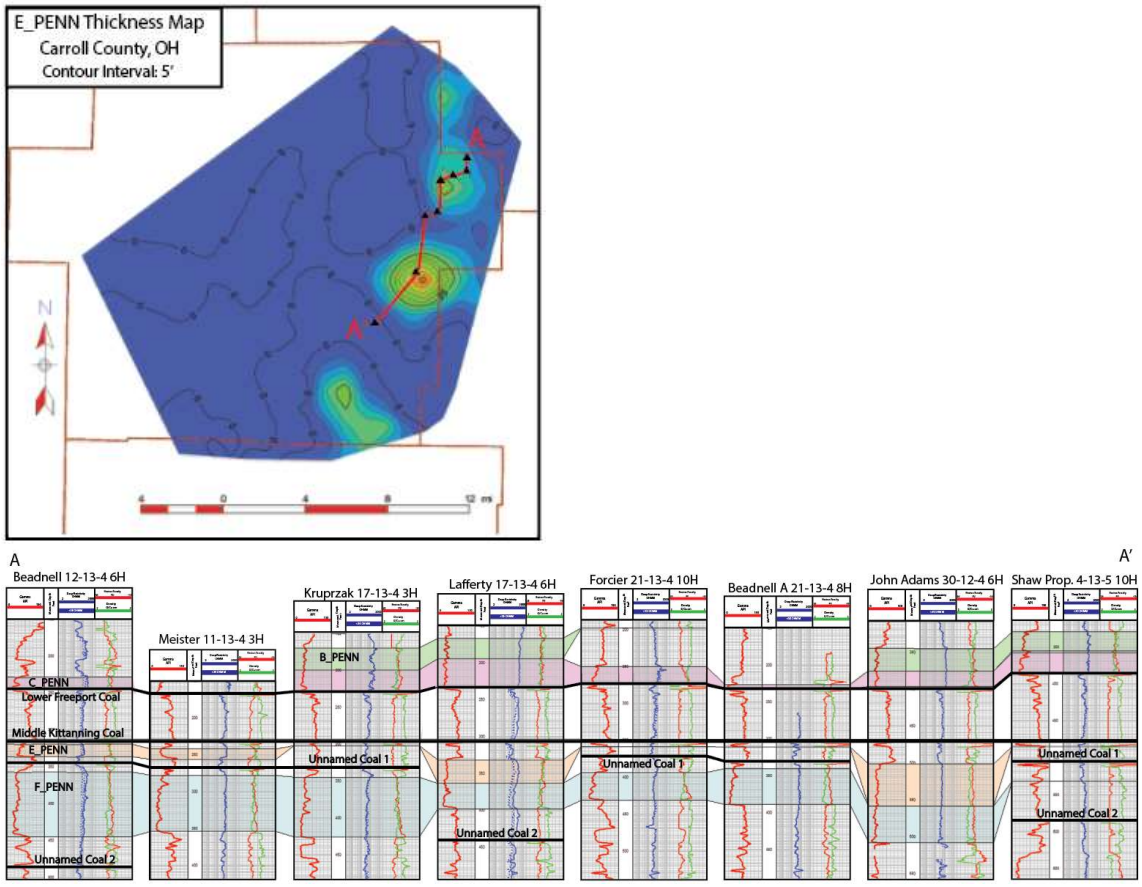

Figure 6.3: Multiple sandstone and coal formations are shown on this cross section, which is hung on the Middle Kittanning Coal. The E_PENN Sandstone (orange) is shown below the Middle Kittanning Coal and above the Unnamed Coal 1. The coal beds, in addition to confining the possible position of the E_PENN in these logs, act as marker beds for the E_PENN horizon where there is no sandstone deposition. In these cases, the top and base of the E_PENN was placed at the base of the Middle Kittanning Coal.

Using coals as marker beds to trace horizons outside of sandstone depositional areas was particularly helpful in correlation of sandstone deposits that meander in and out of the study area boundaries. As discussed previously, correlation of fluvial deposits is often ambiguous, and this uncertainty when tracing zero-foot thickness horizons is a large cause of that ambiguity. Using coals as marker beds in the same manner they were used for reducing vertical uncertainty did help

increase confidence in lateral correlation of sandstone horizons in areas of zero thickness, in addition to using other well log curve patterns such as limestone beds or very thin sandstone beds where possible. Generally, except for the E_PENN formation which was mapped at the base of the Middle Kittanning Coal throughout the study area, the zero-thickness picks on well logs for the sandstone equivalent horizons were restricted to only one to two wells in any direction from the nearest well with sandstone deposition for any given formation. This was done in order to properly see the edges of the beds in thickness maps and followed available markers on the log as discussed above where possible, and if none were available, position between sandstone or coal formations above and below were used to keep consistent positions of the horizons as much as possible. While there is some uncertainty to tracing the equivalent horizons in fluvial settings such as this, the impact to the study is extremely low since the structure of sandstone horizons outside of actual sandstone depositional areas did not influence the outcome of any of the TDS interface maps in this study due to the methods used to map the interface. Since structure maps were only referenced for formations within areas with sandstone deposition and TDS interface transitions, the zero-thickness areas have no bearing on the interface elevation interpretations.

TDS CALCULATIONS

SC Sample Uncertainty

Some amount of error is expected in the returned-fluid samples since they were taken in uncontrolled conditions during drilling, without direct supervision, and by many different people. Before any widespread sampling took place, procedures were handed out and field training on sampling methods was given to mudloggers in the study area in order to reduce these errors. Still, there is potential for error in these samples due to the general fast-paced nature of oil and gas drilling operations.

One possible error considered when reviewing these data was inaccurate depths of sample collection. Oil and gas drilling in the study area can be fast-paced, and site layout can cause mudloggers to be unable to collect samples at the correct interval. During drilling, the mudloggers who collected samples for this study worked out of trailers on drill sites, where they would bring fluid samples for field analysis after collecting them from the discharge of the flowline on the rig. This creates potential for delayed or missed samples if the mudlogger is physically unable to retrieve samples at the rate of drilling due to site layout or other circumstances. Additionally, there was no depth-monitoring equipment at the sample collection points on the rigs, so mudloggers only had depth-monitoring equipment in their trailers and were required to preempt the correct sample depth at the flowline, which may have caused some inaccuracy of recorded sample depths.

With this information considered, large discrepancies are not suspected in sample collection depths recorded vs. actual sample depths due to sample collection errors. The sampling procedures indicated a sampling interval of 15.24 m (50 ft), which means mudloggers returned to on-site trailers frequently between samples, allowing them to monitor depth regularly. Missed samples were noted on very few reports, so mudloggers were for the most part able to maintain sampling intervals in accordance with drilling rate.

Another possible source of error in depth of sample is due to the mechanics of air rotary drilling. This was the most commonly used method to drill through the Pennsylvanian interval in the study area when these fluid samples were collected. This method, which uses large amounts of compressed air to propel formation cuttings and fluids in the wellbore up to the surface, causes cuttings and fluid to mix in the annular space of the borehole. The amount of mixing is unknown, but likely increases when air pumps are turned off and drilling is suspended for any amount of time. This is due to cuttings and fluid settling in the bottom of the borehole together when the pumps are off, then mixing further when the pumps are turned back on. Air compressors can be

shut off due to rig issues, drilling issues, as well as when a new string of drill pipe is connected to the drill string, which occurs regularly at 9.14-27.43 m (30-90 ft) intervals in the study data. To counter issues with this, mudlogs were consulted when reviewing SC data since they notate both drilling issues and drill pipe connections. Anomalously high or low SC readings were compared with mudlog notations and discarded if drilling operations were suspected to have caused the anomalous readings.

Even when pumps are running consistently, downhole mixing of formation fluids can still be a potential source of error in SC data measurements simply due to the physics of air drilling operations. While there is no real way to reduce this, the overall impact to the study is likely low. With the air pumps running steadily at a high rate to keep the borehole from building up with formation cuttings and fluid, these contents are likely mostly interacting with other fluids and cuttings from similar depths rather than vertically distant intervals.

Additionally, the regional stratigraphy of the study area, with low-porosity beds frequently separating higher-porosity sandstones, may help further restrict mixing of fluids in the borehole. As the drill bit drills through a porous sandstone, then encounters a low-porosity unit such as a shale, most of the fluid in the borehole should be attributed to fluid that came from the sandstone interval since low hydraulic conductivity shale beds don't hold as much fluid as a high hydraulic conductivity porous sandstone. As the bit continues to drill through underlying low-porosity units, fluid from the sandstone interval is continuously pushed up the borehole by the air compressors so that when another porous unit is encountered, there is likely some vertical separation of fluids and cuttings attributed to each sandstone formation as the material is pushed up the annulus of the borehole. This, of course, only holds true where there is sufficient thickness of low-porosity units separating sandstone units, though an exact number for sufficient thickness is unknown. Additionally, the rate of drilling and pressure of air used to circulate the fluids up the borehole can influence the level of fluid mixing in the borehole. According to mud logs in the

area, drilling rate ranged from 15.24-45.72 m/hour (50-150 ft/hour) while drilling through the study interval and at the deepest part of the interval, cuttings took less than 30 minutes to reach the top of the wellbore from the bit. This was calculated based on annular volume and output of the air compressors. This means that there was only potential for mixing of fluids from formations with less than 30.48 m (100 ft) of vertical separation at any given time while drilling through this interval. Realistically, mixing would have been much less since it is unlikely that the fluid at the very top of the wellbore would have had the chance to mix with fluids at the bottom of the wellbore, especially since the time for fluids to return to surface was calculated at depths of 304.8-457.2 m (1,000-1,500 ft) and would be considerably lower when the wellbore was shallower. Still, since there is some variability between distances of separation between sandstone beds, as well as the drilling rate and time it takes for fluids to return to surface, mixing is still a necessary consideration in evaluating SC data.

Drilling fluid additives are another potential source of error in the returned fluid sample SC data. The likelihood of this being a major source of error in this study is low since air-drilling operations use a very small amount of water and additives, meaning the majority of the returned fluid is formation fluid. Furthermore, drilling procedures call for the use of fresh water while drilling through the study interval due to regulatory requirements of drilling through fresh water aquifers in Ohio. Mudloggers took samples of the make-up water prior to drilling to ensure the SC was less than 1,000 µS/cm to ensure these procedures were being followed, which furthers our confidence in the assertion that the returned fluid SC samples are minimally impacted by drilling fluid chemistry. The two wells that used mud-drilling methods instead of air-drilling were not used for this study due to the uncertainty of the mud composition and quantity. If the mud composition were known prior to drilling and monitored throughout the study interval, along with changes in volume of the mud versus returned fluids, these uncertainties could potentially be accounted for and mud-drilling methods could be used.

Although there are several sources of uncertainty in the SC samples and data, careful evaluation of all these data prior to incorporation into the overall analysis reduced the likelihood of issues with the samples affecting the study. Quality control procedures were incorporated on multiple levels, including prior to beginning the analysis, as well as additional scrutiny of anomalous data and results throughout the analysis. SC datasets were compared to other sources of data, including associated mudlogs and well logs, as well as SC datasets from nearby wells. For example, coupling returned fluid SC evaluation with well log evaluation for a given well by comparing SC values with log resistivity values and patterns or changes in both, was very useful in determining whether or not to use SC data from that well in the final evaluation.

TDS Calculation Uncertainty

Method 1 TDS calculations are based on simple mathematical manipulation of Archie's Equation, which is a very well-known and widely-used equation within the oil and gas industry. In addition to manipulating Archie's equation, this method operates on the assertion that measured SC values can be substituted directly for R_w (after converting SC units to ohm-m) and deep log resistivity can be used directly for R_t. The theory of these assumptions is logical and based on literature from previous studies (Turcan, 1962; Roberts, 2001).

Per Archie (1942), R_w is defined as the resistivity of the connate formation water. As discussed earlier in this chapter, this study uses the assumption that returned drilling fluids consist of nearly 100% formation fluid with negligible impacts from added drilling fluids. The potential drawbacks to this assumption have also been discussed, and the conclusion is that the returned fluid is a good proxy for formation fluid after undergoing rigorous quality control.

R_t is defined as the true formation resistivity (Archie, 1942). Since the wells in this study were logged using induction logging tools, which were designed to measure formation resistivity for wells drilled using air or oil-based mud, no corrections are needed to convert deep log resistivity

to R_t (Tiab and Donaldson, 2015). The induction tools used during this study measured 228.6 cm (90 inches) from the borehole for the deep resistivity curves, which is likely far enough from the borehole to be undisturbed from drilling operations. With air drilling, fluid invasion from the borehole is negligible as any borehole fluids are pushed up-hole rapidly by the high air pressure. Any invasion would likely consist of formation fluids from deeper formations and would likely not extend to 228.6 cm (90 inches) past the borehole. Additionally, logs were run within 24-48 hours of drilling according to mud logs, meaning there was little time for fluid to migrate from the borehole deep into the formation. Considering these factors, directly correlating R_t to deep log resistivity is a valid assumption for this study.

With the factors discussed above lending validity to the assumptions used regarding R_w and R_t for this study, Method 1 is an accurate means to calculate TDS in this study area with the available data. The assumptions are based in previous literature and manipulation of a well-known mathematical relationship between water saturation, R_w, R_t, and porosity.

Method 2 operates under a simpler relationship than Method 1. The main assumption in this method is that there is a direct mathematical relationship between deep log resistivity and SC of the formation water. It also relies on the accuracy of using returned fluids from drilling as a proxy for formation water like Method 1. As discussed previously, this study operates under the assertion that this is a valid means of analyzing formation water chemistry.

In determining the relationship between deep log resistivity and SC of formation fluids, a simple scatter plot is used to plot the data (Figure 4.3) similarly to Roberts (2001). Since this analysis was restricted to medium-high porosity sandstone beds, the actual formation compositions should be somewhat similar throughout the study area, which would lessen the impact of lithology on log resistivity measurements. However, there are differences in mineralogical composition and other

physical factors like porosity, which is as high as 56% in this dataset, that affect resistivity readings between different formations and data points, accounting for the R^2 value of 0.46.

Due to the poor correlation of the data points to the trend line, the upper envelope trend line of the formation water SC and deep log resistivity relationship was used for Method 2. This step was also taken to assure that this method errs on the side of calculating lower salinity from log resistivity in comparison to Method 1, which may be useful in some environmental or water well applications. By using the upper envelope of data points on the scatter plot, any given deep log resistivity value will correlate to a higher formation water SC value when compared to using the trend line of the entire data set. This means that the particular log resistivity value associated with any given TDS transition will be higher when using the upper envelope trend line. This results in a higher resistivity cutoff corresponding to each TDS transition and, thus, shallower TDS transition elevations than those that would be found using the trend line from the entire data set. Even with using the upper envelope trend line, the Method 2 5,000 mg/L TDS median interface was deeper than Method 1 by 5.4 m (18 ft). Method 2 for this interface was deeper in 31% of wells in which this interface was determined using both methods and by a median of 18.3 m (60 ft). In fact, Method 2 resulted in shallower interface elevations in only 13% of these wells by a median of 40.5 m (133 ft), with 56% resulting in the same elevation for both methods within the same wellbore. The disparities within individual wellbores between Methods 1 and 2 would likely have been much greater, with Method 2 resulting in much deeper interface elevations, had the upper envelope trend line not been utilized.

Another notable pattern is that the difference between the two trend lines decreases with decreasing salinity in Figure 4.3, as the points on the scatter plot show tighter spread with decreasing salinity. It appears on the scatter plot that SC values show greater variability when corresponding resistivity values are less than 100 ohm-m. In the same vein, SC values equal to or greater than approximately 1,000 μS/cm correspond exclusively with deep resistivity values of

less than 100 ohm-m (Figure 4.5). This could simply be a product of drilling, possibly indicating increased mixing of fluids from different horizons in the borehole with increased depth. This could cause dilution of deeper, higher salinity groundwater with shallower, fresher groundwater, which would cause SC measurements for these samples to be low relative to the actual deepest formation water. The deep resistivity measurements on the well logs would be unlikely to be affected by this dilution, causing the relatively lower SC values to correspond with lower resistivity readings deeper in the borehole. By using the upper envelope of the data instead of the entire data set, this potential issue should have a decreased effect on the results of Equation 4.7 since the upper envelope takes into account only the highest SC values and their corresponding deep log resistivity values, which should ensure the SC measurements used for this trend line were not affected by excessive dilution from shallower formations within the borehole.

Comparison of Methods 1 and 2

The main merit Method 1 has over Method 2 is that it accounts for porosity influences as well as log resistivity and groundwater SC when calculating TDS, where Method 2 only uses log resistivity and groundwater SC. This makes Method 1 more accurate in determining TDS, but it is also highly dependent on log data quality. In this study, several well logs showed anomalously high or low TDS calculations from Method 1 in relation to adjacent well logs. These anomalies were almost always attributable to either high or low neutron porosity, density, and/or resistivity curves that were visually apparent when viewing well logs in cross sections with nearby wells (Figure 6.4). These errors were likely due to incorrectly calibrated logging equipment or curves being normalized incorrectly after logging. The errors were often not large and mostly apparent while picking TDS transitions on logs, especially when comparing transition elevations from each method on individual logs. Where questionable porosity data caused large discrepancies or anomalously deep or shallow TDS transition elevations, Method 1 TDS transition elevations were not picked in order to limit the level of uncertainty in the results of this study.

This resulted in fewer data points for TDS transitions from Method 1, especially for the 5,000 mg/L TDS transition, which had 64 data points from Method 1 versus 75 data points from Method 2, and a total of 11 well logs that could only determine this transition from Method 2 and none that were only able to be determined from Method 1. The 10,000 mg/L TDS transition elevations calculated from Method 1 had 71 data points, versus 77 data points with Method 2, so this transition was seemingly less affected inadequate by log porosity data. This is mostly likely due to increased presence of porosity curves with increasing depth in the study area, especially in the interval below surface casing as noted previously.

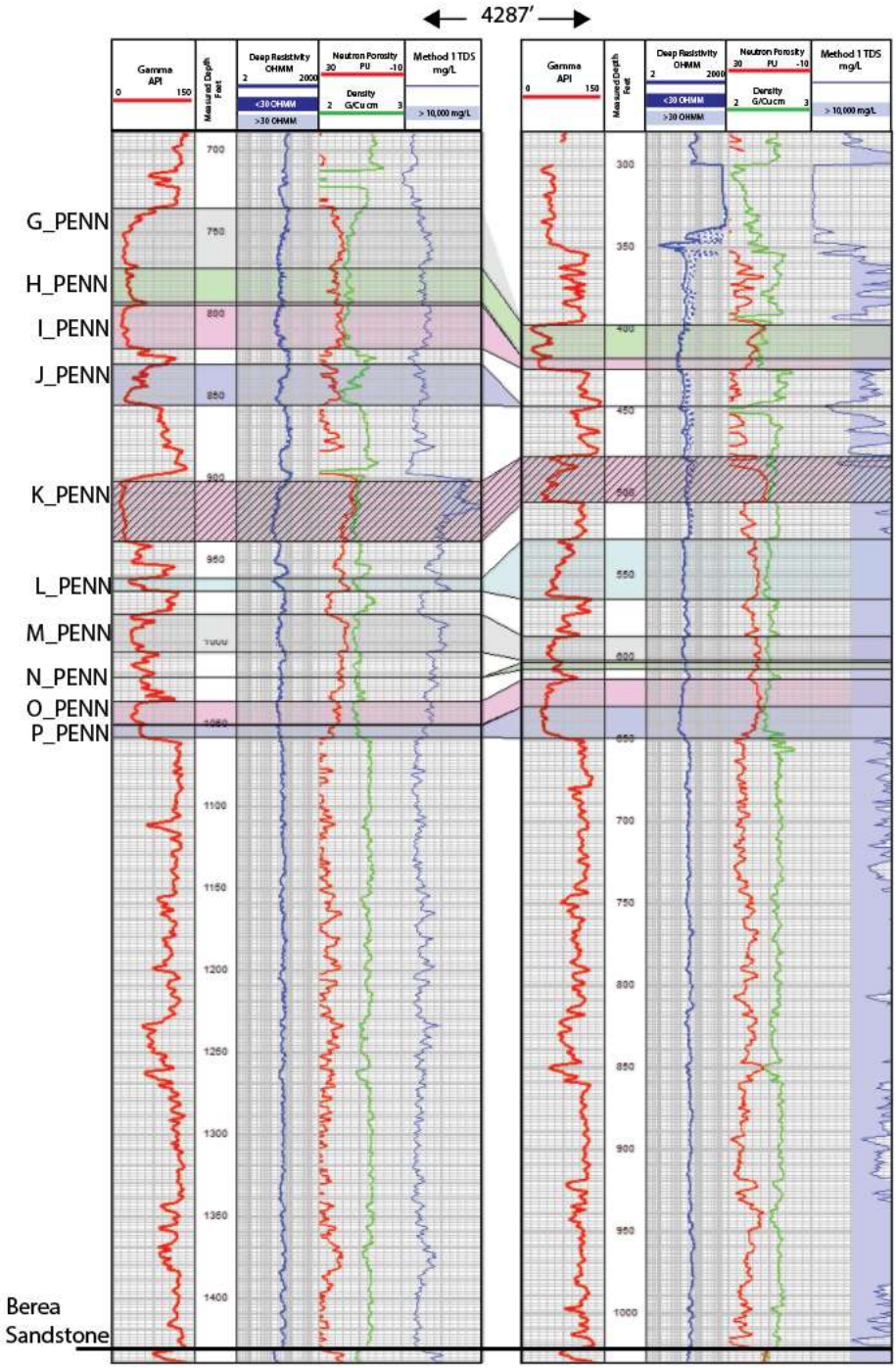

Figure 6.4: The TDS curve in the log on the right shows anomalously high TDS when compared to the left log, which is less than 1.61 km (1 mile) away (both TDS curves are calculated using Method 1). This anomaly was found to be caused by low readings in the resistivity curve, which is especially notable in the shaley sections of the log since the study area typically shows around 30 ohm-m resistivity as in shales as discussed previously. Wells are hung on the top of the Berea Sandstone.

Overall, the results from Method 1 showed shallower 5,000 mg/L TDS transition elevations than Method 2 and deeper 10,000 mg/L TDS transition elevations than Method 2. The Method 1 5,000 mg/L TDS transition elevation showed shallower transitions than Method 2 in 20 wells by a median of 18.3 m (60 ft), with Method 2 showing shallower transitions in 8 wells by a median of 40.5 m (133 ft), and 36 wells showing the same transition elevation for both methods. For the 10,000 mg/L interface, Method 1 determined a deeper transition than Method 2 in 27 wells, as opposed to only 8 wells having a deeper transition as calculated from Method 2. In total, 33 wells had the same transition elevations for both methods. In wells where Method 1 resulted in deeper 10,000 mg/L TDS transitions, the results were a median of 50.55 m (166 ft) deeper than those determined using Method 2.

The fact that Method 1 resulted in shallower interface elevations than Method 2 for the 5,000 mg/L interface despite using the upper envelope was an unexpected result. This may be due to lower porosity in sandstones resulting in Method 1 calculating TDS greater than 5,000 mg/L while deep log resistivity is less than 59 ohm-m, which is the cutoff determined from Method 2 for this TDS interface. Porosity influence is often at least part of the cause of many of the larger TDS elevation disparities in individual wells for both interfaces between Method 1 and Method 2. With average porosity as high as 56% in the dataset, there were many instances of high porosity offsetting the influence of decreasing resistivity during Method 1 TDS calculations, especially in the 10,000 mg/L interface. In some cases, this caused the Method 1 TDS interface to be placed much deeper than the Method 2 interface within the same well. In these instances, Method 1 is likely more accurate than Method 2 as it is based on the relationship between porosity, formation resistivity, and groundwater resistivity, which is designed to account for the influence of both fluids and rock on log resistivity.

The range of discrepancies in elevations between the two methods for the 10,000 mg/L TDS interface within individual wells spans from Method 1 being deeper than Method 2 by 2.74-

202.69 m (9-665 ft) to Method 1 being shallower than Method 2 by 6.09-90.53 m (20-297 ft). There are two wells with greater than 91.44 m (300 ft) of difference between the 10,000 mg/L TDS transition depths calculated from each method, both showing Method 1 deeper than Method 2. These are significant depth differences which would result in very different well casing depths, potentially resulting in negative environmental impacts to the freshwater aquifer depending on which method's results are closer to actual groundwater conditions.

Despite these two wells with large TDS transition depth differences, the majority of the wells in this study show much smaller depth differences between the two methods with 49% of wells that have determinations from both methods showing them both at the same elevation for the 10,000 mg/L interface. Of the 35 wells (51%) that show different elevations between Method 1 and Method 2 results, 10 wells (29%) show 0-15.24 m (0-50 ft) of difference, 5 (14%) show 15.24-30.48 m (50-100 ft) of difference, 11 (31%) show 30.48-60.96 m (100-200 ft) of difference, and 6 show 60.96-91.44 m (200-300 ft) of difference between the elevations as calculated from each method. The differences in the two cases with depth differences greater than 91.44 m (300 ft) can be explained by stratigraphic variances as well as effects of porosity causing Method 1 to deviate from Method 2. These forces often work at the same time and with opposing influences on each method in individual wells, usually causing Method 2 to be much shallower than expected due to missing deeper porous intervals that could allow for a deeper interface to be identified, while at the same time causing Method 1 to result in a deeper interface elevation due to increased porosity in deeper sandstones as resistivity decreases, which results in lower TDS calculations.

An example of this can be seen in the Colescott 11-12-5H well (Figure 6.5). This well shows 202.69 m (665 ft) of difference in the elevations of 10,000 mg/L TDS interfaces between the two methods, and this large difference is partially related to stratigraphic causes including the absence of porous units that cause the Method 2 transition elevation to be greater than 30.48 m (100 ft) shallower than it is in adjacent wells. Additionally, the Method 1 transition elevation is

approximately 30.48-60.96 m (100-200 ft) deeper than adjacent and nearby wells due to slightly higher porosity in the sandstone unit in which this transition occurs. The correlative sandstone unit in the adjacent and nearby wells is slightly greater than 10,000 mg/L TDS, showing that the Method 1 transition elevation difference is not likely due to anomalous log readings, but rather due to differences in porosity related to this well's location within the fluvial depositional structure, as well as increasing salinity within the sandstone unit which cause it to be transitional in the adjacent well. The relatively deeper Method 1 transition combined with the relatively shallower Method 2 transition when comparing this well's log to those of nearby wells cause the large difference between the two elevations, but in reviewing the data from nearby well logs, each depth is easily explained and verified to be accurate.

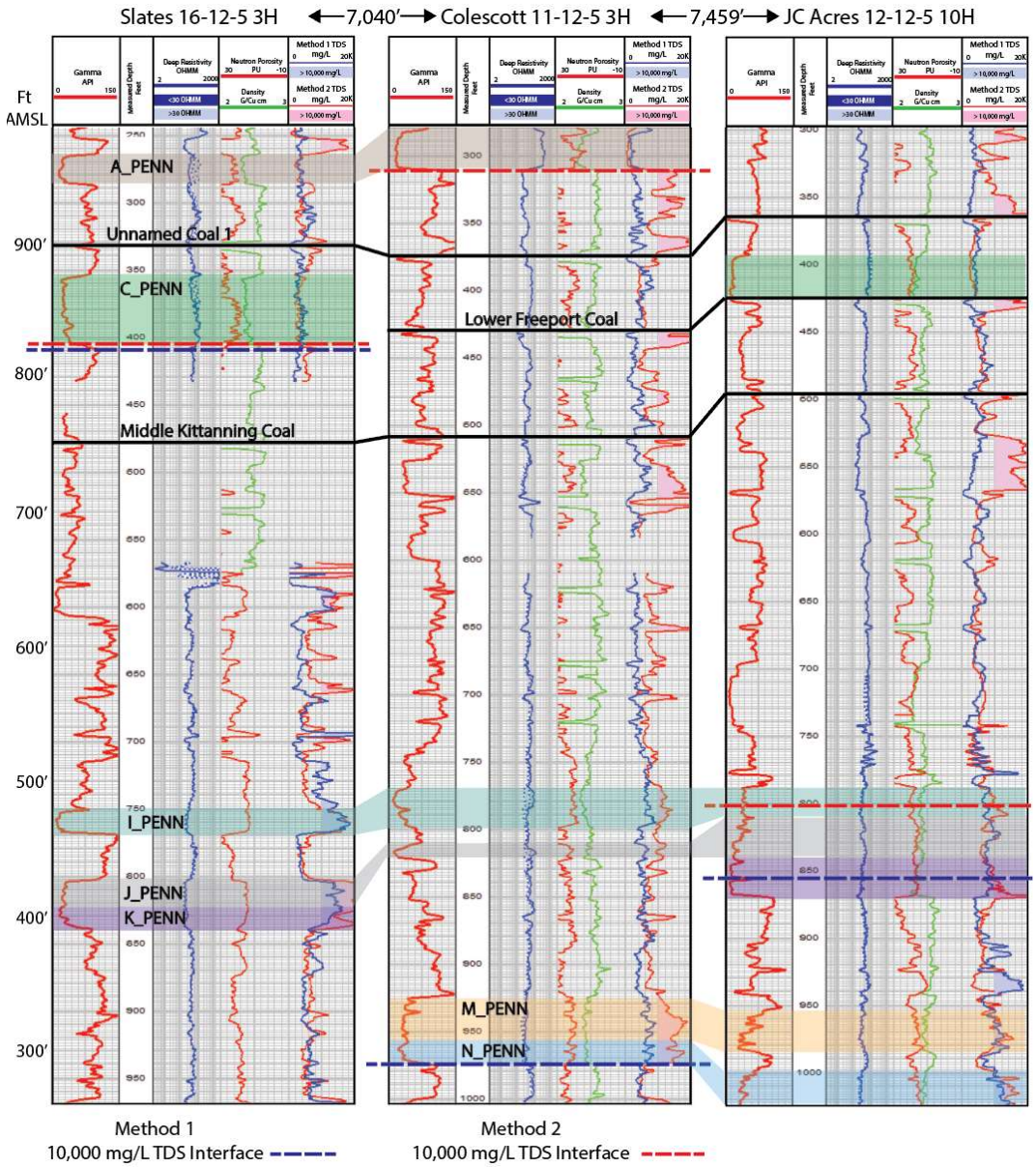

Figure 6.5: The Colescott 11-12-5 3H well shows 202.69 m (665 ft) of difference between the Method 1 and 2 10,000 mg/L TDS interfaces. This cross section shows that this well is missing a porous sand interval between 106.68-137.16 m (350-450 ft) MD (C_PENN) that is visible on adjacent logs, causing the Method 2 interface to be marked at the next-shallowest porous interval. At the same time, the Method 1 interface is deeper than in the adjacent logs due to increased porosity and fresher formation water in the N_PENN sandstone at 281.94-297.18 m (925-975 ft) MD as indicated by relatively higher resistivity.
Note: not all mapped sandstones are shown on these logs, only those relevant to TDS interface zones. Formation colors are correlative. Sea level is structural datum.

Another example of the variation in results between the two methods can be seen in the Mitchell 34-13-5H well, where a transition difference of 174.04 m (571 ft) is again explained by physical

differences in the stratigraphy and porosity (Figure 6.6). The Method 1 transition is slightly deeper than adjacent wells due to higher porosity within the transitional sandstone unit in this well relative to the correlative unit in nearby wells, which causes lower TDS results in Method 1 calculations. The Method 2 transition in this well is slightly shallower than the adjacent wells due to the absence of porous units like the Colescott well as previously discussed, resulting in the large separation between transition elevations calculated from each method.

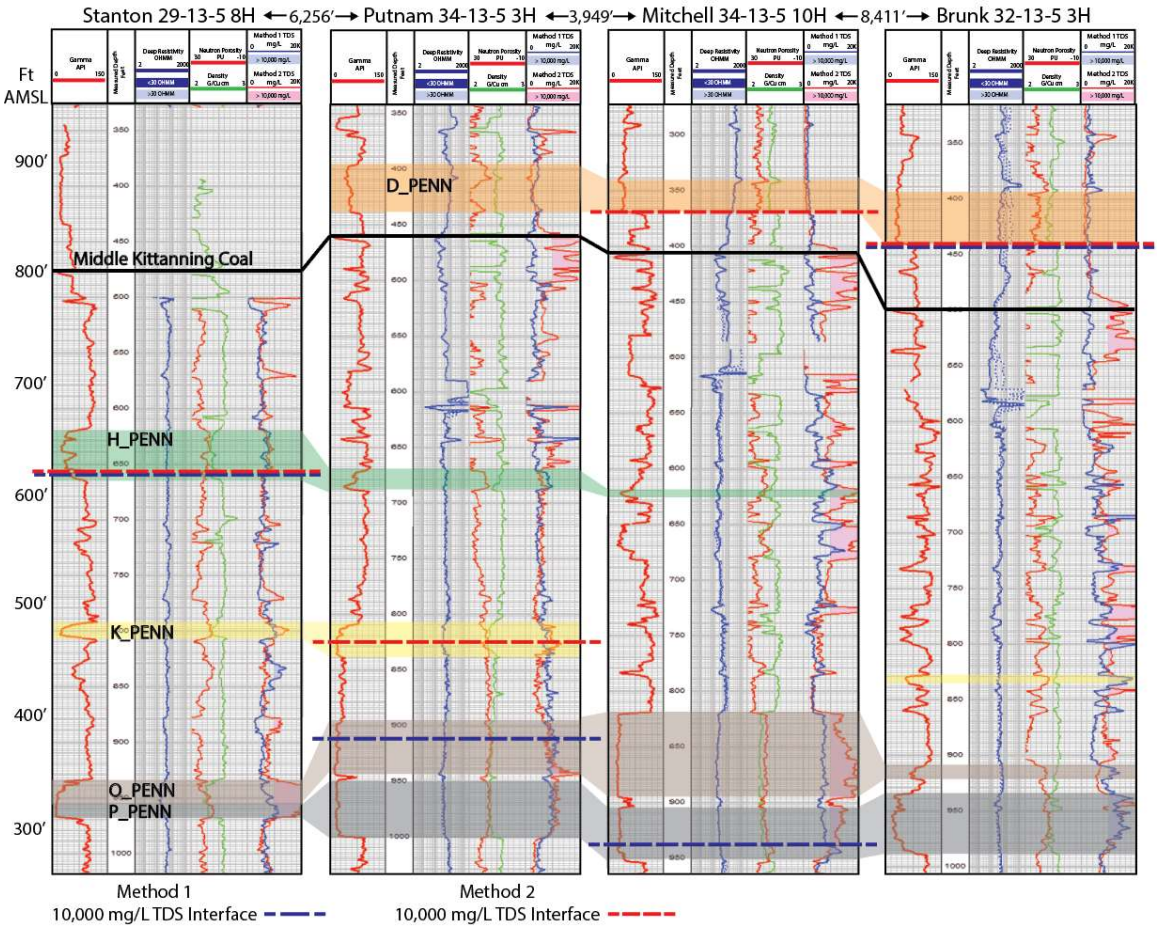

Figure 6.6: The Mitchell 34-13-5 10H well shows a difference of 174.04 m (571 ft) in the 10,000 mg/L TDS interfaces between Method 1 and 2. The Method 1 transition is deeper than that of the adjacent logs due to lower porosity in the correlative sandstone unit within the Mitchell log, which results in lower TDS values calculated from Method 1. The Method 2 interface is shallower than adjacent wells due to absence of correlative porous units in the Mitchell well log. Note: not all mapped sandstones are shown on these logs, only those relevant to TDS interface zones. Formation colors are correlative. Sea level is structural datum.

While Method 1 is more accurate than Method 2 due to the incorporation of porosity into the evaluation, it did result in deeper 10,000 mg/L TDS interface elevations in 38% of wells where both methods were used. With this in mind, the preferred method of TDS calculation when used for any particular study and location may need to be determined based on the environmental application, geologic setting, and data set available. In oil and gas drilling within the study area, state regulations require surface casing to be installed a minimum of 15.24 m (50 ft) below the base of the deepest USDW, which is defined as 10,000 mg/L TDS, and fully cemented from the base of the surface casing string to the top of the wellbore before continuing to drill through formations with greater than 10,000 mg/L TDS groundwater per OAC 1501:9-1 (M)(4). The goal of this rule is to isolate all fresh water behind surface casing to prevent communication of higher salinity formation fluids through the outer annulus of the cased wellbore after cementation, as well as prevent communication between highly saline groundwater in the wellbore with freshwater zones during later drilling operations.

Setting surface casing too deep can allow higher salinity formation fluids to travel up the borehole and into less saline formations during drilling; however, the communication between formations from the base of the surface casing depth to the surface of the wellbore should be cut off after surface casing is installed and cemented properly. On the other hand, when surface casing is set too shallow, it leaves potential drinking water sources below surface casing depth open to contamination by deeper formation fluids with higher salinity, along with potential hydrocarbons during later drilling operations or even during production if they are not isolated behind a cemented intermediate casing string. In the study area, intermediate casing is required when drilling oil and gas wells into, or deeper than, the Marcellus formation, and cement is required to extend 152.4 m (500 ft) past the top of the intermediate casing string and overlap with the surface casing string per OAC 1501:9-1 (M)(6). This allows for additional protection of

shallower formations with less than 10,000 mg/L TDS groundwater as they are further isolated from higher salinity fluids and hydrocarbons from deeper formations.

For determining oil and gas surface casing depths, the potential for contamination of fresh water with saline water is most likely to cause long-term issues if mixing occurs due to casing and cement issues after drilling is complete and production has begun, as opposed to relatively minor mixing that may occur during drilling. Therefore, the conservative method to use for this application would be Method 1 since it results in deeper fresh-saline groundwater interface depths, which would result in deeper surface casing depths and a larger zone protected behind adequately-cemented surface casing. This way, there is reduced long-term potential for direct communication between the shallow freshwater aquifer and deeper hydrocarbon zones or highly saline groundwater zones since the surface casing and cement separates the shallow zone from the annuli of deeper casing strings. For applications such as ensuring fresh groundwater in new drinking water wells, Method 2 may be suitable as it is meant to result in bias towards lower-salinity groundwater correlative to any given log resistivity reading, and would therefore have less potential of resulting in an undesirably saline water well, though the variation in porosity may need to be taken into consideration based on the results of the 5,000 mg/L TDS interface being deeper with this method than Method 1. One additional consideration is that although Method 2 is meant to err on the side of higher resistivity values correlative to any given TDS value (and the actual outcomes varied in this result), the groundwater TDS at surface casing depth for oil and gas wells in the study area is likely still fairly close to 10,000 mg/L, so significantly fresher groundwater would not be left un-isolated below the casing depth.

Overall, each method has merits and drawbacks in data requirements, accuracy, and environmental implications and applications. The application of either method will depend on the unique dataset and hydrogeological conditions for any given study area as well as the purpose of the study. The ability to compare results from each method for a single study area is also

beneficial in evaluating data quality if all required datasets are available, as it lends the possibility of determining sources of discrepancies, as well as ultimately improving confidence in the study's results.

Analysis Improvement

A large component of this study's data was the SC measurements of the returned drilling fluids. While there were procedures in place for sample collection, the nature of oil and gas drilling operations likely have some level of impact on sample test results, and standardizing procedures in this area could offer improved accuracy in the results of the study. Either writing procedures to ensure no drilling fluid additives are used while drilling through the sample collection interval, or at the very least monitoring and recording drilling fluid additives accurately and in a scientific manner would be ideal improvements to this study. Additionally, monitoring the volume of additives and the flow rate at the time of sample collection could allow better SC calibration. This would allow for potential evaluation of the impact certain additives might have on SC sample results, as well as help determine validity of outlier data during the review process.

Additionally, in terms of improving accuracy of sample SC measurements, adding a step to the procedures for filtering sediment from the samples before measurement would be beneficial. This would remove effects of sediment particles on the SC meter readings and improve accuracy of SC measurements of actual groundwater. Furthermore, adding a step to ensure the water samples are within a specific temperature range could be beneficial. This step may not be as important since the readings are corrected to a temperature of 25 degrees Celsius by the meter, but this may reduce potential for error in temperature corrections, especially in very cold samples which were common as shown in the sampling records.

Actual sample collection procedures could potentially be improved by engineering a continuous sample collection method throughout each sampling interval, rather than spot sampling at a

particular footage depth. This would involve setting up a large collection container of some sort to capture returned fluids continuously for 15.24 m (50 ft) and measuring this mixture at the end of each interval, which theoretically would result in an average SC measurement for an entire interval. Additionally, attaching a conductivity probe to the flowline that could measure and record continuous SC data could be another potential way to increase the accuracy of these data. There may be benefits with both of these options as a greater amount of groundwater can be measured, but may not materially improve results, especially since the spot samples collected during this study were tied directly to the correlative log resistivity measurements at each sampling depth. This was done to mitigate erroneous association of any SC measurement at a particular depth with a resistivity value from a different depth within the sampling interval since resistivity values could be quite variable within a 15.24 m (50 ft) interval. Additionally, continuous sample collection may not be physically feasible on an oil and gas drilling rig, not to mention large containers of water can be quite difficult to manage, especially during continuous and often fast-paced drilling operations.

In terms of improving well log data, tool calibration records could aid in determining individual log quality and help decipher if tool error is a cause of apparently anomalous data. Since this information was handled by third-party vendors, there was no way to acquire this information for this particular study. Records such as these could help improve confidence in the data, and thus, the results of the study.

Other Methods

Each of the two methods used in this study incorporates principles from multiple studies discussed in Chapter II, with some slight alterations due to this particular study area and available datasets. One main factor that sets this study apart, and has been discussed throughout this study, is the method of gathering groundwater samples from which to measure SC. The lack of deep

water wells or scientific test wells throughout the study area, in concert with the abundance of oil and gas air-rotary drilling operations, led to the opportunity to capture groundwater samples through less conventional means. Although this method can lead to greater amounts of potential sample contamination, careful review of the sampling results reduced the likelihood of errors impacting the results of the study. While this method of groundwater sample collection is not common in similar studies, it is not unheard of and was evaluated with positive results by Brassington and Taylor (2012).

The relationships between R_w, R_t, and formation porosity used in this study were discussed in Archie (1942) and have been used in other groundwater salinity studies (Turcan, 1962; Roberts, 2001). Method 1 does not stray from Archie's (1942) relationship (Equation 3.1) but does rely on manipulation of the original equation. The assumptions are discussed previously in this chapter. One notable issue with using Archie's (1942) equation is that it was designed for use in saltwater-bearing formations, specifically NaCl-dominant water (Roberts, 2001; Gaither, 1994). To address this, the data for this study were parsed similarly to Roberts (2001) and only water greater than 3,000 mg/L TDS was included in the analysis when determining the mathematical relationship for calculating TDS using porosity and R_t (Equations 5.4 and 5.6).

Method 2 is most similar to the methods described by Turcan (1962) and Roberts (2001). These authors specifically used the relationship of R_w and R_t to calculate formation factor (F) for each well (Equation 3.2), then averaging those values to find F for the study area. This value for F was then used to determine R_t values that directly correspond to specific TDS values for that study area. Method 2 ultimately uses this principal and determines a direct relationship of log resistivity and TDS values, but through direct comparison of formation water SC and log resistivity instead of converting SC to R_w first. This difference does not materially change the relationship used in Method 2 from that used by Turcan (1962) and Roberts (2001) since it is only forgoing the unit

conversion of SC to resistivity. It ultimately results in a slightly simpler method to determine this relationship for the study area.

One other way Method 2 differs from previous methods is that instead of averaging individual ratios of R_t/R_w to find F for the study area like Turcan (1962) and Roberts (2001), this method involves plotting SC and log resistivity on a scatter plot and determining a mathematical relationship from the trend line of these data. This method leads to a more accurate mathematical relationship than calculating a mean F for the study area, as the data is less convoluted this way since it is a direct comparison of all data points. The method accounts for potential changes over different resistivity and conductivity ranges. The importance of this is illustrated by the resultant exponential equation for the trend line, which shows that the data relationship is not linear. This method is also arguably simpler and should yield more predictive results due to a more representative relationship between the data, and it also allows objective evaluation of the data relationship.

This study includes the final step of using the upper envelope trend line to determine the final formation water SC and log resistivity relationship instead of the trend line of the entire data set. This was done for environmental implications unique to this study's location and purpose, as it results in TDS corresponding to relatively higher resistivity values, ensuring that this method is not under-estimating groundwater salinity from well log data. Since one of the purposes of this study was to compare Methods 1 and 2 for oil and gas surface casing applications, and since this study area is far from arid with average annual precipitation between 93.98 and 99.06 cm (37 and 39 inches), opting to use the upper envelope ensured results erred on the side of fresher groundwater protection, rather than protecting a larger quantity of potentially more saline water. In other studies, depending on the application of this method as well as the quality of the data relationship as shown in the R^2 value, this step may or may not be useful.

Both of the TDS calculation methods used in this study are based off of methods described in previous peer-reviewed literature (Archie, 1942; Turcan, 1962; Roberts, 2001; Brassington and Taylor, 2012; Robinson and Lupton, 2018). The changes applied to those methods for this study are based on the unique study site, study purpose, and application of the methods, and they also result in higher accuracy of TDS calculations. The general agreement of results between the two methods in this study increase confidence in the accuracy of both. Additionally, by using two methods to calculate TDS, this study also reveals the significant impact the local stratigraphy has on groundwater movement and recharge in the study area, as discussed in the analysis of the three wells with large elevation differences in the 10,000 mg/L TDS transition calculated from each method. As discussed previously, each method has merits and drawbacks, so the choice to use one or both will depend which is most useful based on study purposes, study area, and data set.

CHAPTER VII

CONCLUSION

Through integration of geophysical well log data and fluid SC data collected during oil and gas drilling operations, the elevation of the fresh-saline water interface for Carroll County, Ohio has been determined and mapped. Two separate methods of determining groundwater TDS from these data are outlined, each with distinct merits and drawbacks and each suited to different datasets, study purposes, and study areas. The comparison of the results of each of these methods during this study ultimately leads to increased confidence in both methods due to the mostly small magnitude of differences in TDS interface depths determined from each method in individual well logs, as well as the reasons for the few larger discrepancies.

One key aspect of the success of each of these two methods was the thorough review of all data for quality control purposes prior to inclusion in the study. This included initial review of fluid SC data and well logs, as well as further review of anomalous data throughout the study. This was especially important since much of the data was captured during drilling operations in a field environment, which meant the data had higher potential for measurement and/or recording errors. Fortunately, due to the abundance of data collected in the study area, there were ample data available that passed quality control reviews and allowed for lateral comparisons between wells.

The stratigraphic analysis performed during this study revealed that the rapidly changing stratigraphy has a large control on groundwater movement in the study area. The fluvial depositional environment resulted in complex layering of porous sandstone beds and low-porosity shale beds in the Pennsylvanian aquifer interval, restricting groundwater flow to specific porous zones. Due to this, delineating the connectivity of porous sandstone beds was imperative to this study's results. This stratigraphic analysis was integrated with the groundwater TDS analyses to aid in interpretation of TDS transition depth contour patterns during mapping, ultimately resulting in accurate and predictive fresh-saline groundwater interface depth maps.

As a result of this study, four separate maps were created for the study area: two maps of the 5,000 mg/L TDS transition elevation as determined from each of the two methods, and the same for the 10,000 mg/L TDS transition elevation. The 1,000 mg/L TDS interface was not able to be mapped since it was presumably above the top of the shallowest data in most logs. While no maps were able to be made, this result allows us to draw the conclusion that the 1,000 mg/L interface is generally likely to be shallower than 61 meters (200 ft) BGS in the study area.

Using the four maps created from this study, elevations of the 10,000 mg/L and 5,000 mg/L TDS interfaces can be accurately predicted throughout the study area by utilization of the maps for each respective TDS value. This has regulatory implications for the study area, which include safer oil and gas well casing designs that better protect fresh groundwater resources. With two maps available for each TDS cutoff, the decision of which map to reference will depend on the method that best suits the purpose of the map user and the study area, though since Method 1 results in a much more accurate calculation of groundwater TDS from well logs than Method 2 due to the incorporation of porosity, the Method 1 interface maps are likewise more accurate maps of each interface elevation. Where the need to protect greater quantities of potentially treatable groundwater prevails, such as with oil and gas surface casing operations, Method 1 may be the better choice not only because it is more accurate, but also because it results in deeper

transition depths, and thus a higher volume of groundwater being isolated. In drinking water well applications, where there is far lower likelihood of porosity data being available and the priority is to have low-salinity groundwater suitable for human consumption, Method 2 may be more beneficial since it does not require porosity data and it skews towards calculating higher groundwater TDS from correlative resistivity values on well logs, resulting more conservative water well depths that are unlikely to penetrate undesirably saline groundwater.

Overall, the methods of this study show two means of calculating groundwater TDS from well logs and fluid SC data, as well as integration of stratigraphic analysis to create predictive fresh-saline groundwater interface maps. These robust methods have resulted in maps of 5,000 mg/L and 10,000 mg/L TDS transition elevations for the study area, which did not exist previously. These maps may be useful for regulatory and other environmental applications within the study area, and the methods may be applied to other areas where sufficient data sets exist.

REFERENCES

Adams, M., Eddy, G., Hewitt, J., Kirr, J. and Rightmire, C., 1984. Geologic overview, coal resources, and potential methane recovery from coalbeds of the northern Appalachian coal basin – Pennsylvania, Ohio, Maryland, West Virginia, and Kentucky in AAPG SG 17: Coalbed Methane Resources of the United States, p. 15-43.

Alger, R. P., 1966. Interpretation of electric logs in fresh water wells in unconsolidated formations: Transactions of the 7th Annual Symposium of the Society of Professional Well-Log Analysts, Tulsa, Oklahoma, May 8011, p. 1-25.

Alger R. P. and Harrison, C. W., 1989. Improved fresh water assessment in sand aquifers utilizing geophysical well logs: The Log Analyst, v. 30, no. 1, p. 31-44.

Alqahtani, F. A., 2013. Subsurface analysis of fluvial systems of Epsilon and Toolachee formations, Cooper Basin, Australia: Arab J Geosci (2015) v. 8, p. 3285-3297, DOI: 10.1007/s12517-014-1344-8.

Archie, G. E., 1942. The electrical resistivity log as an aid in determining some reservoir characteristics: Transactions of the A.I.M.E., v. 146 (1942), p. 54.

Arp, J. J., 1953. The effect of temperature on the density and electrical resistivity of sodium chloride solutions: Journal of Petroleum Technology., v. 5, no. 10, p. 17-20.

Atwia, M. G., Hassan, A. A., and Ibrahim, Sh. A., 1997. Hydrogeology, log analysis, and hydrochemistry of the unconsolidated aquifers south of El-Sadat City, Egypt: Hydrogeology Journal, v. 5, no. 2, p. 27-38.

Asquith, G. and Krygowski, D., 2004. Basic well log analysis: AAPG Methods in Exploration 16.

Barker, R. A. and Ardis, A. F., 1996. Hydrogeologic framework of the Edwards-Trinity aquifer system, west-central Texas: USGS Professional Paper 1421-B, 61 p.

Becker, J. B., 2013. A combined field, laboratory, and numerical study of cutter roof failure in Carroll Hollow Mine, Carroll county, Ohio (UMI no. 1572870) [Master's thesis, University of Akron, Ohio]. ProQuest UMI Dissertation Publishing.

Belknap, W. B., Dewan J. T., Kirkpatrick, C. V., Mott, W. E., Pearson, A. J., Rabson, W. R., 1959. API calibration facility for nuclear logs: Drilling and Production Practice. American Petroleum Institute, 289-316.

Beuthin, J. D., 1994. A sub-Pennsylvanian paleovalley system in the central Appalachian Basin and its implications for tectonic and eustatic controls on the origin of the regional Mississippian-Pennsylvanian unconformity, *in* Dennison, J. M. and Ettensohn, F. R., eds. Tectonic and Eustatic Controls on Sedimentary Cycles: SEPM, Concepts in Sedimentology and Paleontology 4, p. 107-120.

Branson, C., 1962. Pennsylvanian system of central Appalachians, *in* C. Branson, ed., Pennsylvanian system of the United States: AAPG Special Publication 23, p. 97-116.

Brassington, F. C. and Taylor, R., 2012. A comparison of field methods used to define saline-fresh groundwater interfaces at two wites in north west England: Quarterly Journal of Engineering Geology and Hydrogeology, v. 45, p. 173-181, DOI: 10.1144/1470-9236/11-018.

Bridge, J. S. and Tye, R. S., 2000. Interpreting the dimensions of ancient fluvial channel bars, channels, and channel belts from wireline-logs and cores: AAPG Bulletin, v.84, no. 8, p. 1205-1228.

Carter, D. C., 2003. 3-D seismic geomorphology: insights into fluvial reservoir deposition and performance, Widuri field, Java Sea: AAPG Bulletin, v. 87, p. 909-934.

Channas, J., 1971. Petroleum Potential of Ohio: Region 10, *in* AAPG Memoir 15: Future Petroleum Provinces of the United States – Their Geology and Potential, v. 2, p. 1254-1257.

Coogan, A. H., 1994. Shallow Berea sandstone gas fields on the Suffield fault zone, Portage county, Ohio: Ohio Geological Society Second Annual Technical Symposium: Major Natural Gas Plays of the Appalachian Basin of Ohio and Surrounding areas, Canton, Ohio, 10 p.

Crawley, A. and Atkinson, C. H., 1982. An approximation of continuity of lenticular Mesaverde sandstone lenses, utilizing close-well correlations, Piceance Basin, northwest Colorado: Western Gas Sands Project, 32 p.

Donselaar, M. E. and Overeem, I., 2008. Connectivity of fluvial point-bar deposits: an example from the miocene Huesca fluvial fan, Ebro Basin, Spain: AAPG Bulletin, v. 92, no. 9, p. 1109-1129.

Eberle, M. and Razem, A. C., 1985. Effects of surface coal mining and reclamation on ground water in small watersheds in the Allegheny plateau, Ohio: USGS Water-Resources Investigations Report 85-4205, 17 p.

Elizalde, C., Grifffiths, W. A. and Miller, T., 2016. Thrust fault nucleation due to heterogeneous bedding plane slip: evidence from an Ohio coal mine: Engineering Geology, v. 206, p. 1-17.

Fanty, F. and Catuneanu, O., 2010. Fluvial sequence stratigraphy: the Wapiti Formation, west-central Alberta, Canada: Journal of Sedimentary Research, v. 80, p. 320-338, DOI: 10.2110/jsr.2010.033.

Flores, R. M., 1984. Comparative analysis of coal accumulation in cretaceous alluvial deposits, southern United States Rocky Mountain basins *in* The Mesozoic of Middle North America: Canadian Society of Petroleum Geologists Memoir 9, p. 373-385.

Gaither, B. E., 1994. Some considerations in the application of wireline logging to environmental investigations: Gulf Coast Association of Geological Societies Transactions, v. 44, p. 237-244.

Gibling, M. R., 2006. Width and thickness of fluvial channel bodies and valley fills in the geological record: a literature compilation and classification: Journal of Sedimentary Research, v. 76, no. 5, p. 731-770.

Gillespie, H., Kong, D. and Anderson, S. D., 2018. Groundwater salinity in the southern San Joaquin Valley: AAPG Bulletin, v. 101, no. 8, p. 1239-1261.

Gray, J. D., Struble, R. A., Carlton, R. W., Hodges, D. A., Honeycutt, M., Kingsbury, R. H., Knapp, N. F., Majchszak, F. L. and Stith, D. A., 1982. An integrated study of the Devonian-age black shales in eastern Ohio: US DOE, DOE/ET/12131-1399.

Hamlin, S. H. and de la Rocha, L., 2015. Using electric logs to estimate groundwater salinity and map brackish groundwater resources in the Carrizo-Wilcox aquifer in south Texas: Gulf Coast Association of Geological Societies Journal, v. 4, p. 109-131.

Hem, J. D., 1985. Study and interpretation of the chemical characteristics of natural water, third edition: USGS Water-Supply Paper 2254.

Hansen, M. C. and Fox, J. L., 2020. Earthquakes in Ohio: Ohio DNR Educational Leaflet No. 9.

Jordan, D. W. and Pryor., W. A., 1992. Hierarchical levels of heterogeneity in a Mississippi River meander belt and application to reservoir systems: AAPG Bulletin, v. 76, no. 10, p. 1601-1624.

Lockett, J. R., 1927. General structure of the producing sands in eastern Ohio: AAPG Special Publication 3: Structure of Typical American oil Fields, v. 1, p. 138-147.

McAuley, S. D. and Kozar, M. D., 2006. Ground-water quality in unmined areas and near reclaimed surface coal mines in north and central Appalachian coal regions, Pennsylvania, and West Virginia: USGS Scientific Investigations Report 2006-5059 57 p.

Mrakovich, J. V. and Coogan, A. H., 1974. Depositional environment of the Sharon Conglomerate member of the Pottsville Formation in northeastern Ohio: Journal of Sedimentary Petrology, v. 44, no. 4, p. 1186-1199.

Nadon, G. C. and Kelly, R. R., 2004. The constraints of glacial eustasy and low accommodation on sequence-stratigraphic interpretations of Pennsylvanian strata, Conemaugh Group,

Appalachian Basin, U.S.A., *in* Pashin, J. C. and Gastaldo, R. A. eds, Sequence stratigraphy, paleoclimate, and tectonics of coal-bearing strata: AAPG Studies in Geology 51, p. 29-44.

Ohio Division of Geological Survey, 1990 (rev. 2000, 2004). Generalized column of bedrock units in Ohio: Ohio Department of Natural Resources, Division of Geological Survey, 1p.

Ohio DNR GIS Mapping Services, accessed March 2022. Shapefiles available online at https://gis.ohiodnr.gov/arcgis_site2/rest/services

Ohio EPA, 2008. Ohio's Ground Water Quality: 2008 305(b) Report, 94 p.

Ohio EPA Ambient Ground Water Quality Monitoring Program, 2016. Inorganic ground water well summary report (multiple), www.epa.ohio.gov/ddagw, accessed March 2020.

Potter, P. E., DeReamer, J. H. Jackson, D. S. and Maynard, J. B., 1983. Lithologic and environmental atlas of Berea Sandstone (Mississippian) in the Appalachian Basin: Appalachian Geological Society Special Publication No. 1, 157 p.

Razem, A. C. and Sedam, A. C., 1985. Ground-water quality and geochemistry of aquifers associated with coal in the Allegheny and Monongahela formations, southeastern Ohio: USGS Water-Resources Investications Report 85-4034, 39 p.

Riley, R. A., Mcdonald, J. and Martin, D. R., 2012. Elevation contours on the base of deepest underground sources of drinking water in Ohio: Columbus, Ohio Department of Natural Resources, Division of Geological Survey, Map EG-6, scale 1:500,000.

Roberts, J., 2001. Characterizing and mapping the regional base of an underground source of drinking water in central Oklahoma using open-hole geophysical logs and water quality data: Prepared for the Ground Water Protection Research Foundation, Oklahoma City, OK.

Robinson, M. C., and Lupton, D. M., 2018. Brackish groundwater resources of the Northern Trinity Aquifer, Texas: Gulf Coast Association of Geological Societies Transactions, v. 68, p. 445-459.

Root, S. I. and MacWiliams, R. H., 1986. The Suffield Fault, Stark County, Ohio: Ohio Journal of Science, v. 86, no. 4, p. 161-163.

Root, S. I. and Martin, R. J., 1995. The influence of basement tectonics on oil and gas traps in eastern Ohio: a synthesis: Structural Influences on Oil and Gas Reservoirs: Third Annual Technical Symposium, October 25, 1995, p. 31-47.

Sanders, L., 1991. Geochemisty of formation waters from the lower Silurian Clinton formation (Albion sandstone), eastern Ohio: AAPG Bulletin, v. 75, no. 10, p. 1593-1608.

Ryder, R. T. and Zagorski, W. A., 2003. Nature, origin, and production characteristics of the Lower Silurian regional oil and gas accumulation, central Appalachian basin, United States: AAPG Bulletin, v. 87, no. 5, p. 847-872.

Shepherd, M., 2009. Meandering fluvial reservoirs *in* M. Shepherd, Oil field production geology: AAPG Memoir 91, p. 261-272.

Siegel, D. I., Smith, B., Perry, E., Bothun, R. and Hollingsworth, M., 2015. Pre-drilling water-quality data of groundwater prior to shale gas drilling in the Appalachian basin: analysis of the Chesapeake Energy Corporation dataset: Applied Geochemistry, v. 63, p. 37-57.

Stout, W., 1944. Sandstones and Conglomerates in Ohio: Ohio Journal of Science, v. 44, no. 2, p. 75-88.

Stout, W., Lamborn, R. E. , Ring, D. T., Gillespie, J. S. and Lockett, J. R., 1935, Natural gas in central and eastern Ohio, in H. A. Ley, ed.,Geology of Natural Gas: AAPG Special Publications 7, p. 897-914

Sunwall, M. T. and Pushkar, P., 1979. The isotopic composition of strontium in brines from petroleum fields of southeastern Ohio: Chemical Geology, v. 24, p. 189-197.

Tasker, T. L., Warner, N. R. and Burgos, W. D., 2020. Geochemical and isotope analysis of produced water from the Utica/Point Pleasant shale, Appalachian basin: Environmental Science: Processes and Impacts, v. 22, p. 1224-1232.

Thomas, M. A., 2018. Chemical and isotopic characteristics of methane in groundwater of Ohio, 2016: USGS Scientific Investigations Report 2018-5097, 42 p.

Tiab, D. and Donaldson, E. C., 2015. Reservoir Characterization, *in* Tiab, D. and Donaldson, E. C., eds: Theory and Practice of Measuring Reservoir Rock and Fluid Transport Properties, p. 583-640.

Tibert, N. E. and Gibling, M. R., 1999. Peat accumulation on a drowned coastal braidplain: the Mullins Coal (upper carboniferous), Sydney Basin, Nova Scotia: Sedimentary Geology v. 128, p. 23-28.

Tomastik, T. E., 1995. History and reservoir analysis of the Berea sandstone in the Chatham oil field, Medina County, Ohio: Ohio Geological Society Third Annual Technical Symposium: Structural Influences on Oil and Gas Reservoirs, 25 p.

Turcan, A. N. Jr., 1962. Estimating water quality from electrical logs: Geological Survey Research, Baton Rouge, LA, article 116, p. C135-C136.

Van Horn, S. R., Esselburn, J. D. and Tarbert, J. A., 2007. Major-ion chemistry of surface water and identification of hydrogeochemical processes in a recovering surface-mined watershed, The Wilds, southeastern Ohio: GSA Denver Annual Meeting (28-31 October, 2007), GSA Abstracts with programs, v. 39, no. 6, p. 405.

Ver Steeg, K., 1944. Some structural features of Ohio: The Journal of Geology, v. 52, no. 2, p. 131-138.

Walker, A. C., 1991. Groundwater resources of Carroll County Map: Ohio Department of Natural Resources, Division of Water.

Waxman, M. H. and Smits, L. J. M., 1968. Electrical conductivities in oil-bearing shaley sands: Society of Petroleum Engineers Journal, v. 8, p. 107-122.

Whieldon, C. E. and Pierce, C. I., 1965. Oilfield in Mahoning, Columbiana, Carroll, Jefferson, and Harrison counties, Ohio: U. S. Bureau of Mines Information Circular 8250, 20 p.

YSI, 2017. EcoSense EC300A EcoSense EC300M User Manual, Document 606042REF.

APPENDICES

Sandstone Thickness and Structure Maps

This appendix contains all thickness and structure of the top and base of each mapped sandstone formation.

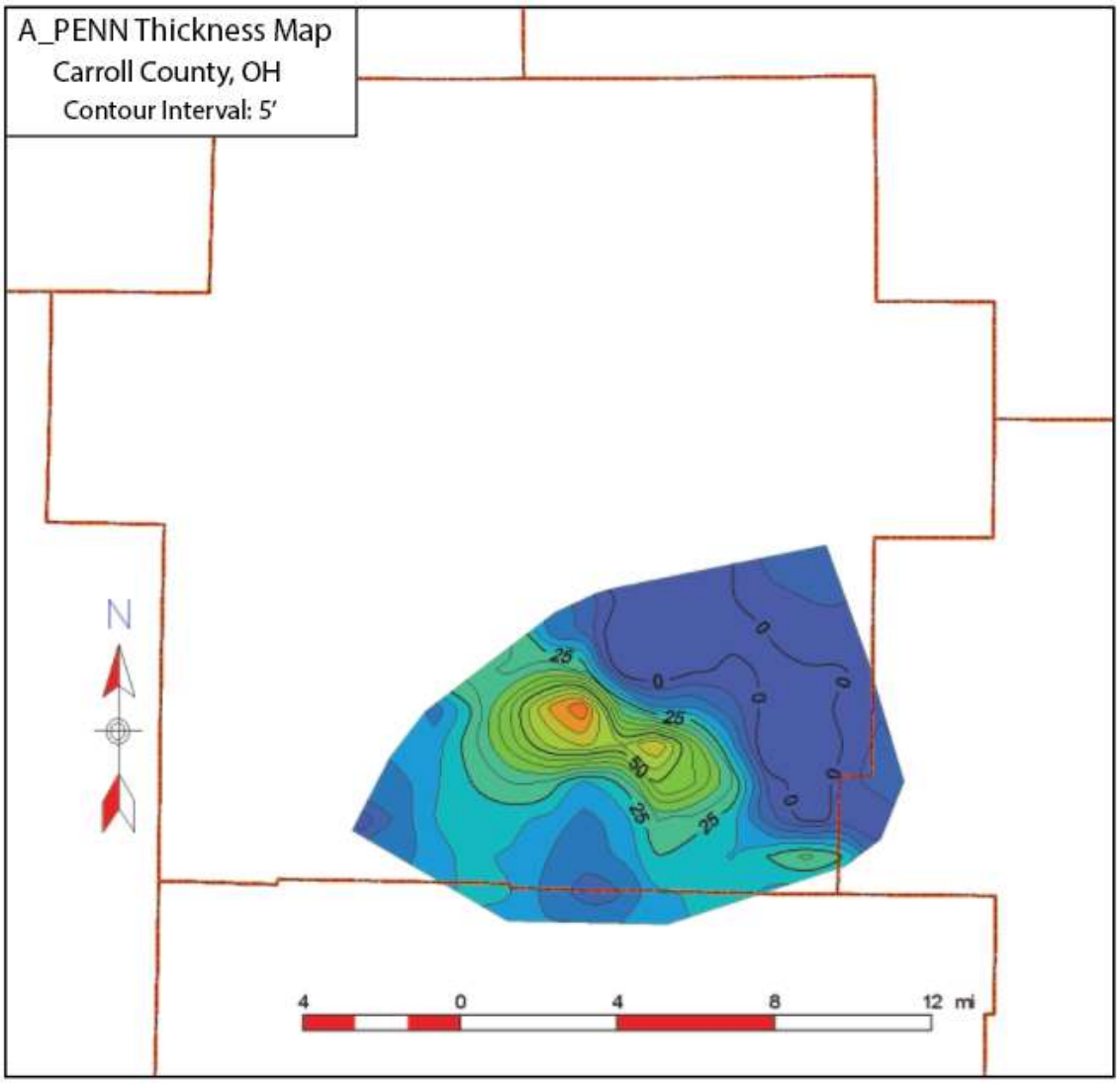

Figure A1: Thickness map of the A_PENN formation.

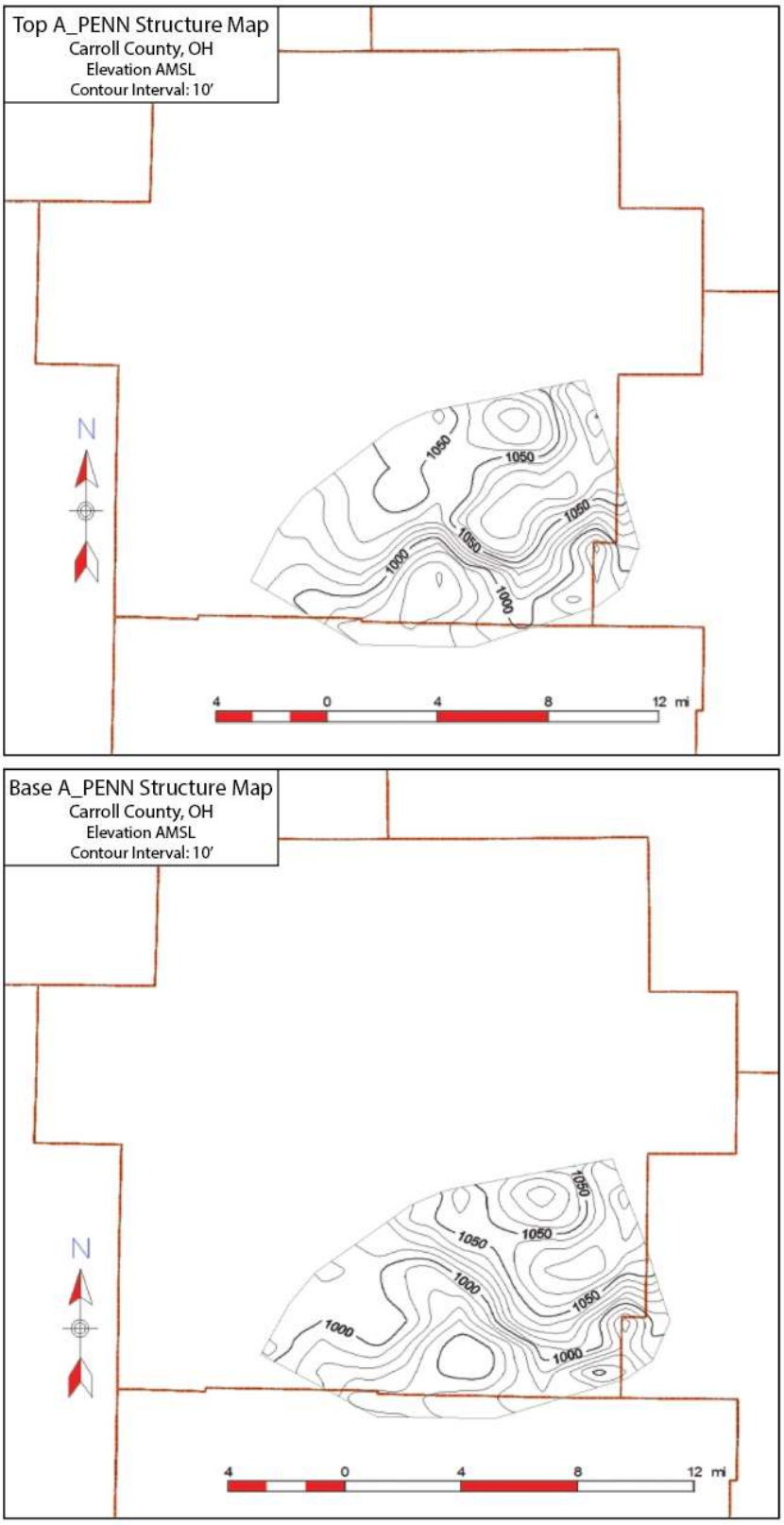

Figure A2 (Upper): Structure map of the top of the A_PENN formation.
Figure A3 (Lower): Structure map of the base of the A_PENN formation.

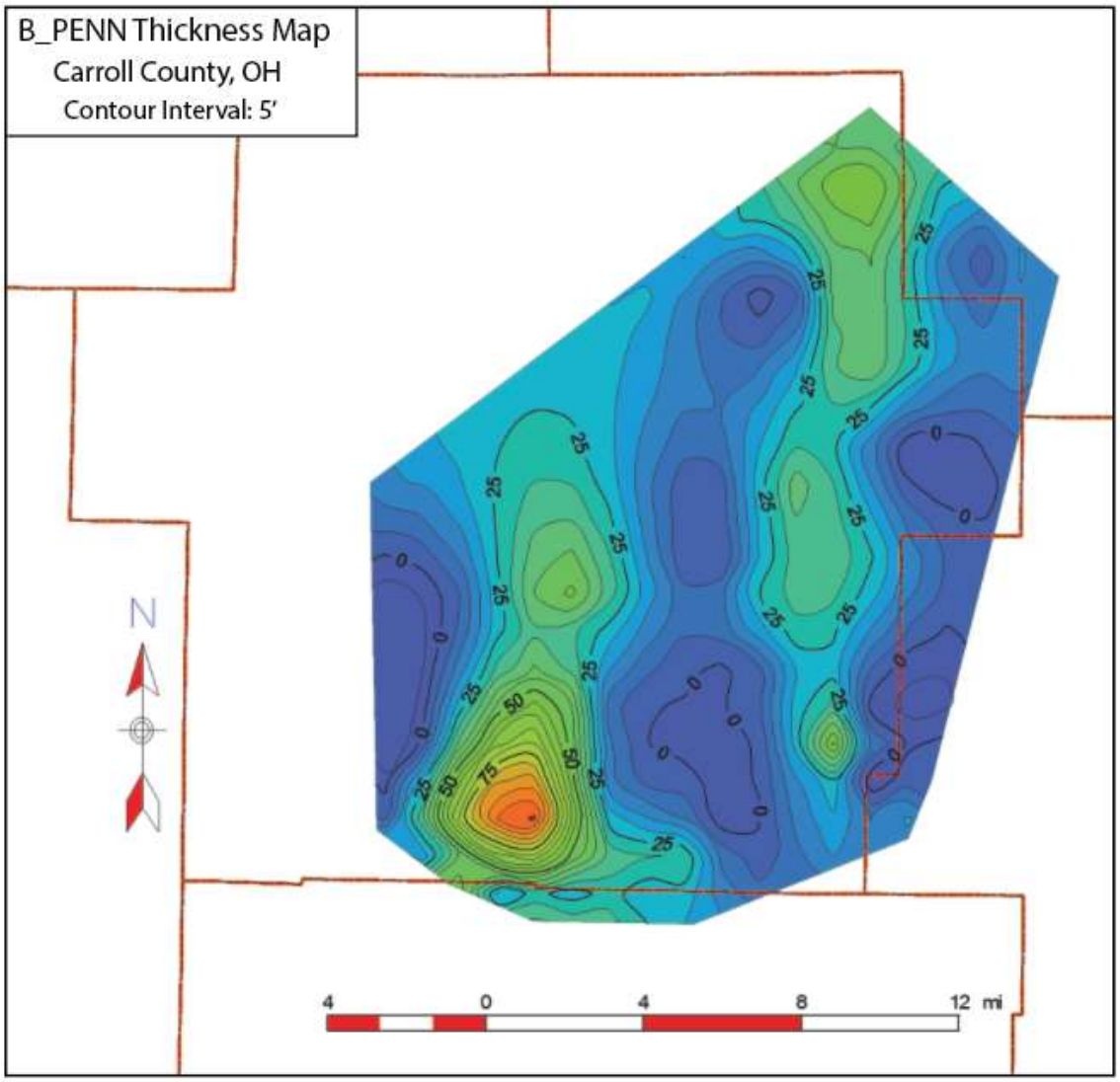

Figure A4: Thickness map of the B_PENN formation.

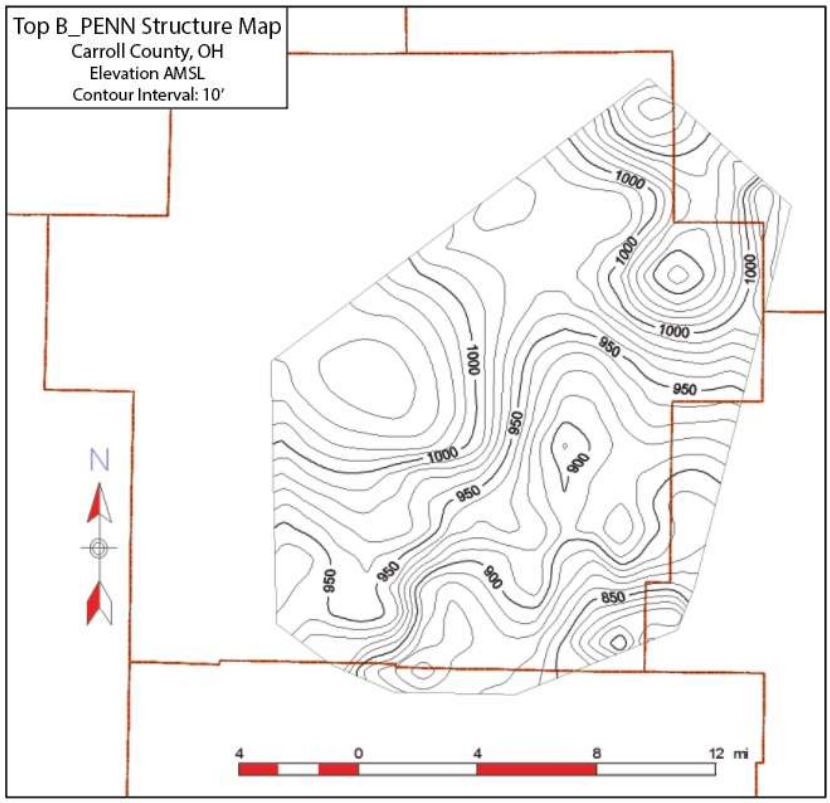

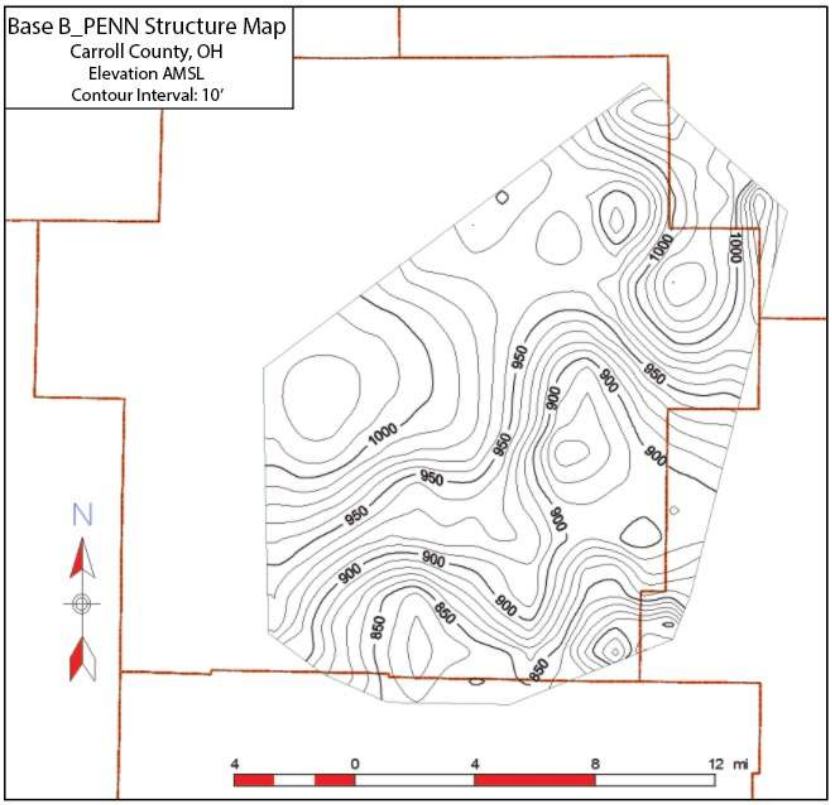

Figure A5 (Upper): Structure map of the top of the B_PENN formation.
Figure A6 (Lower): Structure map of the base of the B_PENN formation.

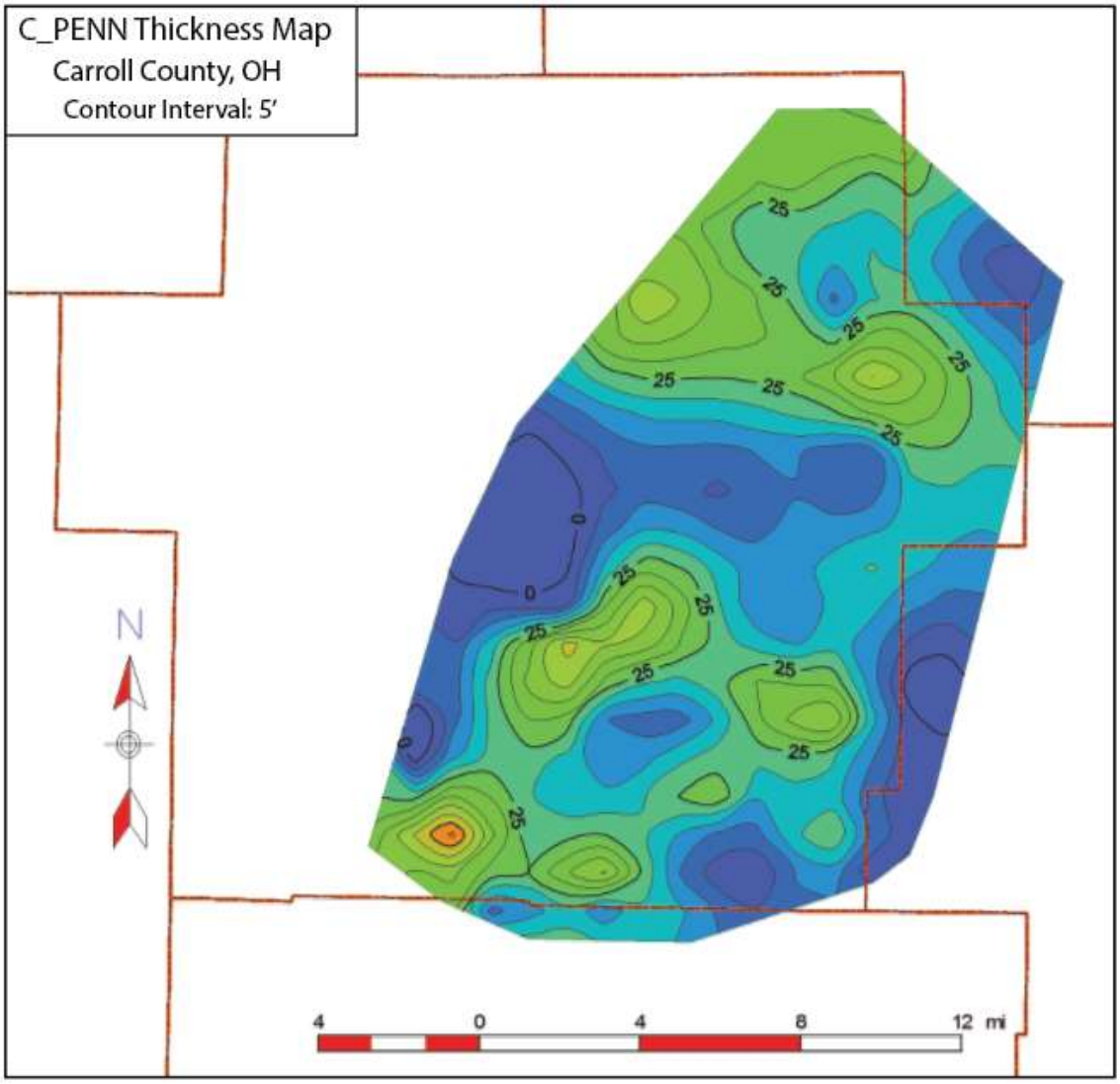

Figure A7: Thickness map of the C_PENN formation.

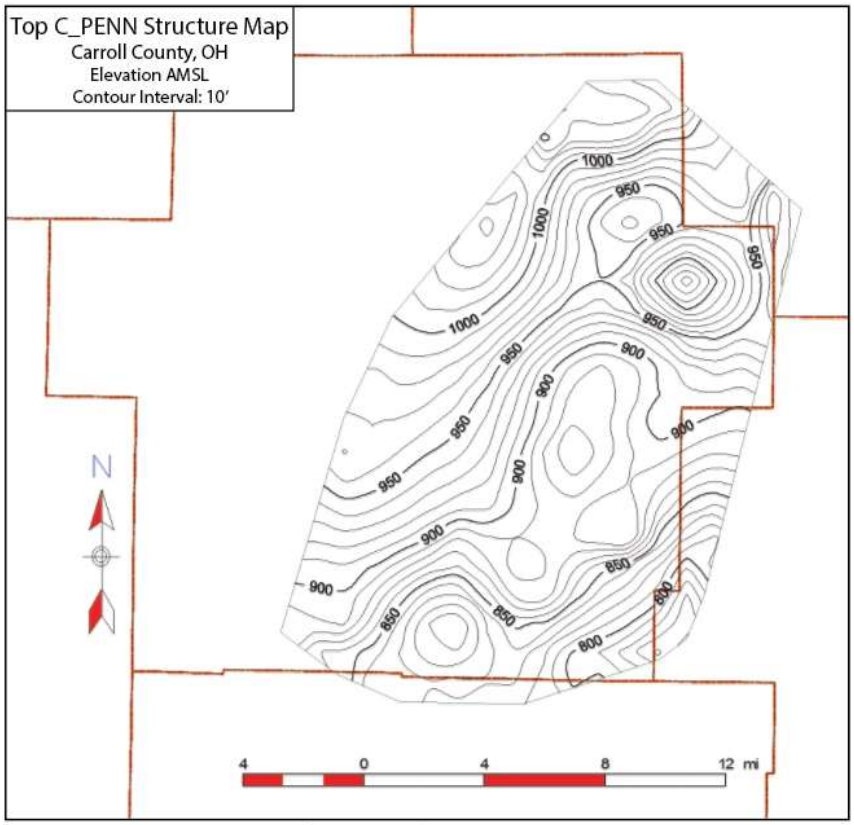

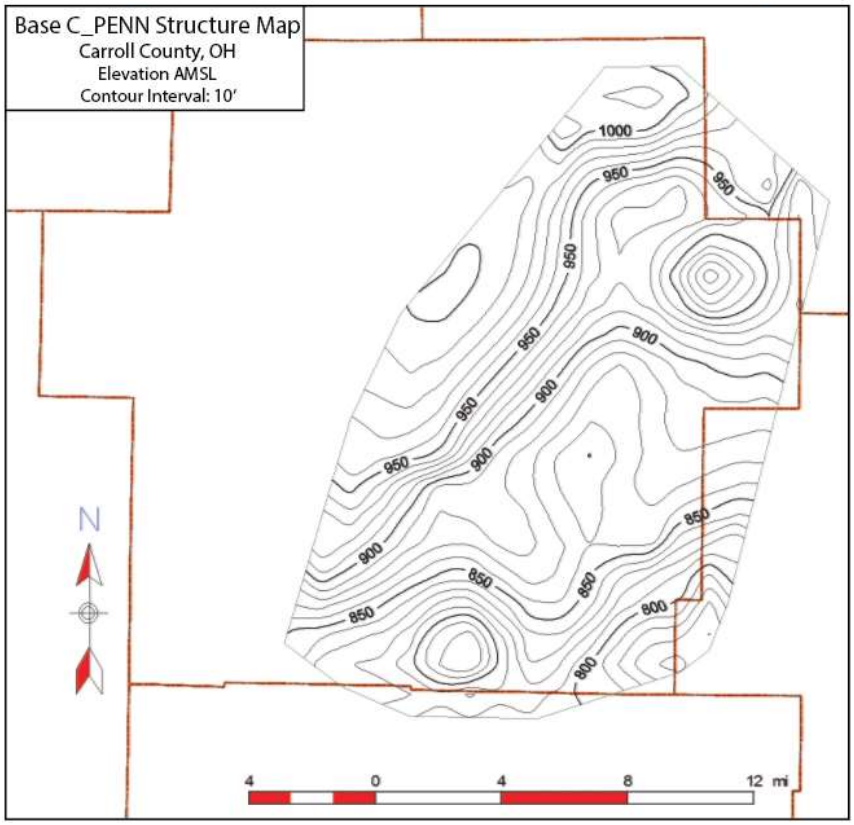

Figure A8 (Upper): Structure map of the top of the C_PENN formation.
Figure A9 (Lower): Structure map of the base of the C_PENN formation.

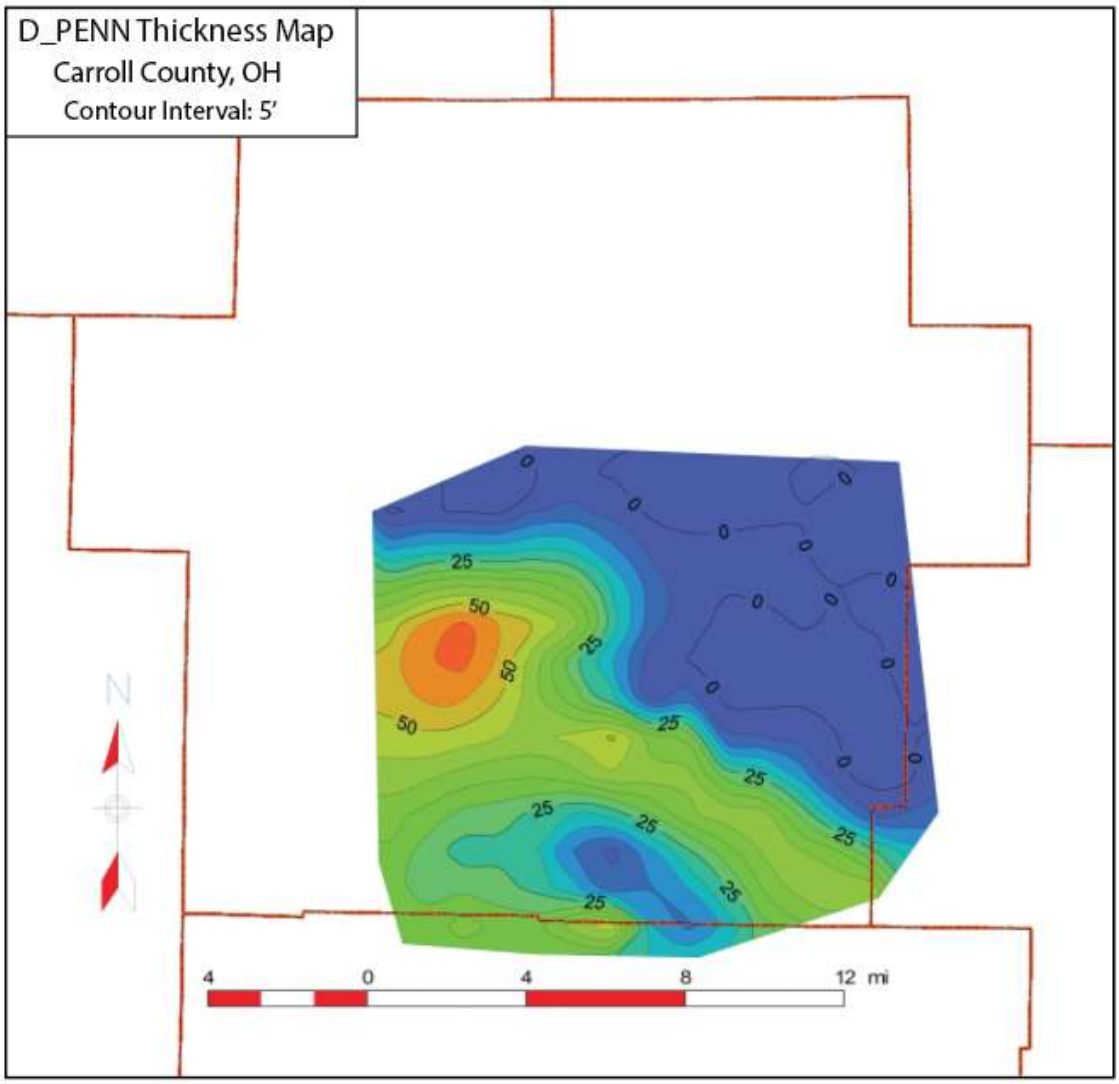

Figure A10: Thickness map of the D_PENN formation.

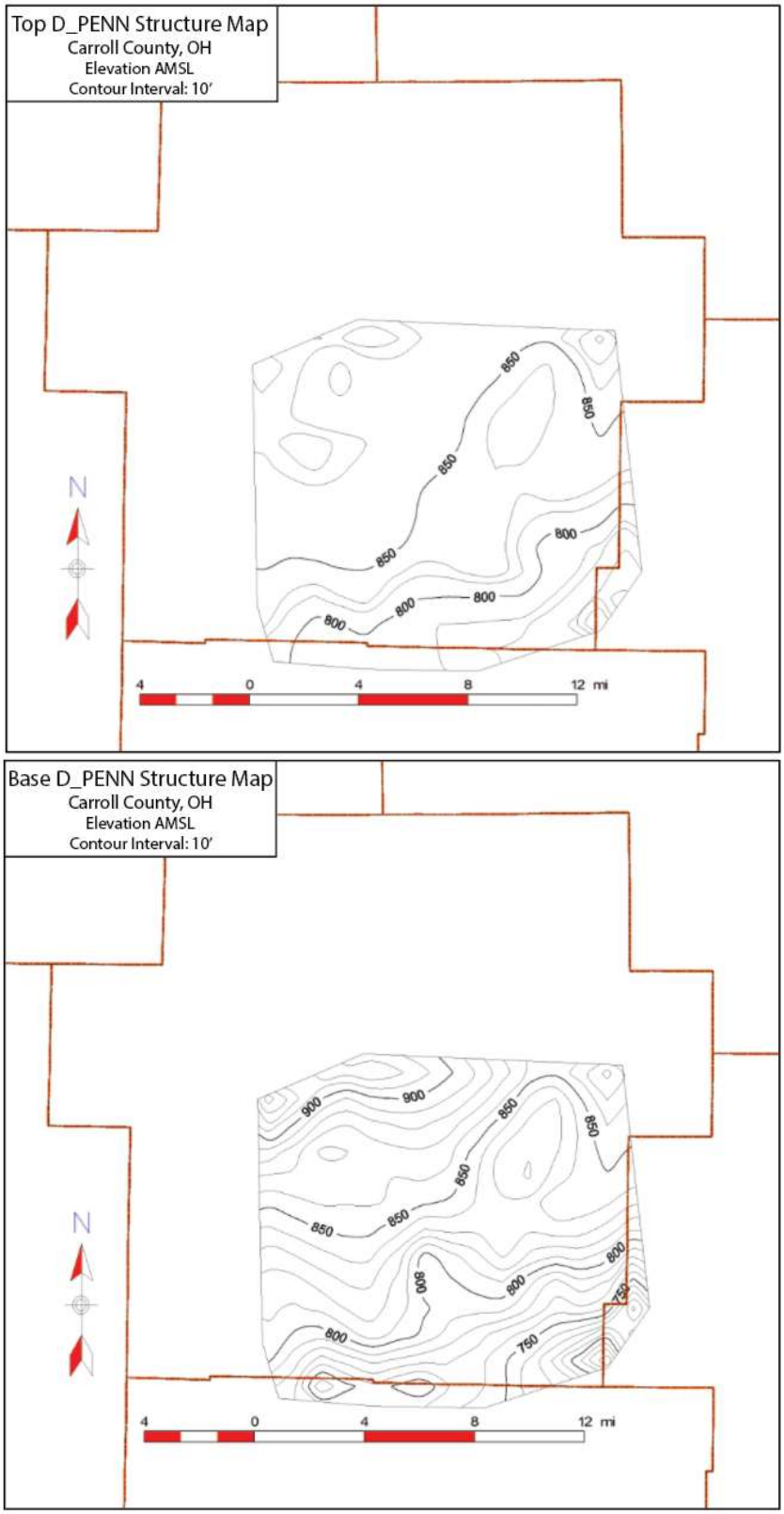

Figure A11 (Upper): Structure map of the top of the D_PENN formation.
Figure A12 (Lower): Structure map of the base of the D_PENN formation.

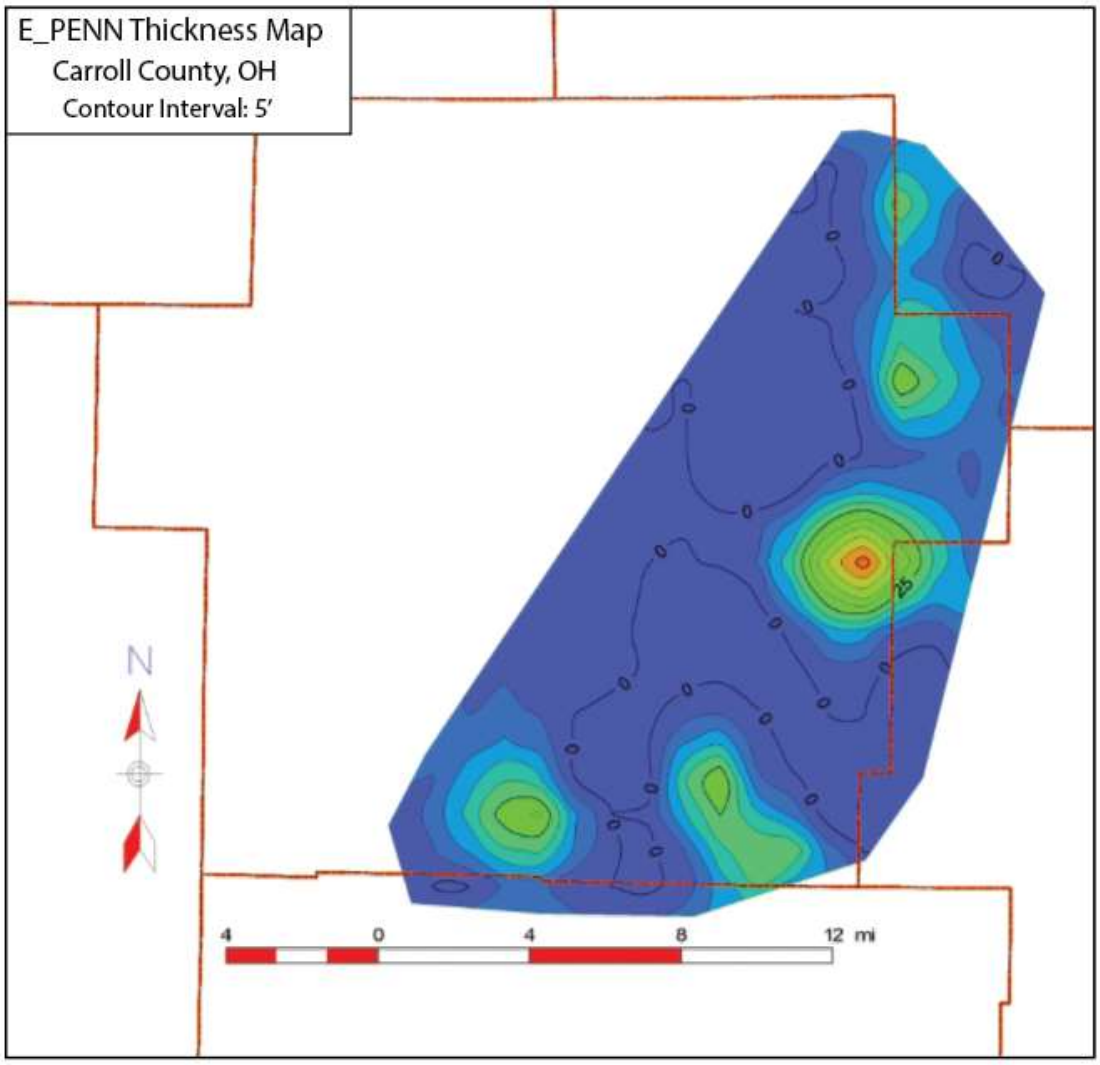

Figure A13: Thickness map of the E_PENN formation.

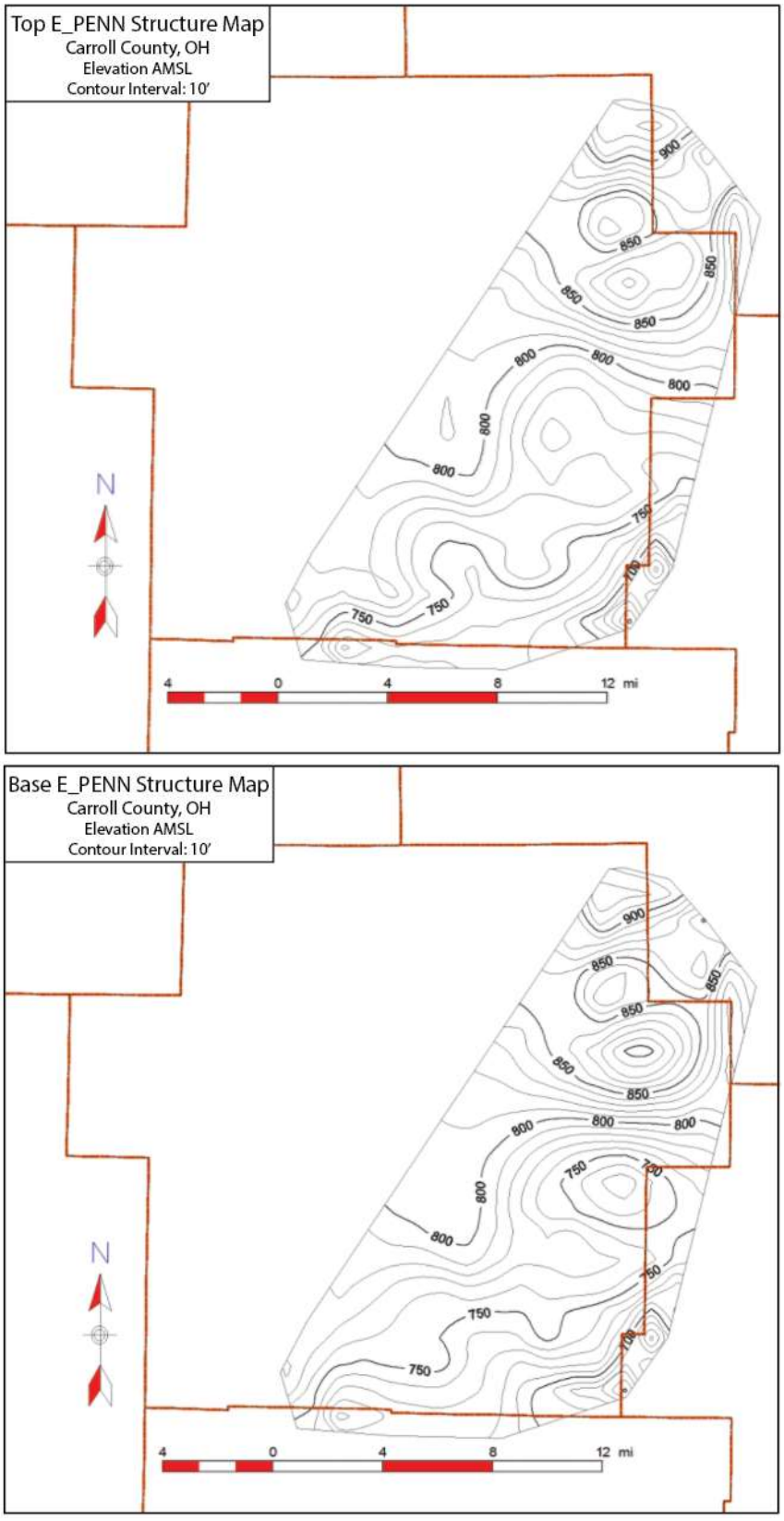

Figure A14 (Upper): Structure map of the top of the E_PENN formation.
Figure A15 (Lower): Structure map of the base of the E_PENN formation.

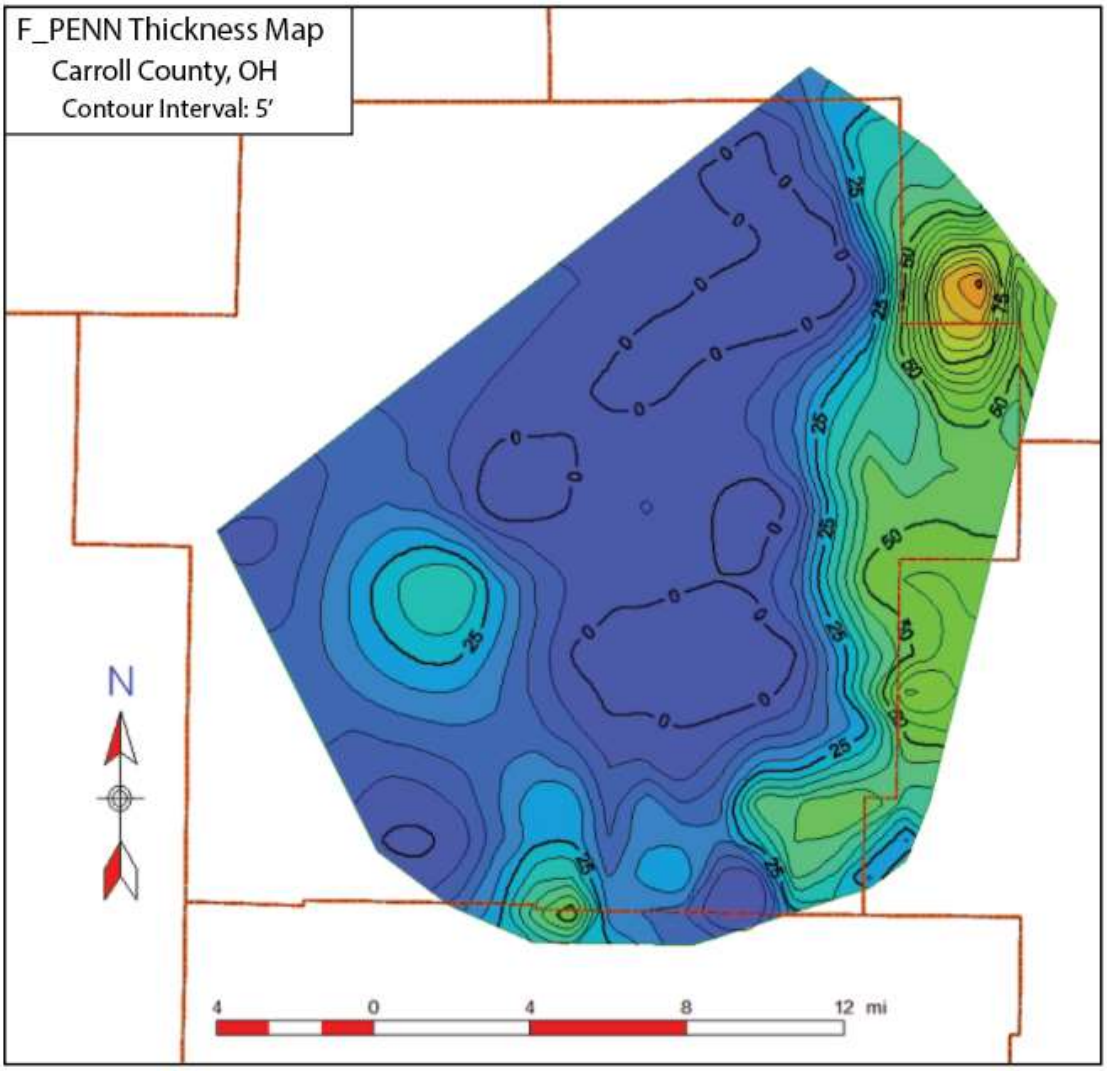

Figure A16: Thickness map of the F_PENN formation.

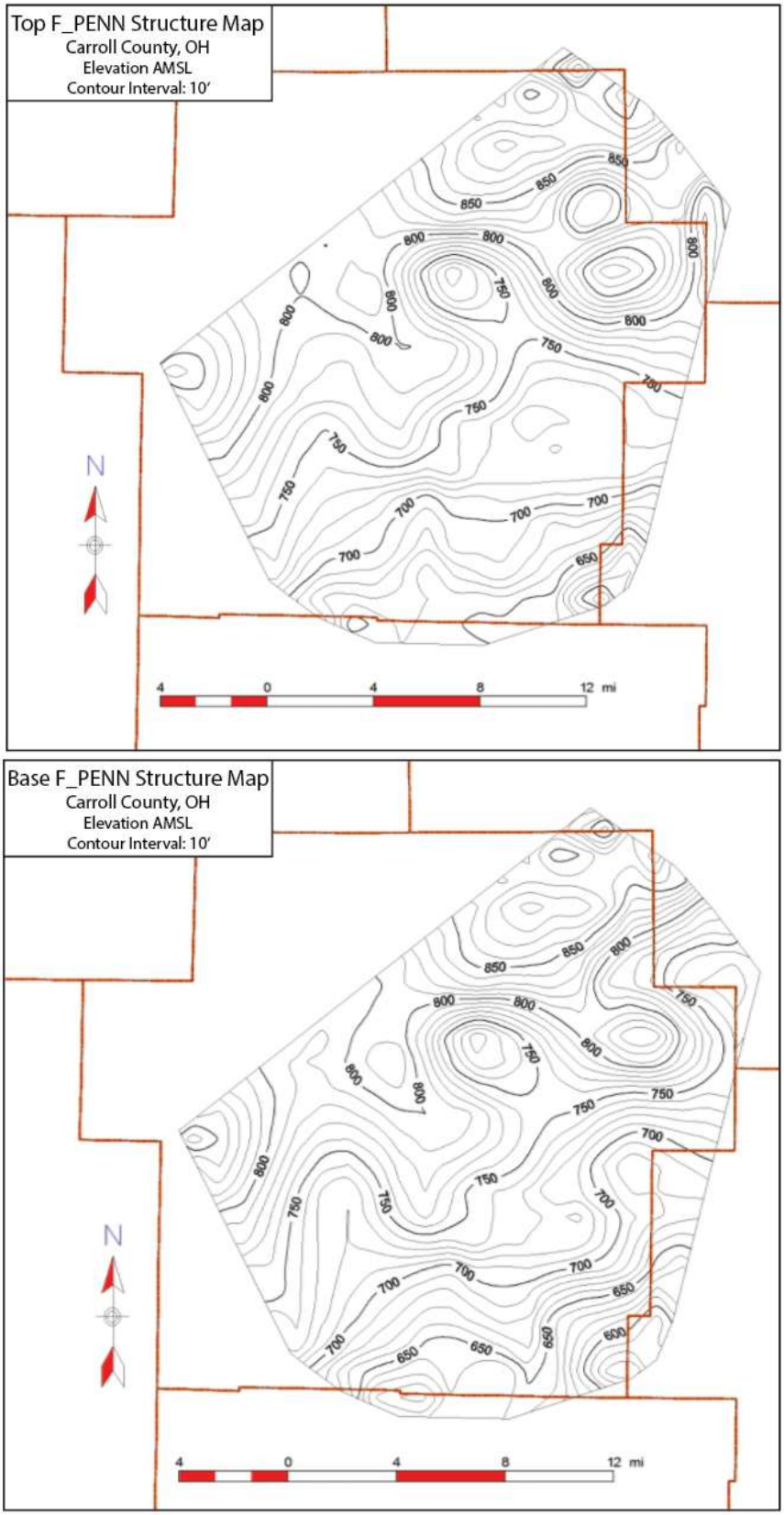

Figure A17 (Upper): Structure map of the top of the F_PENN formation.
Figure A18 (Lower): Structure map of the base of the F_PENN formation.

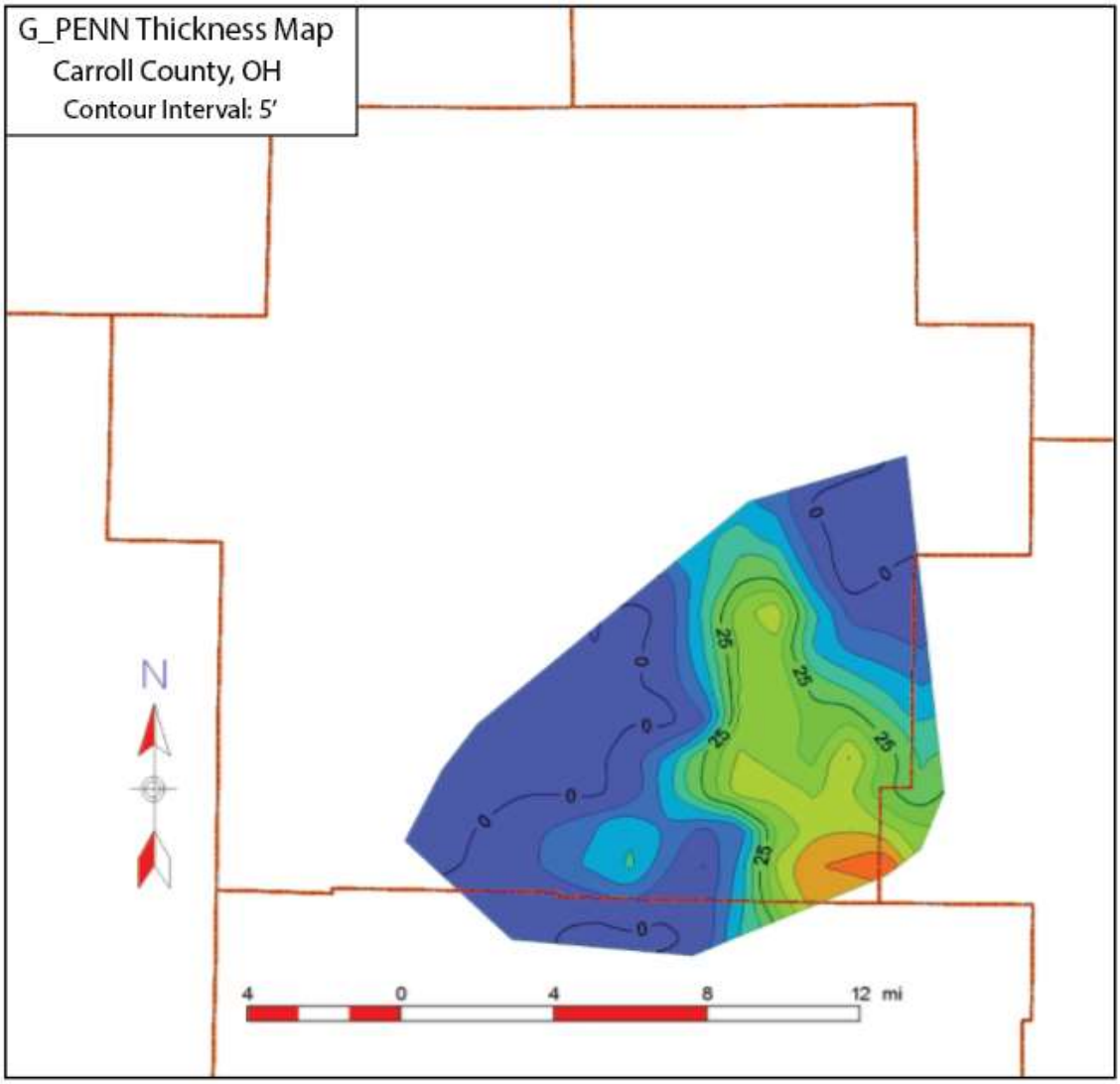

Figure A19: Thickness map of the G_PENN formation.

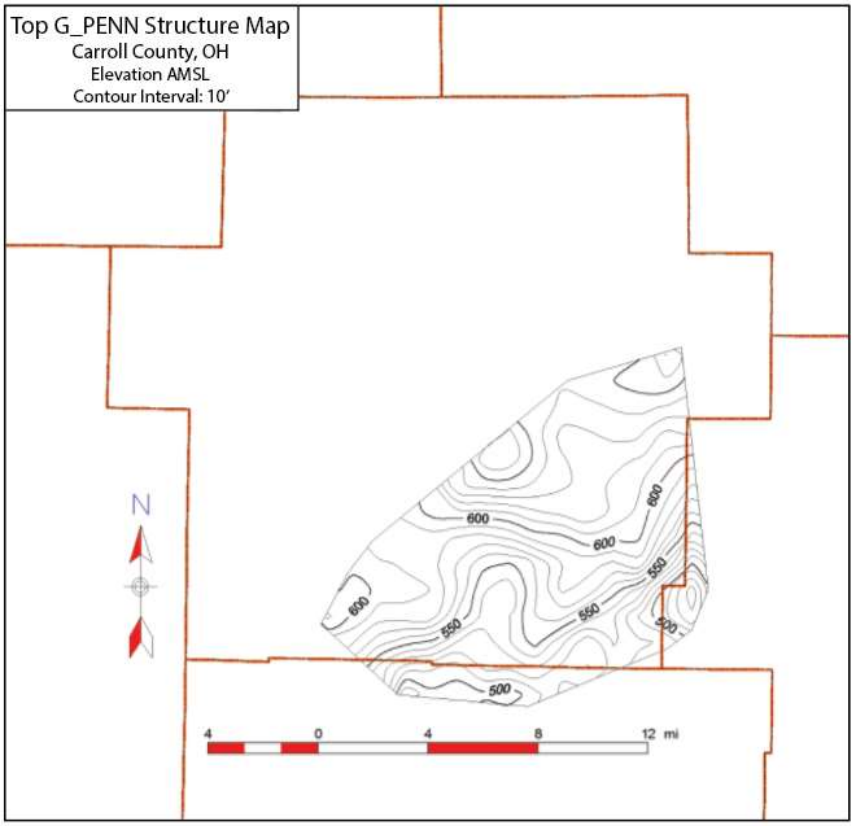

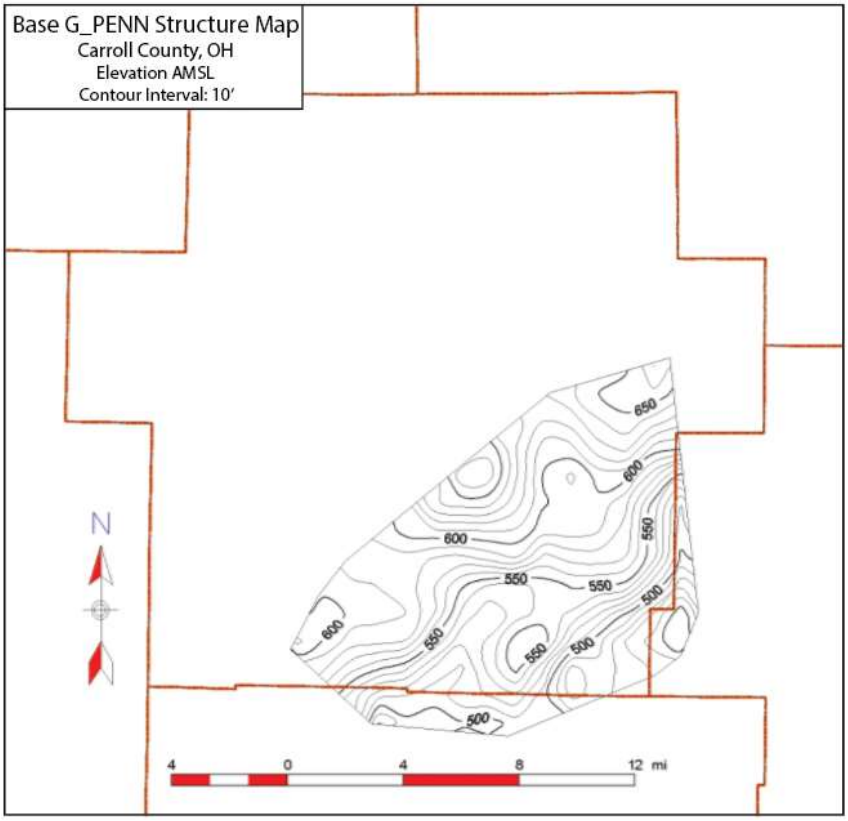

Figure A20 (Upper): Structure map of the top of the G_PENN formation.
Figure A21 (Lower): Structure map of the base of the G_PENN formation.

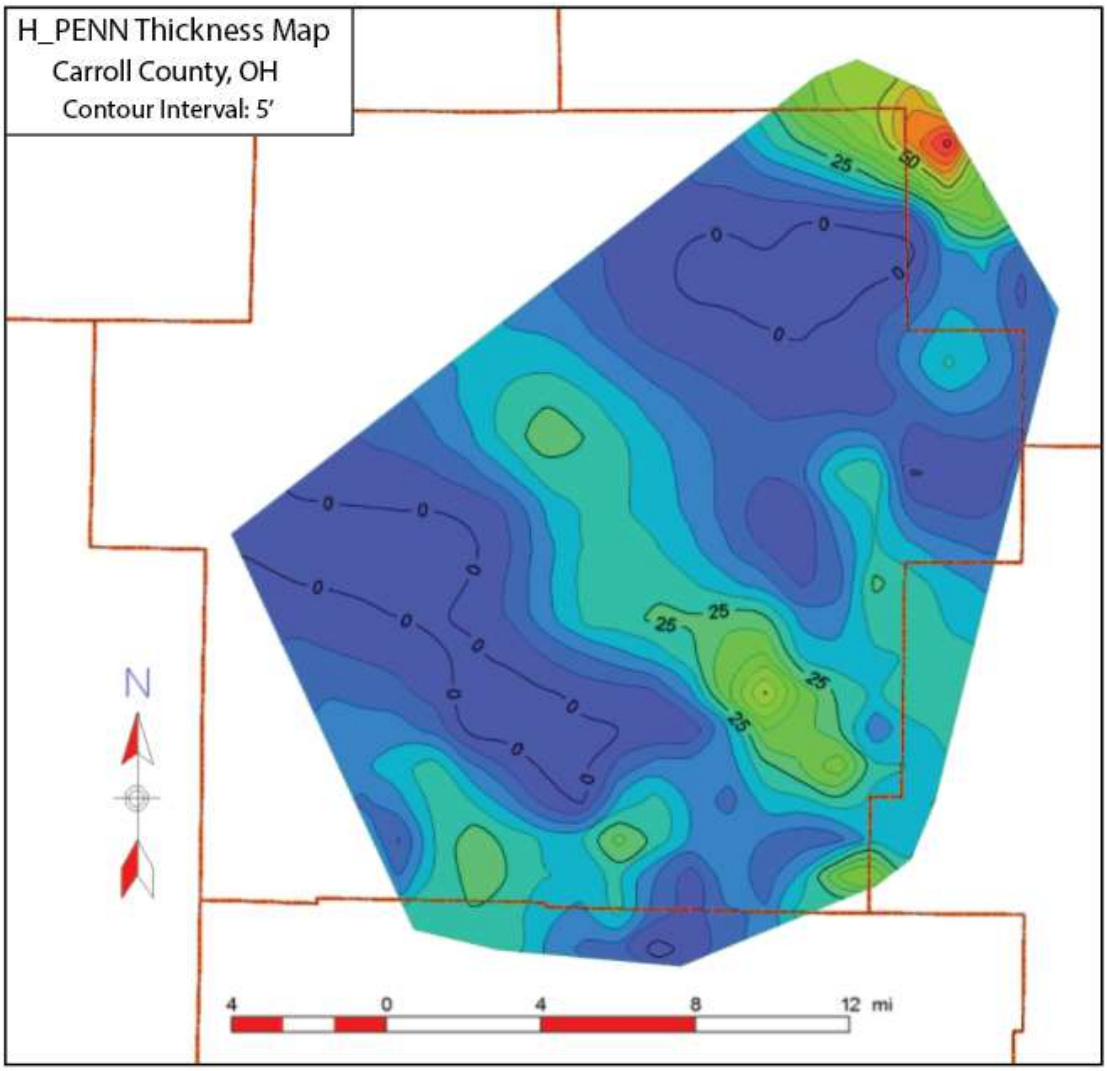

Figure A22: Thickness map of the H_PENN formation.

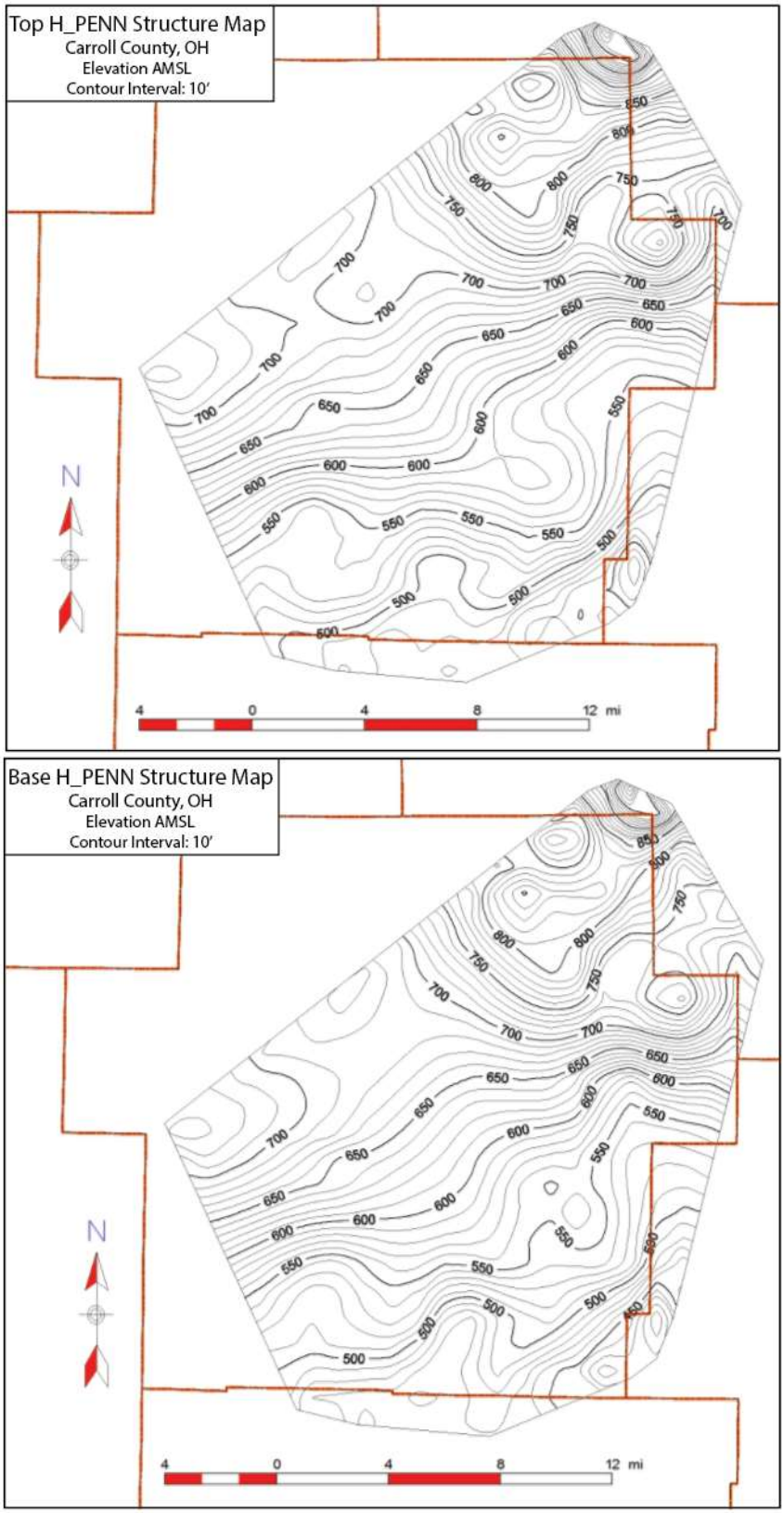

Figure A23 (Upper): Structure map of the top of the H_PENN formation.
Figure A24 (Lower): Structure map of the base of the H_PENN formation.

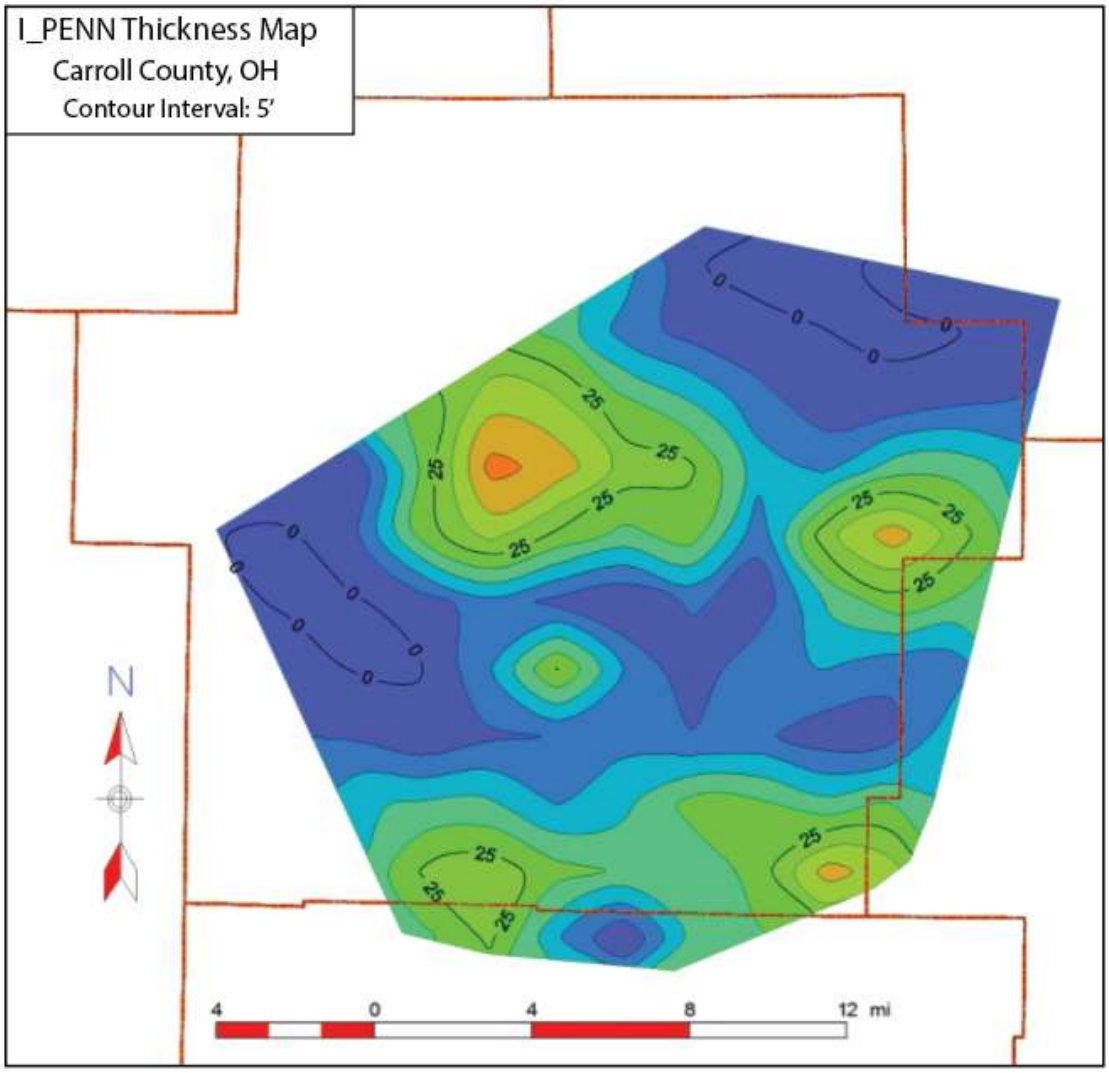

Figure A25: Thickness map of the I_PENN formation.

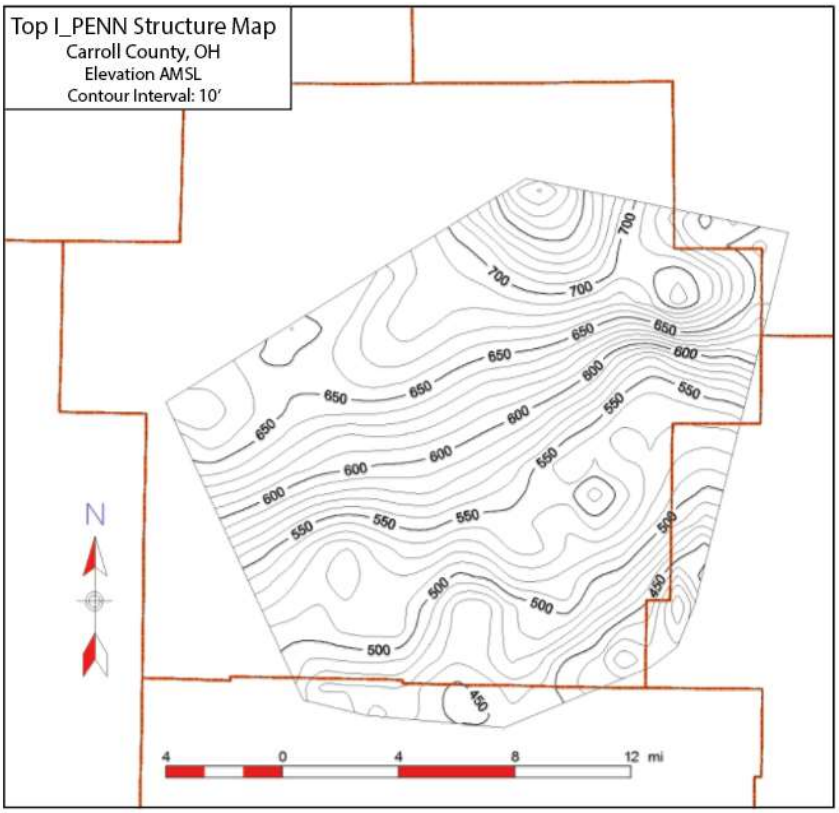

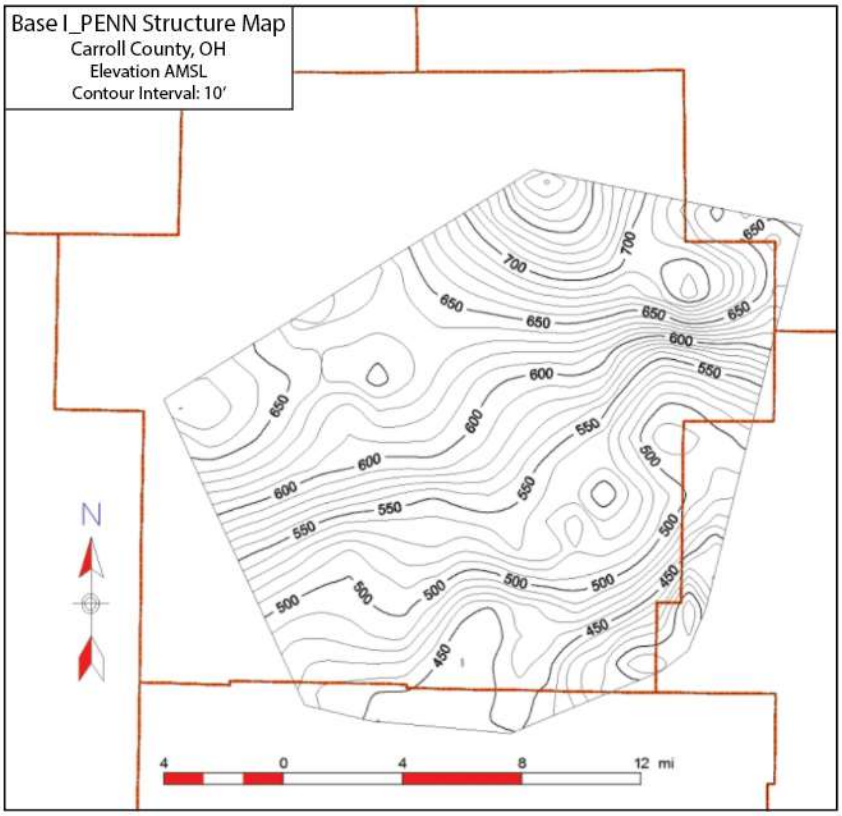

Figure A26 (Upper): Structure map of the top of the I_PENN formation.
Figure A27 (Lower): Structure map of the base of the I_PENN formation.

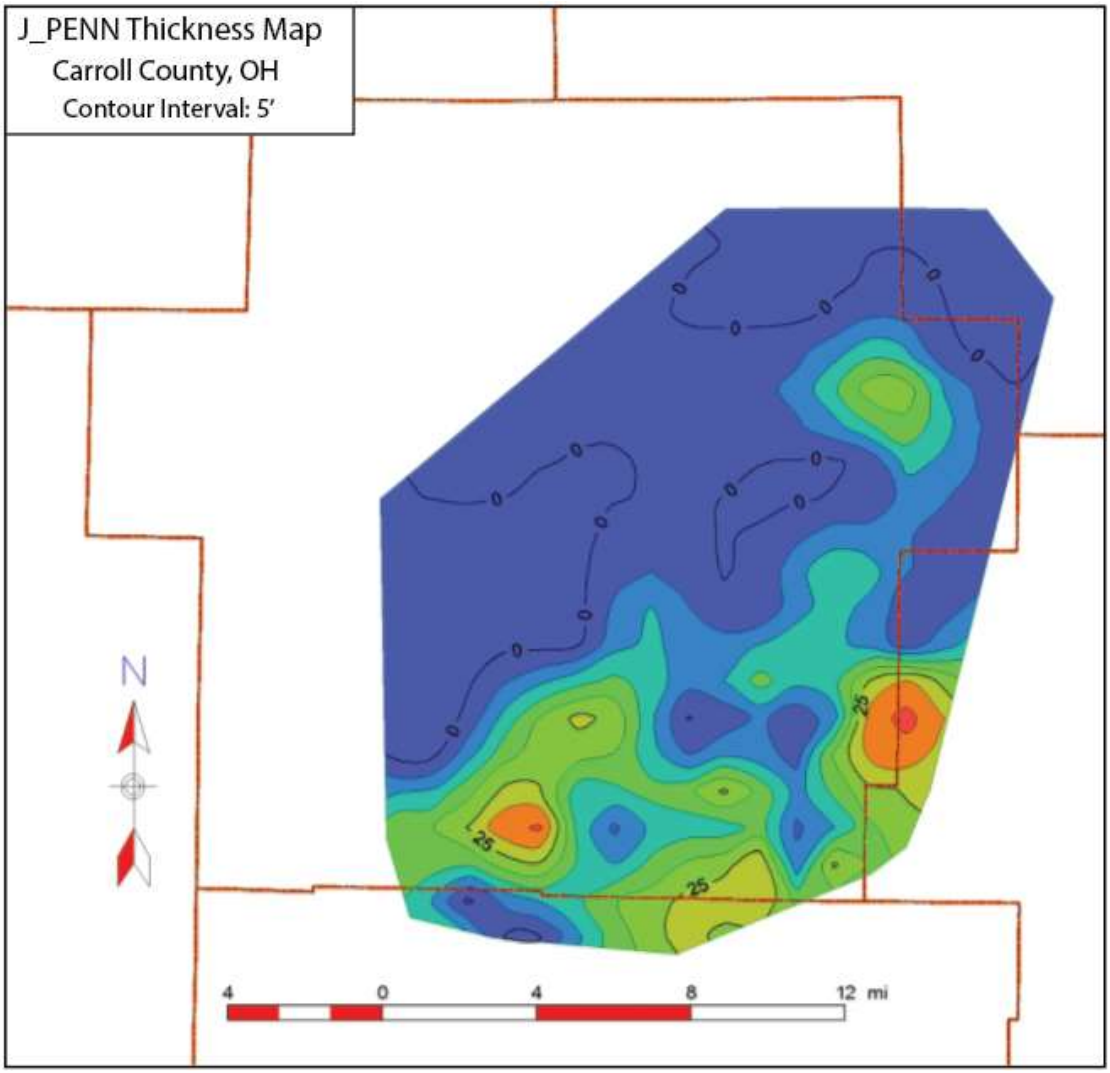

Figure A28: Thickness map of the J_PENN formation.

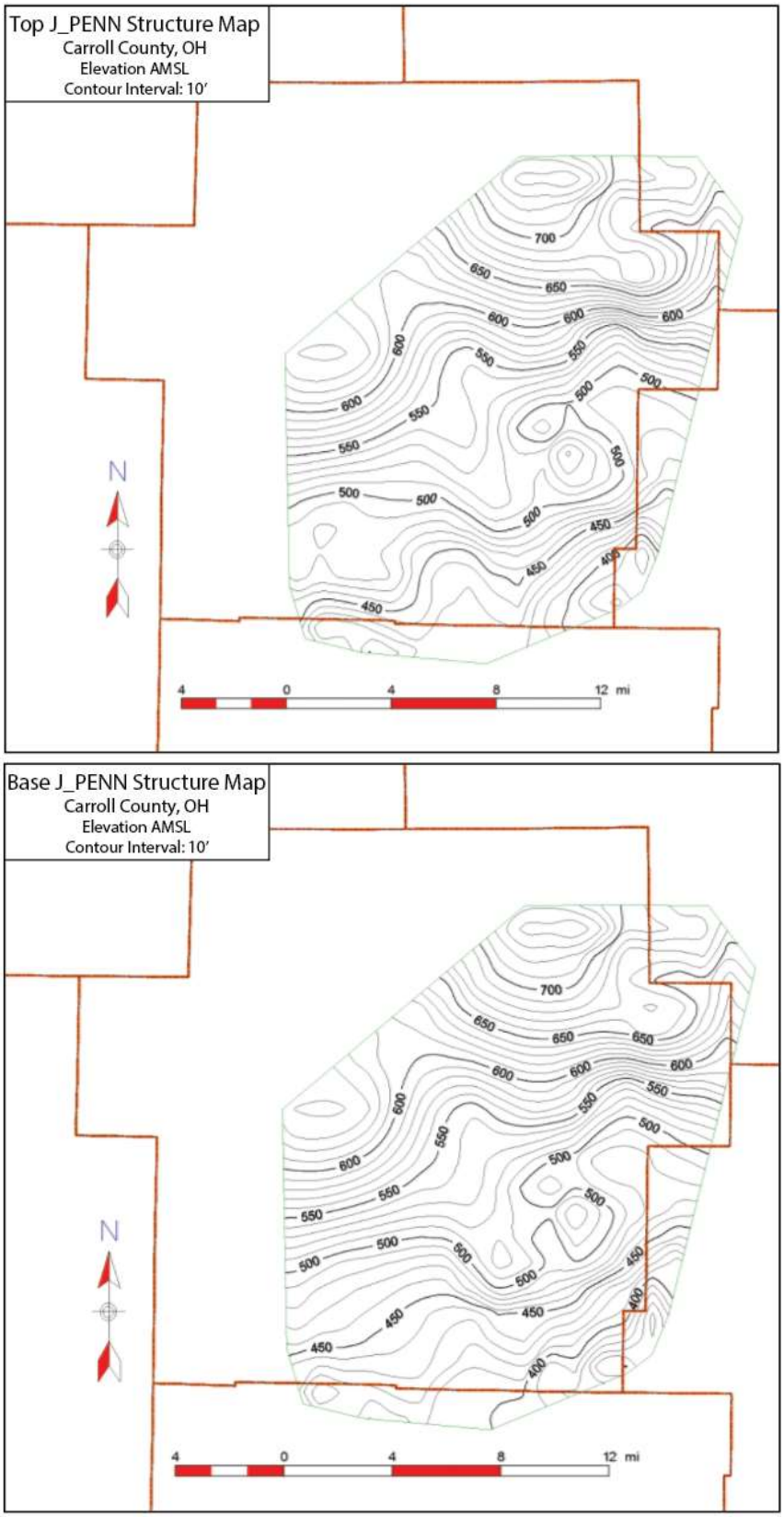

Figure A29 (Upper): Structure map of the top of the J_PENN formation.
Figure A30 (Lower): Structure map of the base of the J_PENN formation.

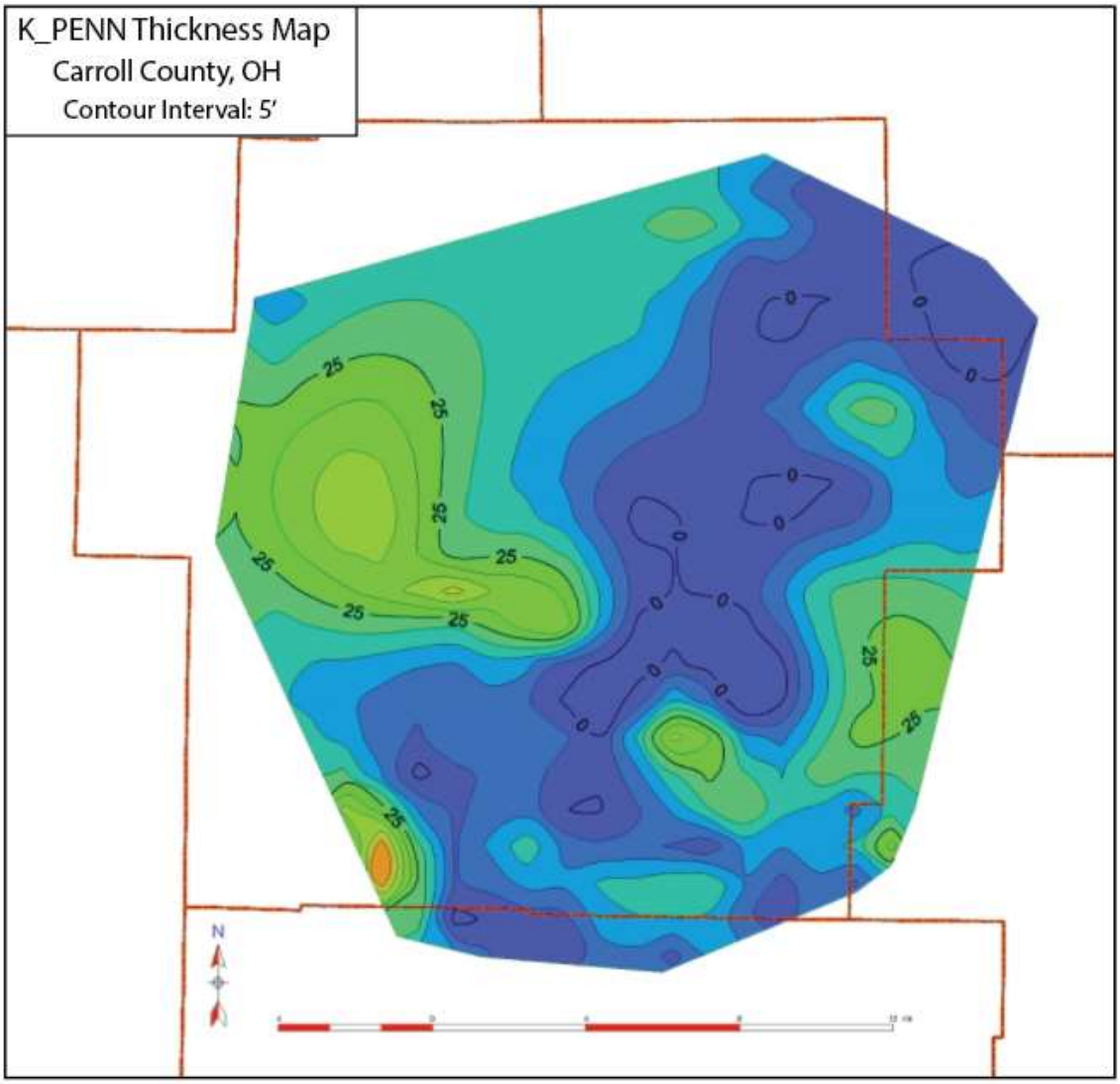

Figure A31: Thickness map of the K_PENN formation.

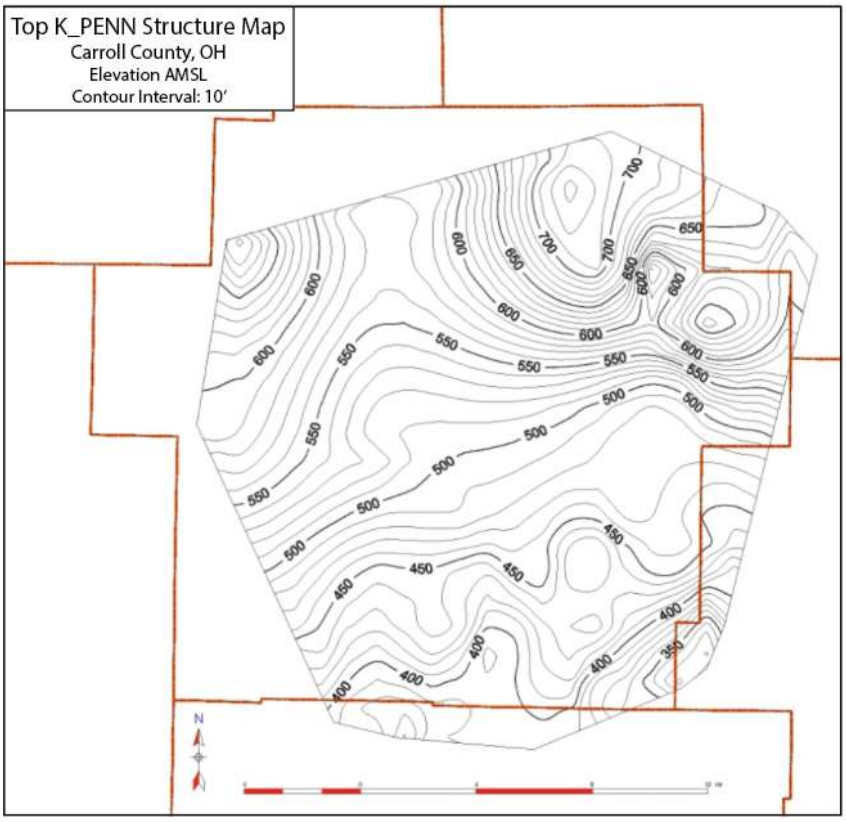

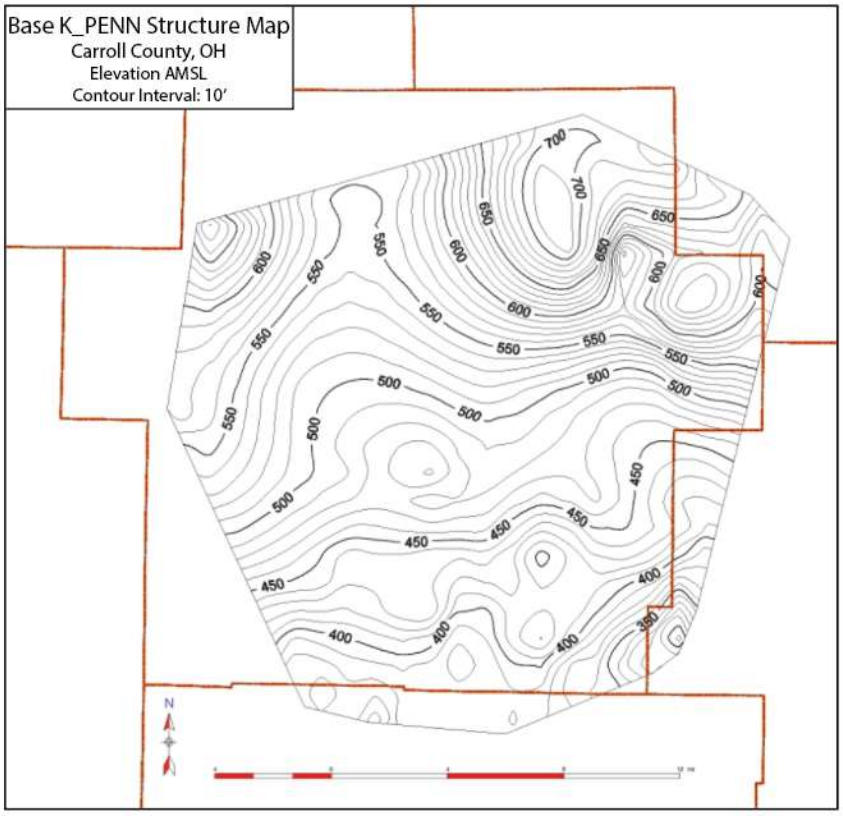

Figure A32 (Upper): Structure map of the top of the K_PENN formation.
Figure A33 (Lower): Structure map of the base of the K_PENN formation.

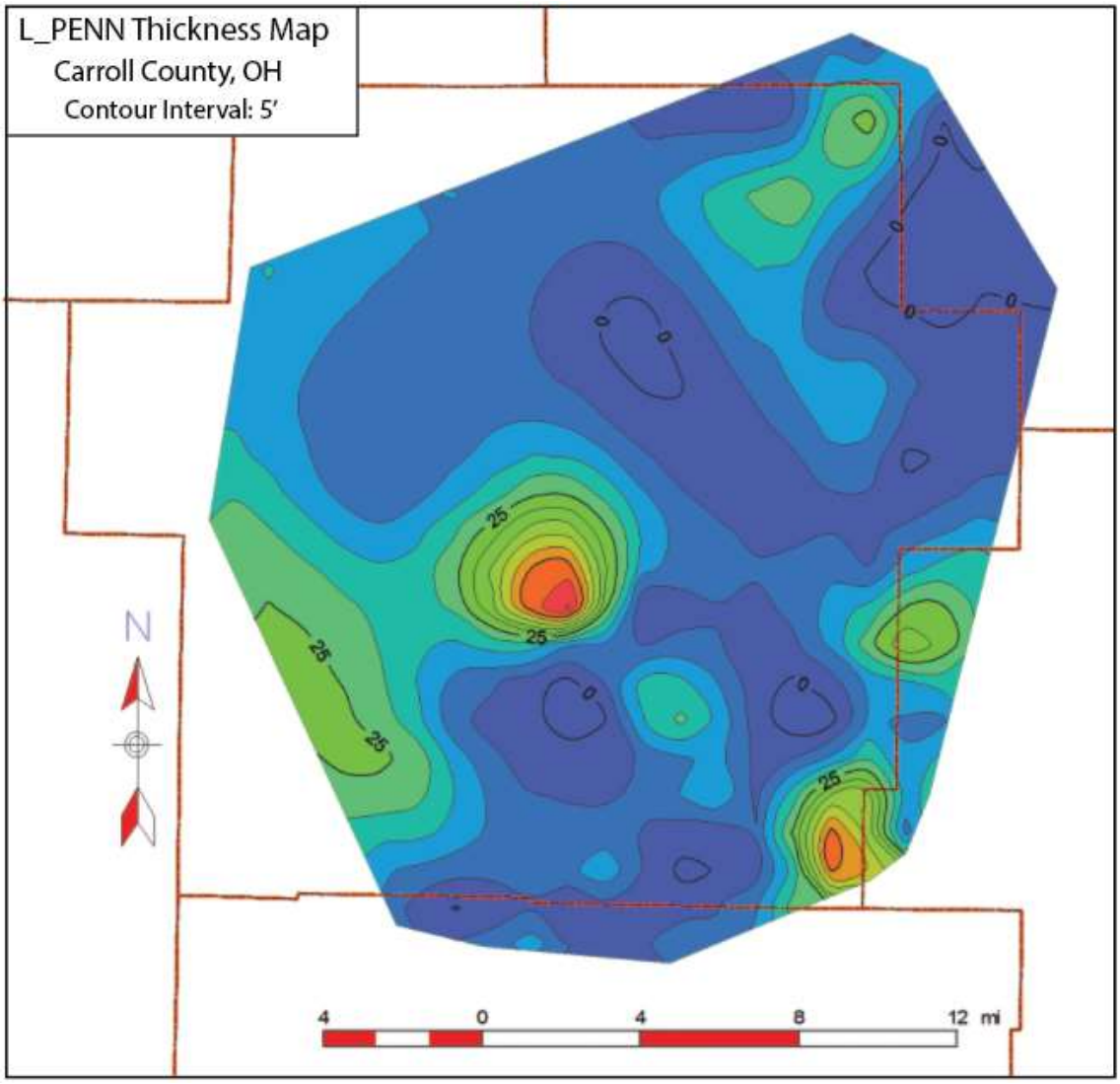

Figure A34: Thickness map of the L_PENN formation.

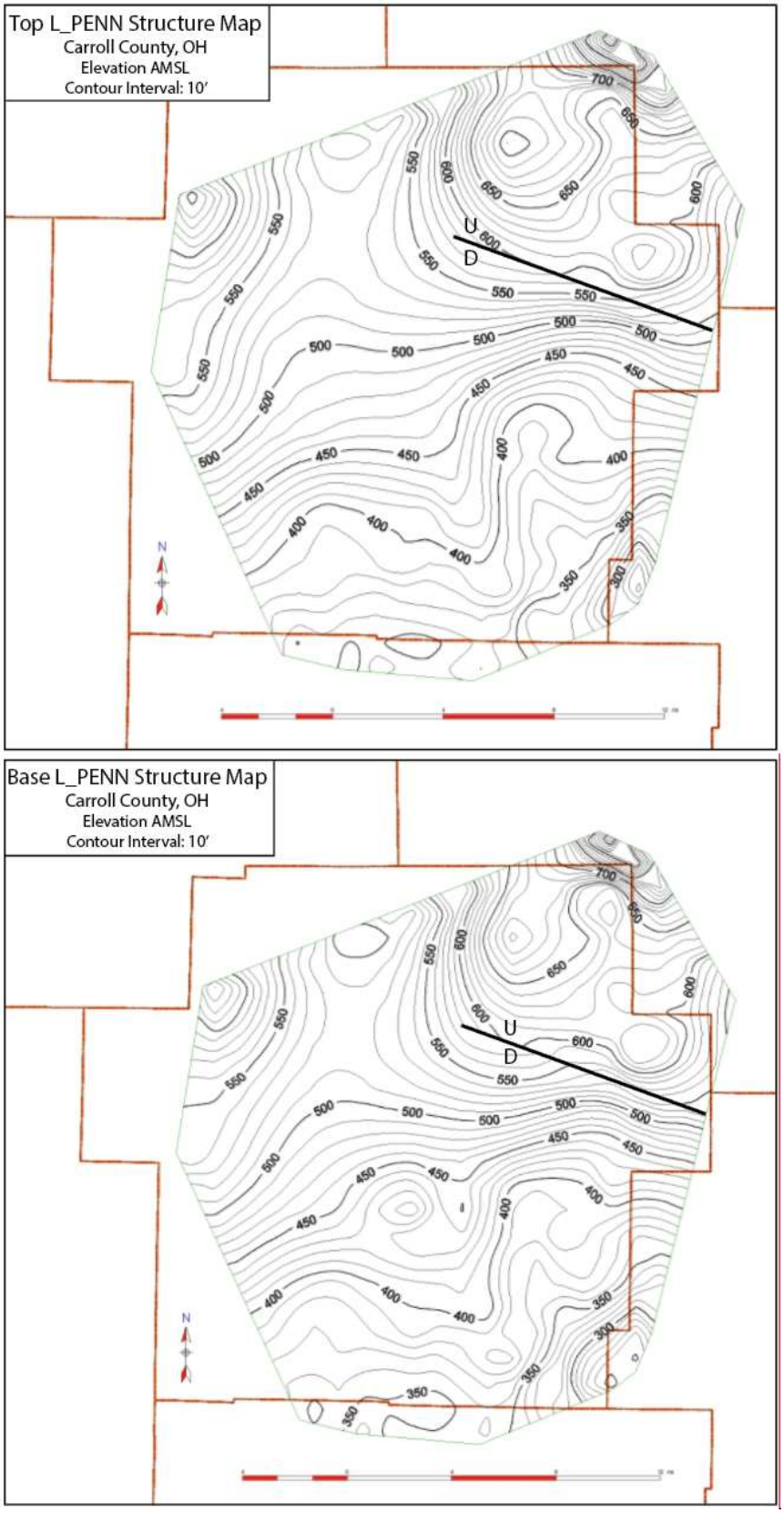

Figure A35 (Upper): Structure map of the top of the L_PENN formation.
Figure A36 (Lower): Structure map of the base of the L_PENN formation.

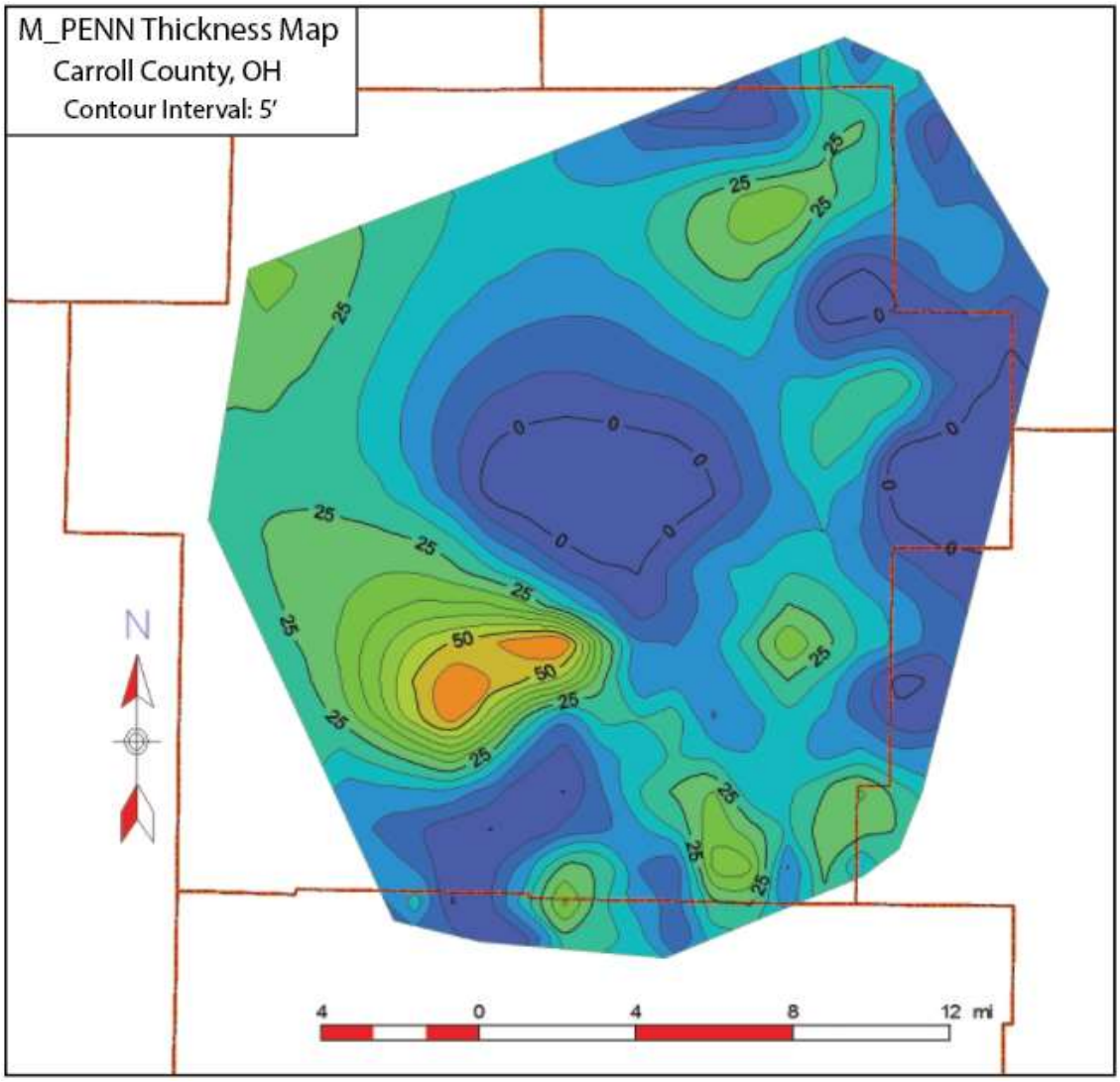

Figure A37: Thickness map of the M_PENN formation.

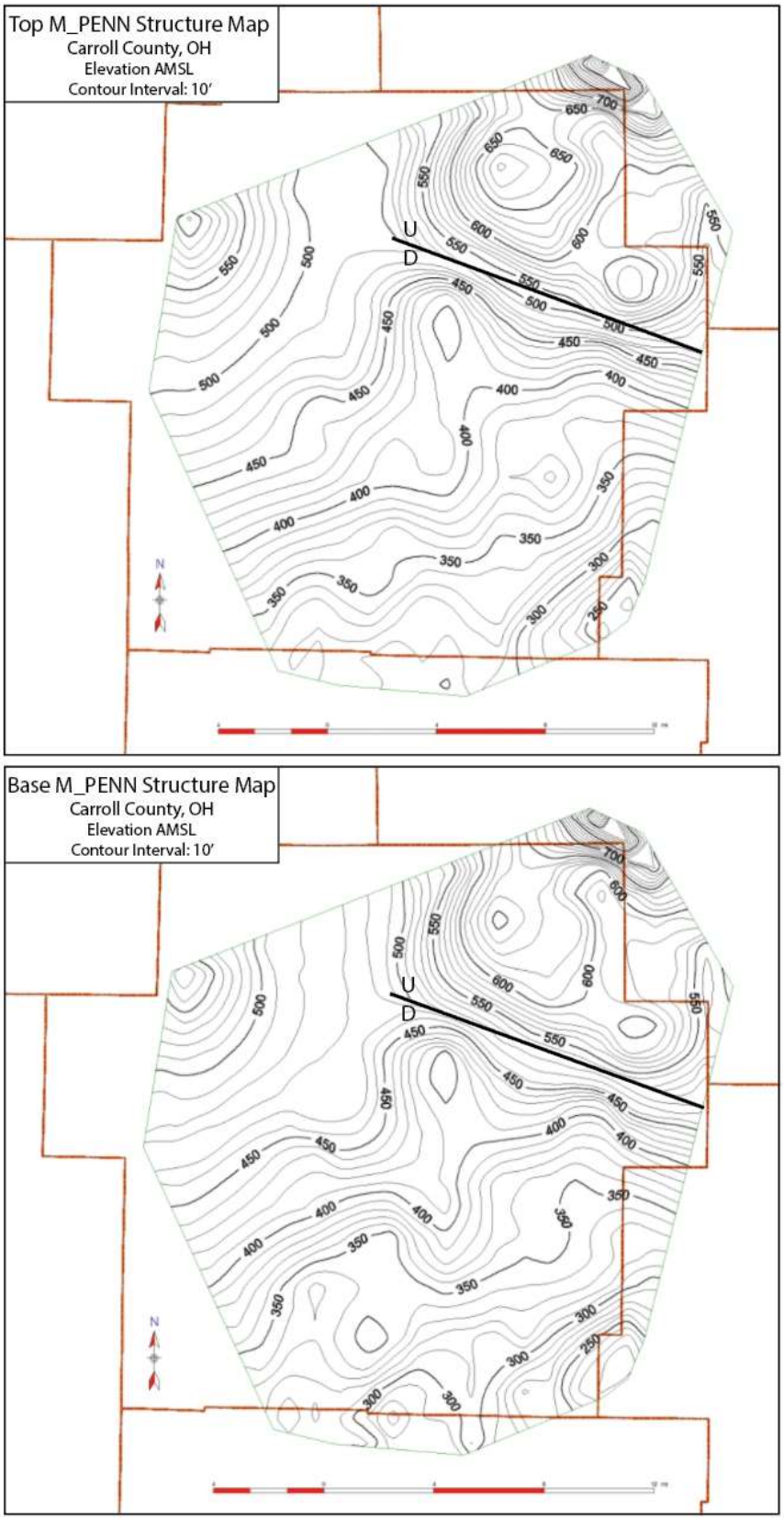

Figure A38 (Upper): Structure map of the top of the M_PENN formation.
Figure A39 (Lower): Structure map of the base of the M_PENN formation.

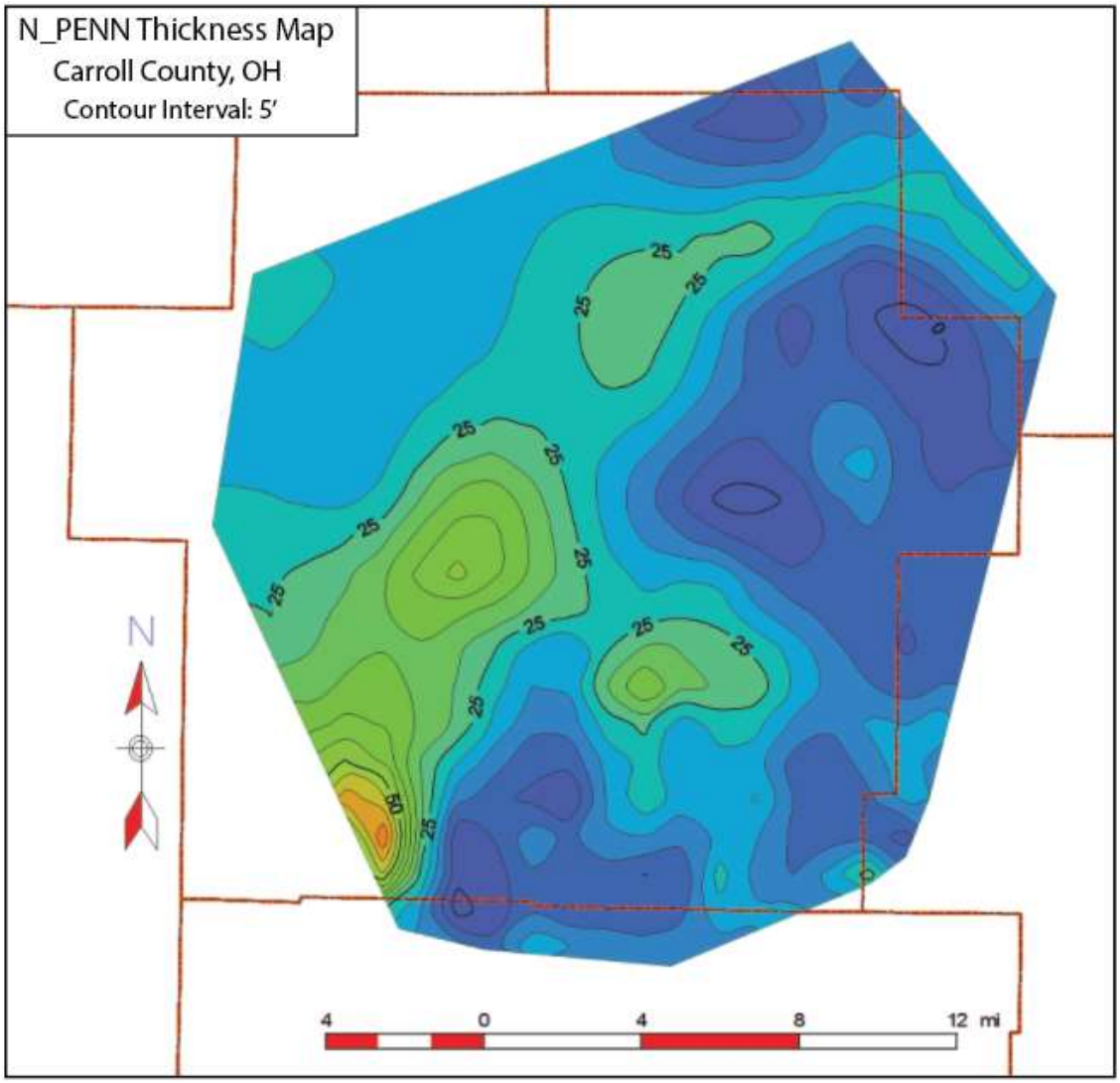

Figure A40: Thickness map of the N_PENN formation.

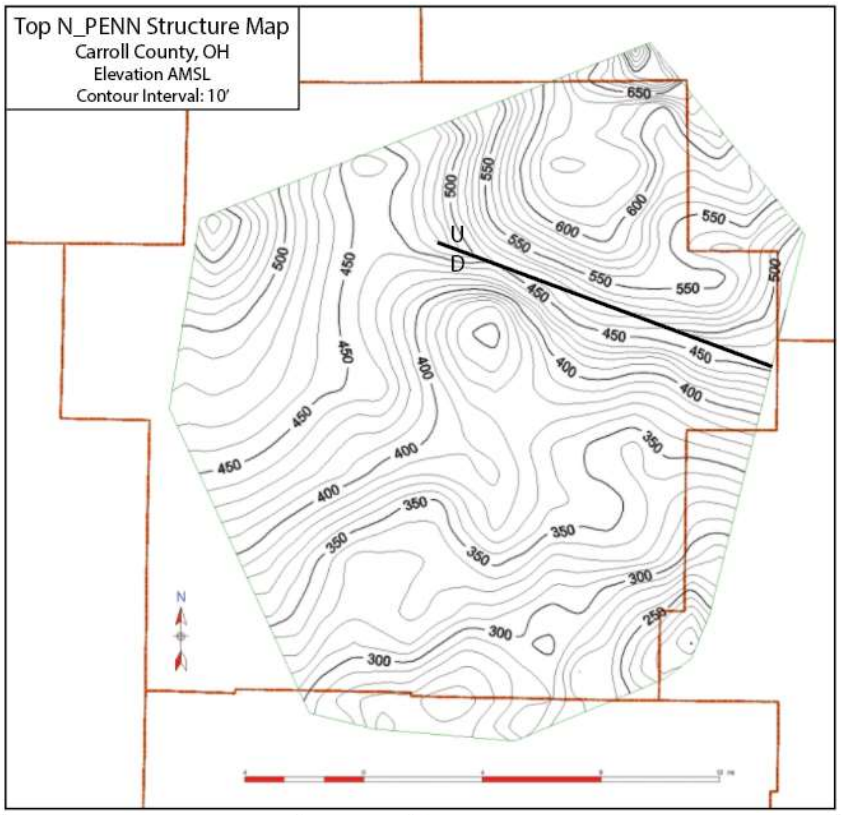

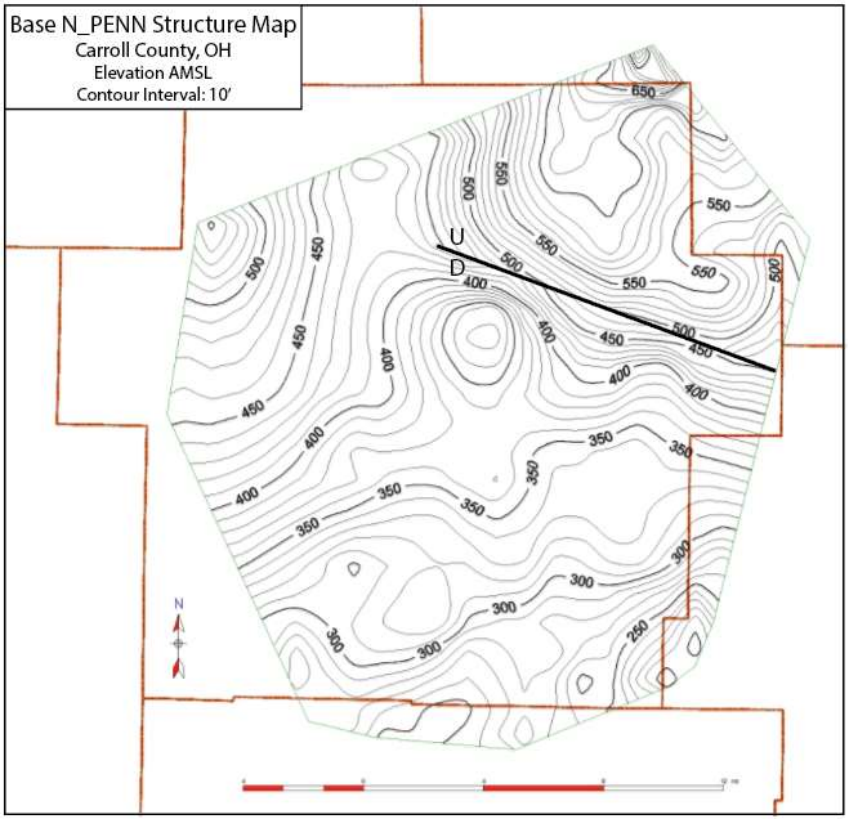

Figure A41 (Upper): Structure map of the top of the N_PENN formation.
Figure A42 (Lower): Structure map of the base of the N_PENN formation.

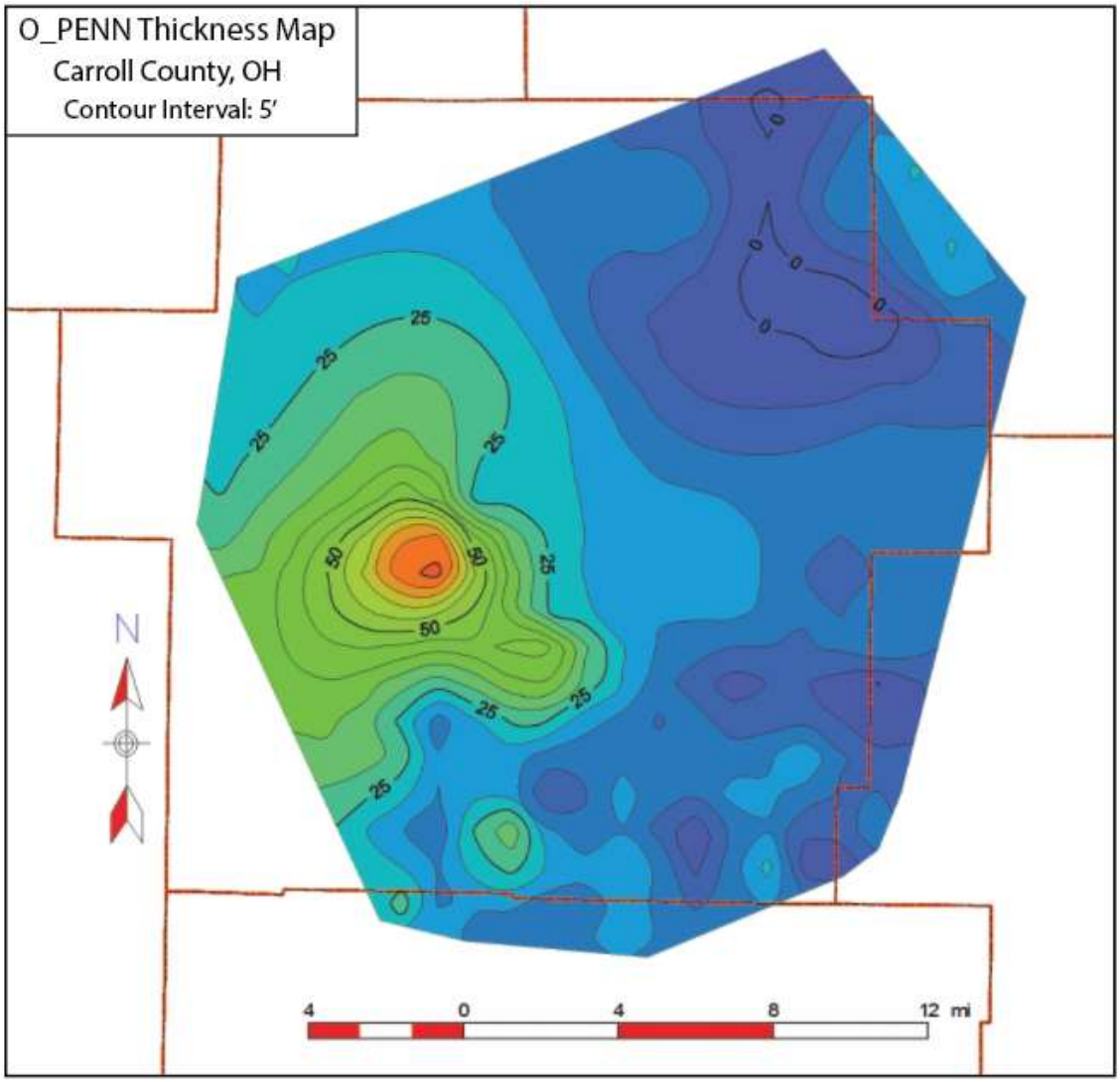

Figure A43: Thickness map of the O_PENN formation.

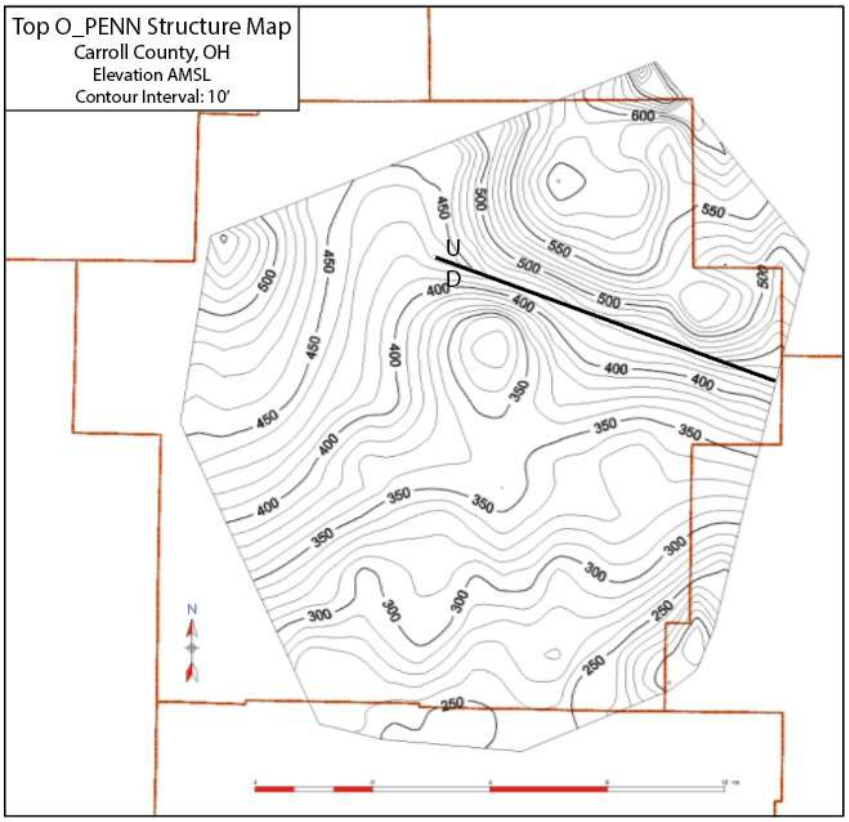

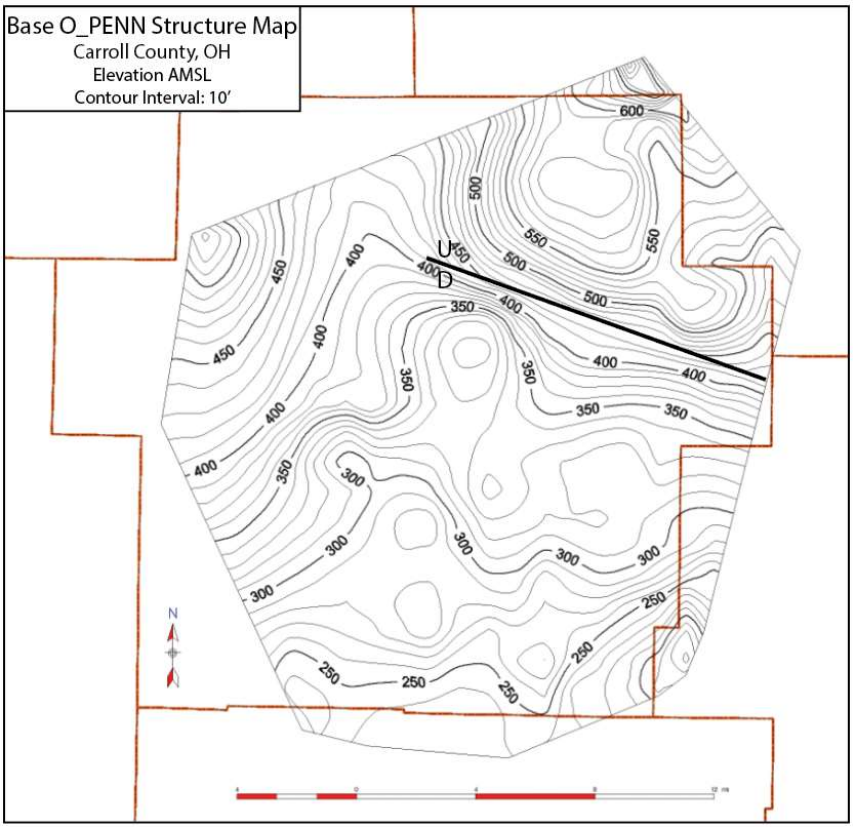

Figure A44 (Upper): Structure map of the top of the O_PENN formation.
Figure A45 (Lower): Structure map of the base of the O_PENN formation.

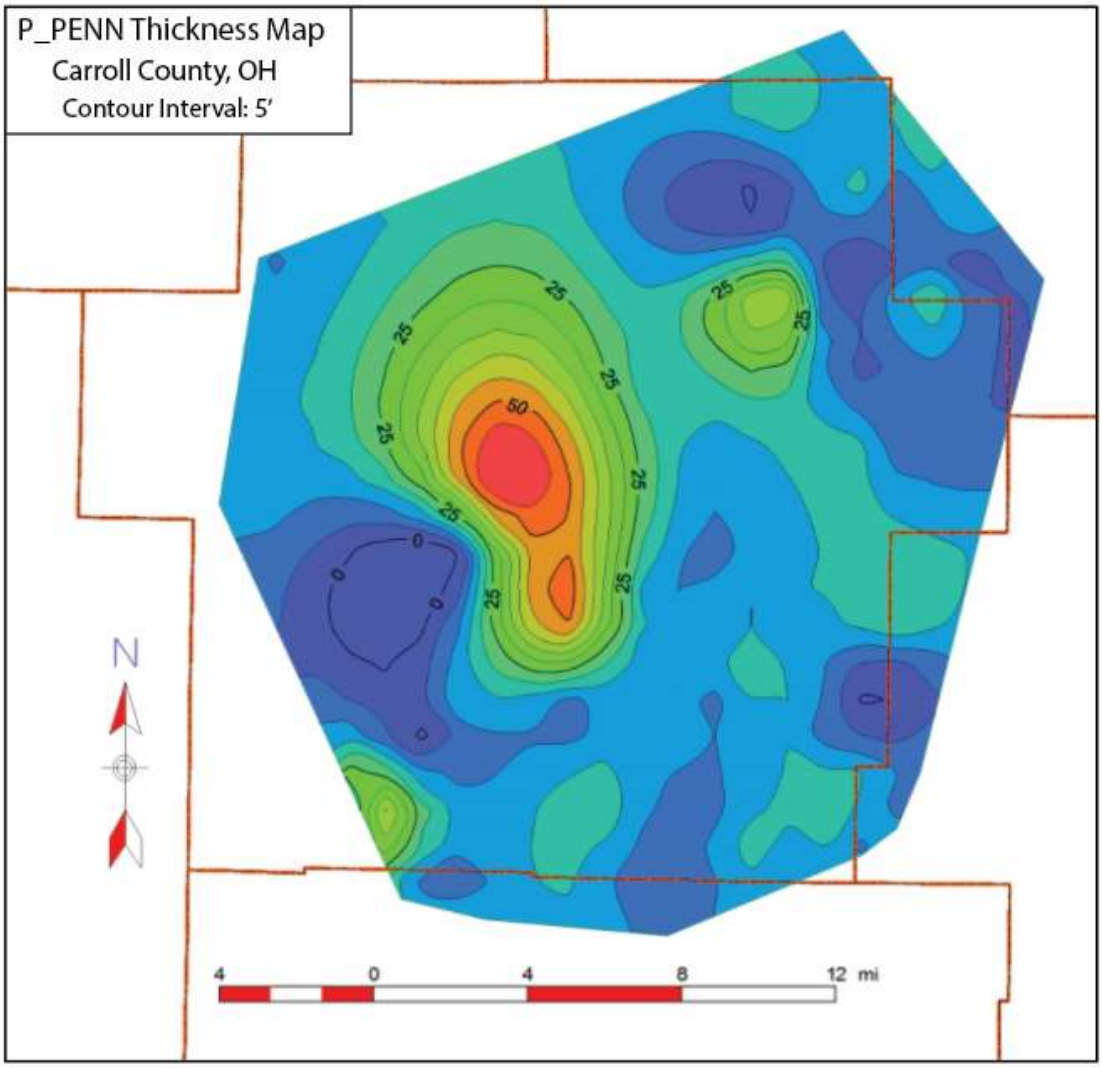

Figure A46: Thickness map of the P_PENN formation.

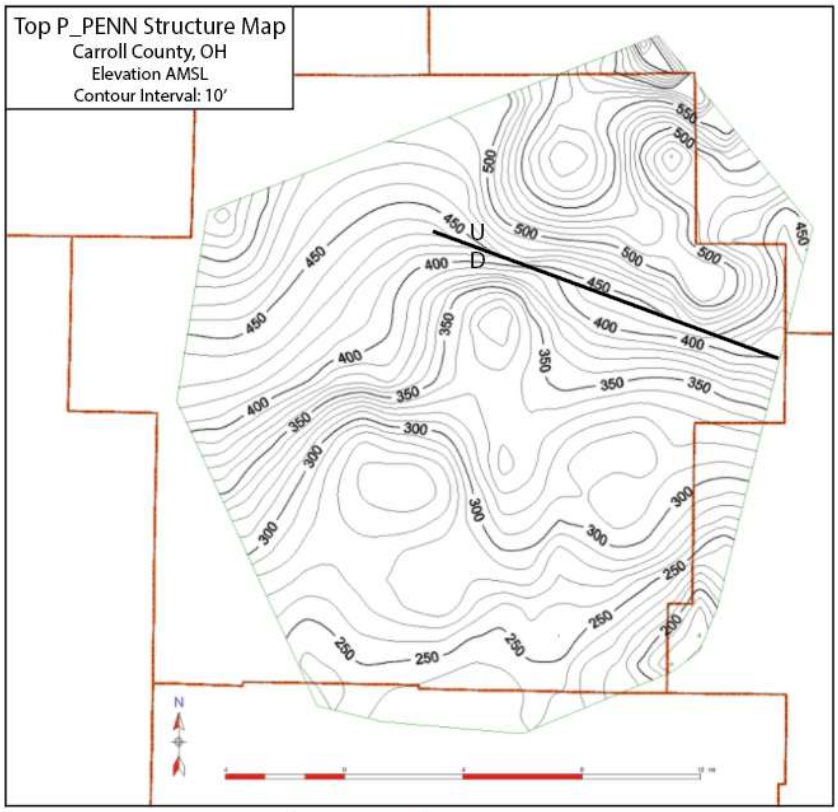

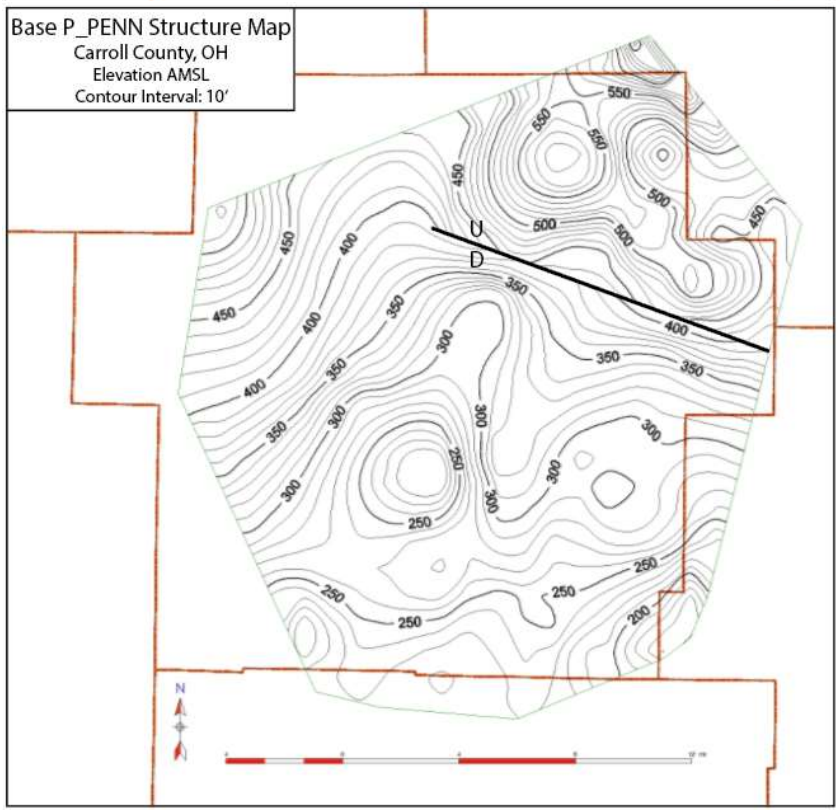

Figure A47 (Upper): Structure map of the top of the P_PENN formation.
Figure A48 (Lower): Structure map of the base of the P_PENN formation.

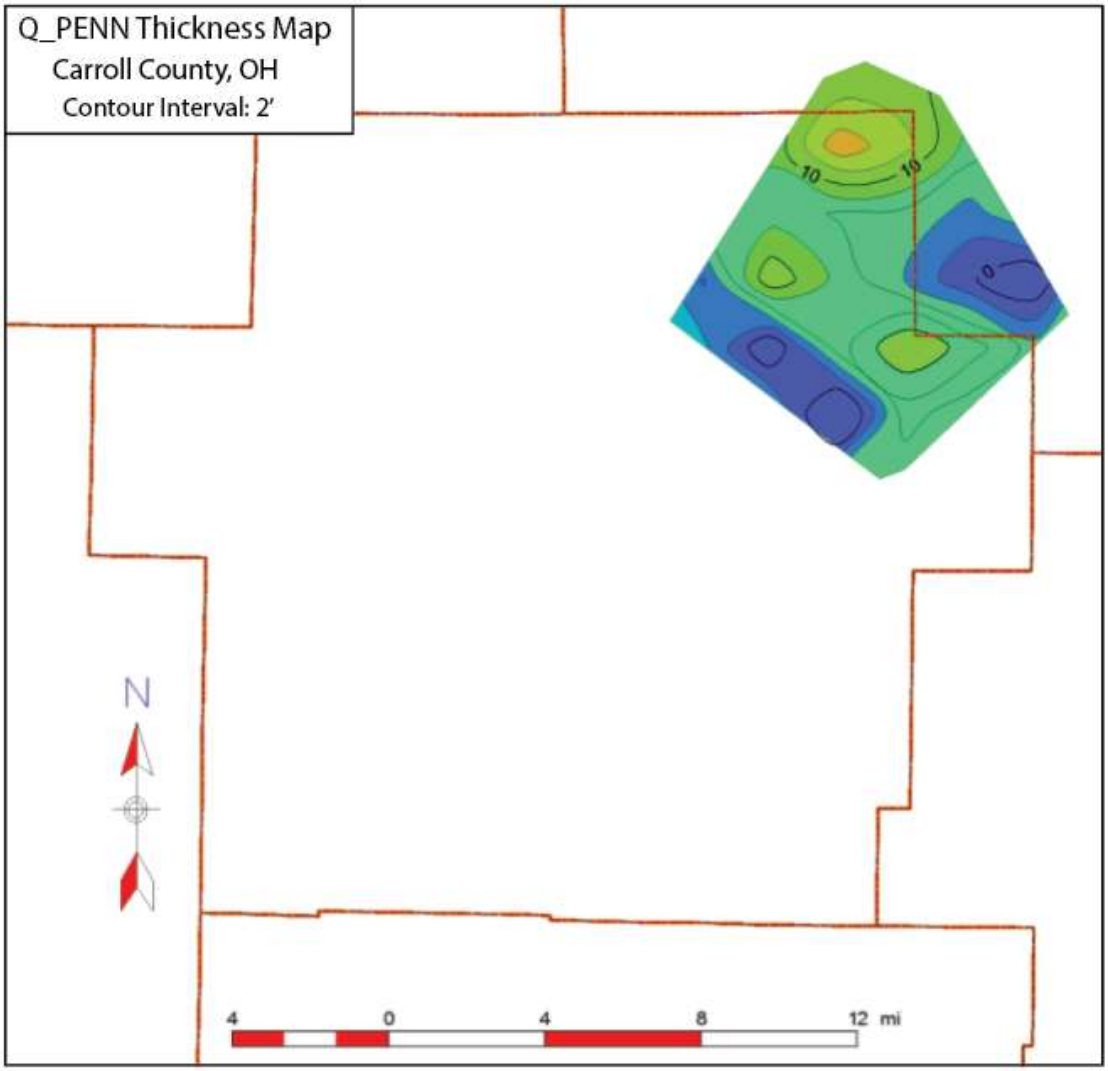

Figure A49: Thickness map of the Q_PENN formation.

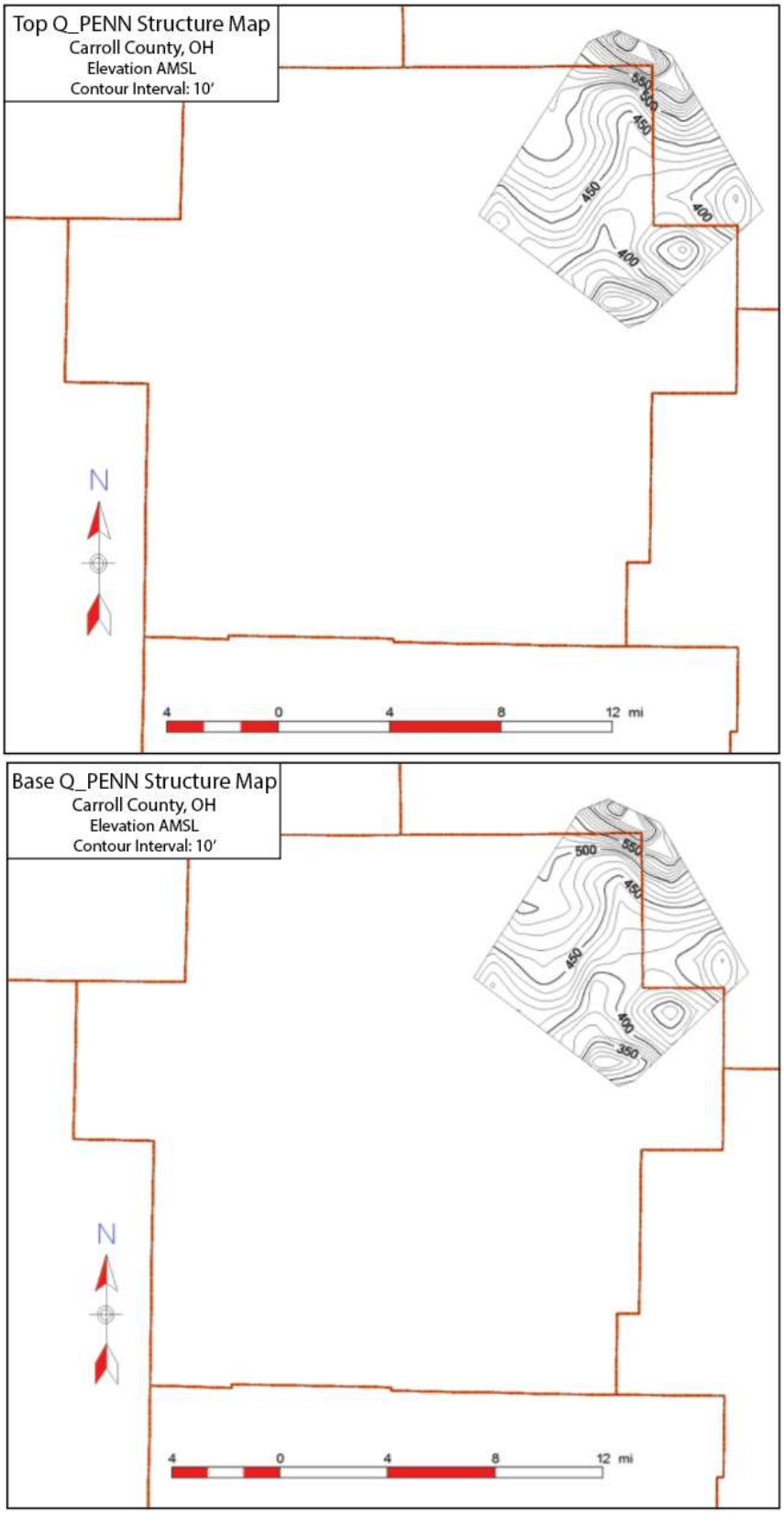

Figure A50 (Upper): Structure map of the top of the Q_PENN formation.
Figure A51 (Lower): Structure map of the base of the Q_PENN formation.

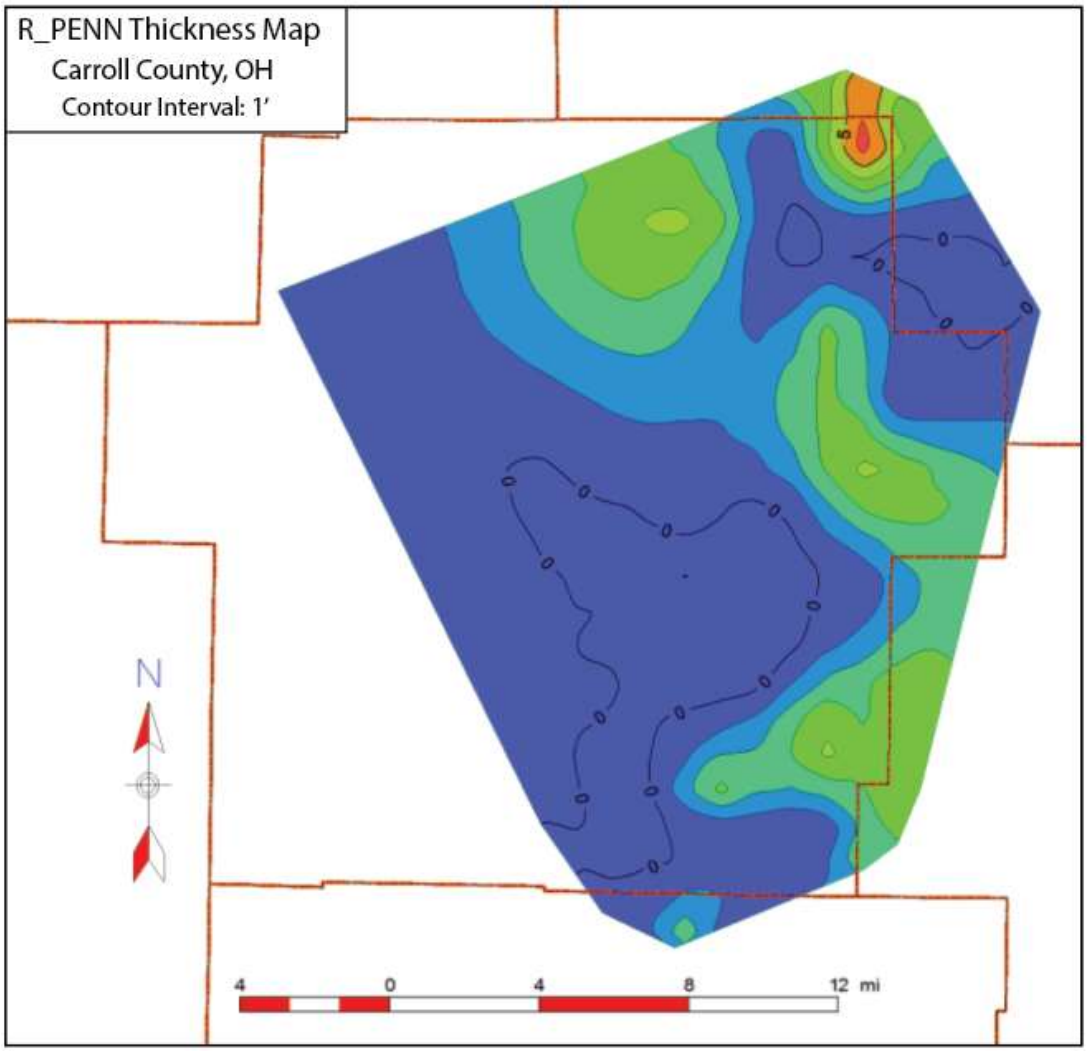

Figure A52: Thickness map of the R_PENN formation.

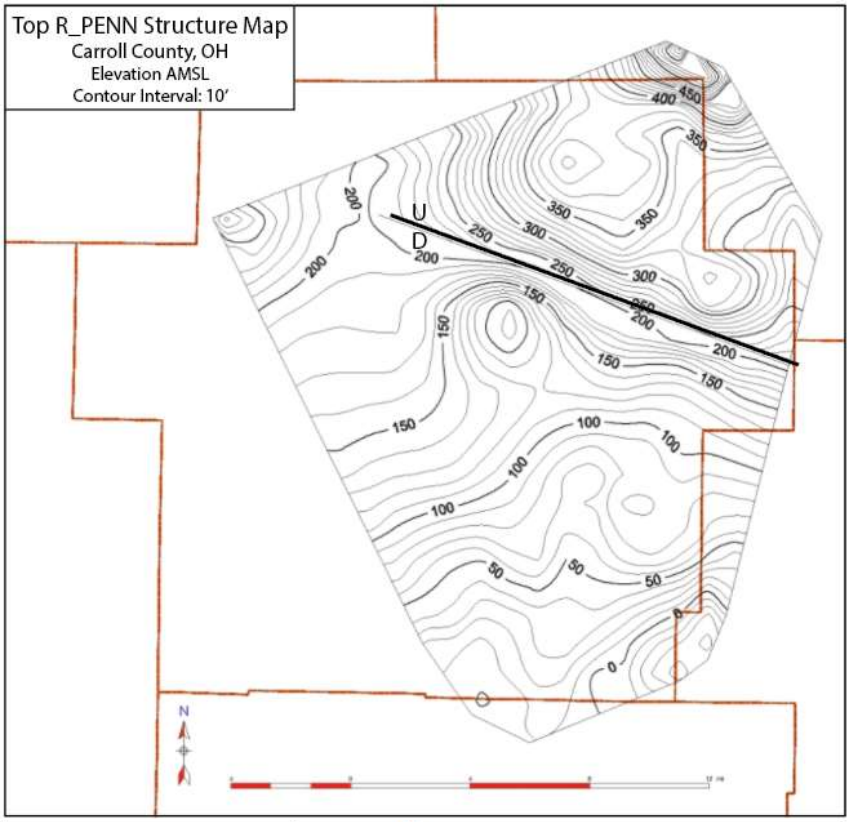

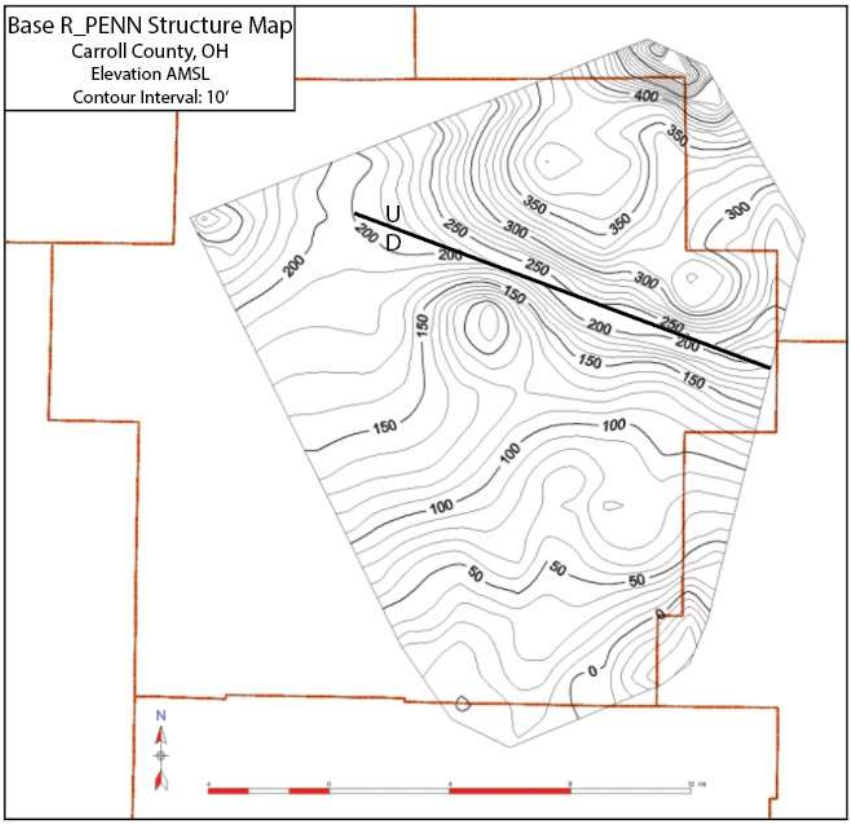

Figure A53 (Upper): Structure map of the top of the R_PENN formation.
Figure A54 (Lower): Structure map of the base of the R_PENN formation.

VITA

Laura Erichsen

Candidate for the Degree of

Master of Science

Thesis: MAPPING PENNSYLVANIAN STRATIGRAPHY AND ELEVATION OF THE FRESH-SALINE GROUNDWATER INTERFACE USING GEOPHYSICAL WELL LOGS IN CARROLL COUNTY, OHIO

Major Field: Geology

Biographical:

Education:

Completed the requirements for the Master of Science in Geology at Oklahoma State University, Stillwater, Oklahoma in December, 2022.

Completed the requirements for the Bachelor of Science in Geology at Northland College, Ashland, Wisconsin in 2010.

Experience:

2022-Present: Regulatory Analyst, Formentera Operations, Oklahoma City, OK
2017-2022: Senior Federal Regulatory Specialist, Continental Resources, Oklahoma City, OK
2015-2017: Geologist, Oklahoma Corporation Commission, Oklahoma City, OK
2013-2015: Hydrogeologist, Chesapeake Energy, Oklahoma City, OK
2012-2013: Mudlogger, Nomac GEO, Uniontown, PA
2011-2012: Geologist, Groundwater and Environmental Services, Fairmont, WV